FINAL REPORT

STRENGTH AND FRACTURE GRADIENTS FOR SHALLOW MARINE SEDIMENTS

Andrew K. Wojtanowicz, Adam T. Bourgoyne, Jr., Desheng Zhou, Kathy Bender
Louisiana State University

Submitted to:

US Department of Interior
Minerals Management Service
381 Elden Street
Herndon, Virginia 20170-4817

Baton Rouge, Louisiana
December 15, 2000

TABLE OF CONTENTS

ATTACHMENTS:

- **Shallow LOT Database from SMS: *OffshoreLOT.xls***
- **Shallow LOT Database from land drilling: *OnshoreLOT.xls***
- **Software: LOTUMS**

EXECUTIVE SUMMARY

Strength of conductor/surface casing shoe cemented in shallow marine sediments (SMS) is analyzed in this study. In this work, SMS are defined as sedimentary deposits below the sea floor to a depth of about 3000 ft. Qualitatively, SMS are soft and ductile compared with the sediments at depth.

The upper part of SMS is known better from soil borings. The soil is rather soft with Poisson's ratio around 0.4, Young's modulus about 3×10^4 psi at 300 ft, and low density with pressure gradient around 0.73 psi/ft. A plastic zone will appear around a well drilled in shallow marine sediments. Compared with leak-off tests (LOTs) in deep wells, LOTs form SMS display non-linearity of early pressure buildup plots, fewer tested points, and maximum pressure stabilization with continuing mud pumping. Also, the maximum stabilized pressure often corresponds to pressure gradients close to overburden pressure.

Properties of SMS are evaluated in this work using soil borings data from within the upper 1000-ft depth range below sea floor. Typical geotechnical data (bulk density, shear strength) have been collected, first. Then, rock mechanics properties (Young modulus, Poison Ratio, Cohesion, and friction angle) were calculated. The properties were used to evaluate in-situ stress in SMS.

Conventional LOT from deep wells and modified procedures used by operators in SMS have been compiled and analyzed in this report. The analysis of shallow LOTs, included the land and offshore operations. Although this report pertains mostly to marine sediments, some statistical observations regarding strength of shallow sediments onshore (in Canada) provide useful perspectives to this study. Analysis of shallow LOTs from land drilling used the attached database file *OnshoreLOT.xls* containing data from tests performed at the surface casing shoe in over 10,000 wells in Canada. Most of the results indicate large values of pressure gradient – close to the value of overburden pressure in the area.

The analysis of shallow LOTs from SMS offshore has been performed using data from the attached database, *OffshoreLOT.xls*. The objective was to – similarly to deep wells - identify trends in formation strength with depth, so a correlation could be developed and used for SMS strength prediction. All data showed that for SMS dispersion data is so large that no correlation or trend could be identified based on the data. Thus, it was concluded that SMS strength should be estimated from direct testing using a theoretically sound methods and simple-to-use procedures.

Traditional method of in-situ stress analysis is based on elastic theory and is not applicable to SMS. An analytical mathematical model of SMS stress in-situ, based on elastic-plastic theory, was derived in the study. Also, a finite element program was set up and used to simulate the transition process from elasticity to plasticity at depth. The analytical model is supported by the finite element analysis results. In addition to the theoretical modeling, empirical formulas for overburden stress in SMS were developed using bulk density data from soil borings. The formulas consider any combination of clayey or sandy sediments subsea.

Also reported is theoretical work addressing change of stress in SMS around drilled wells. Again the process was studied analytically. Based on elasto-plastic theory, formulas were set up to determine the critical condition for transition from an elastic to a plastic wellbore, the size of the possible plastic zone, and stress distribution around the wellbore. Stress variation during leak-off test was also analyzed.

Three types of possible failures caused by pressurization of the casing shoe (LOT or migration) were studied: vertical fracture, horizontal fracture, and cement-rock parting. (For

clarity, no fluid loss to the rock matrix was assumed in this study.) It has been proved theoretically that vertical fracture is the most unlikely failure of the three. Although horizontal fractures are initiated at low pressure in the plastic zone around the wellbore, they cannot propagate beyond the plastic zone until wellbore pressures exceed overburden pressures. On the other hand, an annular channel resulting form the cement-rock parting may propagate upwards at pressures lower than overburden pressure. (Unlike a conventional cement channel that occurs during cementing, cement-rock parting represents conditions when separation may be initiated between cement and rock by high wellbore pressure with no pre-existed channels assumed.) The study shows that cement parting is initiated at pressures equal to the contact stress between cement and rock and their propagation pressure is, on average, 3.5 - fold greater than contact stress. These findings were again supported by the results from the finite element method.

The study identified two factors, related directly to drilling technology, that control critical pressure of cement parting in SMS: contact stress at casing shoe – resulting from cementing operations, and rock penetration by liquid – an invasion of drilling fluid into the rock around the casing shoe. The results show that contact stress is developed during the process of cement setting as a result of volumetric changes in cement annulus. A mathematical model of contact stress around casing shoe was set up based on cement volume reduction and compensation from casing string, and cement and wellbore compressibility. It was shown in the study that changes in cementing and drilling practices may increases casing shoe integrity and reduce the need for cement squeeze treatments.

A general pressure-volume model of LOT and computer software are presented including volumetric effects of wellbore expansion, mud loss into the rock, and propagation of both cement parting and plastic fracture. The proposed model describes all possible mechanisms and therefore could explain linear, non-linear or combination patterns of the LOT plots.

Software LOTUMS - attached to this report - was developed to simulate LOT in SMS. A detailed instruction on using LOTUMS is provided in Chapter 5 and Appendix C. The software enables simulation studies of LOT or a casing shoe pressurization caused by fluid migration outside the well. Also presented is a LOTUMS simulation study of various mechanisms affecting the shape of the pressure-volume plots. The study shows that all mechanisms give very similar response patterns so qualitative analysis is difficult. Moreover, quantitative analysis with the software would require a detailed input data. However, since most of the system properties are unknown there is no reliable data input for the application software. Thus, LOTUMS software could only be used either for simulation studies or demonstration and training.

A simple method for analyzing LOTs in SMS is presented in this report. The method considers separately the pressure stabilization and the pressure buildup and fall-off sections of the LOT plot. Also used in the analysis is drilling data that includes overburden pressure (calculated from the SMS correlations developed in this project) and the maximum cementing pressure at the time of slurry placement.

The analysis of stabilized LOT pressure identifies the maximum strength of the casing shoe controlled by the rock stress (overburden pressure) and the failure by rock fracturing. Also presented is a graphical procedure for comparing the plots of actual and equivalent pressure fall-off. The graphical procedure provides a pattern-recognition method to distinguish the mechanism of cement-rock parting from the fluid loss mechanism.

1. BACKGROUND INFORMATION

A flow from unexpected shallow gas sand is one of the most difficult well control problems faced by oil and gas well operators during drilling operations. Current well control practice for bottom-supported marine rigs usually calls for shutting in the well when a kick is detected if sufficient casing has been set to keep any flow underground. Even if high shut-in pressures occur, an underground blowout is preferred over a surface blowout. However, when shallow gas is encountered, casing may not be set deep enough to keep the underground flow outside the casing from breaking through to disturbed sediments near the platform foundations. Once the flow reaches the surface, craters are sometimes formed that can lead to loss of the rig and associated marine structures.

1.1 Shallow Blowout Statistics

Numerous disastrous blowouts have occurred after gas unexpectedly flowed into the well from a shallow formation. By the time the rig crew can recognize the problem and react to it, gas may have already traveled a considerable distance up the open borehole. Closing the blowout preventers may allow the wellbore pressure to build up to a value exceeding the formation breakdown pressure. When this happens, one or more flow paths can travel to the surface or to disturbed soil near a platform leg. In some cases, a crater forms in the seafloor. If the rig structure is bottom supported, the entire rig may be lost.

Hughes (1986) compiled information on 425 Gulf Coast blowout events that covered the period between July 13, 1960 and January 1, 1985. The data, broken down by area, included 242 blowouts in Texas, 56 in Louisiana, 121 in the Outer Continental Shelf (OCS), 3 in Mississippi, and 3 in Alabama. Gas was present in 82% of the Texas blowouts. The two major operations that were underway when the blowout occurred were (1) coming out of hole (27%) and (2) drilling (25%). Seventeen Texan blowout reports (7.02%) noted that the well blew out around the casing. A total of twenty events (8.26%) reported that the underground flow reached the surface either to form a crater around the well, at a nearby surface site, or caused blowouts from nearby water wells. All the blowouts that reached the surface outside of casing had drilling depth to casing depth ratios greater than four.

Of the 56 Louisiana blowouts included in the Hughes study, gas was present in 73% of wells that reported the type of blowout fluid. The rig operations reported to be underway at the time of the blowout included: workover operations, 37%; coming out of hole, 21%; circulating, 13.2%; and drilling, 13.2%. Hughes does not give details about flows around casing or cratering for the Louisiana blowouts.

Of the 121 OCS blowouts reported by Hughes, gas was present in 77% of the cases. Descriptions of the operations were available for 46 events. The rig operations reported to be underway included: workover operations, 28%; coming out of hole, 24%; and drilling, 20%. Descriptions of the procedure used to control the blowout were given for 66 of the wells. The majority (55%) of the blowouts bridged naturally. Both the date the blowout occurred and the date the well was killed were given for 70 wells; about 49% of these were controlled within one day.

Danenberger (1993) performed a study of blowouts that occurred during drilling operations on the Outer Continental Shelf of the United States during the period from 1971 to 1991. During this period, 21,436 oil and gas wells were drilled; eighty-three blowouts occurred. Four additional blowouts occurred during sulfur drilling operations. Eleven of the blowouts resulted in casualties with 65 injuries and 25 fatalities. Fifty-eight of the blowouts that occurred

while drilling for oil and gas came from shallow gas zones. Exploratory wells accounted for 37.4% of the wells drilled and 56.9% of the shallow-gas blowouts. Conversely, development wells accounted for 62.6% of the wells drilled and 43.1% of the shallow-gas blowouts.

According to Danenberger (1993), a shallow gas blowout in 1980 was the most serious blowout in the OCS, accounting for 6 of the 25 fatalities and 29 of the 65 injuries. However, no casualties due to blowouts were reported during the last seven years of the study.

Oil was not associated with the shallow gas blowouts and environmental damage has been minimal. Two blowouts prior to 1971 are known to have caused oil pollution in the portion of the Outer Continental Shelf under U.S. jurisdiction. An estimated 80,000 bbl of crude oil was released into the Santa Barbara Channel, and about 1,700 bbl of condensate was released into the Gulf of Mexico.

Although no statistics are given for the OCS on crater developments affecting rig foundations, Danenburger (1993) reported that 71.3% of the blowouts stopped flowing when the well bridged naturally. This bridging is thought to be due to the collapse of the uncased portion of the borehole. Flow from 57.5% of the blowouts ceased in less than a day, and flow from 83.9% ceased in less than a week. A list of shallow gas blowouts compiled by Adams (1991) indicates that 18 bottom-supported structures were damaged on the OCS by shallow gas blowouts during the 1971-91 period of the Danenburger study. Seven of the U.S. structures shown in the Adams study were reported to be a total loss, and extensive damage was reported for another three cases. These ten cases account for 17.2% of the 58 shallow gas blowouts reported by Danenburger (1993). Thus 10 lost structures out of 21,436 wells drilled is a rough estimate of the risk from significant cratering.

We were not successful in compiling an estimate of economic loss associated with shallow gas blowouts. However, an operator reported that the cost due to one event outside the U.S. was approximately 200 million dollars.

1.2 Significance of Sediment Strength Determination

Modern contingency plans for handling a shallow gas flow call for diverting the flow away from a bottom-supported rig using a diverter system. The diverter system is used to reduce the wellbore pressure so that it does not exceed the formation breakdown pressure. However, results of this study indicate that using diverter systems does not always prevent cratering. Crater formation during diversion can occur when the diverter is too restricted, thus allowing formation breakdown pressure to be exceeded even though the well is not shut-in.

Cratering and underground blowouts can be prevented only through appropriate casing design, cementing practices, and shut-in procedures. A successful well design must be based on a realistic estimate of the fracture resistance of the sediments. Thus, improvements in the analysis and procedure of leak-off testing for wells in shallow marine sediments (SMS) are needed.

The sediment failure mechanisms around wells traditionally have been poorly understood. In addition, the best choices of well design parameters and well control contingency plans that will minimize the risks associated with a shallow gas flow are not always clear. The objectives of this study were:

- To identify properties of SMS that control the sediment strength and failure around boreholes;
- To study and model mathematically several possible sediment failure mechanisms around over-pressured wellbores;

- To survey and analyze currently used procedures for testing strength of SMS at the wellbores;
- To collect industry data from leak-off testing (LOT) in SMS;
- To develop mathematical models and software for simulating stress-strain (pressure-volume) relationship at the pressurized wellbore (LOT simulator);
- To formulate guidelines for LOT procedure and result analysis in SMS.

2. CHARACTERIZATION OF SHALLOW MARINE SEDIMENTS (SMS)

For the purpose of this work, we define SMS broadly as the depositional environment below the sea floor to a depth of about 3000 ft. According to widely accepted thinking, SMS are soft and ductile compared with the sediments at depth.

2.1 Shear Strength of the Upper SMS

Properties of the upper layers of SMS, just below the seafloor, can be visualized using well-known concepts of effective stress:

$$\sigma_z = s - p \tag{1}$$

in which s is the total overburden stress and p is the formation pore pressure, and modified Mohr-Coulomb failure criteria, as shown in Figure 1.

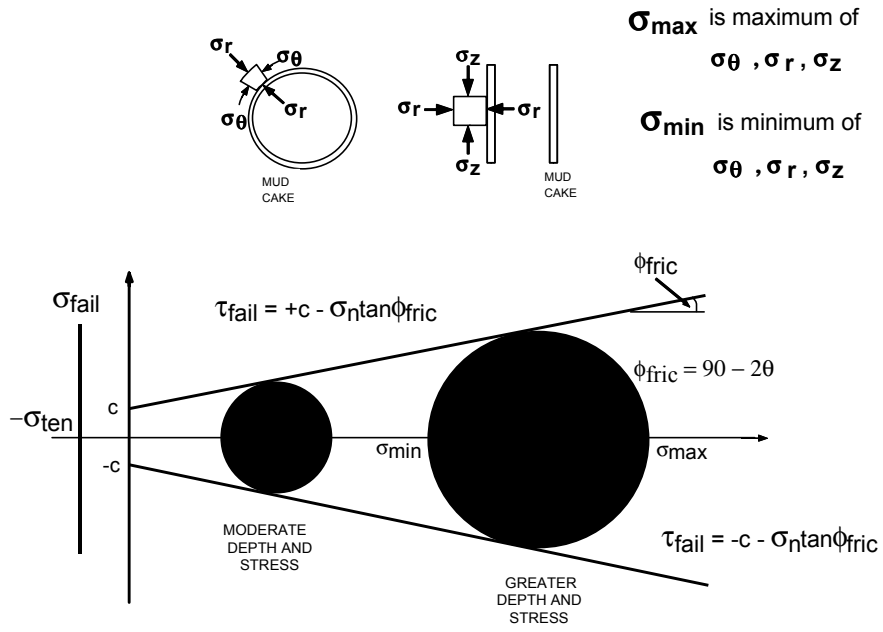

Figure 1. Mohr-Coulomb failure criteria.

In Figure 1 the Mohr's circles are drawn with their centers on the abscissa. Minimum and maximum principal effective stresses (σ_{min} and σ_{max}) are also on the abscissa. Sediment failure is predicted to occur whenever a Mohr's circle touches one of the failure lines given by:

$$\sigma_{fail} = -\sigma_{ten} \tag{2a}$$

$$\tau_{fail} = \pm c \pm \sigma_n \tan(\phi_{fric}) \tag{2b}$$

When the Mohr's circle touches the tensile strength line, σ_{fail}, a hydraulic fracture-type failure occurs. This failure mode is the most common during well control operations for deeper sediments, and the hydraulic fracture orientation is generally near vertical.

When the Mohr's circle touches a shear strength line, τ_{fail}, a shear-type failure occurs. The shear failure begins with the formation of numerous micro-cracks, which can be followed by linking and propagation of the micro-cracks to form a gouge zone. The reduced tensile strength and increased permeability associated with the formation of micro-cracks is believed to sometimes cause the shear failure mode to change to a tensile failure mode.

Figure 1 indicates that the angle of internal friction is the slope of the failure criteria line. Deep unfractured rocks that are well cemented have a high cohesion (shear strength), c, and a high angle of internal friction, ϕ_{fric}, of about 30°. In this case, the shear strength and compressive strength increase rapidly as the confining stress is increased with increasing depth. Additionally, tensile strength is usually very low compared to the maximum effective stress, σ_{max}, and compressive strength, σ_{comp}. The tensile strength will be zero if natural fractures are already present. In well design, sediment tensile strength is usually assumed to be zero.

Marine sands near the surface containing little or no clay usually are cohesionless (c = 0) and have no tensile strength (σ_{ten} = 0). Failure of these sediments during an underground blowout can lead to formation liquefaction (fluidization) if the vertical pressure gradient due to flow of formation fluids in the sand reaches or exceeds the static effective vertical stress present prior to the underground blowout.

In the upper section of the SMS, marine clays not only have low cohesion and tensile strength, but also have a low angle of internal friction ($\phi \sim 6$ degrees). Shallow formations found in many areas of the Gulf of Mexico are predominantly marine clays. Shallow marine clays tend to behave plastically, making the effective matrix stress in the horizontal direction essentially equal to the vertical matrix stress. In shallow plastic formations, the sediment failure mechanism may not be a true hydraulic fracture. A shear stress failure followed by seepage and tunneling-type erosion is believed to be a possible mode of failure. Failure modes in which flow through the sediments occurs in pipe-like channels have been documented extensively in the geotechnical literature concerning failure of earthen dams. Exit holes in the seafloor consistent with these piping-type channels have also been observed by divers and remote cameras during underground blowouts.

2.2 Horizontal Stress - Stress Ratio - Elastic Behavior

Properties of the bottom section of the SMS approach those of deeper rocks which, when pressurized, fail by vertical fracturing. To initiate a vertical fracture, horizontal stress

concentrations present near the borehole wall must be exceeded. As the rock is removed by the bit action, more stress is added to the remaining rock around the wellbore. Hence the stress concentration is created. Additionally, mud is generally present in the well when sediment failure is initiated. Since permeable zones are always covered by a filter cake, the wellbore fluids do not easily penetrate the borehole walls as the pressure is increased above the pore pressure.

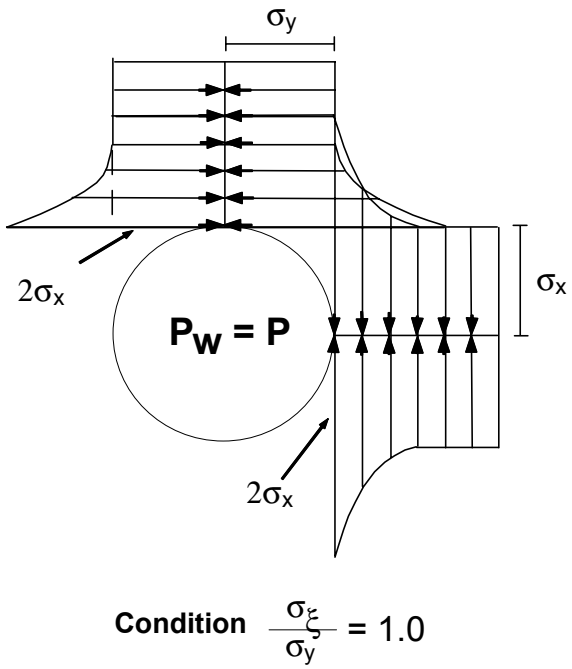

Figure 2. Stress concentration around elastic borehole.

Shown in Figure 2 is a plot of the horizontal stress as a function of distance from the wellbore wall for the case of uniform horizontal stress. This calculation was presented by Hubbert and Willis (1957) for the case of elastic rock behavior and a smooth and cylindrical borehole with axis parallel to a principal stress. Note that the stress concentration near the wellbore results in a horizontal effective stress twice that of the undisturbed (far-field) horizontal stress.

The principal stresses present at the borehole wall for a non-penetrating fluid, uniform horizontal stress, and elastic rock behavior are given by [Rocha, 1993]:

$$\sigma_{rw} = p_w - p \tag{3a}$$

$$\sigma_{\theta w} = 2\sigma_h + p - p_w \tag{3b}$$

$$\sigma_{zw} = \sigma_z \tag{3c}$$

Equation (3b) predicts that in order to initiate a vertical hydraulic fracture, the compressive hoop stress at the borehole wall, $\sigma_{\theta W}$, must be reduced to a tensile stress equal to

the tensile strength of the rock, σ_{ten}. This occurs if the wellbore pressure increases to the following fracture initiation pressure:

$$p_{init} = p + 2\sigma_h + \sigma_{ten} \tag{4}$$

However, once the hydraulic fracture propagates beyond the area near the borehole wall where the stress concentrations are present, the predicted fracture propagation pressure reduces to:

$$p_{frac} = p + \sigma_h + \sigma_{ten} \tag{5}$$

When natural fractures or fissures already exist in the rock, tensile strength can be neglected. Thus we have:

$$p_{frac} = p_{init} = p + \sigma_h \tag{6}$$

This situation is assumed to be true in many areas because of the following observations:

(1) Significant reductions in pumping pressure are seldom seen after fracture initiation during leak-off tests.
(2) Repeated leak-off tests seldom show a decrease in the observed leak-off pressure.

Ratio of horizontal to vertical stress

Before fracture pressure can be predicted from Equations (4) through (6), the effective horizontal stress must be estimated. For sediments between the surface casing depth and the total well depth, the most common approach has been to correlate the minimum observed ratio, F_σ, of horizontal-to-vertical effective stress with depth. Leak-off test data and incidents of lost-returns have been used to develop empirical correlations for various geographic areas. The correlations were heavily weighted to represent the weaker sediments found at a given depth so that a conservative estimate of fracture pressure could be predicted for use in well design calculations. Once F_σ is obtained from the empirical correlation, the fracture pressure can be estimated using:

$$p_{frac} = F_\sigma \, \sigma_z + p = F_\sigma (s - p) + p \tag{7a}$$

Several correlations are commonly used to estimate the horizontal-to-vertical effective stress ratio for the Louisiana Gulf Coast Area. In these correlations the stress ration value decreases for the shallower sediments and approaches a value of about 0.33 at the surface. As reported in Bourgoyne et al (1991), Hubert and Willis determined this value for unconsolidated sands in sandbox experiments conducted in the lab. At greater depths, the ratio F_σ approaches a value of one as the sediments become more plastic with the increasing confining stress. Extrapolating the empirical correlations to very shallow depths gives a low value of F_σ, and thus very low values for shallow fracture pressure are often predicted. Using the correlations for these sediments could result in using unrealistic formation breakdown pressures in the casing design calculations.

Shown in Figure 3 are F_σ values estimated from leak-off tests from five wells drilled in the Green Canyon area, offshore Louisiana. The values were calculated from Eq. (7a). Note that the average observed value of the horizontal-to-vertical effective stress ratio ranges from 0.8 to

1.4 and averages about 1. The observed values in excess of 1 are likely due to: experimental errors that occur while running and interpreting the leak-off tests; the presence of stress concentrations in and around the borehole; and the presence of non-zero tensile strengths in the sediments exposed during the test. Thus, the theory of vertical fracturing gives an unrealistic conclusion that vertical and horizontal stresses are equal.

Researchers (Rocha and Bourgoyne, 1994) also noticed that F_σ approaches unity for most SMS from the gulf coast area and concluded that fracture pressure in Eq. (7a) becomes equal to overburden pressure, or

$$p_{frac} = 1.0(s_{pob} - p) + p = s_{pob} \tag{7b}$$

If fracture pressure equals vertical stress, another explanation of the field LOT data is possible without using vertical fracturing theory. Assuming the fracture is horizontal so that the fracture initiation pressure equals vertical stress provides a much better explanation because, for a uniform horizontal stress field, no vertical stress concentration exists near the borehole. Thus there is no difference between fracture initiation pressure and fracture propagation pressure, which corresponds with field observations.

Weak interfaces at sediment bedding planes can help promote a horizontal fracture. Moreover, an irregularity in the borehole wall must be present before the mud pressure can apply a vertical component of force to open a horizontal fracture.

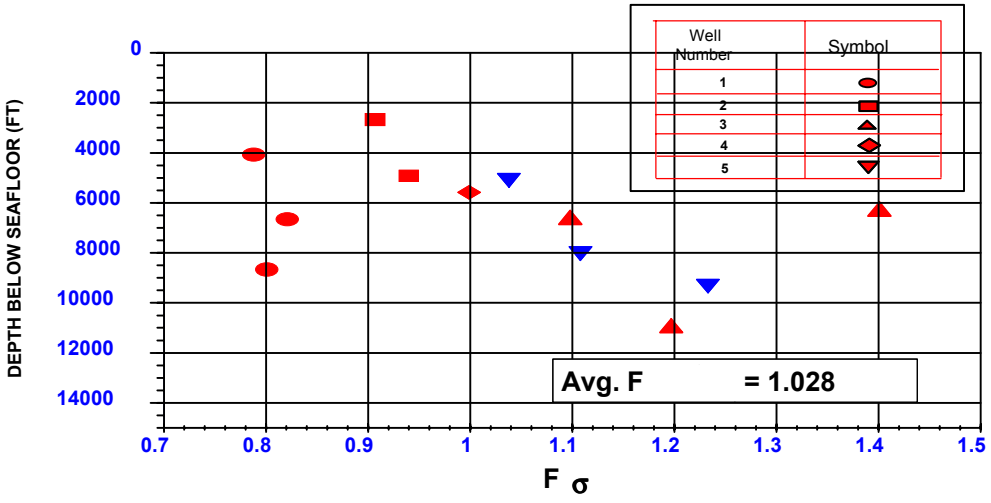

Figure 3. Ratio of horizontal to vertical effective stress determined from leak-off tests in the Green Canyon area, offshore Louisiana.

2.3 Overburden Stress in SMS

The overburden pressure is the most important parameter affecting fracture pressure. The overburden pressure, s, at a certain depth can be thought of as the pressure resulting from the total weight of the rock and pore fluids above that depth. Since bulk density, ρ_b , is a measure of the weight of rock and pore fluids, the overburden pressure at a certain depth can be easily calculated by integrating the bulk density vs. depth profile.

$$s = \int_0^{D_s} \rho_b g dD_s \tag{8}$$

One method for calculating overburden pressure is to sum up the average interval bulk density times interval height for all intervals above the depth of interest. For offshore sediments, hydrostatic pressure due to water depth must also be considered and Equation (8) becomes:

$$s = \int_0^{D_w} \rho_{sw} g dD_w + \int_0^{D_s} \rho_b g dD_s \tag{9}$$

The best source of bulk density data is from in situ measurements made with a gamma-gamma formation density log. Unfortunately such data is seldom available for depths less than the surface casing setting depth. The accuracy of the formation density logs can be poor in large diameter holes, and, hence, a pilot hole may be required to get good measurements in the shallow sediments. Logging-while-drilling (LWD) tools are now available that can measure formation density, but they also require hole diameters no greater than 14 in. Thus a pilot hole may be required to get accurate density measurements in the upper marine sediments.

Sonic travel times determined from well logs or calculated using seismic data can also be used to estimate the formation bulk density. However, Rocha (1993) found that there was a poor agreement between density values obtained with sonic and density logs in the upper marine sediments. The difficulty stems from uncertainty about the proper choice of matrix travel time values for shallow clay sediments.

Cuttings density data obtained while drilling is sometimes available in the shallow sediments. However, the bulk density of cuttings can be highly altered by the release of confining pressure and by exposure to the drilling fluid.

2.3.1 Overburden stress as a function of porosity

Because of the problems discussed above, detailed information on bulk density is often not available at shallow depths. Thus density at shallow depths must often be extrapolated from information obtained at deeper depths. This is typically done using porosity instead of bulk density.

Bulk density can be defined in terms of porosity, ϕ, and other variables using the following equation:

$$\rho_b = (1-\phi)\rho_{matrix} + \phi\rho_{fluid} \tag{10}$$

In this equation bulk density is primarily dependent on porosity since the other variables of grain matrix density and pore-fluid density usually do not have a wide range of values. Porosity often decreases exponentially with depth, and thus a plot of porosity vs. depth on semilog paper often yields a good straight-line trend. This exponential relationship can be described using the following equation.

$$\phi = \phi_0 e^{-KD} \tag{11}$$

The constants ϕ_0 , the surface porosity, and K, the porosity decline constant, are determined graphically or by the least-square fit method. Substituting Equation (11) into Equation (10) gives:

$$\rho_b = +(1-\phi_0 e^{-kD_s})\rho_{matrix} + \phi_0 e^{-kD_s}\rho_{fluid}$$

After substituting into Equation (9) and integrating,

$$s = \rho_{sw} g D_w + \rho_{matrix} g D_s - \frac{(\rho_{matrix} - \rho_{fluid}) g \phi_0}{K}(1 - e^{-KD_s}) \qquad (12)$$

Pseudo-overburden pressure, s_{pob} , can be calculated using Eq. (7b) and data from leak-off tests. The constants of surface porosity, ϕ_0 , and the porosity decline constant, K , are determined in order to get the best fit of the leak-off test data from Equation (12) for $s = s_{pob}$. Rocha (1993) determined values for ϕ_0 and K for several areas in the Gulf Coast and Brazil. These values are given in Table 1.

Table 1. Surface Porosity and Porosity Decline Constant

Area	ϕ_0	K
Green Canyon	0.77	0.000323
Main Pass	0.565	9.9E-08
Ewing Bank	0.685	0.000115
Mississippi Canyon	0.66	1.66E-04
Rio de Janeiro Area	0.67	1.79E-05

2.3.2 New Method for Overburden Stress Estimation in SMS

A set of new correlations have been developed in this project using bulk density data from shallow soil borings analyzed in the following chapter. The correlations are derived and presented in Appendix B.

2.4 Density and Shear Strength of SMS from Soil Borings

Geotechnical engineers routinely run a number of tests on soil borings to determine the load bearing capacity of the shallow sediments. The physical properties tested generally fall into one of three categories: weight/density measurements; Atterberg limits; and shear strength measurements.

Weight/density measurements include moisture content, wet unit weights, and dry unit weights. Atterberg limits tests measure both plastic and liquid limits of the soil. Shear strength measurements are done with miniature vane, Torvane, remote vane, Cone Penetrometer (CPT), and triaxial shear tests. Other tests of chemical properties, such as acid solubility, gas and hydrocarbon content, water salinity, and x-ray analysis, may also be used. Generally, chemical and x-ray tests are performed in the laboratory.

After the sample is retrieved at the surface but before it is extruded from the sample tube, miniature vane tests for shear strength are performed. The sample is then extruded from the sample tube and cut. Representative portions are carefully packaged, sealed, and sent to labs for further testing. The remainder of the sample is tested in the field. Normal field tests are the Atterberg limits tests, visual classifications, and various strength tests. Lab testing includes unconsolidated-undrained tests.

The hole from which the sample was taken can also be tested to obtain in situ values of shear strength, hydraulic fracture pressure, and temperature using specialized tools at the bottom of a drill string.

2.4.1 Geotechnical Tests

Atterberg limits tests

The Swedish scientist, Atterberg, proposed that a soil can exist in one of four possible states—solid, semisolid, plastic, and liquid—depending on the moisture content of the soil. The moisture content is defined as the weight of water per unit weight of matrix material. The higher the moisture content, the more fluid the soil becomes. The moisture content at the point of transition from the semisolid state to the plastic state is known as the plastic limit, and from the plastic state to the liquid state is known as the liquid limit. The plastic limit and liquid limit are known as the Atterberg limits and are quantitatively determined by a standardized method developed by Cassagrande (1932).

Liquid Limit

To determine the liquid limit, the soil is placed in a brass cup, and a groove is cut at the center of the soil pat with a standard grooving tool. Next, the cup is lifted and dropped (using a crank-operated cam) from a height of 0.3937 in (10 mm) onto a hard rubber base repeatedly until the soil flow fills 0.5 in. of the bottom of the groove. The test is repeated at least four times for the same soil at varying moisture contents that require from 15 to 35 blows to close the groove. The moisture content, in percent, and the corresponding number of blows are plotted on semilogarithmic graph paper to produce the flow curve. The flow curve is approximately a straight line. The moisture content corresponding to 25 blows is defined as the liquid limit. For moisture contents above this value, the soil is considered to have negligible cohesive strength and behave essentially as a liquid.

Plastic Limit

The plastic limit test is a simple test in which the soil mass is rolled by hand on a ground glass plate from an ellipse into a thread. The plastic limit is defined as the moisture content, in percent, at which the soil crumbles when rolled into a 1/8 in. (3.2 mm) diameter thread. For moisture contents below this value, the soil behaves more like a semisolid but still has a non-linear (concave downward) stress-strain relationship.

The liquidity index is the ratio of the difference between the in situ moisture content and the plastic limit to the difference between the liquid limit and plastic limit. If the liquidity index is greater than 1, the sediments can be transformed into a viscous form to flow like a liquid. A liquidity index greater than one implies the presence of sensitive clays and behavior somewhat similar to a drilling mud with a high gel strength. A liquidity index less than one implies some degree of consolidation, and a liquidity index less than zero implies over-consolidation. The liquidity index is zero when the soil is at the boundary between a plastic and a semi-solid.

Shear strength: Vane Test
Undrained shear strength, c_u, of very plastic cohesive soils may be obtained directly from vane tests. The shear vane usually consists of four thin, equal-sized steel plates welded to a steel torque rod. The vane is pushed into the soil and then torque is applied to rotate the vane at a uniform speed. The required torque is read from a torsion indicator. In conducting a field vane test, the vane is rotated at approximately 6 degrees per minute. The undrained cohesion, c_u, determined from the vane shear test is a function of clay type and the angular rotation of the vane.

Torvane
The Torvane is a hand-held device with a calibrated spring used to determine the undrained cohesion, c_u , for the tube specimens. This device can be used in both the field and the lab; it is pushed into the soil and then rotated until the soil fails. The undrained shear strength is read from a calibrated dial. *Miniature vane* is a smaller version of the Torvane. Miniature vane tests are done on the retrieved sample before being extruded from the sample tube.

Cone Penetrometer Test (CPT)
The penetrometer consists of a rod with a cone-shaped tip that is pushed into the soil at a standard rate while the required force is recorded. The test can be run in situ at the bottom of a drill string, and the data stored in a downhole memory unit. Data is downloaded from the penetrometer after the unit is retrieved by wire line.

Triaxial Shear Test
In this test, the soil sample [about 1.5 in (38.1 mm) in diameter and 3 in (76.2 mm) in length] is encased within a thin rubber membrane and placed inside a cylindrical chamber filled with water or glycerin. Pressure applied to the water or glycerin is transferred to the soil sample. The soil sample is then sheared with a vertical loading ram. Drainage in or out of the soil sample and pore pressure can also be measured.

Unconsolidated-Undrained Test
In unconsolidated-undrained tests, drainage from the soil specimen is not permitted either during the application of chamber pressure or during the shear failure of the specimen. Since drainage is not allowed at any stage, the test can be performed very quickly. The test is usually conducted on clay specimens because, in saturated cohesive soils, axial stress at failure is practically constant regardless of the chamber confining pressure.

Hydraulic fracture pressure
The hydraulic fracture test can be performed in situ using a wireline retrievable unit (Figure 4) similar to the cone penetrometer test unit. Soil samples are removed from the test hole with a 2.25-in. O.D. thin walled tube. The wall thickness of the tube is about one-sixteenth of an inch to minimize disturbance and lateral compression of the sediments. An extension rod pushes the sampler cylinder into the bottom of the hole and at the same time packs-off a portion of the annulus above the sampler and outside the extension rod. Fluid is injected into the packed-off annular cavity at a constant rate of about 0.5 gal/min while the injection pressure is recorded.

A record of the injection pressure versus time is stored in the unit and then downloaded after the unit is brought to the surface. The unit is pulled from the sediments using the drillpipe and, once free, can be retrieved by wireline.

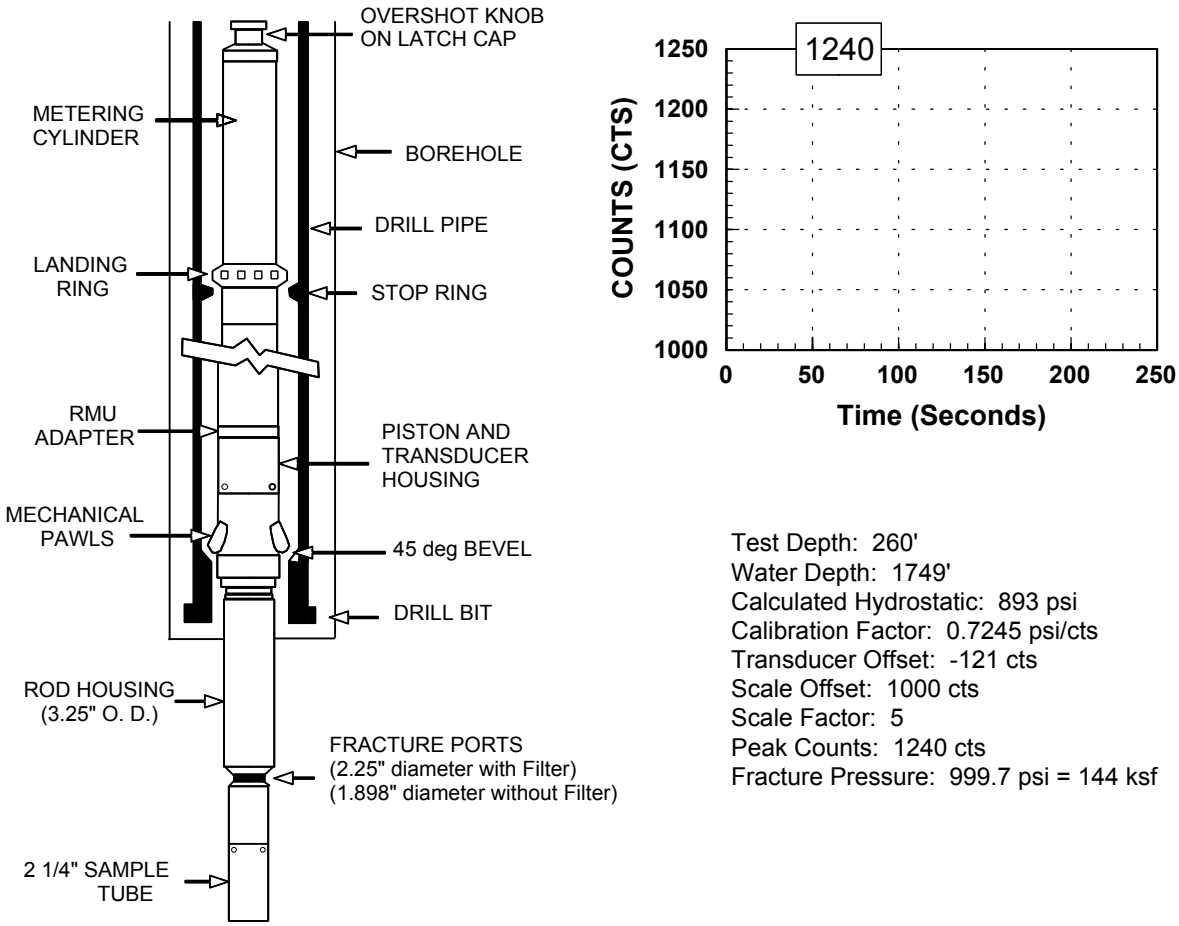

Figure 4. Schematic of wireline retrievable hydraulic fracture tool. (Courtesy of Fugro-McClelland Marine Geosciences, Inc.)

2.4.2 Bulk Density and Shear Strength Data

The most important parameter needed to estimate sediment failure during shallow gas well control operations is the formation bulk density change with depth. Shown in Figure 5 is a composite density versus depth profile for a prospect in the Green Canyon area. The lower portion of the profile (circles) was obtained from a formation density log run in a nearby well. The upper portion of the profile (triangles) was obtained from wet unit weight data collected from soil borings. Integration of this profile produced the overburden pressure versus depth curve shown in Figure 6.

Shown in Figure 7 are plots of moisture content, liquidity index, and shear strength versus depth. Also shown is a lithology description. These data show that the sediments penetrated by the soil borings are impermeable (only clay was found) and that the sediments are plastic. The clays are classified as very soft-to-soft, and the liquidity index dropped below zero only for a small interval near the bottom of the interval penetrated. This indicates the ratio of horizontal to vertical effective stress to be near 1.0 over the entire interval penetrated.

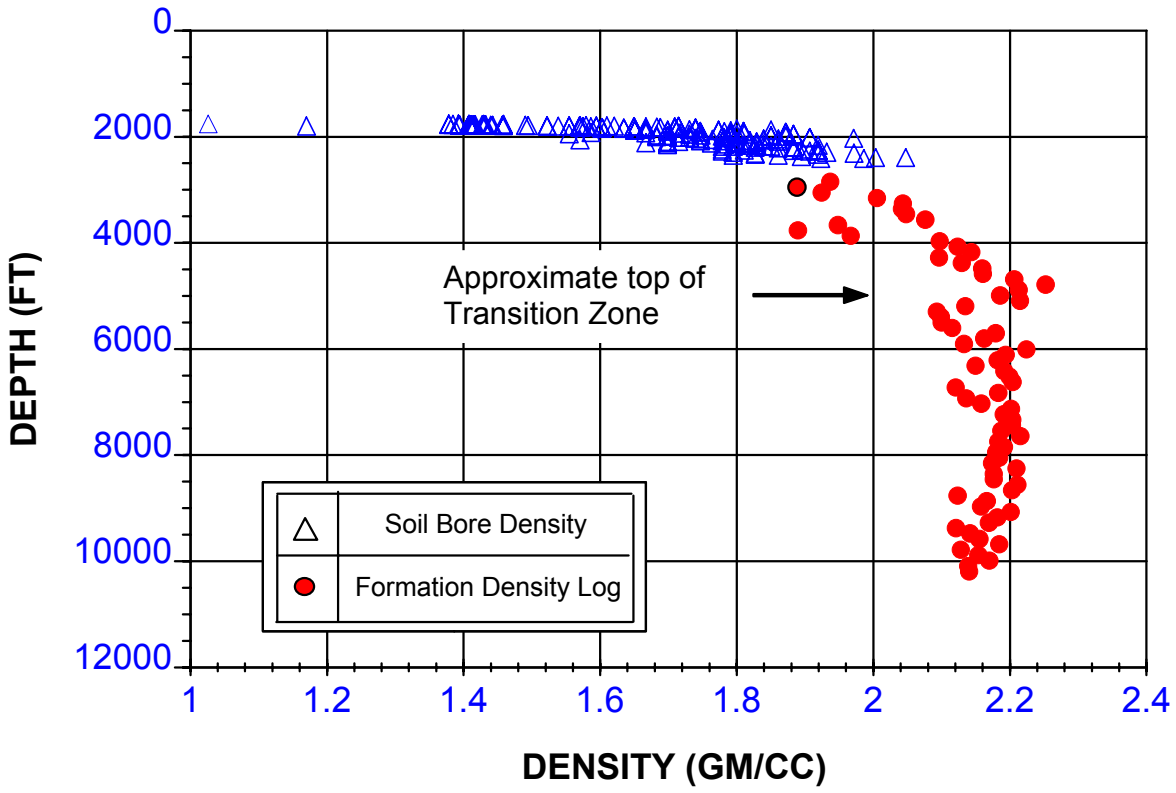

Figure 5. Sediment bulk density vs. depth in Green Canyon.

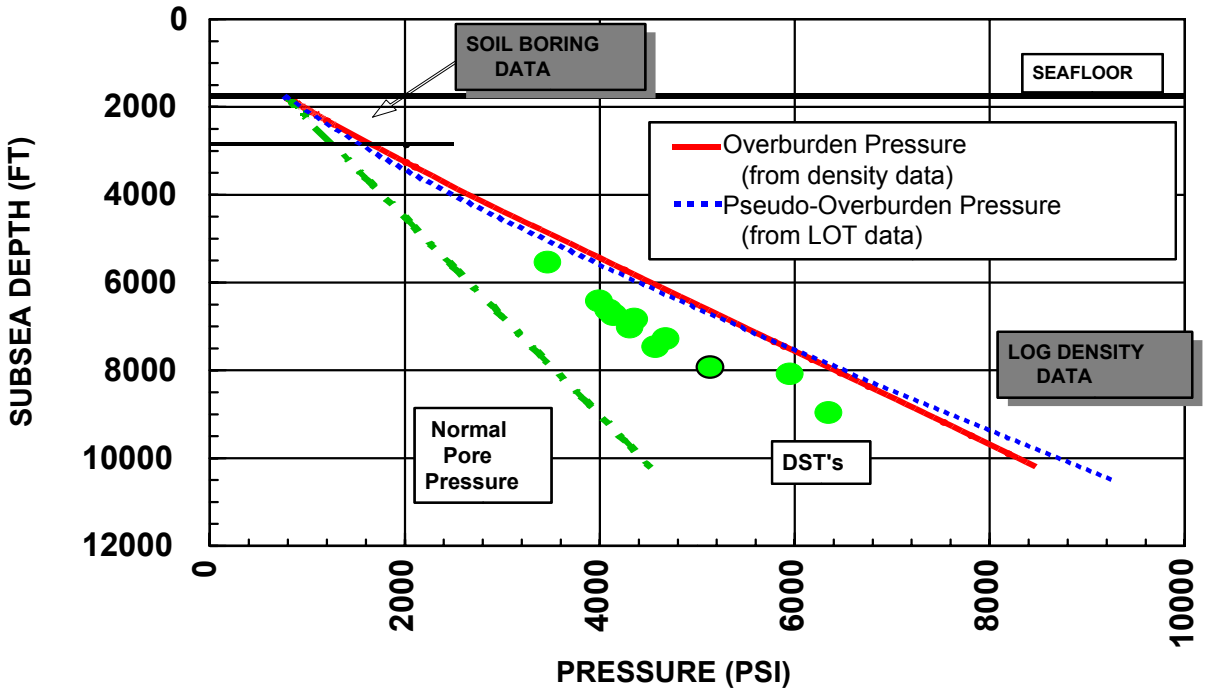

Figure 6. Overburden pressure and pore pressure versus depth in Green Canyon.

Measured shear strengths of the sediments reach values of about 25 psi near the bottom of the interval penetrated. Thus, a significant tensile strength would not be expected. Skempton's formula can be used as an empirical relation between shear strength and effective vertical stress for normally consolidated sediments. Skempton (1957) proposed the formula:

$$\frac{c_u}{\sigma_z} = 0.11 + 0.0037(LL - PL) \qquad (13)$$

which means that the ratio of shear strength to effective vertical stress is about 11%, with a minor correction for liquid limit and plastic limit. At the bottom of the penetrated interval, the effective vertical stress is 210 psi, the liquid limit is 61, and the plastic limit is 22. Using these values in Skempton's formula gives a value of 11.14% and predicts a shear strength of about 30 psi. Thus, Skempton's formula appears to be in reasonable agreement with the field data collected in the Green Canyon area. This formula can be used to estimate the shear strength of shallow sediments for normally consolidated sediments.

Shown in Figure 8 is a plot of the horizontal-to-vertical effective stress ratio, F_σ, calculated from fracture pressure measured by the in situ hydraulic fracture tool that was run when the soil borings were being taken. Note that all of these results show values near one or in excess of one. Since the tool examines such a small sample of sediment (only a few inches), it is much less likely to encounter major flaws in the exposed sediment. The results support our conclusion that fracturing pressure equals overburden stress.

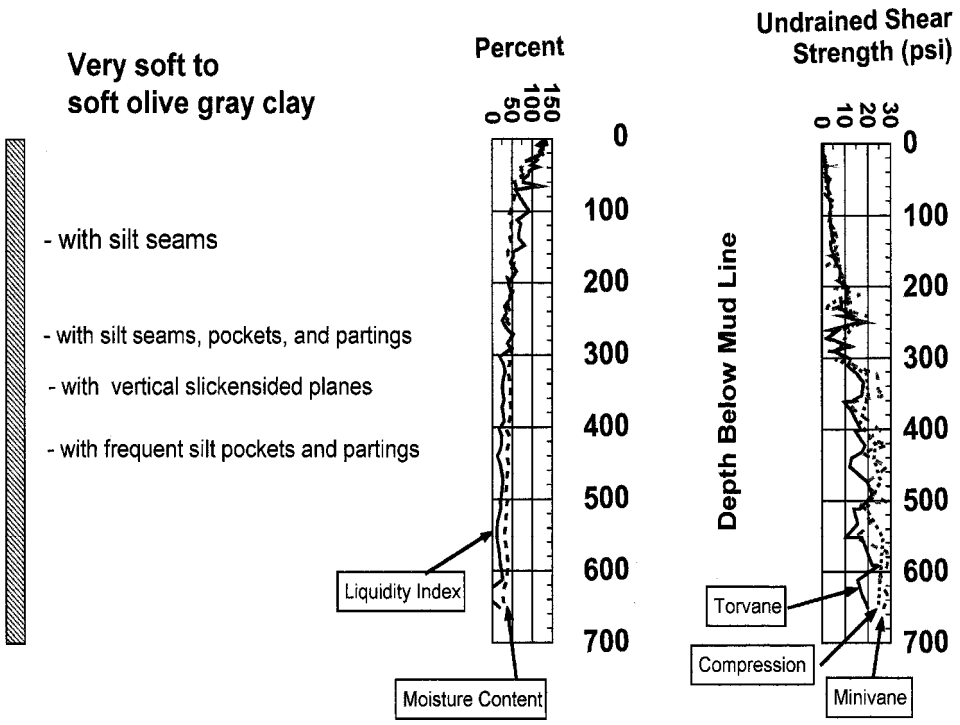

Figure 7. Geotechnical properties of SMS in Green Canyon.

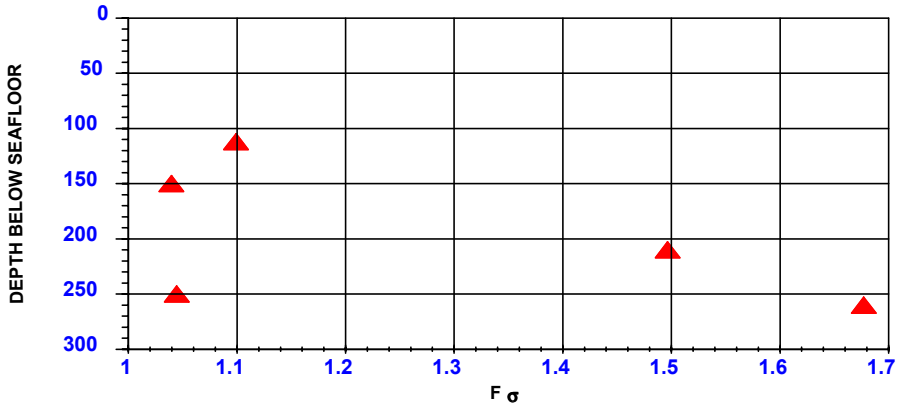

Figure 8. Calculated stress ratio from in situ hydraulic fracture tool data.

2.5 Rock Mechanics Properties of SMS from Soil Borings

Rock mechanics analysis of SMS concerns mechanical properties such as Young's modulus (E), Poisson's ratio (μ), cohesion strength (τ_0), friction angle (ϕ), and effective vertical stress (σ_v). Variability of these properties is a factor here because, unlike the strength of other materials, sediment strength varies not only with depth but also with location.

During the period 1982 through 1986, Conoco, Inc. conducted a geotechnical investigation of the Green Canyon region in the Gulf of Mexico. In our analysis, information from the Conoco data was used to derive mechanical properties of sediments. The borings were collected in upper marine sediments (less than 500 ft below sea floor for all places). Initially, the data was used to determine geotechnical properties, such as liquid limit, plastic limit, water content, unit wet weight, and shear strength, as explained above. Compression tests provided measurements of water content in percent, unit dry weight in lb/cu ft, shear strength in kips/sq ft, strain in percent, lateral pressure in kips/sq ft, and failure strain in percent. Locations of the

borings are shown in Figure 9. Water depth is from 1739 ft to 1767 ft. Also, the major soil strata were classified according to the tested data and tabulated as shown Table 2.

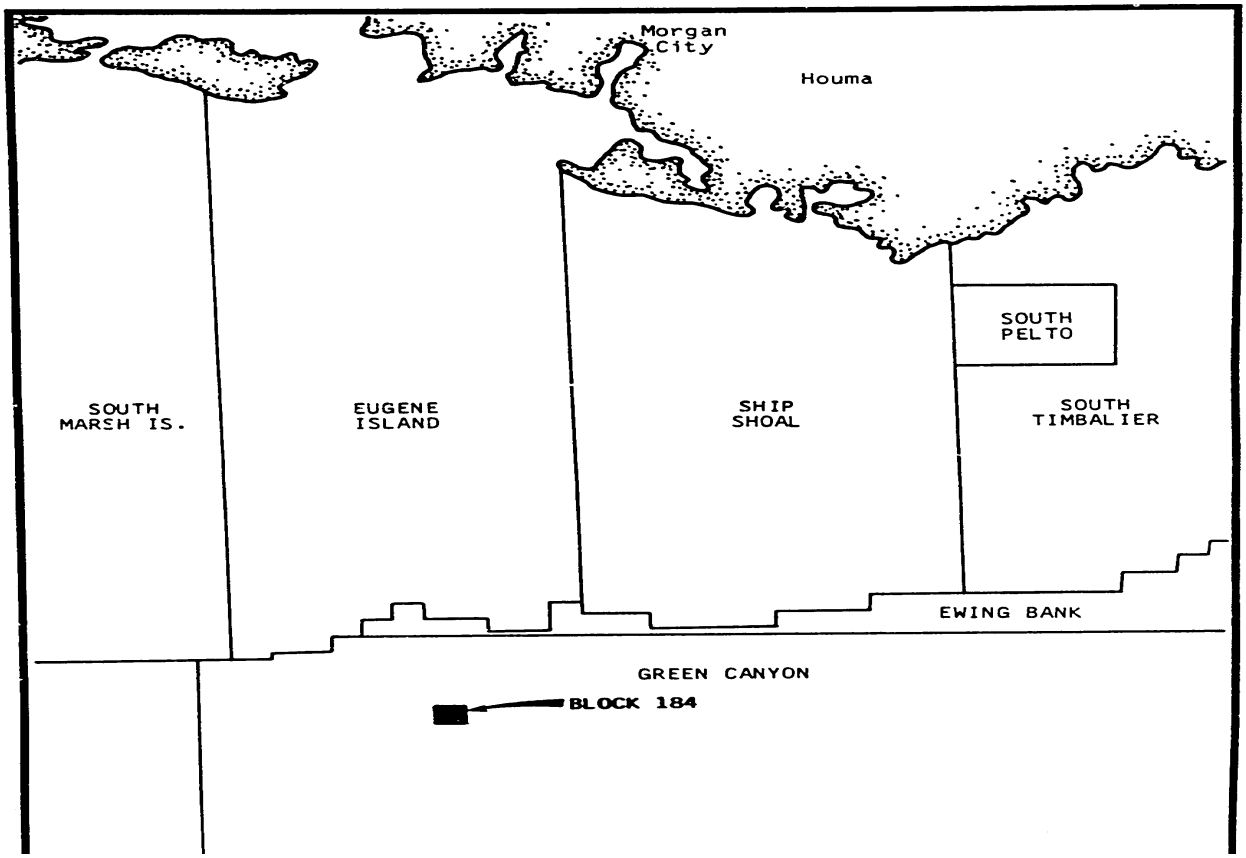

Figure 9. Borings location map (Block 184, Green Canyon in GOM).

Table 2. Main Sediment Strata in Green Canyon

Stratum	Penetration, ft		Description
	From	To	
I	0	50	Very soft to firm clay
II	51	58	Silty fine sand
III	58	124	Firm to stiff clay
IV	124	134	Silty fine sand to clayey fine sand
V	134	300+	Stiff to very stiff clay

The effective stress profile (Figure 10), calculated from the submerged unit weight and the depth, is the difference of overburden pressure and formation pore pressure. Overburden pressure was calculated from the wet boring density and seawater density in the region as:

$$p_{over} = \int_{o}^{D_w} g\,\rho_w\,dD + \int_{D_w}^{D} g\,\rho_b\,dD \qquad (14)$$

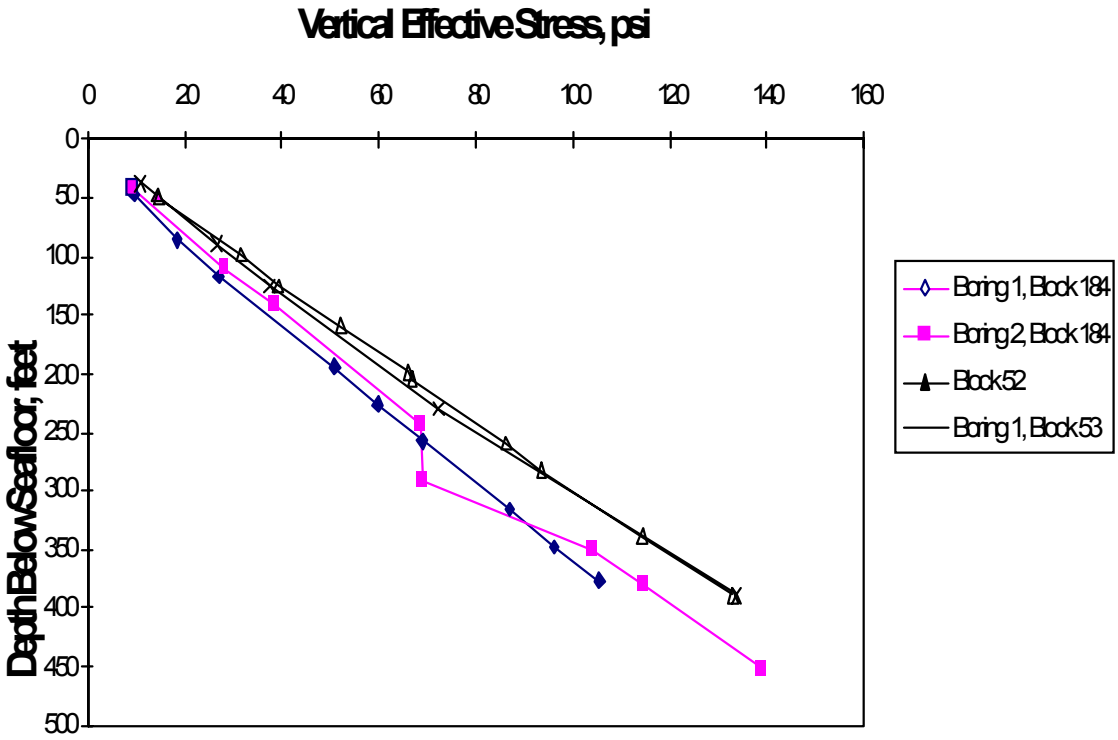

Figure 10. Vertical effective stress vs. depth below sea floor.

Poisson's Ratio μ is defined as the ratio of lateral strain to axial strain, and was calculated based on the confined compression test results as:

$$\mu = k/(1+k) \qquad (15)$$

where k is the confined-vertical stress ratio measured on the borings. The change of Poisson's ratio with depth is shown in Figure 11.

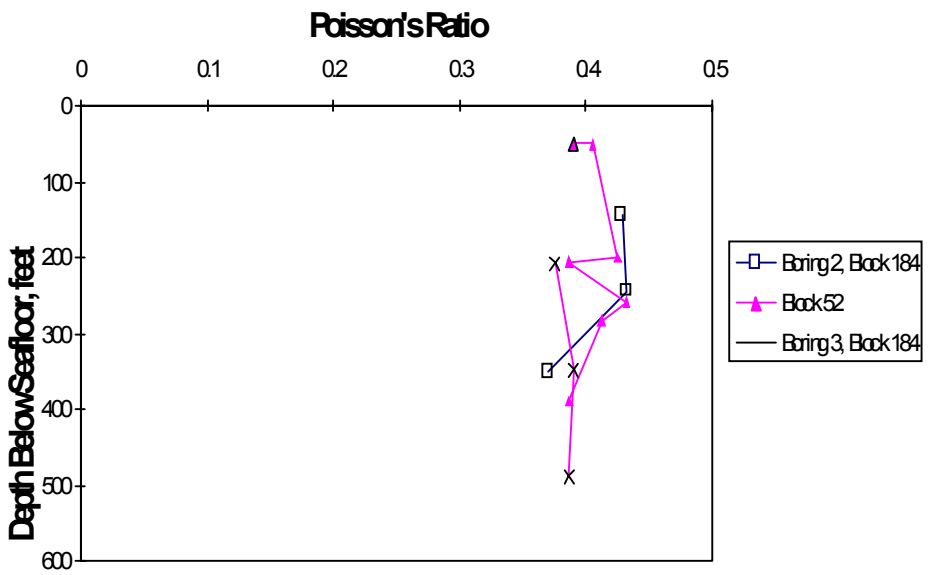

Figure 11. Poisson's ratio vs. depth below sea floor.

Young's Modulus, E, was determined from Equation 17 using the tested shear modulus G. Shear modulus is equal to one-third of the doubled slope of the consolidated undrained triaxial test plot according to its definition and units. Figure 12 is a plot of shear modulus with depth.

$$E = 2G(1+\mu) \tag{16}$$

Cohesion strength, τ_0, is defined as the shear strength when no friction exists and equals the tested unconsolidated undrained shear strength. Figure 13 gives the relation of cohesion strength and depth. Friction angle, ϕ, can be calculated from its definition as:

$$\phi = \arctan\frac{\tau - \tau_0}{\sigma_n} \tag{17}$$

where the numerator is the maximum shear stress and both the numerator and denominator can be read directly from the curve of maximum shear stress versus effective normal stress given by the tests. Figure 14 shows the friction angle change with depth.

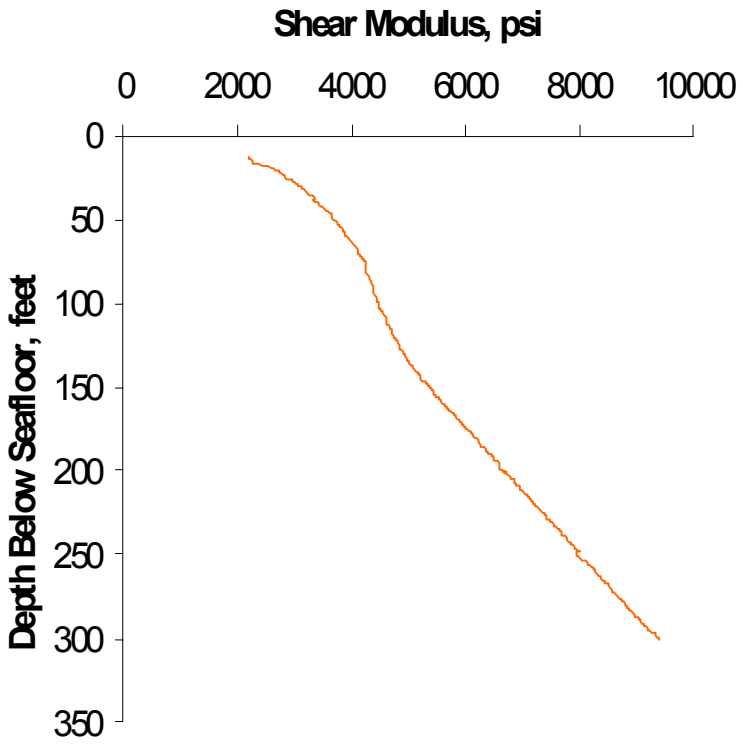

Figure 12. Friction angle change with depth.

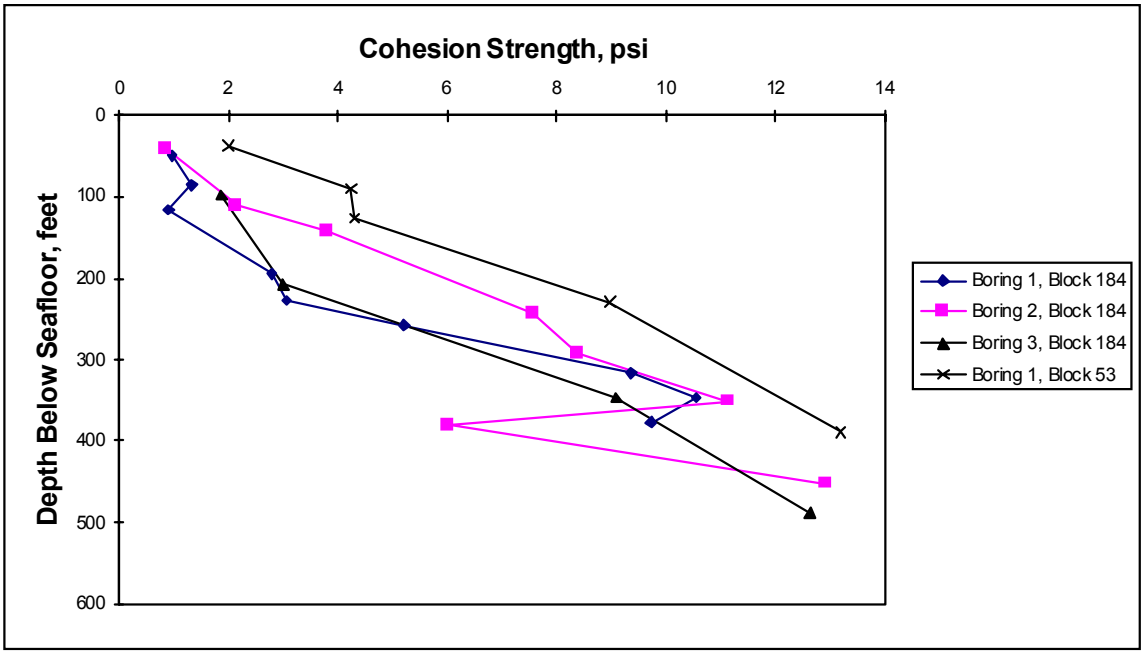

Figure 13. Cohesion strength vs. depth below sea floor.

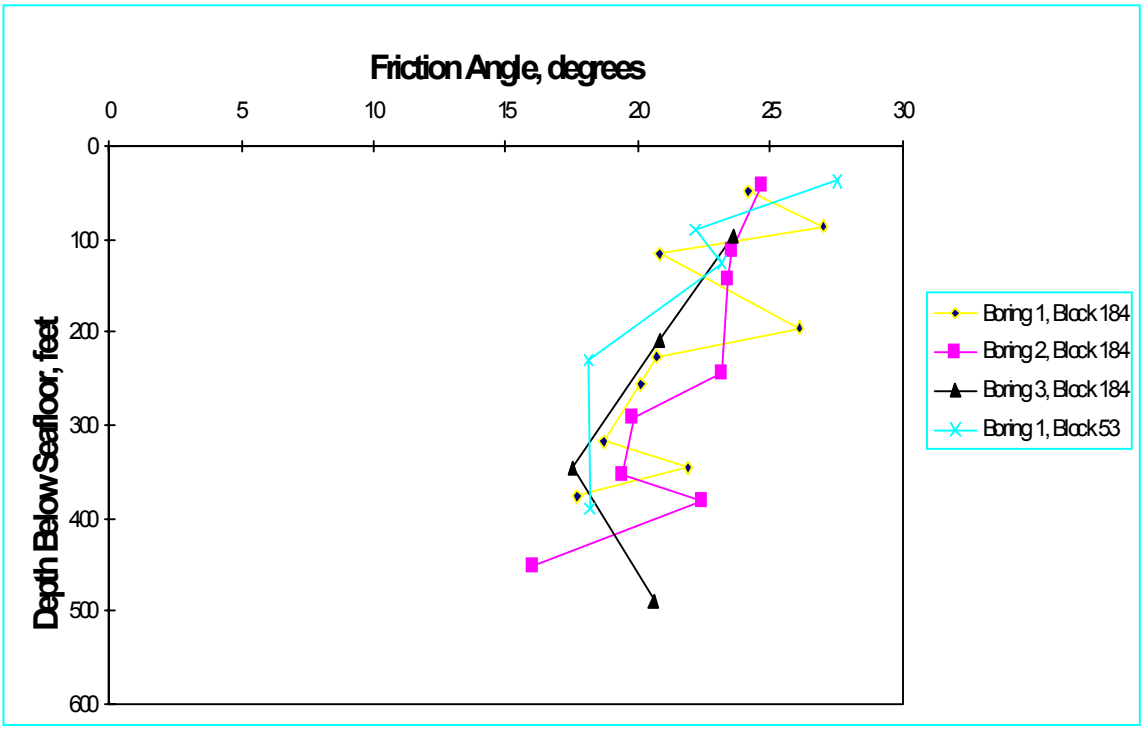

Figure 14. Friction angle vs. depth below sea floor.

2.6 In Situ Stress in SMS

In situ stresses are the bases for stress analysis underground. There are three principle stresses at any underground point. For normal fault sediments, the three in situ principle stresses are one vertical stress and two equal horizontal stresses. The in situ stress can be derived from the basic stress-strain model (D. Zhou, 2000).

2.6.1 In situ Elastic Stresses

As shown above, in situ vertical stress can be calculated from overburden pressure and formation pore pressure that may be estimated from well log information. For horizontal stress calculation, the stress ratio is used. Generally, the stress ratio is given by empirical correlations. Its theoretical formula based on the elastic theory is:

$$F_\sigma = \frac{\sigma_h}{\sigma_v} = \frac{\mu}{1-\mu} \tag{18}$$

However, since the above relation is based on elastic theory, it is not suitable for sediments in plastic state that typically show high in situ values of the stress ratio. To solve this problem, one may assume a 0.5 value of Poisson's ratio for upper marine sediments (UMS), which results in a hydrostatic state of stress. However, since by its definition Poisson's ratio is purely an elastic constant, it does not pertain to sediment in plastic state.

2.6.2 In Situ Plastic Stress Model

Shallow marine sediments are soft and ductile compared with deeper rocks. Also, some agree that "soft shales and unconsolidated sands frequently found in the Texas and Louisiana Gulf Coast can be considered to exist in a plastic state of stress" (Harrison et al., 1954), that "soft, clay-rich materials like shale often act as plastic" (Warpinski and Smith, 1989), or that "shallow marine sediment behaves plastic," (Rocha, 1993). Since there is no correlation of SMS properties with depth similar to those for deeper formations (below 3,000 ft), the problem is open to speculation.

For an elasto-plastic sediment that is continuous, isotropic, homogeneous, and obeys the linear Mohr-Coulomb criterion of perfectly plastic yield, stress ratio in plastic state is (D. Zhou, 2000):

$$F_\sigma = 1 - \frac{2(\sin\varphi + \frac{\tau_0}{\sigma_{zo}}\cos\varphi)}{1+\sin\varphi} \qquad (\sigma_{zo} \geq (\sigma_{zo})_{\lim}) \tag{19}$$

where:

$$(\sigma_{zo})_{\lim} = \frac{2(1-\mu)\tau_0 \cos\varphi}{1-2\mu-\sin\varphi} \tag{20}$$

Equation 20 indicates that plastic and elastic properties together control the stress ratio in SMS. Also, it can be shown that Equation 19 gives values of stress ratio different than one. The only situation when the ratio may reach unity is for frictionless sediment for which the Tresca's yield criterion applies and the stress ratio is:

$$F_\sigma = 1 - 2\tau_0 / \sigma_{zo} \qquad \text{for } \sigma_{zo} > 2\tau_0(1-\mu)/(1-2u) \tag{21}$$

Thus, when the SMS depth exceeds a few hundred feet and vertical stress becomes much greater than cohesive strength, the stress ratio approaches unity, and the state of stress becomes seemingly "hydrostatic" for a soft zone or small cohesive strength with a huge vertical stress, such as the case of very deep wells.

It should be emphasized that the derived in situ stress relations are valid only for sediments in geostatic state (that is, horizontal stress is induced only by overburden pressure). According to the derived formulas, whether or not sediments in UMS will turn into plasticity depends on their properties. Also, the wellbore wall in UMS is not necessarily always in plastic state nor is UMS in a deep well always necessarily in elastic state.

2.6.3 In situ Stresses of SMS in Green Canyon, GOM

The stress state and in situ stresses of the Green Canyon region can be determined from the above formulas by substituting the properties summarized in section 2.5.

From Figure 11, Poisson's ratio is 3.7 to 4.25 for the upper 500 ft of the sediments. The observed trend is a decrease with depth, and the average decrease is about 0.08/100 ft. Cohesive strength increases with depth, from 0.8 psi at 40 ft to 13 psi at 500 ft, at a rate of about 2.6

psi/100 ft (from Figure 13). The friction angle decreases with depth at an average rate of about 2.4 deg/100 ft, with a minimum value of 16 degrees around 450 ft and a maximum value of 27.5 degrees around 30 ft.

Substituting Poisson's ratio, cohesive strength, and friction angle into Eq. (20) leads to the conclusion that all sediments in this area down to 500 ft depth are in a plastic state of stress. The closer the sediments are to the sea floor, the more plastic they become. At a depth of around 450 ft, a sediment having the lowest value of internal friction is almost at the threshold between plastic and elastic states. It is reasonable to assume that sediments below 500 ft may reach elastic state according to the trends of Poisson's ratio and the friction angle and vertical stress shown in Figure 10.

3. SMS FAILURE MECHANISM AROUND OVERPRESSURED BOREHOLES

Two situations pertain to over-pressurized boreholes: shutting in a gas kick and leak-off testing. In the case of a gas kick, an operator of a bottom-supported marine rig may decide to shut in the well if sufficient casing has been set to keep any flow underground. Based upon knowledge of strength of sediments the operator would take a risk of over-pressurizing the borehole, which results in flow outside the well, hoping that the flow would result in an underground blowout rather than a breach to the sea bottom.

In the case of LOT, an operator deliberately pressurizes the borehole to find the strength of sediments at the casing shoe. For simplicity we will use the leak-off testing scenario for analysis of the borehole pressurization effects.

3.1 Stress Distribution Induced by Drilling - Plastic Zone

Base upon the analysis of SMS rock properties and the trends of Poisson's ratio and friction angle—performed in the previous section—we concluded that most SMS in the Gulf of Mexico should be in the elastic state of stress in situ. Although these sediments had been initially in elastic state, a plastic zone was formed due to drilling operations.

The elastic stress distribution around a hollow cylinder can be found in books on rock mechanics (Jaeger and Cook, 1976). When the cylindrical outer radius goes to infinite, the stress relations are

$$\sigma_r = \sigma_h - (\sigma_h - p_w)\frac{r_w^2}{r^2}$$

$$\sigma_\theta = \sigma_h + (\sigma_h - p_w)\frac{r_w^2}{r^2}$$

$$\sigma_z = \sigma_{z0} \qquad (22)$$

At the wall of the wellbore, $r=r_w$, the difference between the maximum and minimum stresses increases to maximum according to the stress distribution.

$$\sigma_{rw} = p_w$$
$$\sigma_{\theta w} = 2\sigma_h - p_w$$
$$\sigma_{zw} = \sigma_{z0} \qquad (23)$$

Equation 24 clearly indicates that at the wellbore wall the radial stress is equal to the effective wellbore pressure (overbalance) and the tangential stress is the difference between effective wellbore pressure and doubled value of far-away horizontal stress (stress concentration). (Interestingly, this value of stress concentration—widely accepted and addressed by many papers and books—is only a special case of a well with zero overbalance.) The principal stresses for the Mohr-Coulomb yield criterion can be written as (Jaeger and Cook, 1976):

$$\sigma_1 - N\sigma_3 = \sigma_0 \qquad (24)$$

where, $N = \dfrac{1+\sin\phi}{1-\sin\phi}$

$$\sigma_0 = \tau_0 \frac{2\cos\phi}{1-\sin\phi}$$

and, σ_0 is the uniaxial compressive strength of the sediment.

Under normal conditions, the radial stress σ_{rw} around a wellbore is the smallest stress (Eq. 22). By substituting the larger stress of $\sigma_{\theta w}$ and σ_{zw} into Eq. 23, the condition to form a plastic annulus around a wellbore is obtained. Shallow marine sediment has a lower friction angle and uniaxial compressive strength, which leads to the proof that a plastic annulus is usually formed around the wellbore for most shallow marine sediments.

If the tangential stress σ_θ is the largest stress, substituting the first two relations in Eq. 23 into Eq. 24 yields

$$p'_w = \frac{2\sigma_h - \sigma_0}{1+N} \qquad (25)$$

The condition for forming a plastic zone around a wellbore occurs when the pure wellbore pressure p_w is less than the critical value p'_w. Compared with the usual drilling case, Eq. 25 indicates a plastic zone around a wellbore will be formed for many kinds of sediments.

If the vertical stress is the largest stress, the critical value of the pure wellbore pressure is $p'_w = (\sigma_{z0} - \sigma_0)/N$. This condition also causes many sediments to change to plastic state around a wellbore.

The ratio of the horizontal to vertical stress at far-field (in situ stress ratio) is discussed by Bourgoyne et al. (1991). For sediment in elastic state, the relation is

$$F_\sigma = \frac{\sigma_h}{\sigma_z} = \frac{\mu}{1-\mu} \qquad (26)$$

The stresses at the plastic-elastic boundary are

$$\sigma_{rc} = \sigma_{rc}$$
$$\sigma_{\theta c} = \frac{2\mu}{1-\mu}\sigma_{z0} - \sigma_{rc}$$
$$\sigma_{zc} = \sigma_{z0} \qquad (27)$$

The condition of $\sigma_{\theta c} \geq \sigma_{zc}$ *is* $\sigma_{rc} \leq \frac{3\mu - 1}{1-\mu}\sigma_{z0}$. At the boundary, the maximum stress $\sigma_{\theta c}$ and the minimum stress σ_{rc} must satisfy Eq. 25. Therefore,

$$\mu \geq \frac{(1+N)\sigma_{z0} - \sigma_0}{(1+3N)\sigma_{z0} - \sigma_0} \qquad (28)$$

This formula gives the critical condition for $\sigma_{\theta c} \geq \sigma_{zc}$. In case Eq. 28 is not satisfied, σ_{zc} becomes the largest stress of the three principal stresses at the boundary.

Stress Distribution in Plastic Zone

The Mohr-Coulomb criterion (Eq. 24) must distinguish the minimum and maximum stresses. As stated in Section 3.1, the radial stress is the minimum stress around a wellbore, and either the tangential stress or the vertical stress may be the maximum stress, depending on the rock properties. Only the larger stress, either tangential or vertical, should be used in Eq. 25. The next section will discuss the stress distribution in a plastic zone for both tangential-radial and vertical-radial combinations.

3.1.1 Maximum Tangential Stress

When $\sigma_{\theta c} \geq \sigma_{zc}$, the method to derive stresses is similar to that for a plane problem. The equilibrium equation in elastic and plastic zones is

$$\frac{\partial \sigma_r}{\partial r} = \frac{\sigma_\theta - \sigma_r}{r} \qquad (29)$$

Substituting Eqs. 22 and 24 into Eq. 29 gives the radial and tangential stress distribution in the plastic zone

$$\sigma_r = (p_w + \frac{\sigma_0}{N-1})(\frac{r}{r_w})^{N-1} - \frac{\sigma_0}{N-1}$$
$$\sigma_\theta = N(p_w + \frac{\sigma_0}{N-1})(\frac{r}{r_w})^{N-1} - \frac{\sigma_0}{N-1} \qquad (30)$$

Vertical stress can be derived from Hooke's law by assuming only radial displacement. Vertical strain in far-field can also be obtained by assuming no horizontal strain. Combining the two relations together, we can obtain the vertical stress around a wellbore:

$$\sigma_z = \frac{E}{\lambda + G}\sigma_{z0} + \mu(\sigma_r + \sigma_\theta) \tag{31}$$

The radius of the boundary between plastic and elastic zones, r_c, can be derived from the continuity of the radial and tangential stresses at the boundary. In the region of elasticity, the stress distribution is (Jaeger and Cook, 1976):

$$\begin{aligned} \sigma_r &= A + \frac{B}{r^2} \\ \sigma_\theta &= A - \frac{B}{r^2} \end{aligned} \tag{32}$$

where A=σ_h for radial distance, r, approaching infinite where tangential and radial stresses become equal to in situ horizontal stress, σ_h. At the plastic-elastic boundary, the radial and tangential stresses should be continuous. Combining Eqs. 31 and 32 with Eq. 33, at $r=r_c$, we get

$$\begin{aligned} \sigma_h + \frac{B}{r_c} &= (p_w + \frac{\sigma_0}{N-1})(\frac{r_c}{r_w})^{N-1} - \frac{\sigma_0}{N-1} \\ \sigma_h - \frac{B}{r_c} &= N(p_w + \frac{\sigma_0}{N-1})(\frac{r_c}{r_w})^{N-1} - \frac{\sigma_0}{N-1} \end{aligned} \tag{33}$$

Solving Eq. 34, the radius between elastic and plastic zones is

$$\begin{aligned} r_c &= r_w \left(\frac{\frac{N-1}{N+1}(2\sigma_h - \sigma_0) + \sigma_0}{(N-1)p_w + \sigma_0} \right)^{1/N-1} \\ B &= \left(\frac{((N-1)p_w + \sigma_0)\left(\frac{r_c}{r_a}\right)^{N-1} - \sigma_0}{N-1} - \sigma_h \right) r_c^2 \end{aligned} \tag{34}$$

3.1.2 Maximum Vertical Stress

For the case of $\sigma_{\theta c} < \sigma_{zc}$, the two principal stresses used in the Mohr-Coulomb criterion should be the radial stress and the vertical stress. The stress relations under this condition can be derived as above, but the vertical stress will be used instead of the tangential stress (Rinses et al., 1982;

Jaeger and Cook, 1976). Vertical stress decreases in the plastic boundary. Tangential stress increases in the plastic region first and then decreases, unlike its behavior in the elastic condition. The radius at which the tangential stress begins to decrease is expressed as r_b , which is given by Rinses et al. (1982).

Each stress has different forms besides the r_b. The correlation is:

For $r_w < r < r_b$,:

$$\sigma_r = (p_w + \frac{\sigma_0}{N-1})(\frac{r}{r_w})^{N-1} - \frac{\sigma_0}{N-1}$$

$$\sigma_\theta = N(p_w + \frac{\sigma_0}{N-1})(\frac{r}{r_w})^{N-1} - \frac{\sigma_0}{N-1}$$

$$\sigma_z = N(p_w + \frac{\sigma_0}{N-1})(\frac{r}{r_w})^{N-1} - \frac{\sigma_0}{N-1}$$

(35)

For $r_b < r < r_c$:

$$\sigma_r = p_w\left(\frac{r}{r_w}\right)^{N-1} + \frac{\sigma_o}{N-1}\left[\left(\frac{\gamma+N}{2\gamma}\right)\left(\frac{r_b}{r_w}\right)^{N-1} - \frac{\gamma+1}{2\gamma}\right]\left(\frac{r}{r_b}\right)^{y-1}$$

$$+\frac{\sigma_0}{N-1}\left[\left(\frac{\gamma-N}{2\gamma}\right)\left(\frac{r_b}{r_w}\right)^{N-1} - \frac{\gamma-1}{2\gamma}\right]\left(\frac{r}{r_b}\right)^{-y-1}$$

$$-\frac{1}{N-2\mu}\left[\sigma_0 - \frac{(1+\mu)(1-2\mu)}{1-\mu}\sigma_{z0}\right]\left[1-\left(\frac{\gamma+1}{2\gamma}\right)\left(\frac{r}{r_b}\right)^{\gamma-1} - \left(\frac{\gamma-1}{2\gamma}\right)\left(\frac{r}{r_b}\right)^{-\gamma-1}\right]$$

$$\sigma_\theta = p_w\left(\frac{r}{r_w}\right)^{N-1} + \frac{\sigma_o}{N-1}\left[\left(\frac{\gamma+N}{2}\right)\left(\frac{r_b}{r_w}\right)^{N-1} - \frac{\gamma+1}{2}\right]\left(\frac{r}{r_b}\right)^{y-1}$$

$$-\frac{\sigma_0}{N-1}\left[\left(\frac{\gamma-N}{2}\right)\left(\frac{r_b}{r_w}\right)^{N-1} - \frac{\gamma-1}{2}\right]\left(\frac{r}{r_b}\right)^{-y-1}$$

$$-\frac{1}{N-2\mu}\left[\sigma_0 - \frac{(1+\mu)(1-2\mu)}{1-\mu}\sigma_{z0}\right]\left[1-\left(\frac{\gamma+1}{2}\right)\left(\frac{r}{r_b}\right)^{\gamma-1} + \left(\frac{\gamma-1}{2}\right)\left(\frac{r}{r_b}\right)^{-\gamma-1}\right]$$

$$\sigma_z = p_w\left(\frac{r}{r_w}\right)^{N-1} + \sigma_0 - \frac{N\sigma_0}{N-1}\left[\left(\frac{\gamma+N}{2\gamma}\right)\left(\frac{r_b}{r_w}\right)^{N-1} - \frac{\gamma+1}{2\gamma}\right]\left(\frac{r}{r_b}\right)^{y-1}$$
$$-\frac{N\sigma_0}{N-1}\left[\left(\frac{\gamma-N}{2\gamma}\right)\left(\frac{r_b}{r_w}\right)^{N-1} - \frac{\gamma-1}{2\gamma}\right]\left(\frac{r}{r_b}\right)^{-y-1} \tag{36}$$
$$-\frac{N}{N-2\mu}\left[\sigma_0 - \frac{(1+\mu)(1-2\mu)}{1-\mu}\sigma_{z0}\right]\left[1-\left(\frac{\gamma+1}{2\gamma}\right)\left(\frac{r}{r_b}\right)^{\gamma-1} + \left(\frac{\gamma-1}{2\gamma}\right)\left(\frac{r}{r_b}\right)^{-\gamma-1}\right]$$

At the wellbore wall the stresses are

$$\begin{aligned}\sigma_r &= p_w \\ \sigma_\theta &= Np_w + \sigma_0 \\ \sigma_z &= Np_w + \sigma_0\end{aligned} \tag{37}$$

Comparing the plastic wellbore with wellbore stresses for the elastic well (Eq. 23), radial stress remains the same, but the tangential stress and vertical stress become much smaller for the plastic wellbore. The tangential and vertical stresses at the plastic wellbore are determined by the rock's uniaxial compressive strength and pressure overbalance and are no longer dependent on in situ stresses.

3.2 Vertical Fracturing of SMS at Pressurized Wellbore

As the wellbore becomes pressurized, radial (minimum) stress increases. Initially, in the plastic zone, the left side value of Eq. 24 equals that on the right side. This balance will be broken if the minimum (radial) stress increases. As the increase in wellbore pressure increases the radial stress and decreases the tangential stress, the left hand value of Eq. 24 becomes smaller than the right-side value. Therefore, further deformation of sediment in the plastic zone around the wellbore could only be the elastic one. Hence, the whole deformation process around the wellbore includes transformation from elastic state before drilling to plastic state after drilling, and then retransformation to the elastic state by well pressurization. Moreover, the sediment may return to the plastic state again when the leak-off pressure increases much higher.

Since this process includes plastic deformation, linear superposition of the elastic theory is not valid. Instead, the resultant stress depends on the loading history (Chen and Han, 1988). In our research, two steps were considered to simulate this process: The first step is the formation of a plastic zone due drilling; the second step is stress re-distribution resulting from pressurization. In the first step, stress distribution in the plastic zone is described by Eqs. 35 and 36. During well pressurization, this plastic zone will transform to elastic deformation, as stated above. As shown in Eq. 22, when the effective wellbore pressure p_w increases to $p_{wlot} = p_w + \Delta p_w$, the stress relation becomes:

$$\sigma_r + \Delta\sigma_r = \sigma_h - (\sigma_h - p_w - \Delta p_w)\frac{r_w^2}{r^2}$$

$$\sigma_\theta + \Delta\sigma_\theta = \sigma_h + (\sigma_h - p_w - \Delta p_w)\frac{r_w^2}{r^2}$$

$$\sigma_z + \Delta\sigma_z = \sigma_{z0} \tag{38}$$

Subtracting Eq. 23 from Eq. 39 gives the stress increase due to the wellbore pressure change Δp_w

$$\Delta\sigma_r = \Delta p_w \frac{r_w^2}{r^2}$$

$$\Delta\sigma_\theta = -\Delta p_w \frac{r_w^2}{r^2}$$

$$\Delta\sigma_z = 0 \tag{39}$$

The resultant stresses around the wellbore are calculated by superimposing the existing stresses before pressurization and the new incremental stresses. Stress in the plastic zone depends on the largest principle stress, tangential or vertical, as discussed above. To make things simple, we used stress distribution for the maximum tangential stress situation. This approach eliminates the complex math calculation of Eq. 36 since we are only interested in the stress around the wellbore. Combining Eq. 30 and Eq. 39 yields the stress distribution during the pressurization.

$$\sigma_r = (p_w + \frac{\sigma_0}{N-1})(\frac{r}{r_w})^{N-1} - \frac{\sigma_0}{N-1} + \Delta p_w \frac{r_w^2}{r^2}$$

$$\sigma_\theta = N(p_w + \frac{\sigma_0}{N-1})(\frac{r}{r_w})^{N-1} - \frac{\sigma_0}{N-1} - \Delta p_w \frac{r_w^2}{r^2}$$

$$\sigma_z = \frac{E}{\lambda + G}\sigma_{z0} + \mu(\sigma_r + \sigma_\theta) \tag{40}$$

According to these formulas, the vertical stress is not changed by the pressurization. However, after a fracture is formed that is large enough to allow gas/fluid migration, the vertical stress will affect the fracture propagation process.

If a wellbore was initially in the elastic state, and the well pressure decreased below a critical value, $p_w < p'_w$, the wellbore wall would fail, resulting in the formation of a plastic zone. An expression for critical pressure is derived by writing Eq. 22 for the wellbore wall and substituting the larger of the two stresses at the wall, $\sigma_{\theta w}$ or σ_{zw}, into the Mohr-Coulomb yield criterion in Eq. 24, which is summarized below.

The critical condition for a wellbore in elastic state due to a drilling operation is

$$p_w \geq p'_w \tag{41}$$

where

$$p'_w = \frac{2\sigma_h - \sigma_0}{1+N} \tag{25}$$

for $\sigma_{\theta w} > \sigma_{zw}$

or $$p_w < \frac{3\mu - 1}{\mu}\sigma_h$$

and

$$p'_w = (\sigma_{z0} - \sigma_0)/N \tag{42}$$

for $\sigma_{\theta w} < \sigma_{zw}$

or $$p_w > \frac{3\mu - 1}{\mu}\sigma_h .$$

Wellbore wall fracture occurs when its stress turns into tensile stress and exceeds its tensile strength. In the following section we will examine fracturing conditions for elastic and plastic wellbores, respectively.

3.2.1 Vertical Fracture at Elastic Wellbore

As wellbore pressure increases, the radial stress around the wall increases and tangential stress decreases, as indicated by Eq. 39, for elastic deformation. The tangential stress may be reduced by tensile stress as the wellbore pressure increases to some value (fracture pressure). The fracture direction is perpendicular to the tangential stress, and thus is vertical, which explains why the wellbore fracture is in the vertical direction. Combining the stress change (Eq. 39) after the leak-off test with the stress (Eq. 22) prior to the test (due to the drilling operation) for the elastic situation yields

$$\sigma_r = \sigma_h - (\sigma_h - p_w)\frac{r_w^2}{r^2} + \Delta p_w \frac{r_w^2}{r^2}$$

$$\sigma_\theta = \sigma_h + (\sigma_h - p_w)\frac{r_w^2}{r^2} - \Delta p_w \frac{r_w^2}{r^2} \tag{43}$$

As the minimum value of tangential stress is at the wellbore wall, the fracture occurs at the wall. At the wellbore wall, $r = r_w$, and Eq. 43 reduces to

$$\begin{aligned} \sigma_{rw} &= p_w + \Delta p_w \\ \sigma_{\theta w} &= 2\sigma_h - p_w - \Delta p_w \end{aligned} \tag{44}$$

Eq. 43 describes the stress distribution during the leak-off test (pressurization), but Eq. 23 is the distribution before the leak-off test, although both are correct for elastic deformation. Of the two formulas, Eq. 23 is typically used in fracturing theory. However, strictly speaking, Eq. 43 is the more accurate for the conditions under study.

Fracturing occurs when tensile stress overcomes tensile strength. That is, tangential stress becomes negative (tensile stress) and less than the tensile strength (S_{ten}): $\sigma_\theta < -S_{ten}$. Substituting this critical condition into Eq. 44 gives the pressure increase (pressurization) needed to initialize a vertical fracture.

$$\Delta p_w > 2\sigma_h + S_{ten} - p_w \tag{45}$$

When pressure overbalance p_w and tensile strength S_{ten} are zero, a well-known condition of double-stress concentration at the wellbore is created.

3.2.2 Vertical Fracture at Plastic Wellbore

Eq. 40 describes stress distribution for a wellbore with a plastic zone. The tangential stress rapidly decreases as well pressure increases. For a long openhole section, vertical stress remains constant during the pressurization. Thus, in Eq. 40, the only two other stresses at the wall that change are

$$\begin{aligned} \sigma_r &= p_w + \Delta p_w \\ \sigma_\theta &= N p_w + \sigma_0 - \Delta p_w \end{aligned} \tag{46}$$

As we know, vertical fracture occurs as the tangential stress becomes less than the tensile strength, $\sigma_\theta < -S_{ten}$. Eq. 46 can give the impression that a vertical fracture may be initialized for a large increase of Δp_w. However, the difference between radial and tangential stresses also increases and may meet the plastic failure criterion before tangential stress reduces to satisfy the fracture criterion.

When the radial and tangential stresses meet the Mohr-Coulomb yield criterion (Eq. 24) during the pressurization, the tangential stress is reduced to initial wellbore pressure, $\sigma_\theta = p_w$. The radial stress is $Np_w+\sigma_0$ at the plastic boundary. As a result, the plastic zone will expand with increasing wellbore pressure. We call this condition of the newly-formed plastic zone a *re-plastic-state condition* since the wellbore was initially in plastic state before the pressurization. The wellbore pressure required for the appearance of re-plastic state is

$$p_w + \Delta p_w = N p_w + \sigma_0 \tag{47}$$

Eq. 47 has been derived by substituting $\sigma_r = \sigma_1$ and $\sigma_\theta = \sigma_3$ into Eq. 24, which gives: $\Delta p_w = (N-1)p_w + \sigma_0$.

After re-plastic transformation, tangential compressive stress at (and close to) the wall starts to increase with increasing wellbore pressure, according to Eq. 24. Analysis of the condition, $\sigma_\theta = p_w$, shows that wellbores in SMS cannot be in tension during the pressurization unless the initial well pressure, p_w, was negative. *Therefore, we conclude that except for underbalance drilling, wellbore pressurization cannot induce vertical fractures in wells that have been in plastic state of stress prior to the pressurization, which is the case for SMS.*

Similar reasoning can be applied to the SMS wellbore in elastic state prior to pressurization, i.e., when $p_w > p'_w$. An increase of well pressure to the critical value, p_w'', would induce plastic yield in the initially elastic wellbore. Also, tangential stress at the wall would reduce to $\sigma_\theta = p'_w$ when $\sigma_r = p''_w$. (Further increase of well pressure would result in the increasing tangential stress.) The critical pressure, p''_w, is determined from combining Eqs. 22, 24, and 39, as

$$p''_w = \frac{2N\sigma_h + \sigma_0}{1+N} \tag{48a}$$

for $\sigma_{\theta w} > \sigma_{zw}$; or, $p_w < \frac{3\mu - 1}{\mu}\sigma_h$

$$p''_w = 2\sigma_h - \frac{\sigma_{z0} - \sigma_0}{N} \tag{48b}$$

for $\sigma_{\theta w} < \sigma_{zw}$; or, $p_w > \frac{3\mu - 1}{\mu}\sigma_h$

Since the minimum value of tangential stress is p'_w, an initiation of vertical fracture requires that $p'_w < 0$. It follows from Eq. 25 that $p'_w < 0$ only if $2\sigma_h < \sigma_0$ or $\sigma_{z0} < \sigma_0$. However, the values of $2\sigma_h$ and σ_{z0} are generally greater than σ_0 below the depth of two hundred feet in SMS due to the sediment's low strength. *Hence, unlike for deep wells, an SMS well cannot be fractured vertically even if its wall was in elastic state of stress before pressurization.*

3.2.3 Verification with Finite Element Method

Results from the analytical study, presented above, have been validated using the finite element method and the software ABAQUS (D. Zhou, 2000). Unlike the analytical model that considers a long section of open hole, the finite element method allows modeling complex geometry of the borehole at the casing shoe.

As discussed above, the sediment deformation process at the wellbore has some relation with plasticity. Plastic deformation depends not only upon plastic strains but also upon loading

history. The actual stress is not a simple addition of the stresses before or during the leak-off test. Modeling plastic deformation was performed in two steps. The first step involved calculating stresses around the wellbore before well pressurization (leak-off test). The second step was a stress-displacement analysis under borehole pressure while the wellbore is in a pre-stressed state.

Three cases were modeled:

Case 1: Elastic wellbore

If the rock in the chosen area is in elastic state before pressurization, it is called an elastic wellbore. Most deep wells should be in this kind of state. Sediment properties used in this study are: Young's modulus (1.04×10^5 psi); Poisson's ratio (0.25); cohesive strength (94.8 psi); and the angle of internal friction (25.4 degrees). Plastic flow is assumed as non-dilatant.

Case 2: Plastic wellbore

The plastic wellbore indicated here is an annulus around the wellbore in plastic state, but the farther part outside the plastic annulus is still in elastic state before pressurization. The sediment properties are: Young's modulus (1.04×10^5 psi); Poisson's ratio (0.3); cohesive strength (31.6 psi); the angle of internal friction (25.4 degrees); and non-dilatant flow.

Case 3: Plastic sediment

This case considers a situation in which sediment around the well is in a plastic state of stress before the wellbore becomes pressurized. The objective of this study is to find out what would happen to the sediment under the action of wellbore pressurization. The properties of this sediment are: Young's modulus (1.04×10^5 psi); Poisson's ratio (0.25); cohesive strength (40.1 psi); the angle of internal friction (12.5 degrees); and non-dilalant flow.

To make the distribution of stress easily understood, some special lines were chosen. As shown in Figure 15, lines 1 through 4 are horizontal and used to describe radial distribution at different depths, while line 5 represents the contact surface between cement and rock and vertical distribution stresses along the wellbore.

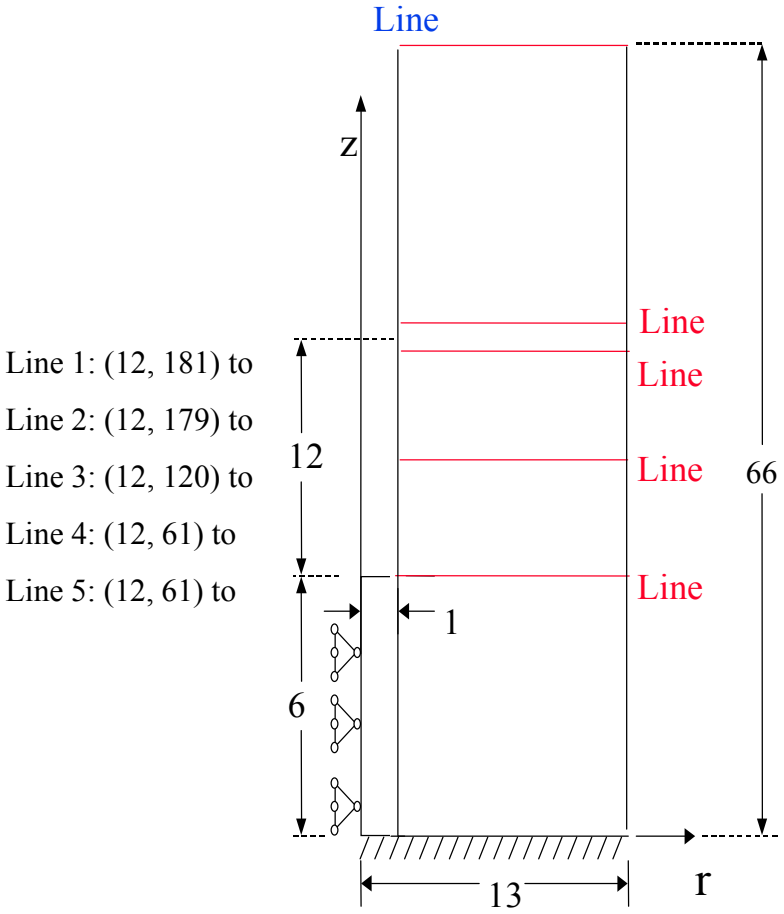

Figure 15. Characteristic locations in finite element analysis.

Finite element results are stored in finite element output files. For our plastic analysis, stress, strain, and displacements are available for every node and at any time. Most results are presented in the plots in Appendix A. They are only a very small part of our finite element outputs. Also, Figure 16 shows an example of the finite element analysis model of the pressurized borehole in Case 2.

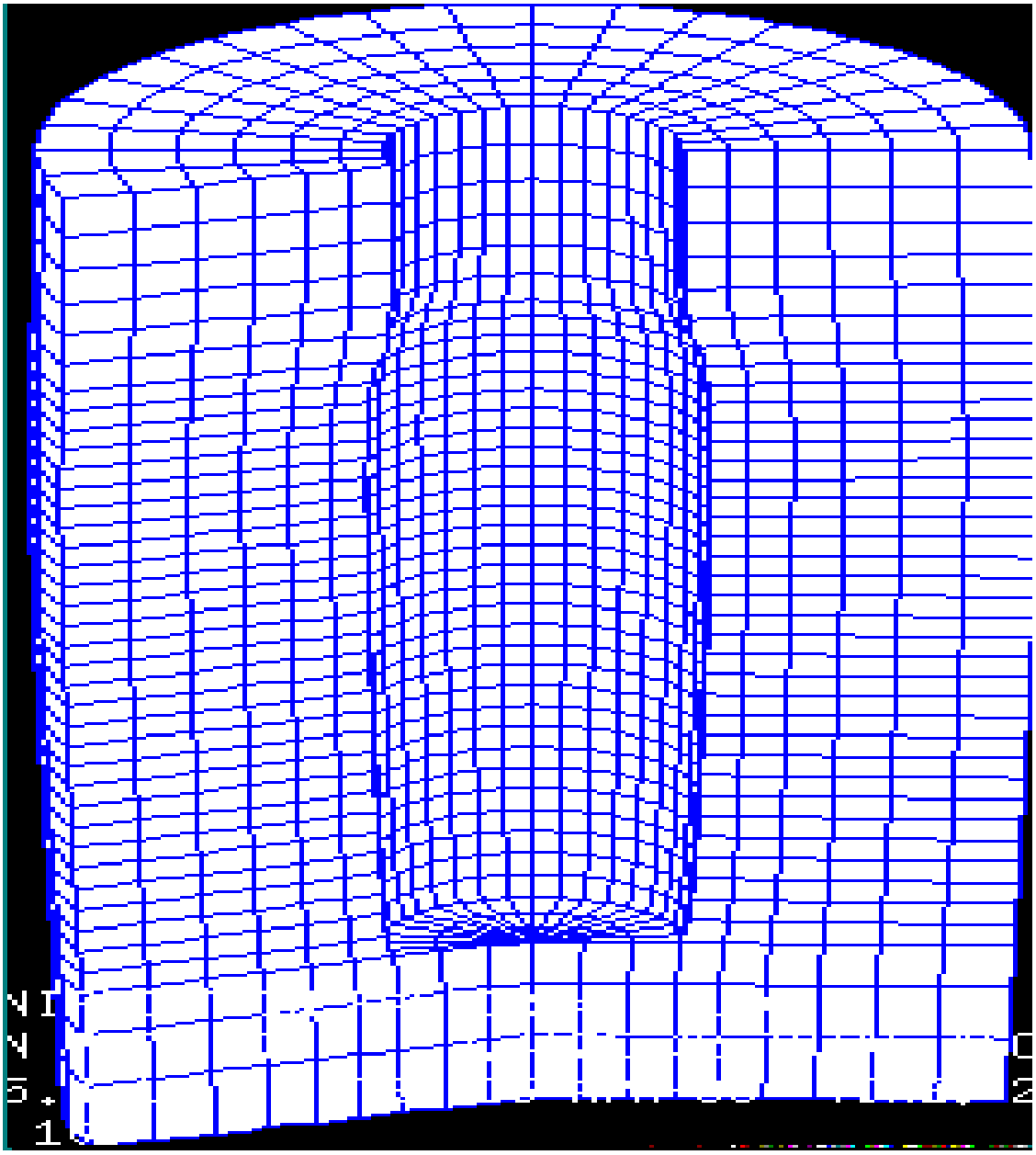

Figure 16. Finite element model of borehole expansion for Case 2.

Case 1: Elastic Wellbore

Plots in Figs. A.1 through A.6 in Appendix A show the results for Case 1. Figures A.1 - A.3 show the results before pressurization and the state of stresses caused by drilling. Note that compression and tensile stresses reported in the finite element analysis are negative.

Figure A.1 gives the distribution of stresses around the wellbore in the radial direction at the middle of the uncased section (Line 3). This distribution is exactly the same as that of many plane strain analyses. In situ tangential stress is equal to in situ horizontal stress and is twice that at the wall of the wellbore. Vertical stress remains constant from the wellbore to the outside boundary. Radial stress decreases from in situ stress to zero. This result proves that plane strain analysis can be used in the middle of the uncased section, even for such a short section as that of LOT (5-15 feet).

Figure A.2 shows the stresses along the wall of the wellbore. Radial, tangential and vertical stresses vary largely at the bottom hole position. Shear stress occurs around the bottom hole as shown in Figure A.3.

Shear stresses are not only concentrated around the bottom hole, but also around the casing shoe, as shown in Figure A.4. Figure A.5 shows that a plastic zone is formed around the wellbore.

Figure A.6 gives the displacement of the wellbore during pressurization. The rock is parted from the cement at the casing shoe. As the information in the figure indicates, cement parting is possible, which is the main reason for the formed shear stress in this area since drilling fluid is not allowed to go into this newly produced channel.

Case 2: Plastic Wellbore

Calculated results for Case 2 (for a wellbore with a plastic zone around it) are shown in Figs. A.7 through A.16. Since wells in shallow marine sediments generally have this kind of plastic annulus, Case 2 is discussed here in more detail. From the analytical analysis it follows that formation of a plastic zone can be prevented in drilling by increasing mud weight. However, this plastic zone is assumed to be stable and will yield only when stresses reach the yield/failure criterion.

Figs. A.7 and A.8 show stresses before pressure increase. As discussed in the analytical section above, in a plastic wellbore, tangential stress rapidly reduces in response to a pressure increase. Figure A.7 clearly shows this result. In the plane-strain analysis, vertical stress is generally regarded to be constant. However, the plot in Figure A.7 clearly indicates that vertical stress will also decrease with increasing borehole pressure.

Shear stresses are present but do not control a possible failure mechanism, as shown in Figure A.8. Also, as shown in Figure A.11, borehole pressurization increases shear stresses without shear fracturing.

Development of sediment failure is demonstrated in Figure A.9. First, tangential stress decreases with increasing wellbore pressure in the middle of the open hole. The phenomenon appears to be similar to that seen in deep wells. However, as shown in Figure A.10, instead of decreasing to tension, tangential stress returns before reducing to zero and begins to increase again in response to further pressurization. Thus, as the borehole becomes pressurized, tangential stress will not reduce to tension, as is the case for deep sediments. Therefore, *vertical fracture is impossible in SMS.* Theoretically, tangential stress returns because of the occurrence of re-yield. The mechanism was discussed in detail in the previous section.

Figures A.12 and A.13 show stress distribution just below and above the casing shoe along lines 1 and 2 in Figure 15, respectively. A small shear stress is generated around the casing shoe, and no fracture will occur below the casing shoe, as shown in Figure A.12. However, the element above the casing shoe looks free of stresses (all stresses reduce to zero), while radial stress reduces to tension, as shown in Figure A.13, which means that cement parting occurred.

The size of the plastic zone is almost insensitive to pressurization, as shown in Figure A.14, which means that plastic strains produced by the drilling operation could not be eliminated during pressurization. It should, however, result in wellbore expansion due pressurization. Figure A.15 gives a plot of wellbore pressure increases. The pressure increase at the wellbore wall is continuous and causes wellbore expansion, as shown in Figure A.16. However, the expansion is very small, which seems to negate the popular concept of wellbore "ballooning" in plastic sediments.

Case 3: Plastic Sediment

As drilling creates a void space in the sediment, the wellbore size reduces to some extend. The sediment in question is soft and moves into the wellbore. (Field experience indicated that using heavy muds might prevent borehole reduction to some degree.) As the open hole section below the casing shoe becomes pressurized, the sediment responds by displacement and concentration of stresses.

Results from the finite element analysis of Case 3 are shown in Figs. A.17 through A.23 in Appendix A. Figure A.17 shows stress distribution in the radial direction at the middle of the open hole section (line 3 in Figure 15) before pressurization. In response to pressurization, stresses around the wellbore become small, and stress concentration occurs in the sediment, which is in plastic state. As shown in Figure A.18 and similar to Case 2, tangential stress does not reduce to tension but returns with increasing borehole pressure. (Note that the turning point of tangential stress is moved to the right compared to that shown in Figure A.7.) Thus, a vertical fracture cannot be initiated.

Figures E.19 and Figure E.20 depict stress distributions just above and below the casing shoe, respectively, and indicate that cement parting has occurred. The tensile radial stress clearly proves this conclusion. Another conclusion is that the bottom end of the casing shoe is a most likely place where horizontal fracture could be initiated when vertical stress at the wall reduces to tension. The horizontal fracture might occur in response to the uplifting effect of the hydraulic pressure applied to the cement at the casing shoe. As shown in Figures A.20 and A.21, no conditions for fracturing exist in the mid and bottom points of the open hole section below the casing shoe. Figures A.22 and A.23 show a summary of the distributions of tangential and radial stress, respectively, along different horizontal planes.

3.3 Horizontal Fracturing of SMS at Pressurized Wellbore

The mechanism of horizontal fracture involves fracture initiation and propagation. The latter is well described by balancing the effective wellbore pressure with overburden matrix pressure (or actual well pressure with overburden pressure). On the other hand, the mechanism of horizontal fracture initiation is typically addressed by assuming that wellbore liquid somehow invades the rock through pre-existing fractures or discontinuities and without addressing the invasion mechanism. Our assumption regarding non-penetrating fluid precludes such hypothetical speculations and requires some quantitative description of the mechanism of fluid invasion into the rock at the casing shoe.

One such mechanism is an uplift of the wellhead at the sea bottom caused by LOT pressure increase. During LOT the well is shut-in around the drill pipe, and pressure pushes the wellhead upwards. As the casing is attached to the wellhead, the uplifting of the wellhead may reduce vertical compression at the casing shoe, which, in turn, may be transferred to the rock. If the reduction of compressive stress were large enough, it could reduce vertical stress at the wellbore wall from compression to tension which would cause horizontal fracture.

Unfortunately, our finite element analysis showed that this uplifting mechanism can only reduce part of vertical compressive stress at the shoe, even for a rigid column of casing and cement. Moreover, our numerical calculations showed that vertical compressive stress at the borehole wall would not be reduced to tension even for bottomhole pressure several-fold greater than overburden pressure.

The mechanism which actually may initiate horizontal fracture involves uplifting of casing and cement at the shoe. There, drilling fluid can easily go under the cement and casing shoe and push them upwards, as shown in Figure 17. This uplifting would cause elastic deformation of the bottom portion of cemented casing. The resulting strain is transferred to the rock and may reduce vertical compressive stress at the wall to tension and initiate horizontal fracture. This mechanism has been confirmed theoretically.

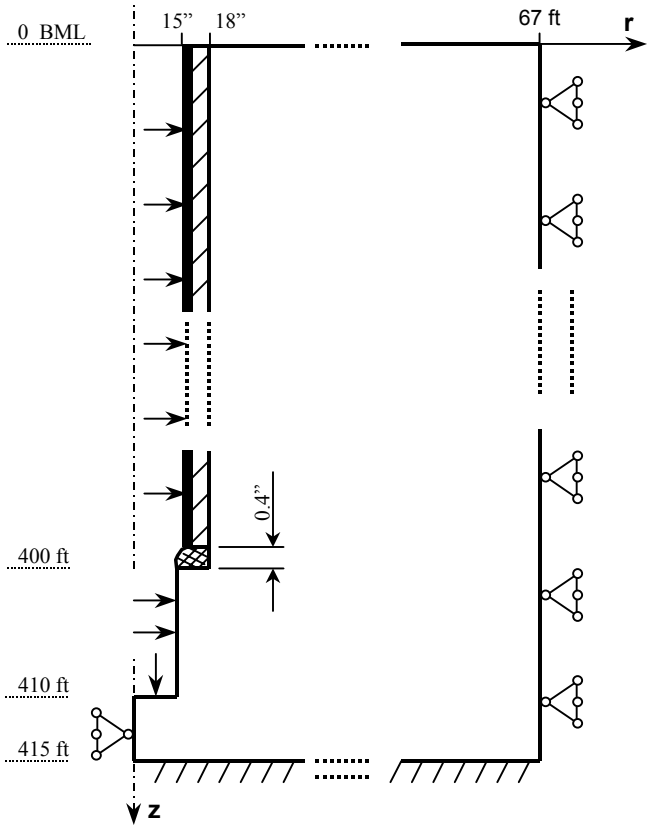

Figure 17. Finite element model of well at casing shoe.

The wellbore configuration used in our finite element studies is shown in Figure 17. The example well has a casing diameter of 30 and wellbore diameter of 26 . The rock properties are: Young's modulus = 1.1×10^4 psi; Poisson's ratio = 0.35; cohesion strength = 9.2 psi; and internal friction angle = 23 degrees. The cemented casing has Young's modulus = 30×10^6 psi and Poisson's ratio of 0.3. The value of contact stress is assumed to be zero. Effective overburden pressure was calculated using average submerged unit weight, 8.345 lb/gal, which represents UMS having a porosity of 61% and wet bulk density, 13.9 lb/gal. During LOT, bottomhole pressure increases from its initial zero value 145 psi, which roughly corresponds to drilling at 415 feet below the sea bottom.

Shown in Figure 18 is an effective vertical stress distribution at the borehole wall from the mud line (sea bottom) to the open hole bottom (finite element results are summarized in Appendix A). Vertical stress increases linearly with depth in the upper section of the well, indicating that the well's wall is in elastic state from surface to the depth at which plastic failure occurs. Below this depth vertical stress steadily decreases, indicating an expansion of the plastic zone with increasing depth. At the casing shoe vertical stress changes dramatically going from compression to tension caused by LOT pressure (points A-B-C). This change represents conditions for initiating a horizontal fracture at the shoe. This mechanism has been verified with ABAQUS in several simulation runs for varying UMS properties and wellbore conditions, shown in Table 3 (Appendix A, Figs. A.24 through A.33). All these calculations showed initiation of tensional horizontal fractures in SMS due to LOT-induced pressurization.

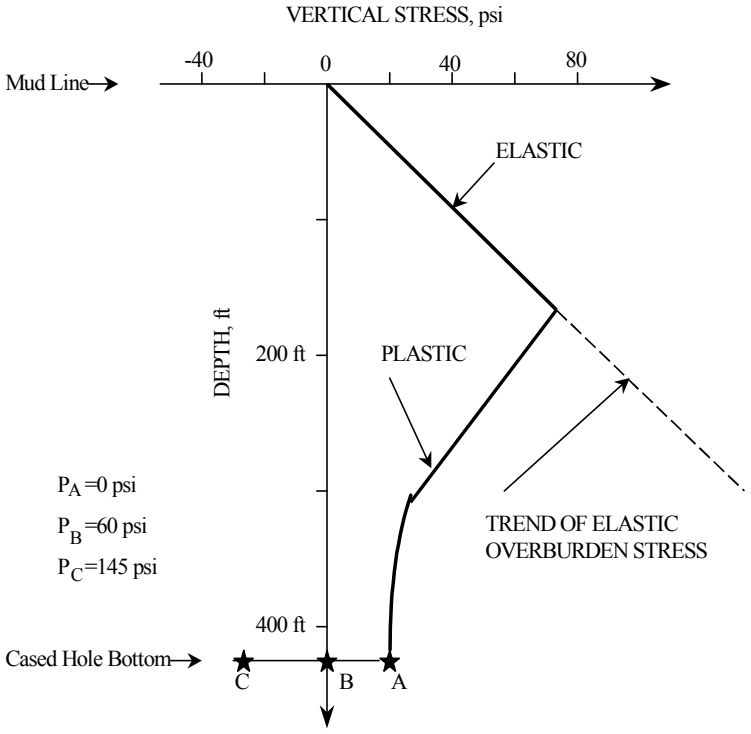

Figure 18. Vertical stress change shows initiation of horizontal fracture at casing shoe during well pressurization.

Table 3. Data for horizontal fracture simulation study

CASE	$2r_w$ (in)	E (psi)	μ	φ (deg)	τ_0 (psi)	γ (lb/gal)	E_{cc} (psi)	D (ft)	d_{cc} (in)
1	26	1.1E4	0.4	12.5	11.6	8.35	3E7	400	30
2	26	1.1E4	0.4	12.5	11.6	8.35	3E7	564	30
3	20	1.1E4	0.4	12.5	11.6	8.35	3E7	400	24
4	26	1.1E4	0.4	12.5	11.6	16.7	3E7	400	30
5	26	1.1E6	0.4	12.5	11.6	8.35	3E7	400	30
6	26	1.1E4	0.4	12.5	11.6	8.35	3E8	400	30
7	26	1.1E4	0.4	15.3	11.6	8.35	3E7	400	30
8	26	1.1E4	0.4	12.5	16.6	8.35	3E7	400	30
9	26	1.1E4	0.35	12.5	11.6	8.35	3E7	400	30

Once a horizontal fracture is formed at the wall of a well, the drilling fluid will penetrate into it and may propagate the fracture. As shown above, however, the vertical stress increases in the plastic zone around the wellbore with increasing distance from the well to the plastic/elastic boundary, where it becomes overburden stress in situ. Hence, within the plastic zone, the horizontal fracture's length is finite and determined by well pressure equal to vertical stress. Unlimited propagation can occur when the horizontal fracture comes to the plastic/elastic boundary and the actual wellbore pressure reaches the value of in situ overburden pressure.

3.4 Cement Parting at Casing Shoe in SMS

Another potential failure resulting from pressurization of wellbores in SMS is initiation of an annular channel (cement parting) that may propagate vertically upwards around the cemented casing. A recent study addressed plastic deformations of the open hole due to well pressurization by LOT (Wojtanowicz and Zhou, 1996). In this study, the authors used finite element simulations assuming no bond and no contact pressure existed between cement and rock. They concluded that drilling fluid may invade the contact surface between cement and rock at the casing shoe. The required size of the opening gap should be on the order of 0.01 in., which was within the critical range (0.01-0.015 in.) for drilling fluid's inflow, as determined by other researchers (Morita, 1990). However, the issue of critical value of well pressure needed for cement-rock parting was not addressed.

Critical pressure for induction of the annular channel is the minimum bottomhole pressure required to change contact stress at the casing shoe from compression to tension. (In order to determine critical pressure, one must assume that a mechanical continuum exists between cemented casing and rock, which means assuming both a bonding and contact stress.) As critical pressure for channeling may be smaller than that for horizontal fracture, both critical conditions should be included in the analyses.

The recent study mentioned above (Wojtanowicz and Zhou, 1998) also included annular channeling and involved a finite element analysis of the mechanical model of wellbore shown in Figure 15. Conceptually, the model was identical to the one for vertical fracture except for a

constant non-zero value of contact stress between the cemented casing and rock. The initial value of the bottomhole effective pressure before LOT pressurization was assumed to be zero. Shown in Figure 19 is the effect of bottomhole pressure on contact stress at the casing shoe. As bottomhole pressure increases from zero to 350 psi, contact stress reduces from 100 psi to zero. Thus at 350 psi annular channeling begins, which means that the critical value of bottomhole pressure is 3.5-fold greater than the initial contact pressure.

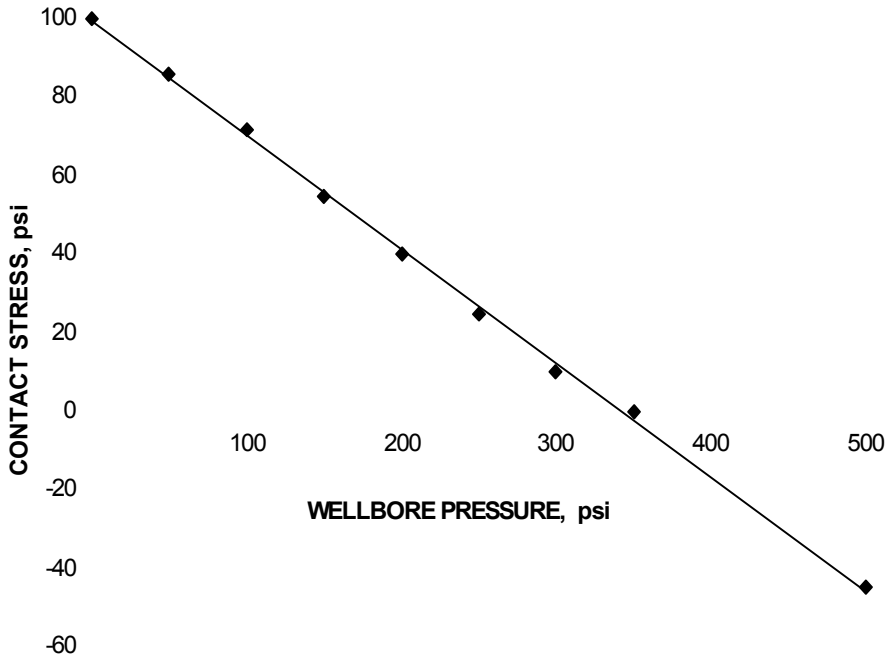

Figure 19. Contact stress change shows initiation of channel at bottom of cemented casing.during LOT-induced pressurization (Wojtanowicz and Zhou, 1998).

Critical pressure for annular channeling strongly depends on contact stress. Intuitively, the larger the contact stress is, the higher the wellbore pressure is needed to create a channel. We believe that the value of the contact stress depends upon time, formation properties, and, to some extent, properties of the cement slurry. Although determination of the contact pressure is beyond the scope of this study, we can estimate its range from zero (for compacted sediments) to horizontal stress in situ for very weak sediments. Thus, the maximum value of contact stress is:

$$\delta_c = \sigma_h = \frac{\mu}{1-\mu}\sigma_{z0} \tag{49}$$

where the value of Poison ratio in UMS can be evaluated using a recent empirical correlation (Eaton, and Eaton, 1997).

The relationship between contact stress and critical (initiation) pressure for cement parting (annular channeling) is shown in Table 4. The data reveals that in all cases considered in

the study, critical channeling pressure was about 3.5-fold greater than the contact stress. Moreover, with this 3.5 value, the pressure ratio was not affected by varying rock properties, such as Young's modulus, Poisson's ratio, internal friction angle, and cohesive strength. In addition, vertical stress and wellbore diameter did not affect the ratio either.

Table 4. Data for annular channeling simulation study

CASE	E (psi)	μ	φ (deg)	τ_0 (psi)	LOAD (psi)	D (ft)	2r (in)	RATIO
1	1.1E5	0.3	25.4	31.6	600	1100	26	3.6
2	1.1E5	0.3	21.6	34	600	1100	26	3.5
3	1.1E5	0.3	25.4	78	600	1100	26	4.3
4	1.1E3	0.3	25.4	31.6	600	1100	26	3.5
5	1.1E5	0.2	25.4	31.6	600	1100	26	3.5
6	1.1E5	0.3	25.4	31.6	600	1100	20	3.5
7	1.1E5	0.3	25.4	31.6	700	1300	26	3.4

4. PRESSURE TESTING OF SMS STRENGTH AT CASING SHOE

In situ measurement (LOT) is the most accurate and direct method for finding formation strength at the casing shoe. Then, the strength is related to the maximum drilling fluid density that can be used to drill the next section of open hole. Obviously, the result of the test is not only indicative of formation fracture but may reflect casing shoe failure through cement sheath (cement parting).

Typically, LOT is performed immediately beneath the cemented casing shoe. The casing should be set in shale. After waiting an appropriate time for the cement to harden, cement plug and 5 to 20 feet of fresh formation are drilled very carefully (almost zero weight on bit) to prevent damaging the casing shoe integrity. Then, the drill bit is pulled into the casing before circulating and conditioning the mud. Mud circulation time should be long enough to remove the effect of entrained gas and even out the mud weight. Next, the BOP is closed and mud pumped down the drill pipe at a constant rate between ¼ and 1 bbl/min until the value or pattern of pressure increase becomes indicative of upcoming shoe/rock failure. In deep wells, this point is represented by a deviation from linear pressure increase with volume pumped. In SMS, however, no straight line pattern occurs and, hence, no clear indication of the onset of failure is evident. Therefore, operators have developed various procedures for conducting and analyzing LOTs in SMS.

4.1 Conventional Leak-off Tests (LOT)

Following is a summary of LOT procedures proposed by various authors. For deep wells the approach is basically the same as summarized by Chenevert and McClure (1978):

1. Construct a graph with dashed lines indicating a "minimum volume" line and the anticipated leak-off pressure line.
2. While coming out of the hole, position the bit in the casing above the shoe.

3. If the mud is not of a known, uniform density it should be circulated until it is. Two common causes of non-uniform density are barite slugs in the drill pipe and formation cuttings in the annulus.
4. Close the ram preventer above the drilling spool.
5. Using a small pump (such as a cementing pump) begin pumping mud down the drill pipe at a constant rate of 0.25 to 1.50 bbl/min. The rate depends on these conditions: with no open hole, use 0.25 to 0.33 bbl/min; with sandstone formation exposed, use 0.75 to 1.5 bbl/min, depending on the amount of open hole. Data obtained should fall very close (within 0.5 bbl) to the "minimum volume" line at leak-off.
6. Record on the graph the pressure after each 0.25 or 0.50 bbl increment is pumped.
7. Continue pumping until the curve starts its decline, or until the anticipated leak-off pressure line is exceeded. Exceeding this line is often caused by only shale being exposed in the open hole.
8. When the pumping is shut off, keep the well shut in and read an instantaneous pressure. Then read pressure values each minute for about 10 min. These should also be plotted on the graph.
9. Release the pressure and record the volume of testing fluid recovered in the trip tank if one is available. The volume of fluid recovered should approximate the volume of fluid pumped.
10. Compare the graph with typical plots to be sure it is a good test.

A procedure developed by Amoco provides for additional information after the leak-off occurs. The procedure is as follows:

1. Pick up drill bottom hole assembly (BHA) and trip in hole. Tag cement. If casing is full of seawater, displace seawater with mud that will be used in subsequent drilling to perform LOT.
2. Circulate and condition mud until mud weight is even in and out.
3. Casing Integrity Test (CIT): Pressure test casing recording pressures every 0.125 bbl (or every 0.25 bbl maximum). Shut in and monitor pressure for 10 min. Enter the pumped volumes and pressures on the CIT sheet.
4. Drill out the float shoe, rat hole, and 10 to 15 ft (3-5m) of new hole. Circulate and condition the mud until mud weight is even in/out, checking in triplicate with pressurized mud balance.
5. Pull out of hole until the bit is about 10 to 15 ft (~3-5m) inside the casing shoe.
6. Rig up cementing unit and test lines. Close blow out preventers, BOP (annular or pipe ram), prepare to monitor volume/pressures on the cement unit, and also monitor pressures at the choke (via the casing pressure gauge on the choke console).
7. Pump mud (via cement unit) at 0.25 to 0.5 bpm constant rate, recording pressures every 0.25 bbl, regardless of pump rate, until the pressure increase shows a definite deviation from a linear trend (leak-off pressure, LOP) or until hard break down. Hard break down occurs if the pressure abruptly drops while pumping. Record data on the LOT sheet and follow the plot. If the pressure plot falls below the maximum volume line during pumping before leak-off, bleed off the pressure and start over using 0.25 bpm faster pump.
8. Confirm leak-off; pump an additional volume (0.75 to 1.0 bbl) into the formation while frequently monitoring injection pressure behavior to ensure that the pressure increases at

a smaller slope. Note: If hard break down has occurred, there is no need to pump this additional volume.

9. Shut down the pump and record the instantaneous shut in pressure (ISIP). Then continue to monitor the pressure decline for 20 minutes or until the shut in pressure stabilizes, whichever time is least. Look for surface leaks.
10. If a pressure decline is observed and the pressure stabilizes, then the test is probably of good quality.
11. Bleed off pressure and record recovered drilling fluid volume. Record the injected and recovered fluid volumes.
12. Retest before squeezing. Retest if the pressure abruptly dropped significantly while pumping (hard break down) to determine a valid LOP; do not use peak pressure as the LOP.

Another procedure, developed by Amerada Hess, emphasizes the dynamic effect of pressure buildup and stabilization in response to pumping:

1. Drill cement and float equipment and 10 of new formation or clean out rathole.
2. Circulate and condition mud until mud weight in and out is uniform (within 0.1 ppg).
3. Pull back into the casing shoe. Make up cementing lines, ensuring they are filled with mud (avoiding pumping air into drill pipe). Break circulation. Close the annulus.
4. Pump mud at ¼ bpm until a pressure response is observed. Record volume pumped.
5. Begin pumping in ¼ bbl installments at ¼ bpm rate. Stop pumps after each ¼ bbl and wait until pressure stabilizes. Record volume of mud pumped, final pumping (dynamic) pressure, and stabilized (static) pressure at each ¼ barrel increment.
6. Plot both dynamic and static pressures vs. cumulative mud volume pumped.
7. Continue in ¼ barrel installments until the static pressure indicates a "leak-off" is occurring or the maximum specified pressure is reached (jug test).
8. A final shut-in pressure should be recorded 5 minutes after pumping has ceased.
9. Slowly bleed off the pressure and record the volume of mud bled back.

Dowell's procedure provides a criterion for LOT quality by comparing leak-off pressure with instantaneous shut-in pressure:

1. Record casing test pressure each 0.25 bbl while pumping @ 0.25 bpm, and plot on the leak-off test chart.
2. Drill out all cement and float equipment and +/-10 of new formation.
3. Circulate the well with the mud pumps until the mud is conditioned (uniform density and rheology throughout the well). If the mud does not have good fluid loss properties, a viscous, low fluid loss pill may be spotted across the open hole.
4. Pull the drill bit into the cased hole.
5. Pump mud to fill treating line and remove any air from the pump and lines before rigging up to the drill pipe. Break circulation. Close BOP.
6. Perform LOT with the cement pump. Level mud in the displacement tanks with a barrel marker, and reset volume to zero.
7. Perform LOT by pumping at a consistent 0.25 bpm and plotting the pressure every 0.25 bbl of volume pumped. The actual LOT is established when the plot of pressure vs. volume injected falls away from the straight line trend. When leak-off is established, stop pumping.

8. At this point in the test, plot shut-in pressure on the same chart. This pressure should be plotted every minute until it levels out, or for about 5 minutes. If ISIP is less than half the leak-off pressure, a possible problem exists. Re-perform the leak-off test. If the same leak-off test is obtained on the new test, then it should be considered an accurate leak-off pressure.
9. Once pressure is stabilized, the well should be bled off into the displacement tanks and the volume recorded.

Slightly different from these procedures are those used by the operators in South China Sea. They recommend stopping the pump in the middle of the leak-off test. Then the falling pressure is monitored during the stop pump period. The pressure fall-off is an indicator of fluid seepage into the rock. After the fall-off, pumping is continued to the breakdown pressure.

4.1.1 LOT Analysis Techniques Used by Operators

It should be emphasized that the methods for LOT analysis have not been developed from the theory of rock fracturing mostly because rock properties are usually not known during drilling operations. Also, leak-off tests measure casing shoe integrity, which encompasses properties of the rock and cemented annulus. Thus, operators set out to develop easy-to-use techniques that would not require much input data.

Typical LOT data is shown in Figure 20. The pressure at point A is the leak-off pressure (LOP) for the leak-off test; i.e., point A is the point at which the pressure-volume plot deviated from a straight line (linear relation). Point B is the maximum pressure point at which pressure no longer increases with further pumping. After the maximum pressure at point B, the well is shut in (Point C in Figure 20). Segment DE is the level-off section of the leak-off test.

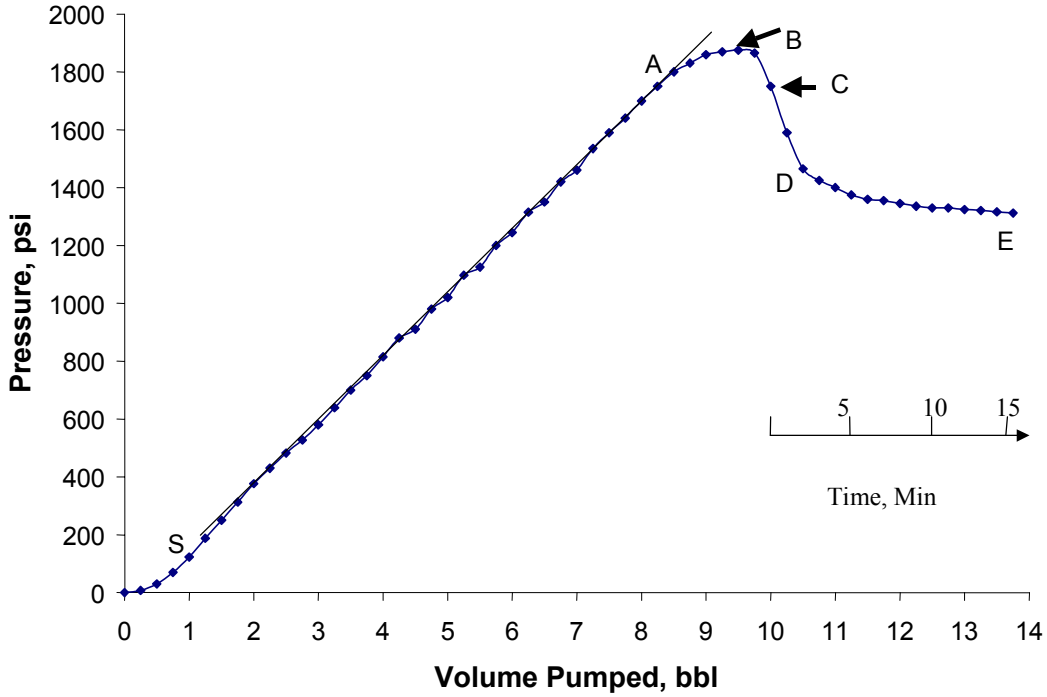

Figure 20. Common interpretation of leak-off test result.

For the leak-off test in Figure 20, the analysis can be summarized as follows: The early exponentially increasing part (segment OS) represents the effect of gas. The straight line segment SA represents linear pressure-volume relationship controlled by the system compressibility. A fracture appears at point A. The fracture propagates at segment AB as new drilling fluid is pumped. After point B, the pumped mud continues to propagate the fracture. Segment SA is called the pressure build-up section. Segment AB is fracture propagation section. As stated previously, point A is the leak-off point, and point B is the breakdown point. Segment BC is the breakdown section. The sharp pressure drop (segment CD) represents the loss of kinetic energy (friction loss of mud) and filtration of mud. The stabilized segment DE represents filtration loss of mud.

Chenevert and McClure (1978) suggest using a minimum volume line (Figure 21) and the anticipated LOP lines, shown in Figure 22, as a guide for determining the pump rates. The

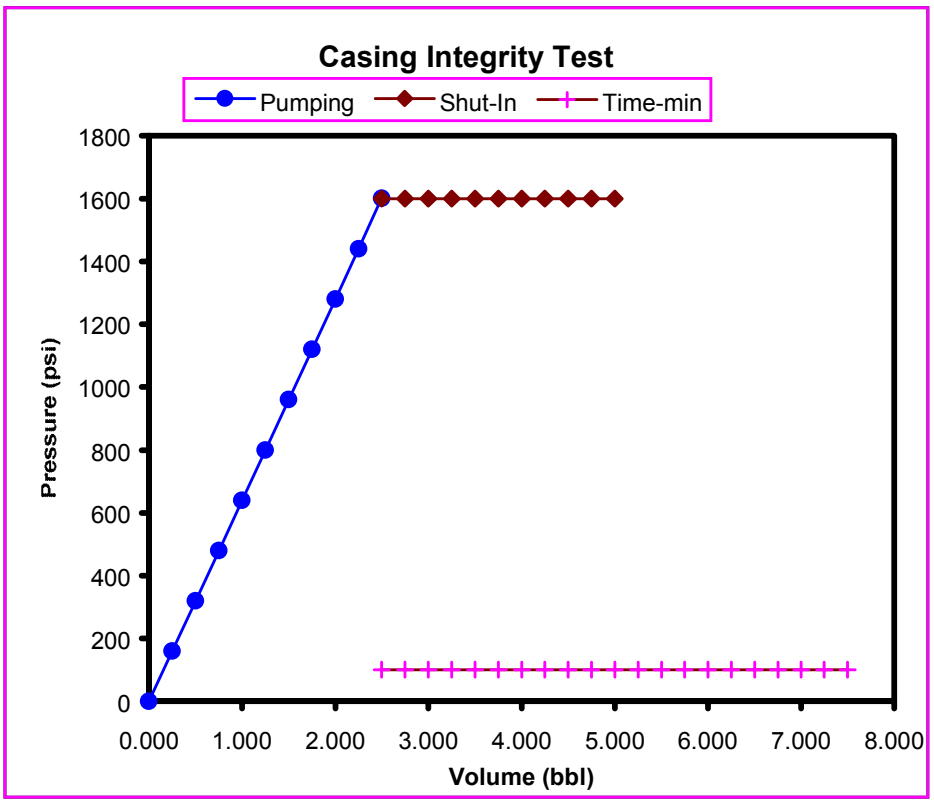

Figure 21. Casing integrity test result (courtesy of Amoco).

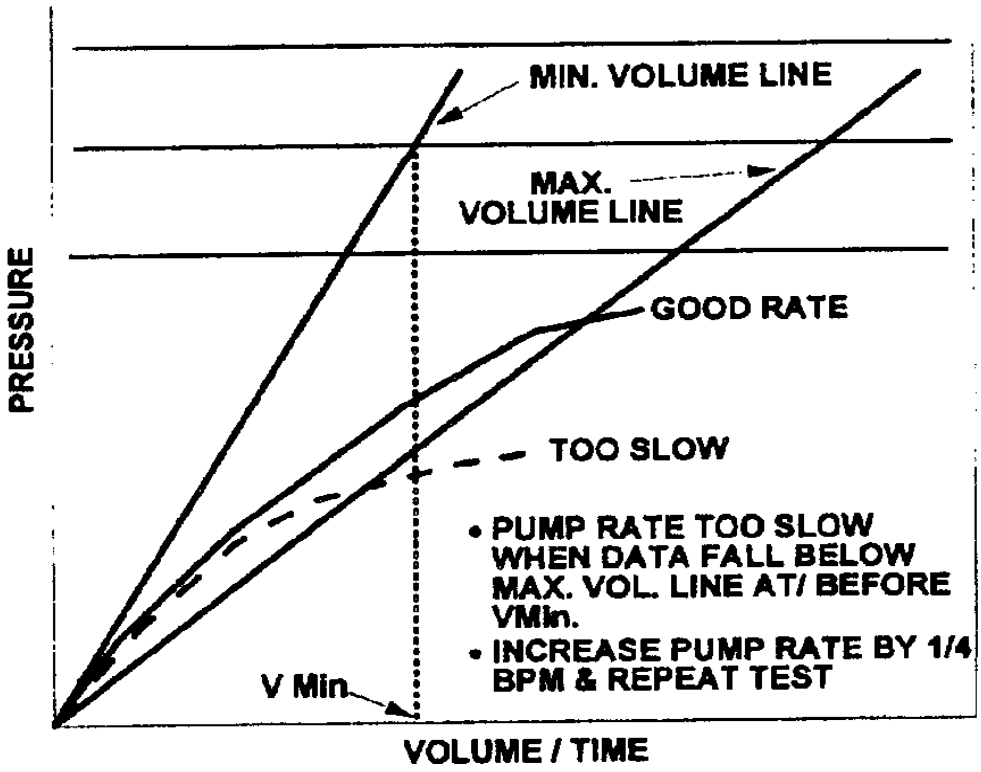

Figure 22. Pumping rate effect (Postler, 1997).

minimum volume line can be estimated from mud compressibility, as the authors suggested, but in practice it is the casing test line, shown in Figure 23. According to the authors, straight-line data of a LOT should stay equal to or very close to the minimum volume line values; otherwise, the pump rate is inadequate. However, the authors do not mention the data limit that may deviate from the minimum volume line. This limit is known as the maximum volume line, shown in Figure 22.

Postler (1997) suggested the following procedure for analysis (Figure 23):

- Predicted value of leak-off pressure should be verified with offset well data and/or local overburden and pore pressure. There should be no guesswork or arbitrary setting of a certain pressure value to reach the next casing shoe. Also, a rightward bend in the plot near the predicted pressure probably indicates leak-off. A bend significantly below this value is probably not leak-off, and pumping should continue.
- Minimum acceptable leak-off pressure: less than ½ ppg of equivalent mud weight of the predicted leak-off pressure line. The ½ ppg represents the margin of error garnered from experience.
- Maximum acceptable pressure plot: maximum pressure based on equipment limitations or lost circulation experience.
- Minimum volume line: a diagonal line represents the mud compressibility and may be taken by the casing integrity test line.

- Maximum volume line: a diagonal line represents the lower limit reference and is generally two times the minimum volume. LOT data that deviate below this line are usually caused by high formation permeability and a too-low pump rate.

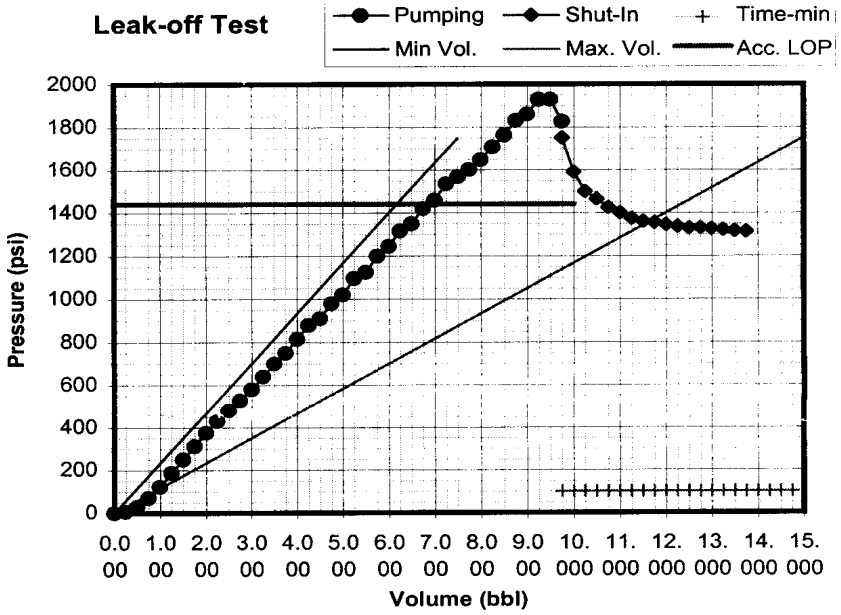

Figure 23. Typical leak-off test plot (Postler, 1997).

Morita et al. (1991) studied the occurrence of formation fracture and its propagation by hydraulic pressure. They conclude that LOT would cause no damage or formation fracture since fracturing is controlled by minimum rock stress and the rock will recover after the leak-off test. They summarize a whole interpretation of formation fracture, as shown in Figure 24.

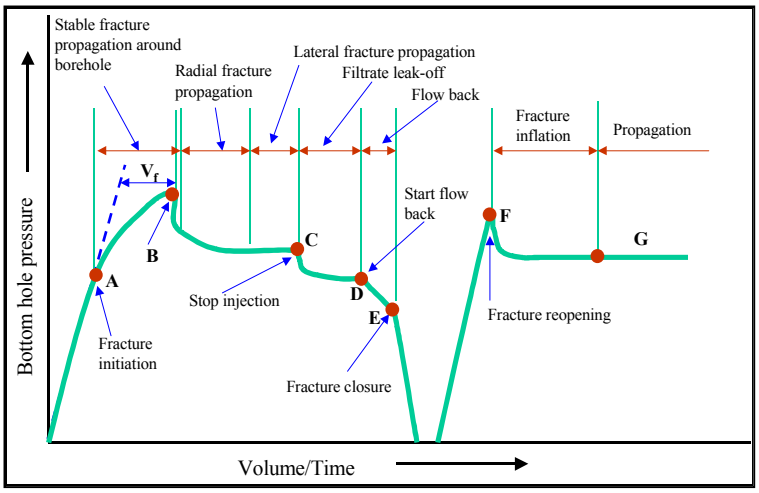

Figure 24. Rock fracture and fracture propagation under leak-off test (Morita et al., 1991).

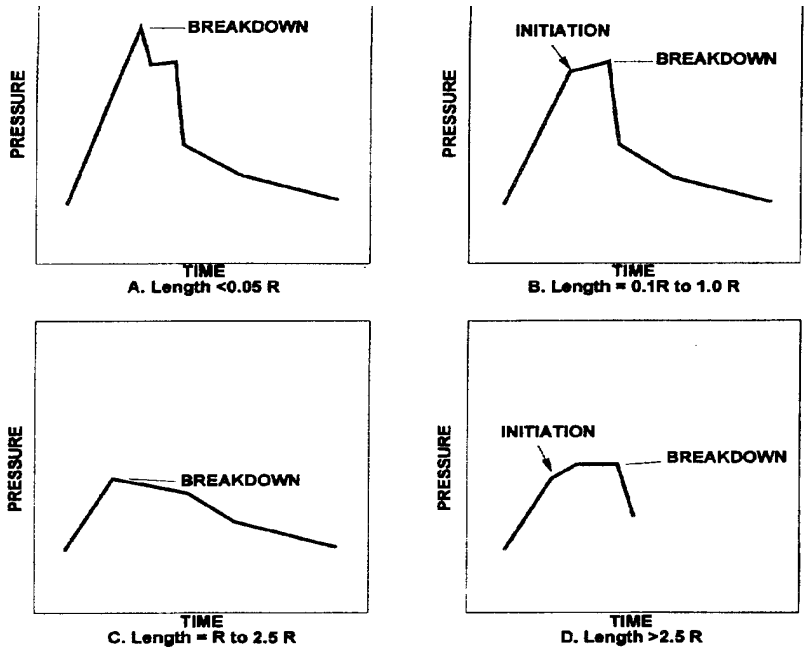

Figure 25. The effect of pre-existing crack length.

Some operators attribute unusual leak-off test results to pre-existing cracks or so-called mini-fractures. Ishijima and Roegiers (1983) studied the effect of the length of the pre-existing cracks on the rock breakdown pressure. They conclude that different crack length might give different initiation and breakdown pattern, as shown in Figure 25.

Amerada Hess developed a diagnostic method that considers various patterns of LOT plots in different formations. The pattern depends upon the rock type, as shown in Figure 26A. Plasticity and permeability are the major factors affecting the LOT pattern.

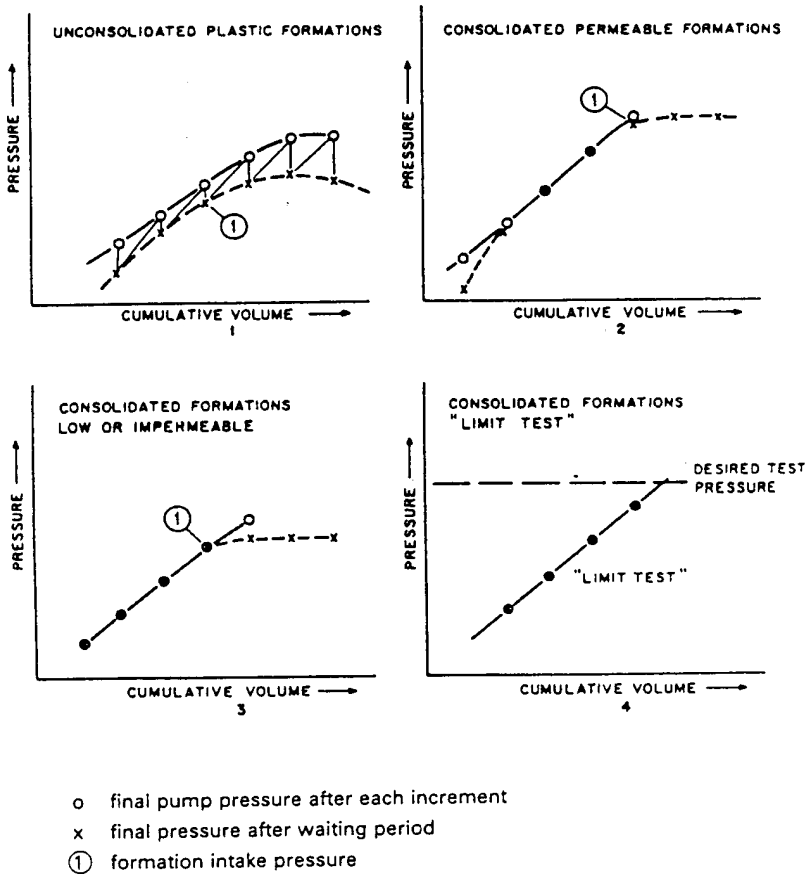

Figure 26A. Schematic representations of the leak-off test pattern for different rocks.

Amoco's approach to LOT analysis focuses on casing shoe quality assurance, i.e., deciding whether to drill ahead or to squeeze cement. The company's guidelines recommend squeezing cement in these cases:

- the leak-off pressure is less than the minimum acceptable value required to drill to the next casing point;
- shut-in pressure has not leveled off; or,
- the ratio of leak-off pressure (LOP) to minimum stress (MS) is greater than 1.1.

This general interpretation technique, also used by most operators, is demonstrated in Figure 26B.

Date: 22-Mar-96	Casing Shoe				
Well: XXXXXX	Csg. Size	MD ft	TVD ft	Incl. deg	Azimuth deg
Location: XXXXXX					
Rig: XXXXX	13.38		5686.00	0.00	N/A

Mud Properties						
Mud Wt. ppg	WBM/ OBM	VIS. cp	PV cp	YP lbs/100sqf	API WL cc	Gels. 0/10
13.00	WBM	50.00	21.00	13.00	13.00	4/19

LOT Test Results					Channel Indicators
LOP (psi)	MS (psi)	LOP_{EMW} (ppg)	MS_{EMW} (ppg)	LOP_{EMW}/ MS_{EMW}	Time in 1. LOP_{EMW} < Minimum Acceptable Value 2. Shut-in pressure not leveling off 3. LOP_{EMW}/ MS_{EMW} > 1.10 when leak-off occurs without abrupt pressure drop (hard breakdown)
920.00	860.00	16.11	15.91	1.01	

LOP

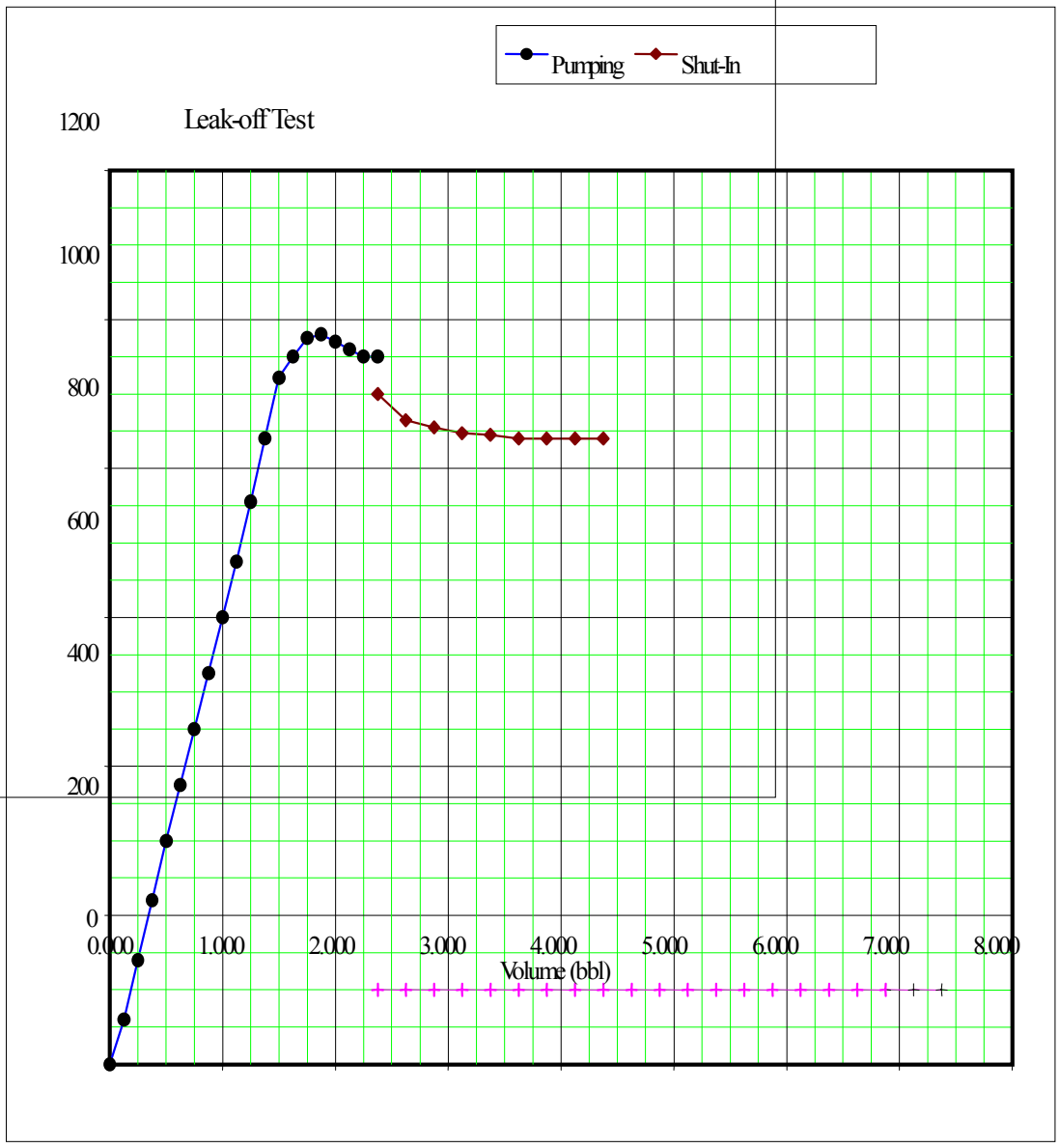

Figure 26B. Interpretation of leak-off test result (courtesy of Amoco).

Other principles commonly used for analyzing LOT plots include the following observations:

1. A concave upward slope early, followed by a constant slope to leak-off, indicates trapped air in the system.
2. A concave upward slope throughout the leak-off test indicates high fluid loss to a permeable formation.
3. A concave downward slope at a much earlier than expected fracture pressure indicates a leak in cement or casing.
4. A leak-off test that does not go through the origin indicates pressure loss due to friction or gellation of mud.
5. After bleeding the pressure and collecting returns in displacement tanks, if significantly less volume returned than was pumped (+/- 1 bbl), then a possible channel exists. This assumes that pressure can be bled off through drill pipe (i.e., no check valves).

Postler (1997) presents a good summary of LOT guidelines and interpretation techniques based on published theories. He suggests evaluation of both the build-up and shut-in portions of the test plot, as well as the judicious use of repeat tests during interpretation of LOT results. He suggested the following general steps: 1. Estimate the leak off; 2. Evaluate LOP; 3. Evaluate the shut-in; 4. Check for a cement channel; 5. Retest when in doubt. He also presents diagnostic patterns of the leak-off test plots indicating annular chanelling (shown in Figure 27). He asserts that a large open channel around the casing shoe will give a lower leak-off pressure than predicted (Case A in Figure 27). On the other hand, a small channel will result in two slopes, which indicate two leak-off points. Also, the two-slope plot will have two small level-off parts in the shut-in section of the plot (Case B in Figure 27). Another alternative is a plugged (non-propagating) channel in cement. Such a channel is demonstrated in the plot by a rapid pressure drop after shut-in the well (Case C in Figure 27).

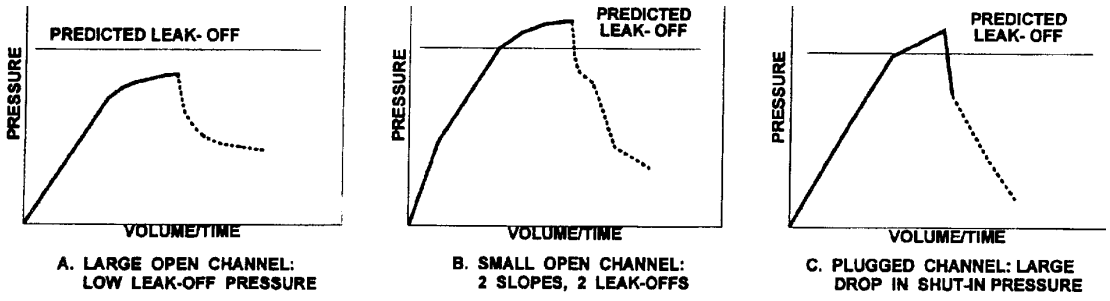

Figure 27. The effect of cement channels on leak-off test result.

In addition to general guidelines, researchers provide suggestions on how to identify some specific problems in LOT. Chenevert and McClure (1978) studied mud gelation effects. They suggest that the formation fracture pressure should be calculated from pumping pressure (LOP) by adding mud hydrostatic pressure and subtracting mud gelation pressure instead of friction pressure. The authors also criticize the procedure of getting mud gelation pressure from the rotational viscometer after the mud has been quiescent for 10 minutes. They assert that this

procedure should be avoided since it does not reflect the downhole pressure and temperature conditions. Instead, they propose using well circulation data to find the mud gelation pressure.

However, pressures due to mud gelation are relatively small and can be ignored without resulting in significant error when calculating the LOP and the fracture pressure. Following the procedure would result in overestimation of the LOP and the fracture pressure. Thus, the industry simply ignores the mud gelation effect during analyzing test results.

Hazov and Hushudov (1993) studied the effect of plastic formation on the leak-off test because operators and researchers thought that wellbore ballooning is a major reason to pump a large volume. The authors calculated the wellbore compressibility in shale formations based on LOTs in the eastern North Caucasus of the former Soviet Union. This work produced the observation that the measured and calculated volumes from the LOT and the drilling fluid compressibility were quite different. The authors report that calculated volumes for cased holes with 100% cement bond and those without good cement bond were significantly different.

The authors also state that the non-linear LOT curves were the result of wellbore expansion, fluid loss, and filtration. However, plastic deformation in shales takes considerable time (10 to 20 hours), and the time needed to pressurize shales during a LOT takes only 10 to15 minutes. Therefore, the authors conclude that plastic deformation might not be the main factor in their study.

The authors also conclude that this large volume change came from elastic hydro-fractures. They considered the fractures to be pre-existing. As pressure increased, the fractures took mud in. The fractures closed under the action of rock stress and returned the mud without any losses as the pressure was reduced.

4.1.2 LOT Data Recording Practices

Typically, a graph describing the relationship of pressure versus pumped volume constitutes a permanent record of LOT. Occasionally, the pressure fall-off after shutting in might also be added to the record. Some operators add to these plots reference lines, such as maximum and minimum pressure lines and maximum and minimum volume lines, as shown in Figure 23.

However, including well information and leak-off condition in the LOT records is generally a good practice. Shown in Table 5 and Figure 28 is a complete record from the leak-off test.

Table 5. Complete data record from LOT (courtesy of Amoco)

Date:	22-Mar-96				Water Depth	Air Gap	Max. TVD	Max. MD
Well:	XXXXXX				ft	ft	(ft)	(ft)
Location:	XXXXXX							
Rig:	XXXXXX				300.00	70.00	5734.00	

LOP Criteria		Mud Properties						
Estimated Ppg	Min. Acc. Ppg	Mud Wt. ppg	WBM/ OBM	VIS. cp	PV cp	YP lbs/100sqf	API WL cc	Gels. 0/10
16.50	15.75	13.00	WBM	50.00	21.00	13.00	13.00	4/19

Casing Shoe					Top of 1st Below Casing Sand			
Csg. Size	MD ft.	TVD ft.	Incl. deg.	Azimuth deg.	MD ft.	TVD ft.	Incl. deg.	Azimuth deg.
13.38		5686.00	0.00	N/A	N/A	N/A	N/A	N/A

LOT Chart Guidelines					
Min. Volume (last point of CIT)		Max. Volume (twice Min. Vol.)		Accepted LOP (horiz. line)	
(bbl)	(psi)	(bbl)	(psi)	(bbl)	(psi)
0.00	0.00	0.00	0.00	0.00	813.10
2.50	1600.00	5.00	1600.00	10.00	813.10

Required Input

Optional Input

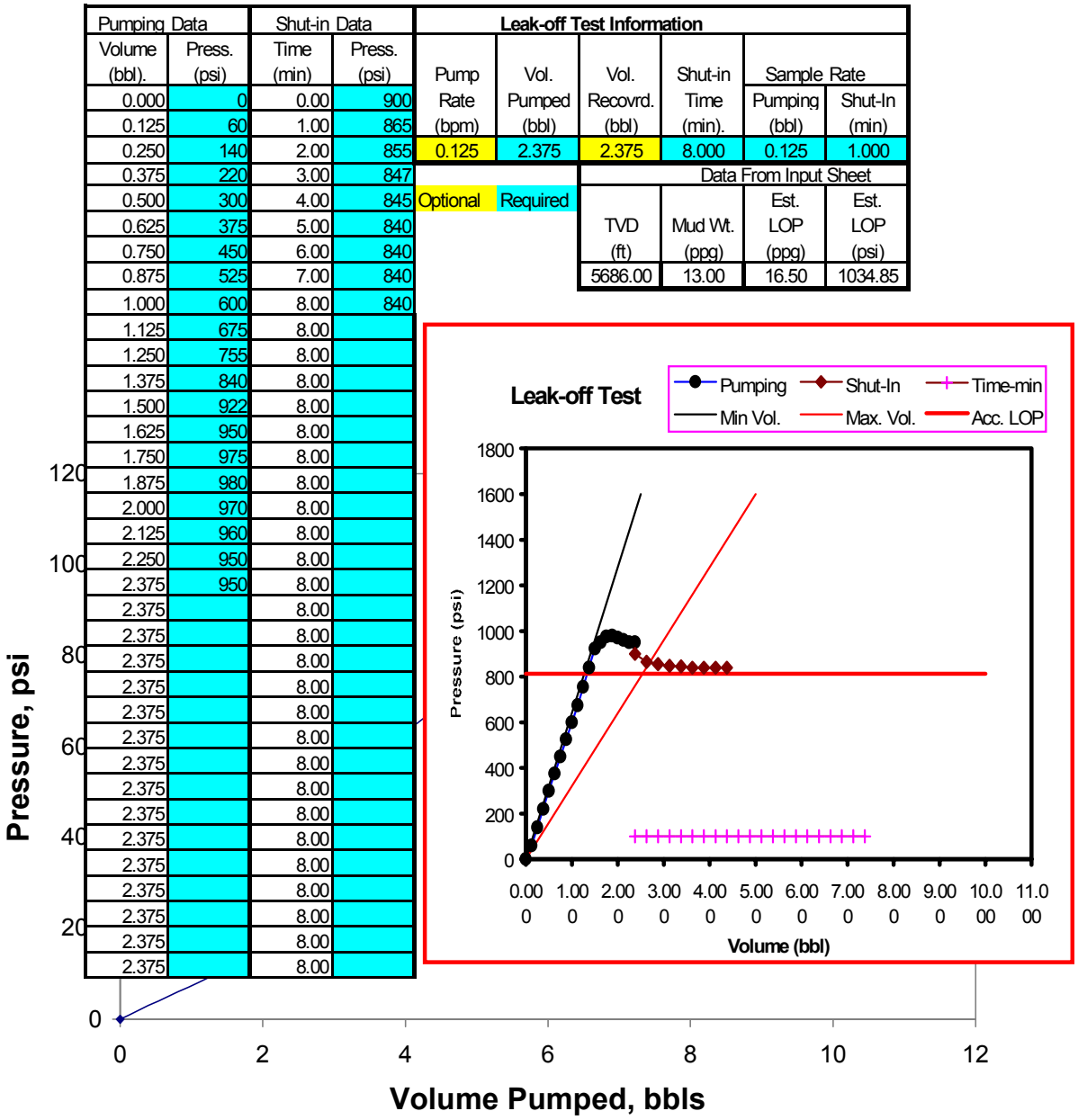

Figure 28. Example of well-documented LOT (courtesy of Amoco).

4.2 Leak-off Tests in Shallow Sediments

In shallow sediments, leak-off tests are performed for the same reason as in the deeper formations: to estimate how much pressure can be applied to the rock just below the casing shoe before the shoe/rock system fails. Also, the LOT procedures for both situations are conceptually the same: to stress out the shoe/rock system until the first sign of failure appears. The problem is that in deep rocks the beginning of failure (fracture) is well supported by theory and relatively easy to recognize, which is not the case for shallow and soft rocks. As shown in Figure 29, for example, this deep-well LOT shows a distinct straight line and rapidly developing curvature, indicating the start of elastic failure. This type of pressure response can be fully explained by the elastic rock model with a linear stress-strain relation and the maximum value of tangential stress at the wellbore wall to be exceeded in order to initiate the fracture.

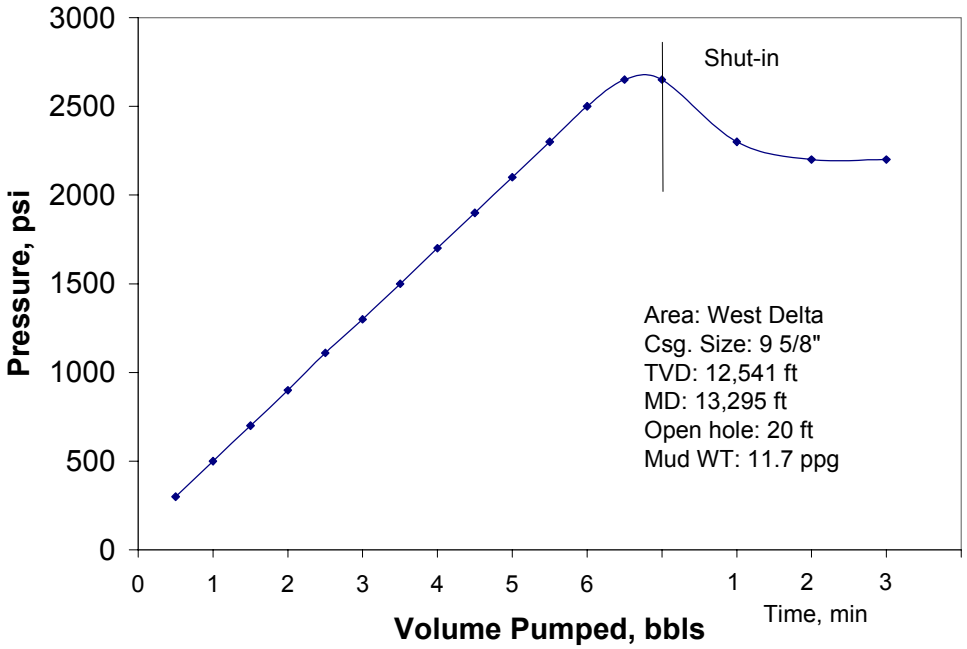

Figure 29. Typical LOT in a deep formation.

In shallow formations, however, particularly SMS, recorded LOTs give various plots with no clear indication of the beginning of failure. Moreover, as the elastic theory cannot explain non-linearity of those plots, other factors must be hypothesized, such as mud filtration, micro-fracturing, or equipment malfunction. Shown in Figure 30 is a LOT record with a nonlinear trend. The trend was confirmed by bleeding back 4.5 bbls of mud, followed by pumping an additional 3 bbls.

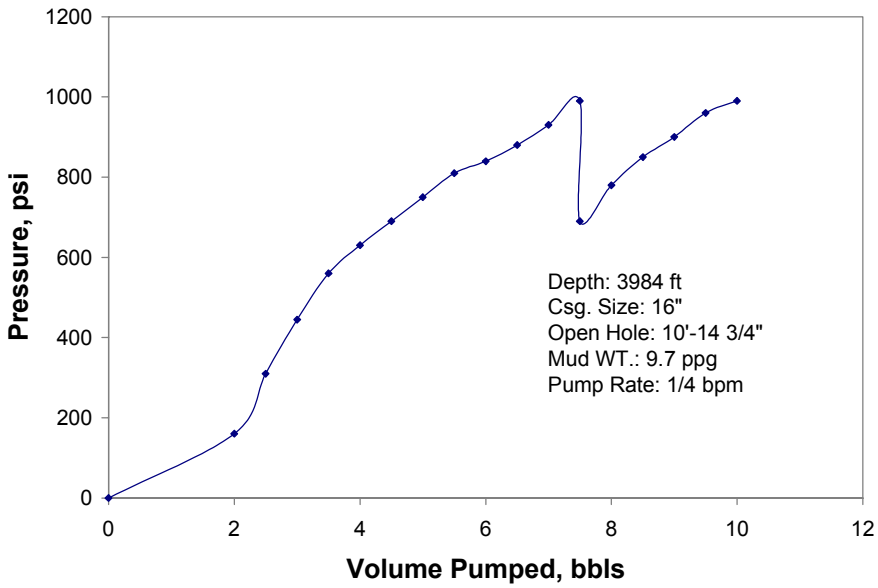

Figure 30. Non-linear LOT in a shallow sediment.

4.2.1 Field Data from Shallow LOTs

Operators have long realized that, because the onset of formation breakdown is not clear in soft rocks, a rock failure may be underway during the test. The failure may result in permanent damage to the annular seal. To avoid potential damage, some operators have eliminated LOTs in SMS, while others put an arbitrary limit (with safety margin) on the maximum pressure during the test. The result of such a test with a limiting pressure of 990 psi is shown in Figure 30. Also, some other operators perform LOTs as a series of slow pumping periods intermittent with stop-pump/hold-pressure periods. Typically, such a test is terminated when the system does not hold pressure any more.

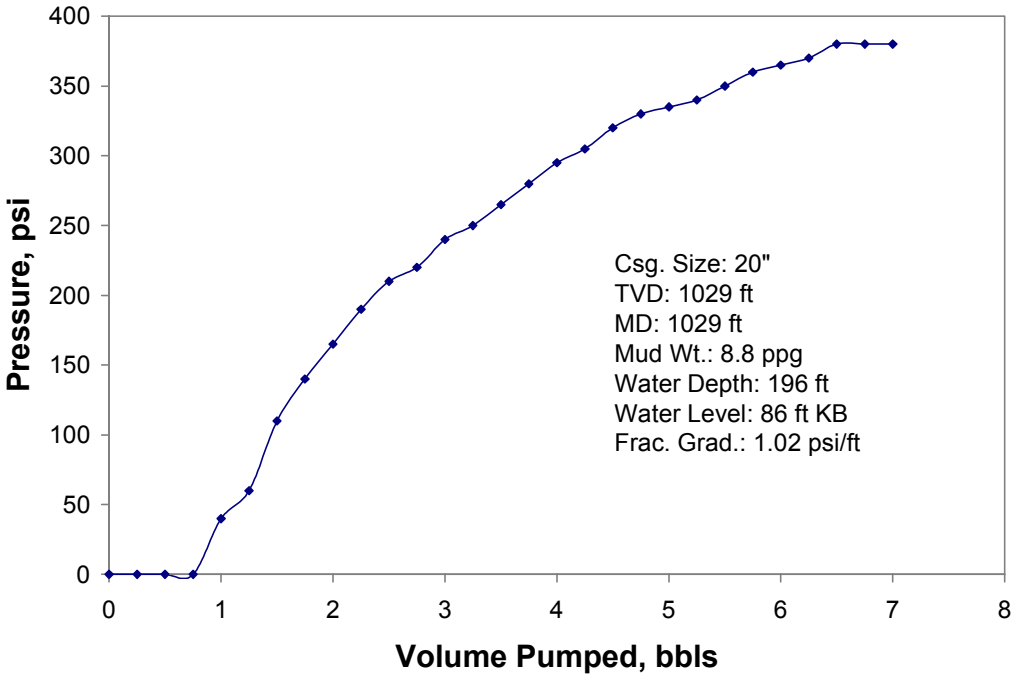

Figure 31. Non-linear LOT in SMS with "yield" pressure.

Shown in Figure 31 is a LOT performed in UMS at 747 ft BML with 196 ft of water depth. Non-linearity of the plot is evident with no pressure peak indicating concentration of stresses around the wellbore. Instead, pressure stabilized at a constant value of 370 psi, at which point the system "yielded." This response bears some resemblance to the stress-strain behavior of elasto-plastic materials.

The pressure response depicted in Figure 31 is typical for LOTs in SMS. The plots may be different in the way that their "yield" pressure behaves; instead of remaining constant, the yield pressure may slowly drop in a linear manner. Also, it has been observed by some operators that the typical values of the yield pressure gradients are high, ranging from 0.75 psi/ft to over 1.0 psi/ft, as documented by data from five LOTs in UMS, shown in Table 6.

High pressure gradients would indicate that SMS are much "stronger" than has been previously believed. Reports indicate that, for some shallow sediments, fracturing gradients can become two-fold greater that those for deeper sediments (Arifun and Wahyu H. Sumpennpo, 1994).

Table 6. Values of yield pressure gradients from LOTs in UMS

PROPERTY	UNIT	LOT 1	LOT 2	LOT 3	LOT 4	LOT 5
Water depth	ft	195	195	196	102	103
Shoe depth, BML	ft	218	534	747	583	582
Pressure @ yield	psi	185	170	380	155	220
Pump rate	bbl/min	5.00	5.00	0.25	0.25	0.25
Mud weight	lb/gal	8.65	8.5	8.8	9.0	8.9
Water gradient	psi/ft	0.44	0.44	0.45	0.44	0.44
Pressure gradient @ yield	psi/ft	1.49	0.84	1.02	0.829	0.94

One way of predicting high strength of shallow sediments is to use equations from the theory of fracturing deep sediments, and make an empirical correlation between the ratio of vertical-to-horizontal stresses versus depth using data from LOTs. Though this approach may work in practical applications, it is theoretically incorrect because it is based upon an implicit assumption that elasto-plastic behavior can be modeled as a pseudo-elastic one. The approach may generate values of the stress ratio greater than unity that are difficult to explain without considering the effects of some external factors, such as tectonic stresses.

Generally, upper marine sediments are weaker and have higher stress ratios than deep sediments. They are also most likely to exhibit plastic rather than elastic behavior under stress loads applied by LOTs. Therefore, the conventional fracturing theory based on elastic analysis cannot fully explain either the behavior of SMS during LOTs or potential damage resulting from these tests.

Also, nonlinear trends are difficult to recognize from a small number of measurements. Figure 32 demonstrates this point. Only three measurements are recorded prior to the shut-in, which, therefore, makes finding out whether (or not) there is an initial linear trend in this plot and where the non-linearity begins impossible. Analysis of the plot's non-linearity becomes inconclusive.

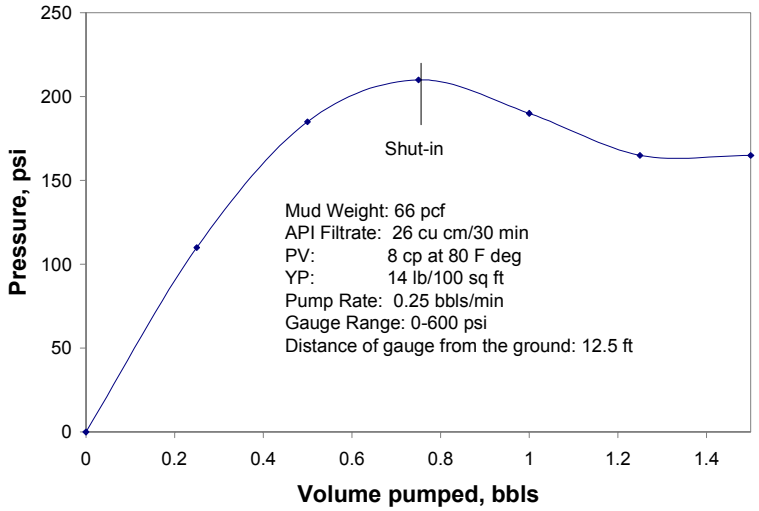

Figure 32. Inconclusive trend of LOT caused by too few measurements.

Unlike LOT data from deep wells that show the maximum breakdown pressure hump, the plots of shallow LOTs indicate pressure stabilization in response to continuous pumping. Figure 33 is an example of such behavior. Once the maximum pressure of the 220 psi is reached after pumping one bbl of mud, the pressure remains constant while pumping an additional 1.25 bbls prior to shut-in.

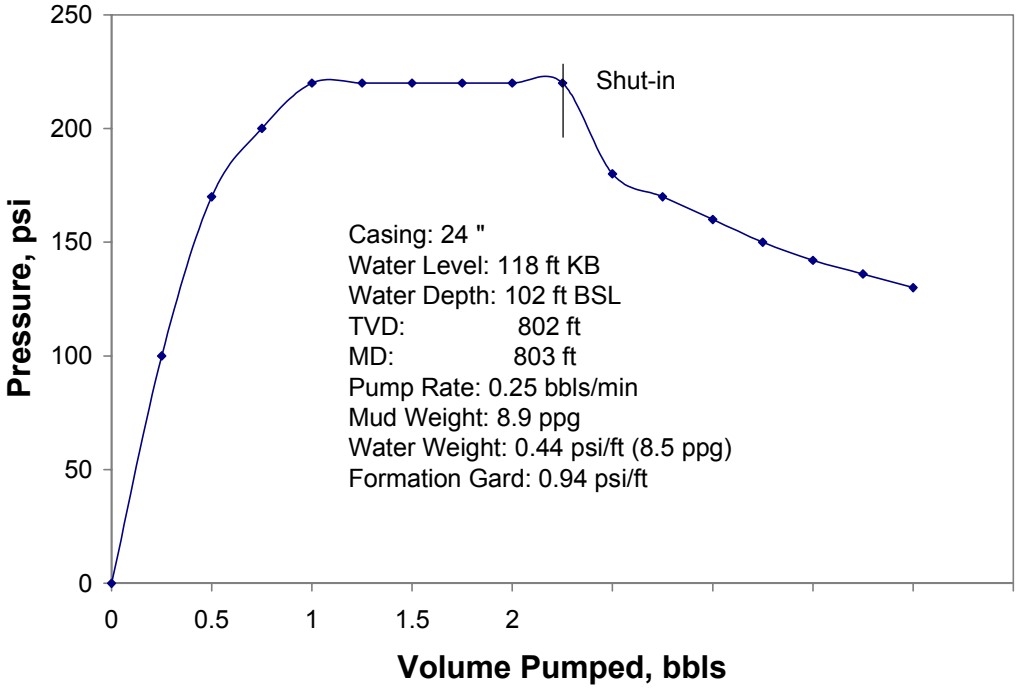

Figure 33. No breakdown pressure hump for shallow LOT.

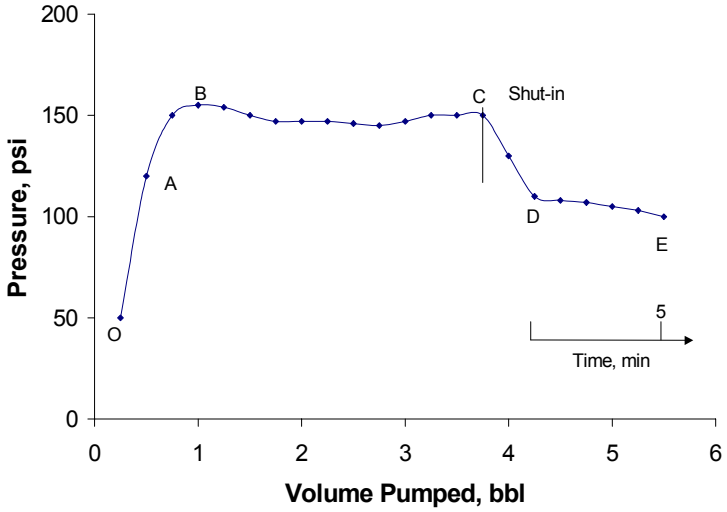

Figure 34. Shallow LOT pattern and characteristic points.

Figure 34 shows the basic patterns of the LOT curve sections in shallow marine sediments: non-linear initial buildup (0-A-B); stabilized maximum pressure (B-C); initial shut-in pressure drop (C-D); and final fall-off (D-E). Some sections of the plot in Figure 34 are similar to those in deep wells (sections C-D-E, for example). The difference stems from non-linearity of the initial buildup and leveling off at the maximum pressure value. Another difference is an incomplete pressure record that does not show the shut-in pressure section of the LOT plot.

These observations are further documented by examples of shallow LOT plots in Figs. 36 through 38. In these figures, "Formation gradients" are the calculated values from the test that represent casing shoe strength.

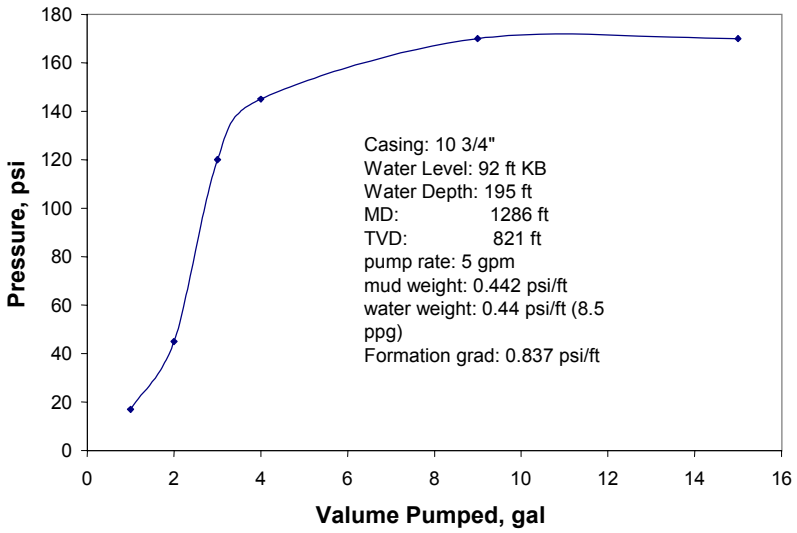

Figure 35. Leak-off test data in SMS.

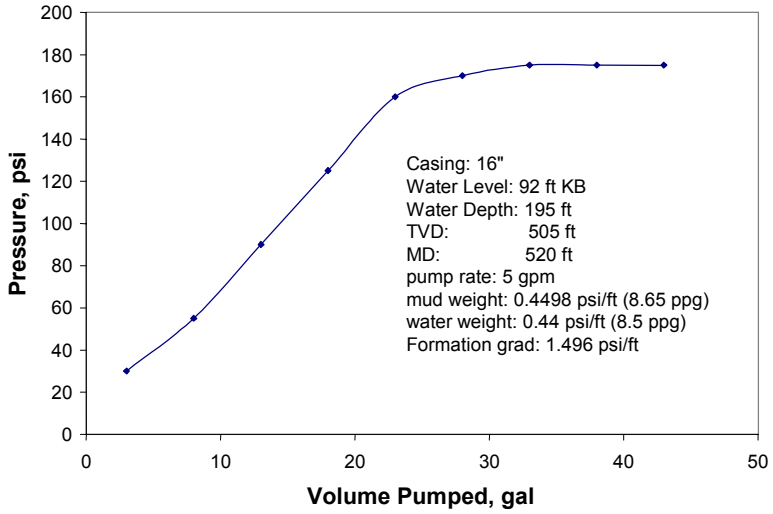

Figure 36. Leak-off test data in SMS.

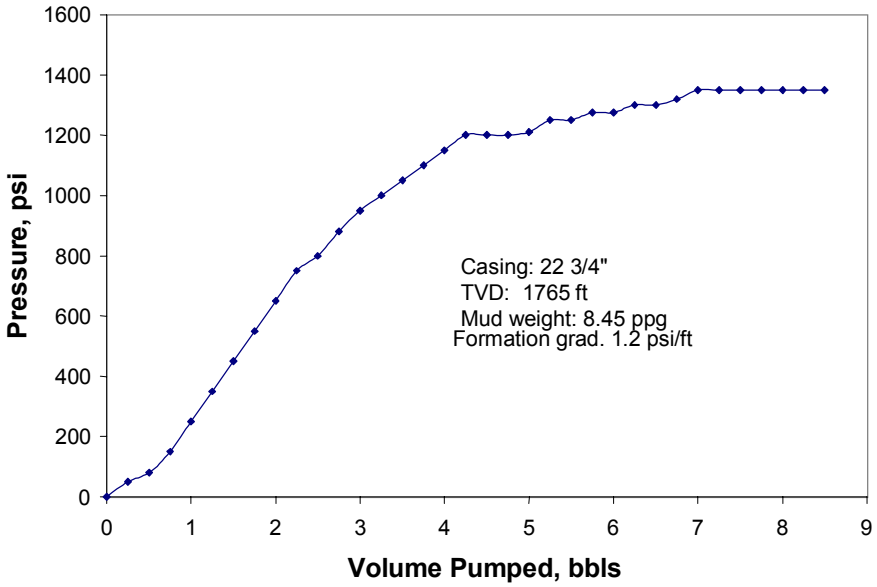

Figure 37. Shallow LOT data onshore.

Typically, pressure response to pumping is a function of time. The pumping can either be performed at a constant rate (dynamic) or in 0.25-bbl increments followed by a waiting period for pressure stabilization (static), the pump-and-wait method. The resulting two plots are parallel and shifted by the value of frictional pressure loss, as shown in Figure 38. The purpose of the pump-and-wait method is to provide a comparison plot that may help locate pressure losses and verify the value of leak-off pressure (LOP). As shown in Figure 39, the mud leakage occurred instantly in this well at 700 psi after pumping the first batch (0.25 bbl) of mud. Figure 40 shows an example of LOT with a very low value of pumping rate.

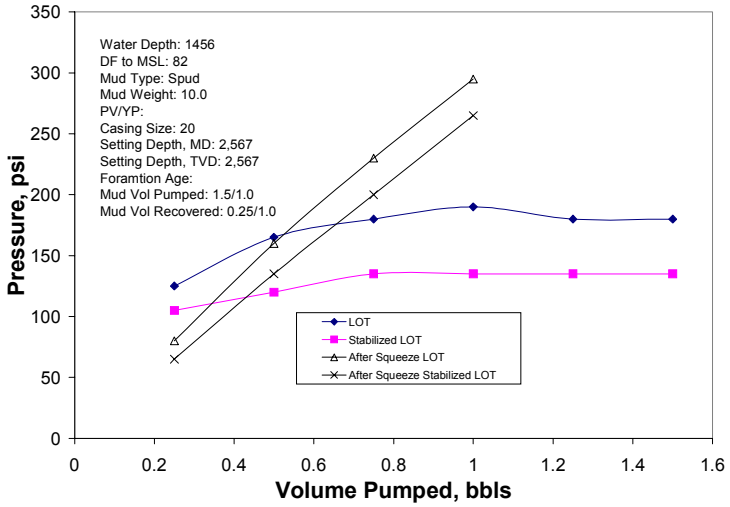

Figure 38. Dynamic and static plots of LOT before and after cement squeeze.

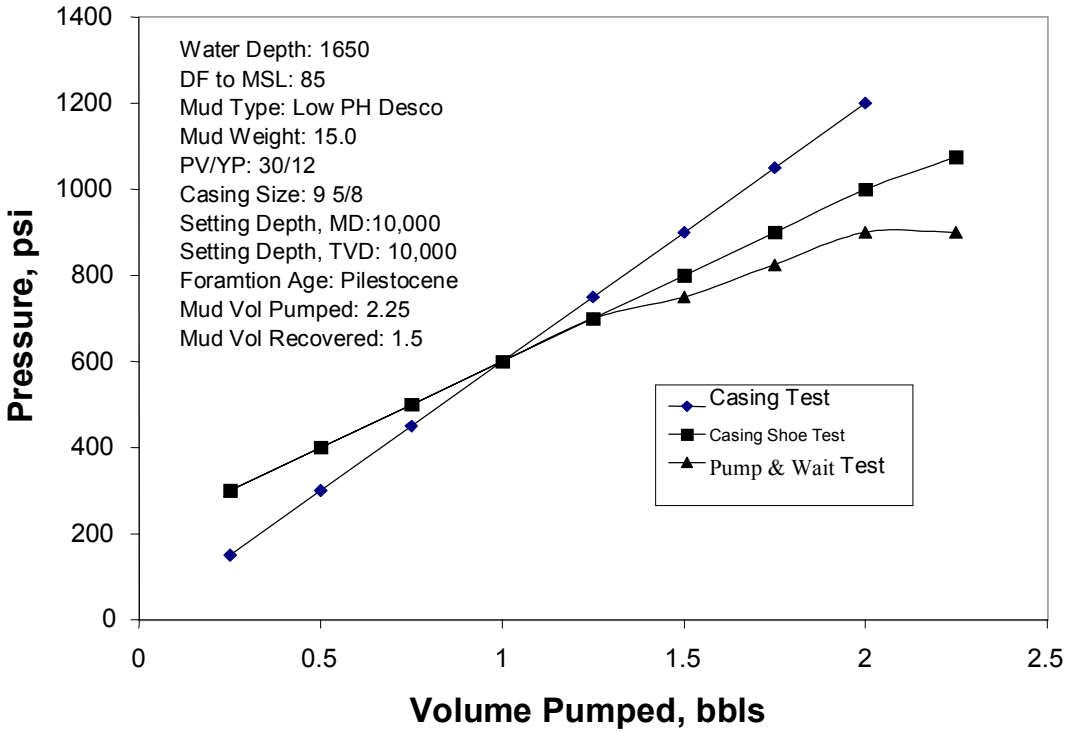

Figure 39. Pump-and-wait test indicates LOP at 700 psi.

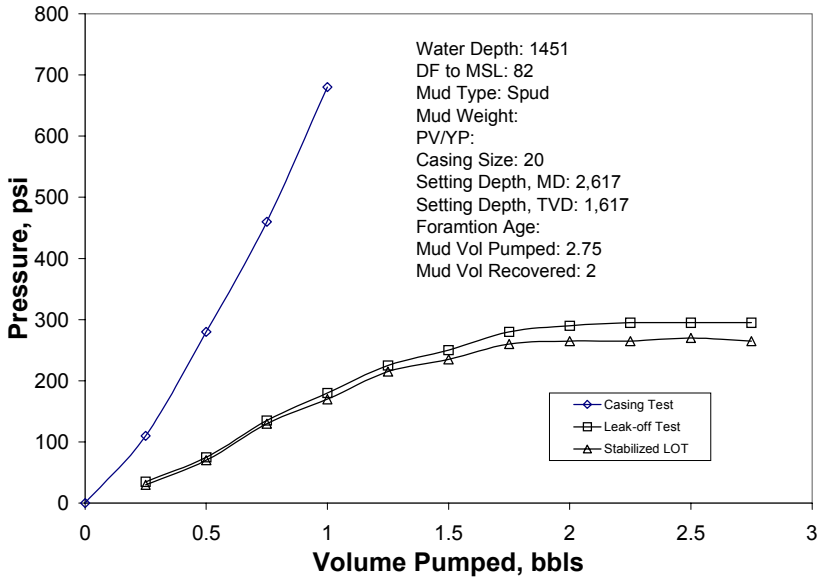

Figure 40. No difference between pump-and-wait and dynamic LOTs.

4.2.2 Shallow LOT Database

Two Microsoft Excel files containing shallow leak-off test results have been attached to this report. The database *OffshoreLOT.xls* contains results of 677 tests performed in SMS. The database *OnshoreLOT.xls* contains results of more than 10,000 tests from land drilling operations collected by the Canadian Energy Resource Conservation Board. Table 7 is an example of the offshore LOT file. Each row contains data from an individual test plus other relevant information, such as well name, water depth, hole size, casing size, casing depth, mud weight, LOT, field, country, operator, DBSF, result, air gap and count.

Table7. Example of LOT Database from SMS

Well Name	Water Depth	Hole Size	Casing Size	Casing Depth	Mud Weight	LOT
M1	1307	17.5	13.38	6775	9.9	13.3
M1	1307	12.25	9.63	9445	12	13.3
M1	1307	26	20	2637	8.5	10.4
	25	26	20	1020	8.7	11
	25	17.5	13.38	4623	9.3	13.6
	230	17.5	13.38	1637	9.1	12.7
	118	17.5	13.38	1306	9.1	16.3
	186	9.88	7.63	4212	9.2	12
	186	13.5	10.75	1883	9.1	12
	186	13.5	10.75	1668	8.7	12
	78	17.5	13.33	5014	9.3	15.2
	78	26	20	1257	9.1	12
	96	20	16	5062	9.1	14.5
	96	10.63	9.63	12300	16	17

Table 7 (Columns ctnd.)

LOT	Field	Country	Operator	DBSF	Result	Air Gap	Count
13.3	LOBM-1	ANGOLA	ELF AQUITAIN	5468			3
13.3	LOBM-1	ANGOLA	ELF AQUITAIN	8138			4
10.4	LOBM-1	ANGOLA	ELF AQUITAIN	1330			5
11	INDA-4	NIGERIA	CHEVRON	995			6
13.6	INDA-4	NIGERIA	CHEVRON	4598			7
12.7	MARINE VIII	CONGO	AMOCO	1407			8
16.3	MARINE VIII	CONGO	AMOCO	1188			9
12	MATA GORDA	USA	HALL HOUSTON	4026			10
12	MATA GORDA	USA	HALL HOUSTON	1697			11
12	MATA GORDA	USA	HALL HOUSTON	1482			12
15.2	MATA GORDA ISLAND	USA	SANTA FE MINERALS	4936			13
12	MATA GORDA ISLAND	USA	SANTA FE MINERALS	1179			14
14.5	MATAGORDA ISLAND	USA	ARCO	4966			15
17	MATAGORDA ISLAND	USA	ARCO	12204			16

Table 8 is an example of the onshore LOT file. It has been organized differently than the offshore file with coded proprietary information on the wells. Also, the file uses the SI metric system of units. Note that the leak-off pressure gradient psi/ft, should be calculated from the file as

Leak-off Pressure [psi/ft] = 0.4421 GRADIENT

Table 8. Onshore LOT data file record example

LE	LS	SE	TWN	RG	M	SFC_DEPTH	PRESSURE	GRADIENT	QUAL_FACT	FORMATION	TD
00	06	06	001	01	4	184.4	4275	32.9	1	SAW/LIV	1189
00	06	17	001	01	4	219.0	5654	35.5	1	SA/BISD	1189
00	06	31	001	01	4	216.0	3516	26.0	1	SAW	1158
00	07	04	001	02	4	189.0	5654	39.7	1	SA/BSLC/BIS	1158
00	07	05	001	02	4	180.0	2750	25.1	1	SWTH	1195
00	06	06	001	02	4	215.0	4068	28.7	1	SAW	1128
00	06	10	001	02	4	189.0	4100	31.5	1	LIV/SAW	1195
00	10	12	001	02	4	181.0	2250	22.2	1	SWTH	1172
00	06	19	001	02	4	219.0	5240	33.7	1	MANN	1188
00	07	29	001	02	4	189.0	4685	33.5	1	SAW/BI	1180
00	06	33	001	02	4	189.0	5378	38.2	1	MANN	1128
00	06	02	001	03	4	193.0	5792	39.7	1	SAW	1158
00	10	03	001	03	4	180.0	1725	19.4	1	SAW/LIV	1182
00	11	05	001	03	4	192.5	3722	29.0	1	SAW/MANN	1170

Table 9. Symbols used in Table 8

LE	=	The well's location exception
LS	=	The well's legal subdivision
SE	=	The well's section
TWN	=	The well's township
RG	=	The well's range
M	=	The well's meridian
SFC_DEPTH	=	The setting depth in meters of the well's surface casing
PRESSURE	=	The surface leak-off pressure in KPa
GRADIENT	=	The leak-off gradient in Kpa per meter
QUAL_FACT	=	A number (1 to 5) based on the following leak-off gradient criteria 1. 17.0 to 40.0 Kpa/m 2. LOT not run to leak-off 3. 0 to 16.9 KPa/m 4. 40.1 to 50.0 Kpa/m 5. 50.1 and greater
FORMATION	=	The projected formation (abbreviation) the well will be terminating
TD	=	The projected total depth of the well in meters

4.2.3 Analysis of Shallow LOT Data

Included here is the analysis of shallow LOTs, including the land and offshore operations. Although this report pertains mostly to marine sediments, some statistical observations regarding strength of shallow sediments onshore (in Canada) provide useful perspectives to this study.

The analysis of shallow LOTs from land drilling uses the database file *OnshoreLOT.xls* containing data from tests performed at the surface casing shoe in over 10,000 wells in Canada. All results have been statistically organized according to the test depth, as shown by Figure 41B. The plot in Figure 41B is of the average LOT pressure gradient versus casing shoe depth. The values are greater than typical overburden pressure gradients for sedimentary rocks, particularly at large depths. The reason might be high strength of volcanic rocks in the area.

For shallow depths, LOT pressure values are also large. Figure 41A shows a frequency plot from 7658 shallow LOTs conducted at depths smaller than 1000 ft. Of the tests, 77% indicated pressure gradients greater than 1.0 psi/ft, which is the overburden pressure value in GOM. This result could only be explained by the fact that shallow formations in the Canadian Rockies are strong volcanic rocks having a considerable value of tensile strength, unlike GOM shallow sediments with tensile strength close to zero.

To support this conclusion, let us consider geological data for one of the shallow LOTs (405 ft) recorded in the Canadian database. The lithology in the well (from surface) included 100 feet of Vitric tuff (100'), 60 feet of Andesite (160'), 180 feet of Dacite (340'), and another 65 feet of Andesite (405'). The value of the LOT pressure gradient in this well was 0.98 psi/ft.

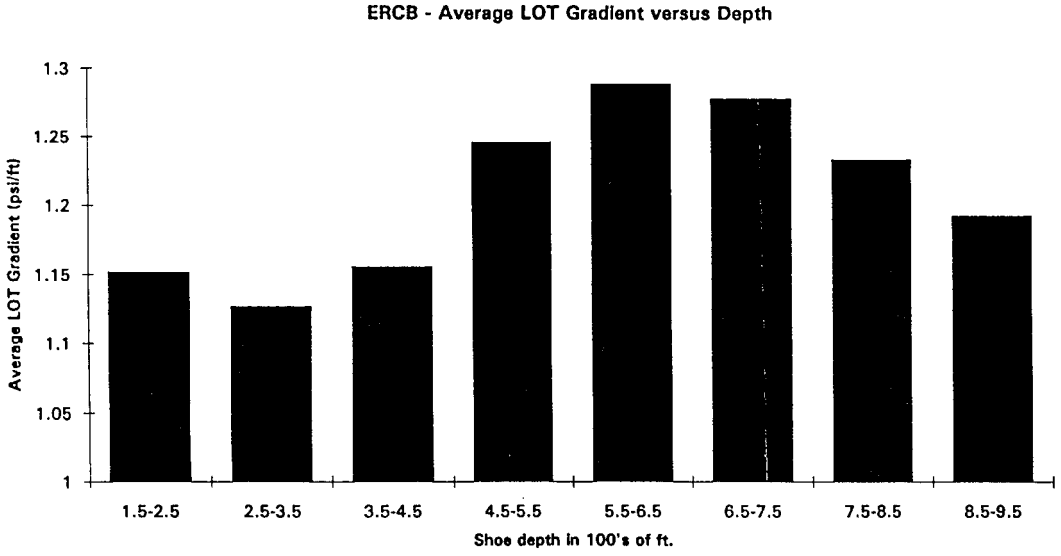

Figure 41A. LOT gradient versus depth for land drilling in Canada.

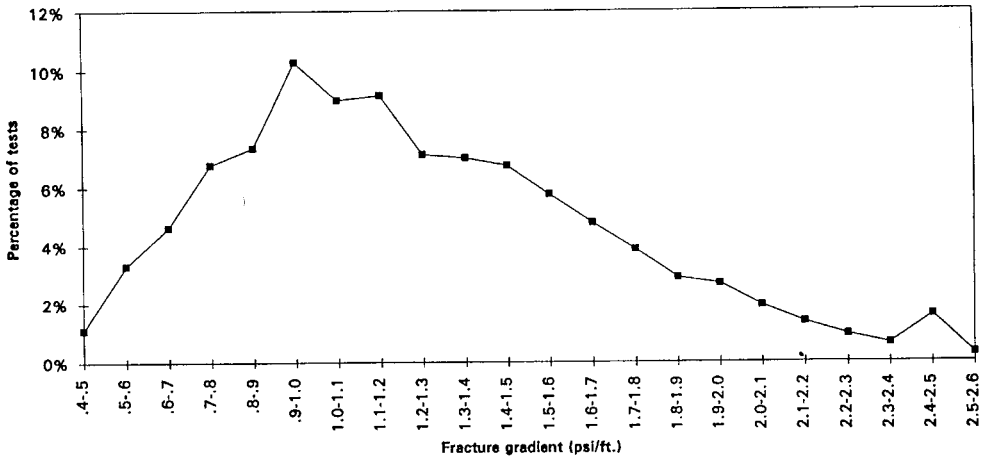

Figure 41B. Frequency plot for pressure gradients from 7658 shallow LOTs on land in Canada.

An analysis of shallow LOTs from SMS offshore has been performed using LOT results from our database, *OffshoreLOT.xls*. The objective was to identify trends in formation strength with depth, an analogical approach to that for deep wells, shown in Figure 42. Then, if trends exist that are similar to those in deep wells, LOT pressure correlations could be used for planning shallow sections of the wells.

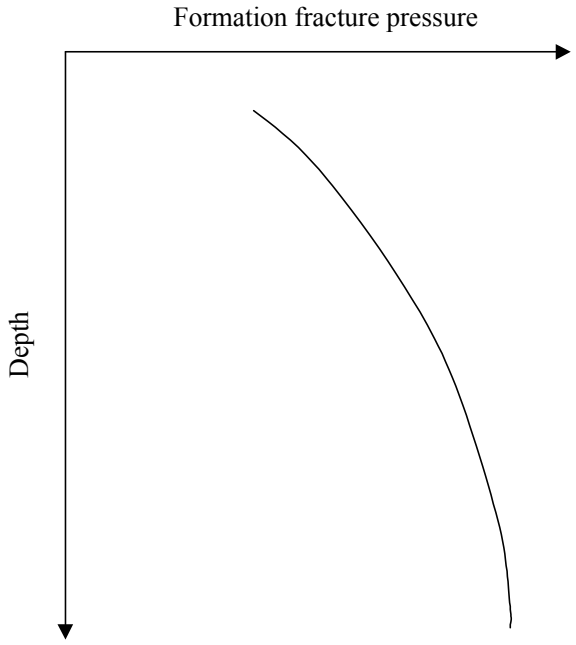

Figure 42. Typical LOT correlation trend for deep wells.

Obviously, a trend line similar to that in Figure 42 would represent a least-square regression fitting of actual LOT data scattered around the line.

The shallow LOT data from SMS that was used in our analysis was grouped for the same drilling areas and the same operators to eliminate geological variation of formation properties and the bias resulting from different LOT analysis procedures. The analyzed data included US Gulf of Mexico (High Island, Eugene Island, West Cameron, Vermillion, South Timbalier, and Main Pass), UK North Sea, and Brazil SES.

We made plots of tested leak-off pressures (LOPs) versus depth. As shown in Figure 43, LOPs are expressed as equivalent mud weight in pounds per gallon (ppg) and depth in feet (ft). For comparison, mud densities are put on the same plot. As shown in the figure, mud density is about 9.2 ppg and LOP is about 12.4 ppg at the depth of 1500 ft. The mud weight is the mud used during the leak-off test. Also, the seawater depth of the well is plotted. For example, the sea water depth is about 450 ft for the well with mud density of 9.2 ppg and LOP of 12.4 ppg.

The analysis of LOT data vs. depth showed a similar large data scatter in all drilling areas considered. At deep depths a fairly good correlation between leak-off pressure and depth (as shown in Figure 42) was evident, while no correlation existed at shallow depths (Figure 43).

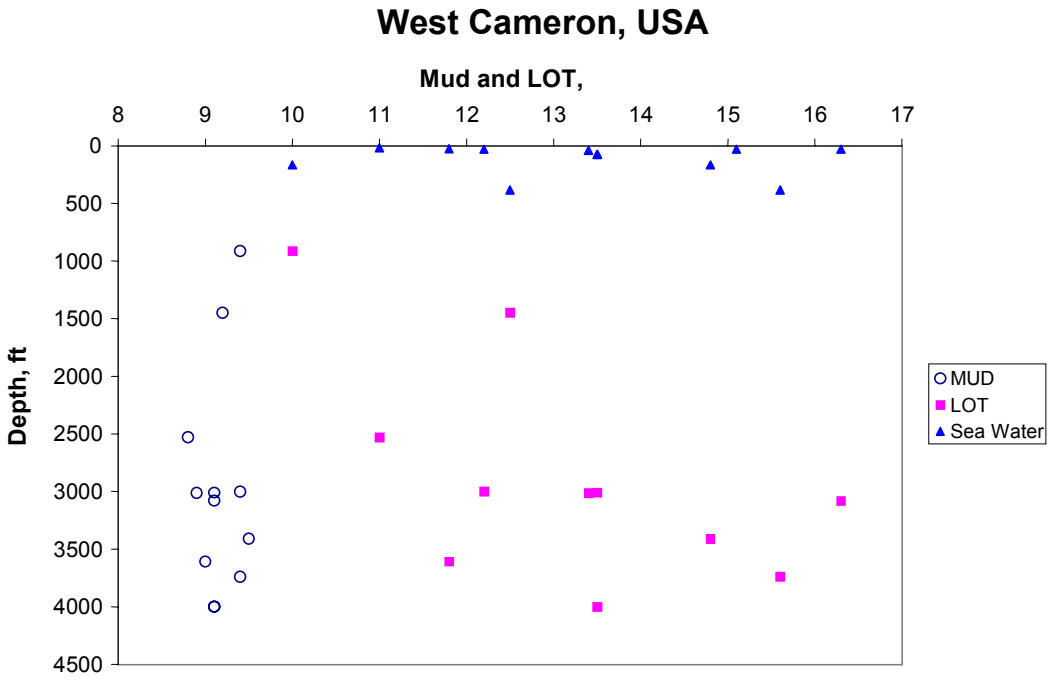

Figure 43. Data scatter from shallow LOTs in SMS.

This observation is demonstrated in Figure 44, where data from deep and shallow LOTs are plotted together. A trend with a small standard deviation could be drawn for the deeper part below 6,000 ft. However, dispersion of shallow data is so large that no correlation or trend could be developed from this data. Thus, we conclude that, unlike deep wells, no generalized fracture gradient correlation could be made for SMS from statistical analysis of LOTs in the area. The reason is that geology-related (overburden, rock consolidation) and drilling-related (cementing, contact stress) mechanisms may control the test and contribute to large data scatter.

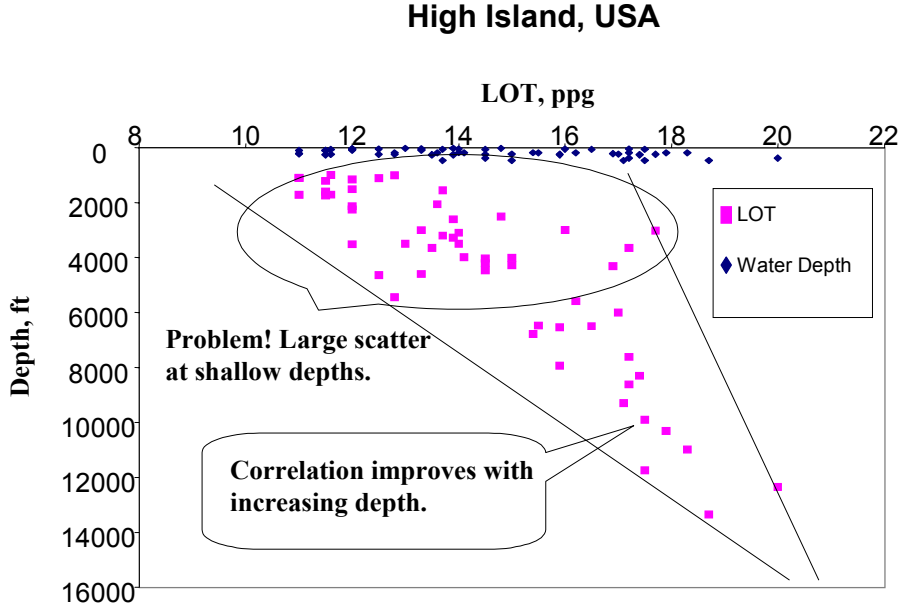

Figure 44. Reduced LOT data scatter with depth.

Figure 45 shows leak-off test pressure in the North Sea area. Again, all the predicted models lose their meaning with the large dispersion of LOT data in SMS.

Another method practiced by some operators is to use the minimum tested leak-off pressure from the depth range for planning the depth of the next well section. Alternatively, operators try to find some "averaged" value of LOT pressure representing all available LOT data from the area. However, for shallow marine sediments, using minimum LOT data is often counter-productive because the data scatter is so great that the minimum pressure gradient might be equal to the equivalent density of mud. Moreover, using an average LOT pressure value may often involve a 50-percent risk of not being able to reach the planned depth of the next well section. All these points are documented in Figs. 46 through 50, below.

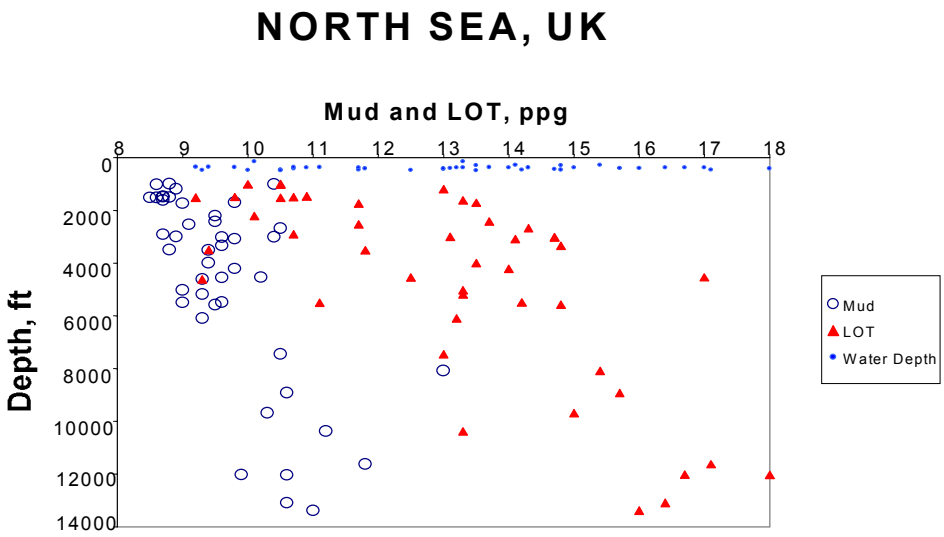

Figure 45. No meaningful correlation of LOT pressure vs. depth (Noth Sea, UK).

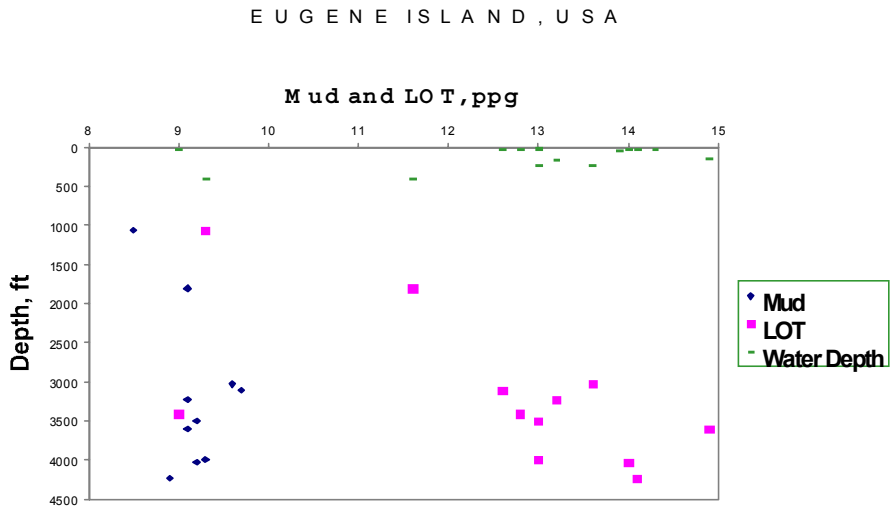

Figure 46. Very large LOT data scatter with no trend for Eugene Island area.

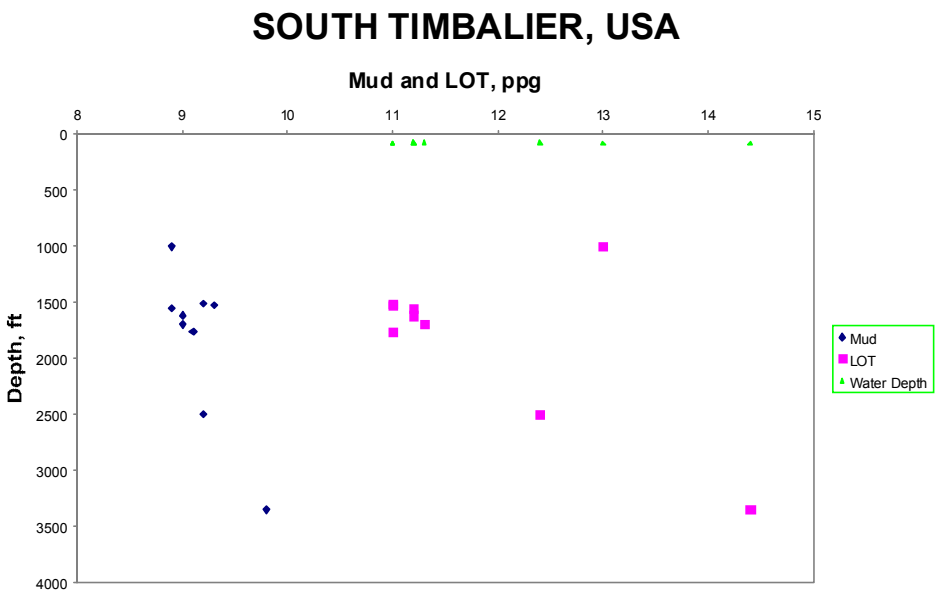

Figure 47. Inconclusive LOT data from South Timbalier area.

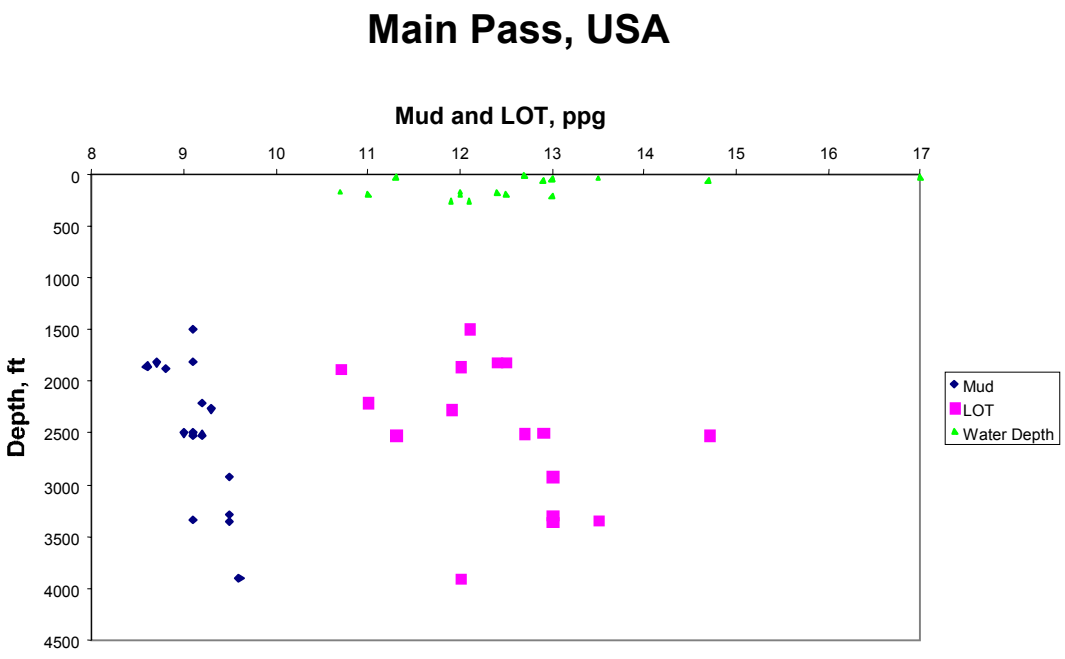

Figure 48. In the Main Pass area, LOT data varies from 11 ppg to 14.5 ppg at 2500 ft.

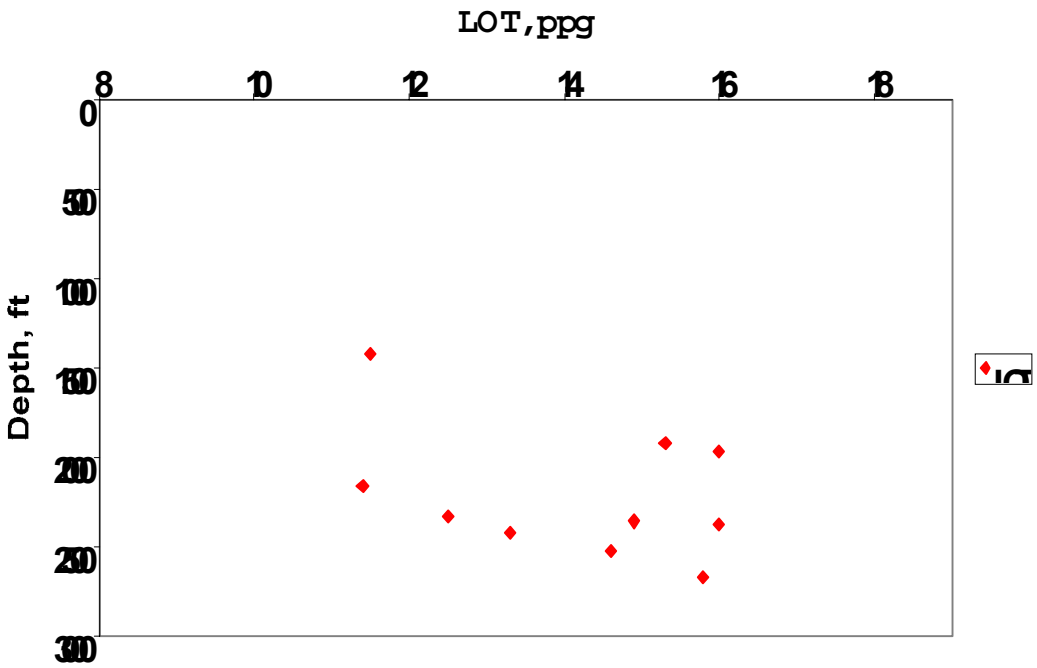

Figure 49. LOT data from offshore Brazil: using LOP=11.5 ppg would be too conservative, while using the average value of 14.2 ppg is too risky.

5. LEAK-OFF TEST MODEL AND SOFTWARE

5.1 Mathematical modeling of LOT in SMS

Conventional modeling of LOT has used a linear relation of pressure versus pumped volume based on the mud compressibility (Chenevert and McClure, 1978). The model proved sufficiently useful in deep well sections with strong impermeable rocks at the casing shoe. Almeida (1986) systematically studied a leak-off test and presented the total compressibility concept, including mud compressibility, wellbore expansion, uncased casing expansion, and filtration. Hazov and Hushudov proposed a similar model in 1993. All these models give a linear relation between pressure and pumped volume that reflects the regular LOT results. Using Darcy's law and assuming pre-existing channels, Altun (1999) modeled a non-linear LOT behavior observed sometimes in deep wells when the casing shoe is set in sand instead of shale.

The LOTs performed in upper sediments, however, display more complex patterns than those for deep wells with generally non-linear plots. The non-linear behavior of LOT is

characteristic for SMS so it could not be explained as the result of pre-existing channels in the cement. Thus, geo-mechanical analysis is needed to build a new model for LOT in SMS.

5.1.1 Wellbore Expansion Volume

In SMS, a plastic zone is generally formed around the wellbore due to the drilling operation. In the plastic zone, vertical stress σ_v reduces significantly from its in situ value to a small value at the wellbore wall (Risnes et al., 1982; Wojtanowicz and Zhou, 1998). Some operators believe that the deformation of a wellbore wall surrounded by a plastic zone is large enough to explain all volumetric implications: the non-linear pressure-volume relation, the large volume pumped, and the volume returned. However, theoretical calculations with finite element analysis proved this concept to be wrong.

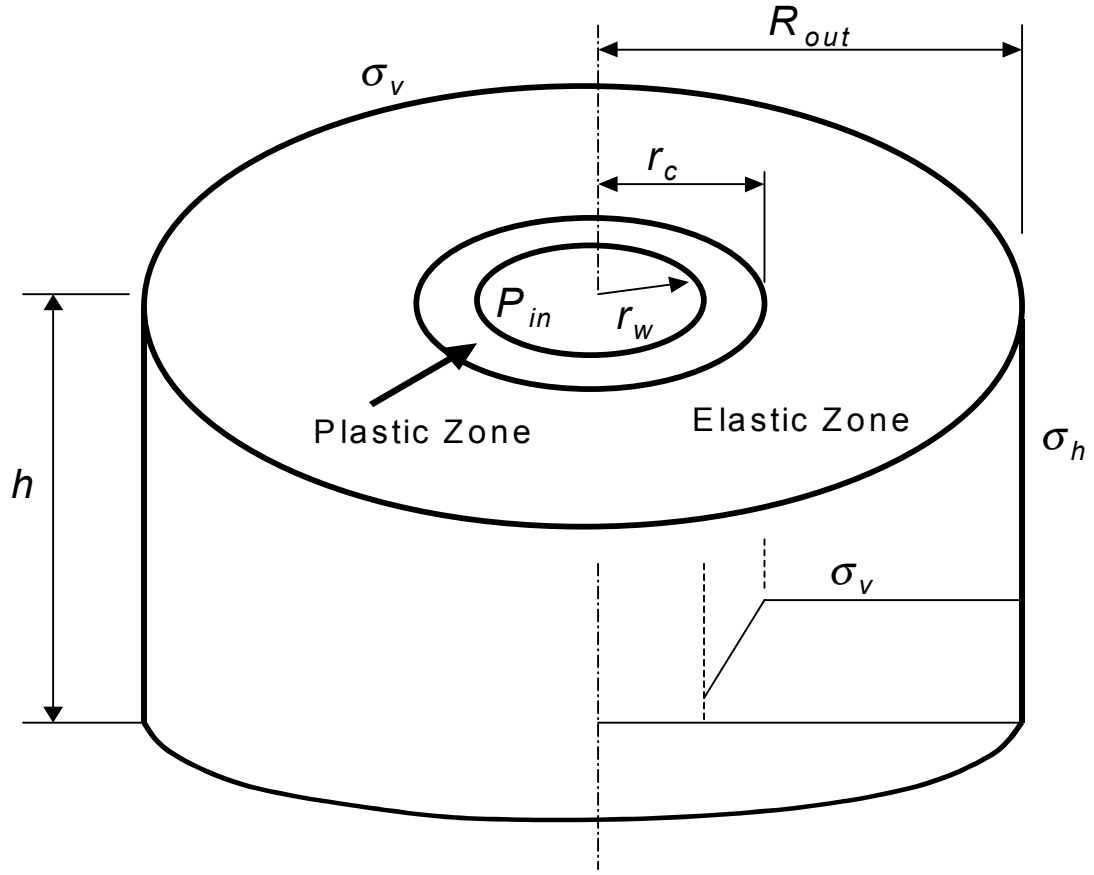

Figure 50. Expansion of the wellbore in a plastic zone is controlled by the outer elastic zone.

Figure 50 is an example of a wellbore with a plastic zone around it. The rock has Young's modulus of 1.04×10^5 psi; Poisson's ratio of 0.3; cohesion strength of 31.6 psi; and internal friction angle of 25.4 degrees. Other dimensions are: r_w=12 in; R_{out}=132 in; and h=60 in. Overburden stress (vertical stress) σ_{z0} is 600 psi; in situ horizontal pressure, σ_h=257 psi; and effective wellbore pressure (the difference between wellbore pressure and formation pore pressure), p_w=0. Based upon the Drucker-Prager yield criterion and associated flow rule (Chen and Han, 1988), the calculated radial size of the plastic zone around the wellbore is r_c=21 inches.

During a simulated LOT (well pressurization), the wellbore wall expanded linearly with increasing wellbore pressure, and the radial displacement of the wall was about 0.109 inches when the wellbore pressure was 600 psi. For comparison, if the same wellbore was in purely elastic state (no plastic zone and no formation fracture), its displacement for 600 psi pressure would be 0.104 inches. Note that plastic displacement was calculated using the finite element method and elastic displacement using this analytical formula (Zhou, 2000):

$$u_w = \frac{3\Delta p_w r_w}{2E} \tag{50}$$

Since the elastic and plastic wellbore deformations are almost the same, we conclude that the effect of the plastic zone deformation on wellbore expansion is negligible. Physically, plasticity means a body can deform easily while its volume is almost constant (Obert and Duvall, 1967; Chen and Han, 1988). There would be no radial displacement if the outside boundary of the plastic zone were fixed. Thus, wellbore expansion depends on the deformation of the elastic zone outside the plastic zone. Therefore, the displacement of a well with a plastic zone should not be much different from that of an elastic well. In conclusion, volumetric wellbore expansion can be estimated by using elastic displacement u_w from Eq. 50 as

$$\Delta V_w = 2\pi r_w u_w H * 12/231 = 0.49 r_w^2 H \Delta P_w / E \tag{51}$$

5.1.2 Well Fluid Loss to Rock

Drilling fluid losses occur either through the mechanism of flow into rock permeability or filtration. Darcy's law is the formula describing the first mechanism as

$$q_{fil} = CA_{fil} p_w \tag{52}$$

where: : = apparent viscosity; p_w = wellbore effective pressure (pressure difference between drilling mud and formation pressures); q_{fil} = flow rate through the wellbore wall; $A_{fil} = \pi d_w \Delta h$ = area of the wellbore section having height Δh and diameter d_w; and C = constant representing rock-mud cake permeabilities and fluid viscosity. Note that pressure p_w increases with time during the leak-off testing pressure increase.

Haberman et al. (1992) measured in situ filtration rate and found that the overall average rate was about 2.0 gal/min (range of 0.8 to 3.2 gal/min). The fluid loss was estimated to be about 5 to 10 times lower than the drilling mud API tests, 100 to 200 lower than the API cement fluid loss from the slurries with fluid-loss additives, and more than 1,000 times lower than the slurries without fluid-loss control. The rate of 0.0002 gal/ft^2/min was the average value. The initial hydrostatic pressure of the slurry column was 0.82*8754=7178 psi, and the pore pressure at 8754 ft was about 3790 psi. An average value of the constant was C=5.9×10^{-8} gal/ft^2/min/psi.

Another fluid loss mechanism is cake (static) filtration. In it, filtration volume is proportional to the square root of time, as

$$q_{fil} = C_w A_{fil} / \sqrt{t} \tag{53}$$

and the wall leak-off coefficient, C_w, is

$$C_w = \sqrt{\frac{k_c \alpha \, p_w}{2v}} \tag{54}$$

where: α = mud cake deposition constant.

5.1.3 Volume of Plastic Fracture

The opening pressure of a horizontal fracture in SMS depends upon the closing stress on the crack and the tensile strength around the tip of the crack The larger the closing stress, the higher the fluid pressure needed to part it. The width of the opened crack depends on the displacements of the crack's two sides which are controlled by the rock's Young's modulus for infinite rock (Sneddon and Lowengrub, 1969).

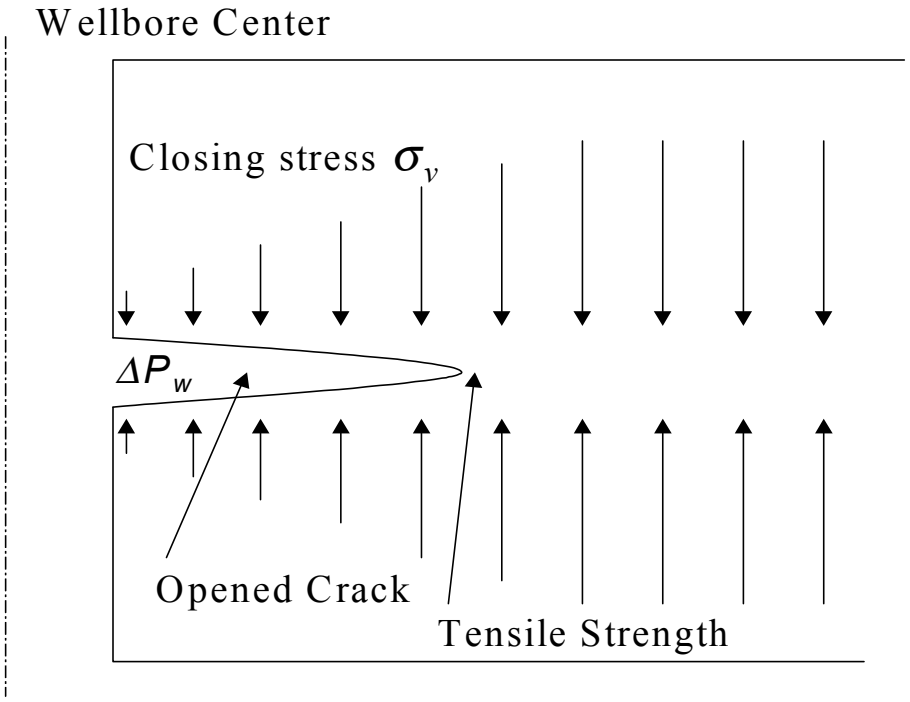

Figure 51. Horizontal non-propagating fracture in the plastic zone around the wellbore.

For horizontal fractures, vertical stress σ_v is the closing stress. Since the vertical stress increases from a small value at the wellbore wall to the overburden stress at the outer (elasto-plastic) boundary of the plastic zone (Figure 50), low wellbore pressures may initiate the fracture but the fracture will not propagate. To make the fracture propagate, wellbore pressure must become equal to the in situ overburden pressure. For the value of wellbore pressure smaller than overburden, fracture in the plastic zone is called a plastic (or non-propagating) fracture (Wojtanowicz and Zhou, 1998).

The plastic fracture extends and widens with increasing wellbore pressure. Eq. (55) gives the relation of the effective wellbore pressure with the space volume in the opened fracture (Zhou, 2000, Appendix D) as

$$\Delta V_{ff}(R) = \frac{1}{110}(R^2 + r_w R - 2r_w^2) w(r_w, R) \tag{55}$$

where: R = radial distance of the fracture tip from the wellbore center; $R \le r_c$, where r_c = radial size of plastic zone (Zhou, 2000, Appendix C, Eq. C-7); and $w(r_w,R)$ = half of the crack width at the wellbore wall (Zhou, 2000, Appendix D, Eq. D-8).

As an example, let us consider a well from the GOP area at a depth of 389 ft below sea bed with the following properties: Young's modulus = 32,915 psi; Poisson's ratio = 0.39; internal friction angle = 17.8; cohesion strength = 10.2; effective overburden stress = 133 psi with a wellbore diameter of 26 inches; and an initial wellbore effective pressure = 0. The size of

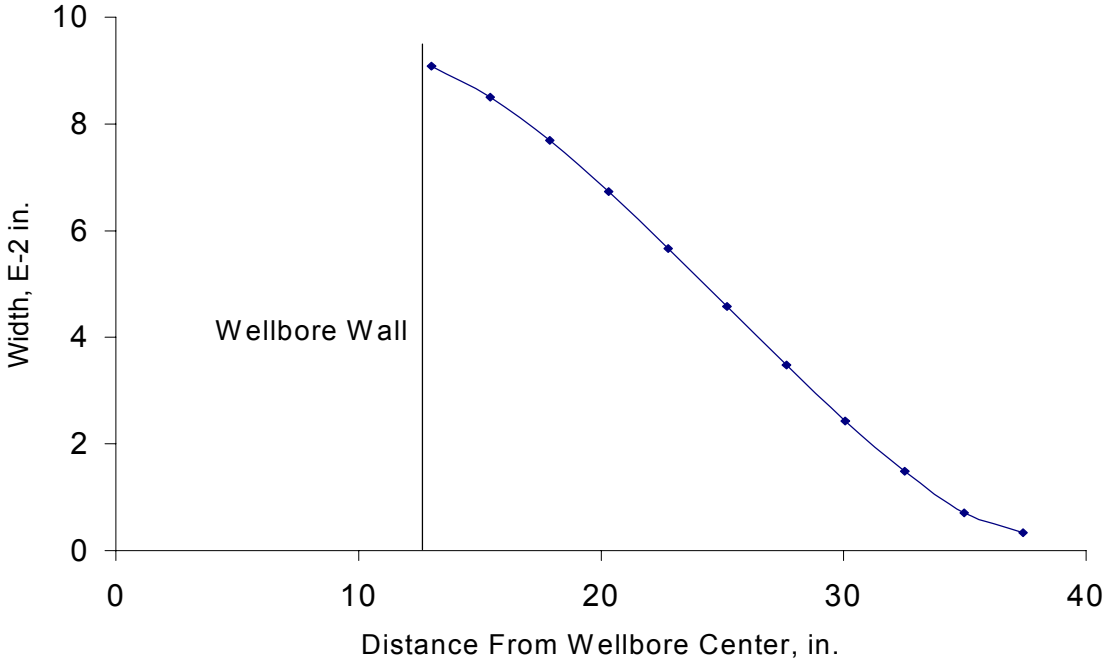

Figure 52. Width of plastic fracture vs. radial distance.

the plastic zone is 37.4 inches away from the wellbore center. The maximum width of a plastic fracture is measured at the wellbore wall when the fracture tip reaches the elasto-plastic boundary and the effective wellbore pressure equals the overburden stress. The distribution of the fracture width along the fracture is shown in Figure 52. A computer program has been written for the width calculations (Zhou, 2000).

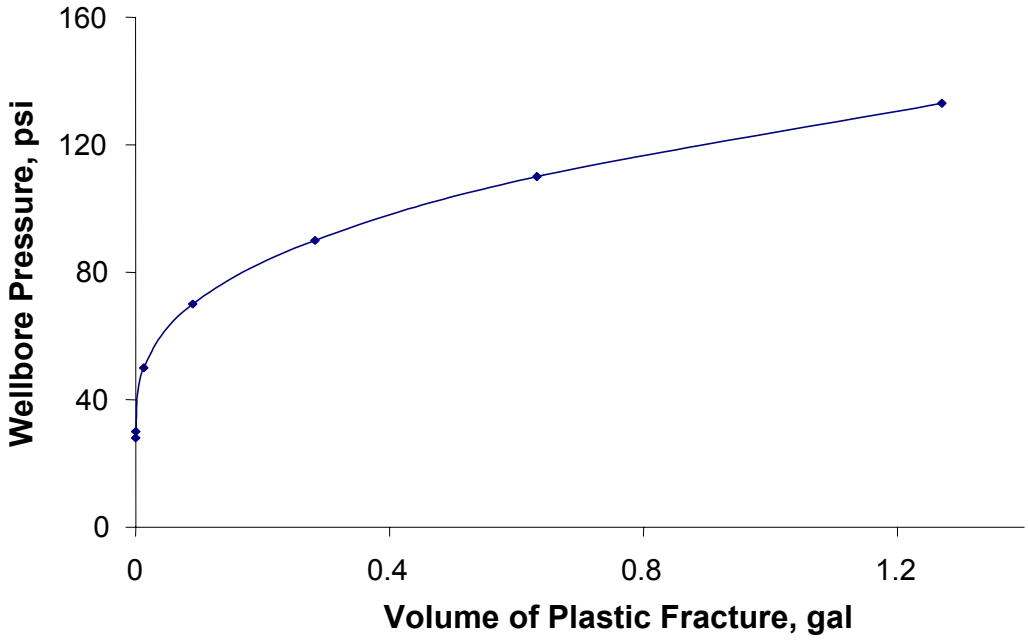

Figure 53. Volume of plastic fracture vs. propagation pressure.

A plot of the effective wellbore pressure versus fracture volume is shown in Figure 53. Maximum fracture width is 0.18 inches, and the maximum volume of fluid filling this fracture is gallons. Also, the fracture initiating pressure is 28 psi. Figure 53 provides evidence that the pressure build-up section of LOT is non-linear for a plastic fracture. However, the fracture volume is extremely small. A plastic fracture will take a larger volume of fluid only for very small values of the Young's modulus *(E)* and/or large size of plastic zone *(R)*. Thus, a non-linear behavior may become significant only when mud leaks off through the newly formed fracture walls to a permeable formation.

5.1.4 Volume of Cement Parting Channel

To date, non-linearity of LOTs has been explained by assuming a pre-existing "cement channel" of certain size and length. The channel supposedly provides a conduit for drilling fluid. Drilling fluid is then supposed to flow or "leak" through the channel to a shallow permeable formation (Poster, 1997; Altun et al., 1999).

Generally, pre-existing channels in cement may result from bad cementing, excessive temperature change, or excessive pressure change inside the casing string (Nelson, 1990). For LOT, however, no high temperature change occurs in the casing string and formation. Also, excessive pressure variation is eliminated by released surface pressure right after setting the top plug during displacing cement. Thus, bad cementing may be the major reason for the pre-existing channels.

Wojtanowicz and Zhou (1998) eliminated the "pre-existence" assumption and proved that cement fracture may be initiated either by LOT or other source of well pressurization at the casing shoe—gas migration, for example. The difference between a pre-existing cement channel and an annular crack is that the cement channel works as a fixed conduit, while an annular crack

must be opened and propagated. The opening mechanism of the annular crack is the same as that of a rock fracturing (shown in Figure 50), with the closing stress equal to the contact stress σ_c between the cement and the rock (Figure 54).

Contact stress is developed during cement setting, and its value can be considered constant across the cement sheath at the same depth. However, tensile strength around a crack tip could depend on the position of the crack within the sheath explained below.

As shown in Figure 54, Crack 1 is the crack between the casing and the cement. Its tensile strength depends on the bonding between the cement and the casing. Crack 2 is in the cement, and its tensile strength is the tensile strength of the cement. Crack 3 forms between the cement and rock. The connection between the cement and the rock is most likely the weakest of the three. Thus, the annular crack will propagate along this surface. The relation between wellbore pressure and volume of the annular crack (Zhou, 2000, Appendix B) is

$$\Delta V_{cem} = \frac{r_w^4 (p_{LOT} - \sigma_c)^3}{E^2} \left(\frac{1}{\frac{\mu_p q E^2}{8262 (p_{LOT} - \sigma_c)^2 r_w^2} + \frac{\tau_y r_w}{75}} \right) \tag{56}$$

For example, let us assume that a mud having plastic viscosity of 40 cp and a yield point of 15 lbf/100 sq ft is pumped into a 26-in well during LOT at a rate of ¼ bbl/min. Also, Young's modulus of the rock is 32,915 psi, total compressibility is 52 gal/psi, and initial effective wellbore pressure and contact stress are zero. The calculated results are shown in Figure 55. The cement-rock parting obviously makes the pressure-volume relation non-linear.

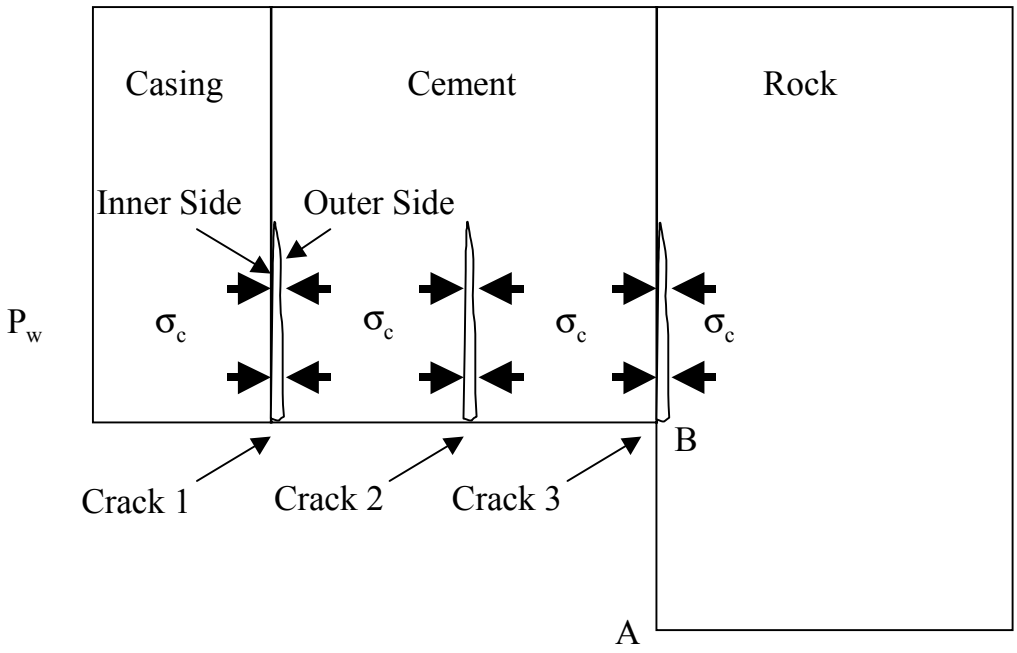

Figure 54. Annular cement parting crack is opened by well pressurization.

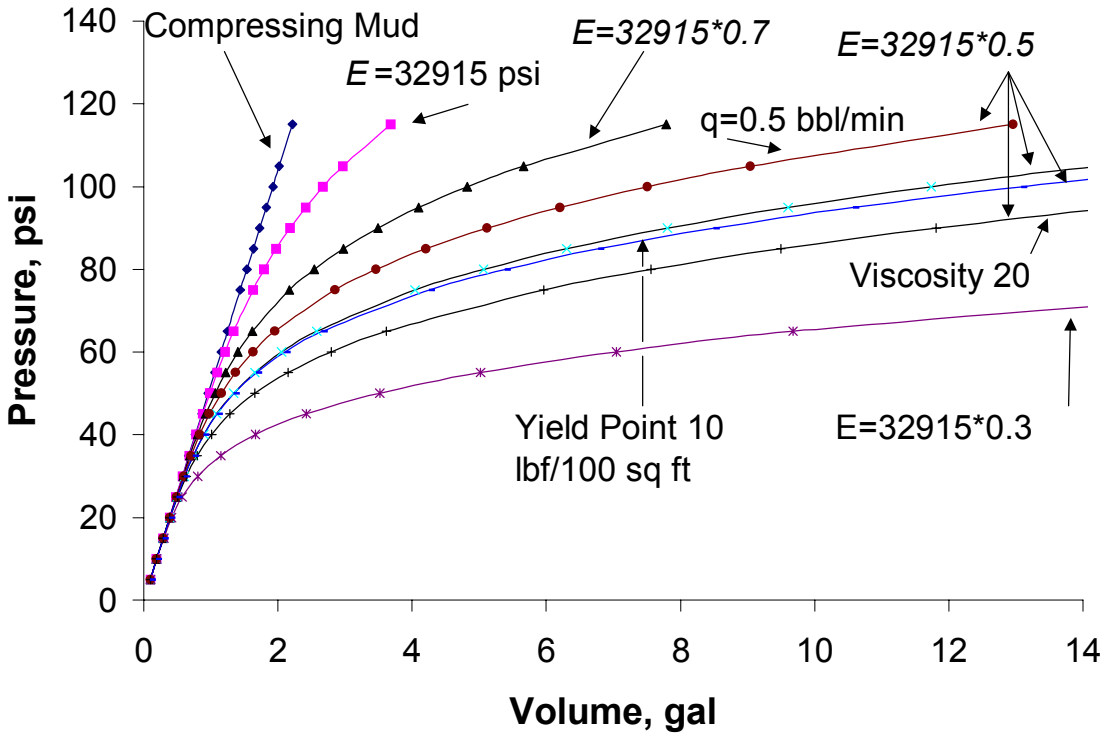

Figure 55. Non-linearity of annular crack volume vs. pressure.

Young's modulus of the rock strongly affects the non-linear behavior. The smaller the Young's modulus is, the more convex the pressure-volume plot becomes. Furthermore, pumping rate, plastic viscosity, and yield point of the mud also affect the curvature of the plot.

The assumed value for contact stress in Figure 55 is zero. However, the effect of contact stress can be easily estimated by shifting the plots in Figure 55 upwards along the "compressing mud" line by the value of contact stress.

5.1.5 Leak-off Test Model

By combining the volumetric effects described above, a mathematical model for the leak-off test has been developed to describe the relationship between well pressure and mud volume pumped. The model is formulated as follows:

Let us consider an annular mud element V_i and relate its volume reduction ΔV_i to increased pressure Δp_i using the fluid compressibility equation:

$$C_{mi} = \frac{1}{V_i}\frac{\Delta V_i}{\Delta p_i} \tag{57}$$

where: C_{mi} = compressibility (1/psi) of the mud in element V_i .
Also, total mud volume V_0 is the sum of all elements,

$$V_0 = \sum_{i=1}^{n} V_i = \sum_{i=1}^{n} \frac{\Delta V_i}{C_{mi} \Delta p_i} \tag{58}$$

where n is the total number of elements. If mud compressibility is constant for all mud elements in the well (no air effect, constant mud density) and mud friction in the well is negligible, the cumulative volumetric effect ΔV_p of the pressure change Δp can be expressed as

$$V_0 = \frac{\Delta V_p}{C_m \Delta p} \tag{59}$$

where ΔV_p is the volume pumped into the well, provided the wellbore is rigid and there are no fluid losses. Thus,

$$\Delta p = \frac{\Delta V_p}{C_m V_0} \tag{60A}$$

Equation (60A) implies that well pressure change is proportional to pumped volume and inversely proportional to total mud volume and mud compressibility. This equation is the basic one used by Chenevert and McClure (1978) to model the leak-off test. However, for an actual well, not all the pumped mud is used to compress the whole mud system. Part of the pumped volume is lost to the rock permeability/filtration, another part flows into the opened fracture, while yet another part expands the wellbore. Wellbore expansion includes volumes of casing expansion ΔV_{cas} and open hole expansion ΔV_w. The lost volume includes filtration ΔV_f (Almeida, 1986; Hazov and Hurshudov, 1993; Altun et al., 1999) and the volume of cement parting ΔV_{cem} and formation fracture ΔV_{ff}, as discussed above. The cement parting and plastic fracture open new rock surface area for drilling fluid flow/filtration. The two new filtration terms are expressed as ΔV_{cemf} for the filtration volume through parted cement surface, and ΔV_{fff} for the leak through the surface of the horizontal plastic fracture.

A complete pressure-volume relationship (pressure build-up section of the LOT plot) is

$$\Delta P = \frac{\Delta V_p}{C_m V_0} - \frac{\Delta V_{cas}}{C_m V_0} - \frac{\Delta V_w}{C_m V_0} - \frac{\Delta V_f}{C_m V_0} - \frac{\Delta V_{cem}}{C_m V_0} - \frac{\Delta V_{cemf}}{C_m V_0} - \frac{\Delta V_{ff}}{C_m V_0} - \frac{\Delta V_{fff}}{C_m V_0} \tag{61}$$

The first term in Eq. (61) represents the compression of the whole mud by the pumped mud volume. The term gives a linear relation between the increased pressure and the pumped volume. The second term can be neglected for cemented casing strings because casing expansion is constrained by cement and formation and thus the expansion volume is almost zero. The third term represents expansion of the open-hole section below the casing shoe. The pressure-volume relation of this term is also linear according to Eq. (53).

The fourth term in Eq. (61) accounts for mud loss into the rock. It may be represented either by a smooth curving relation based on Darcy's law (Altun et al., 1999) or a linear relation if the effect of mud cake is considered (Almeida, 1986). The fifth term represents the effect of cement-rock parting and gives a smooth curving pressure-volume relation starting from some

lower wellbore pressure, as shown in Figure 55. The last term in Eq. (61) also gives a smooth curving relation, representing the effect of a non-propagating plastic fracture (Figure 32). (It has been already proved that the fracture can be initiated at a well pressure much lower than the overburden pressure.)

5.2 LOT Simulation Software

A software package (LOTUMS) has been developed for leak-off test simulation in shallow (upper) marine sediments. The software has been written in Microsoft Visual Basic 6.0. The software is based upon the mathematical model presented above.

Installation and use of the software is explained in Appendix B. Potential users are expected to be familiar with Microsoft Windows and understand principles of borehole mechanics. Shown in Figure 35 is the software main interface. Functions of the software are provided in the menu on the top of the window. The software provides a set of default data. Users may use the default data to complete analysis during learning period. During actual LOT analysis, users may enter all the needed data by modifying the default data. To study the effects of some factors, users may change only one or a group of data and analyze the results.

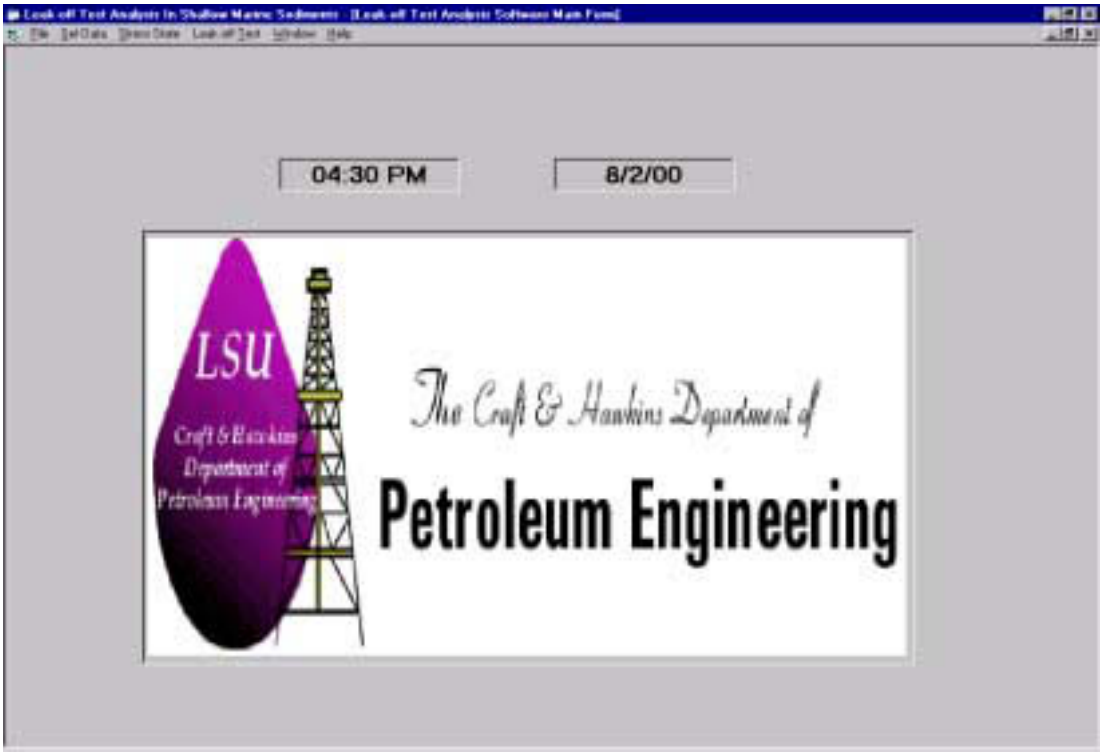

Figure 56. Leak-off test software main interface.

The software input data has been organized in four screens: well and casing; mud and LOT; cement slurry; and rock. For example, Figure 57 shows the mud and LOT screen.

The important initial calculations prior to LOT analysis are the stress status of the formation, wellbore pressure, and formation pore pressure. Figure 58 shows the screen for stress analysis, *Leak-off test Analysis in Shallow Marine Sediments- Stress Analysis Results*.

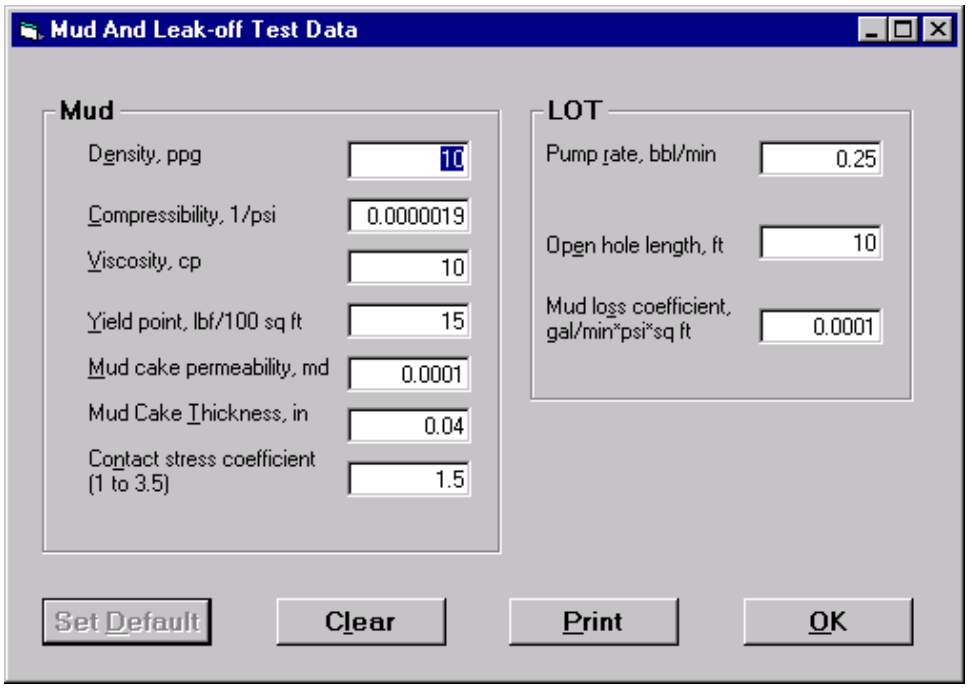

Figure 57. Main data input screen.

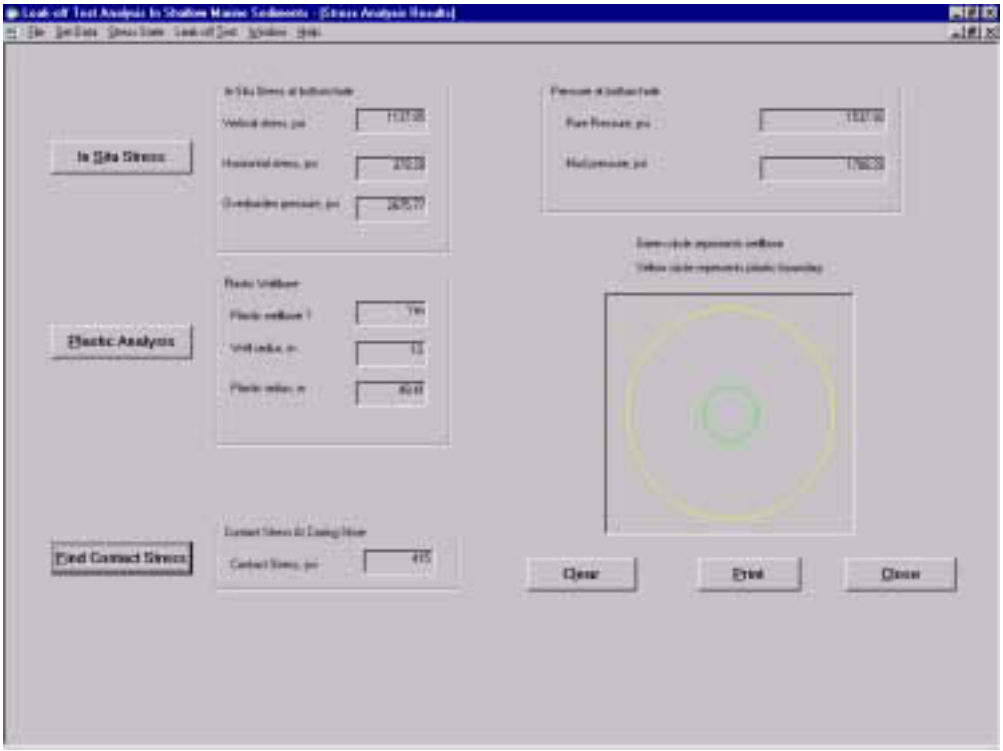

Figure 58. Initial stress analysis screen.

On this screen, the command button, *In Situ Stress,* initializes the stress module of the software that calculates the in situ stress of the formation and displays the results in the three windows next to the button. Another module, controlled by the button labeled *Plastic Analysis* performs elastic-plastic stress analysis of the well and displays the results in the three windows next to the button. An appropriate plot is developed to display the stress analysis results. The button labeled *Find Contact Stress* controls another important module for stress analysis. The module performs cement slurry analysis and calculates the contact stress between cement and rock.

The *Clear* button on the stress-analysis screen (Figure 58) clears all the results and plots on the screen for further analysis. Another button, *Print*, sends the results to a printer. If no printer is connected to the user's computer or if the user wants to use another printer, he may use the main data screen menu function, *Print,* to select the printer, as shown in Figure 59.

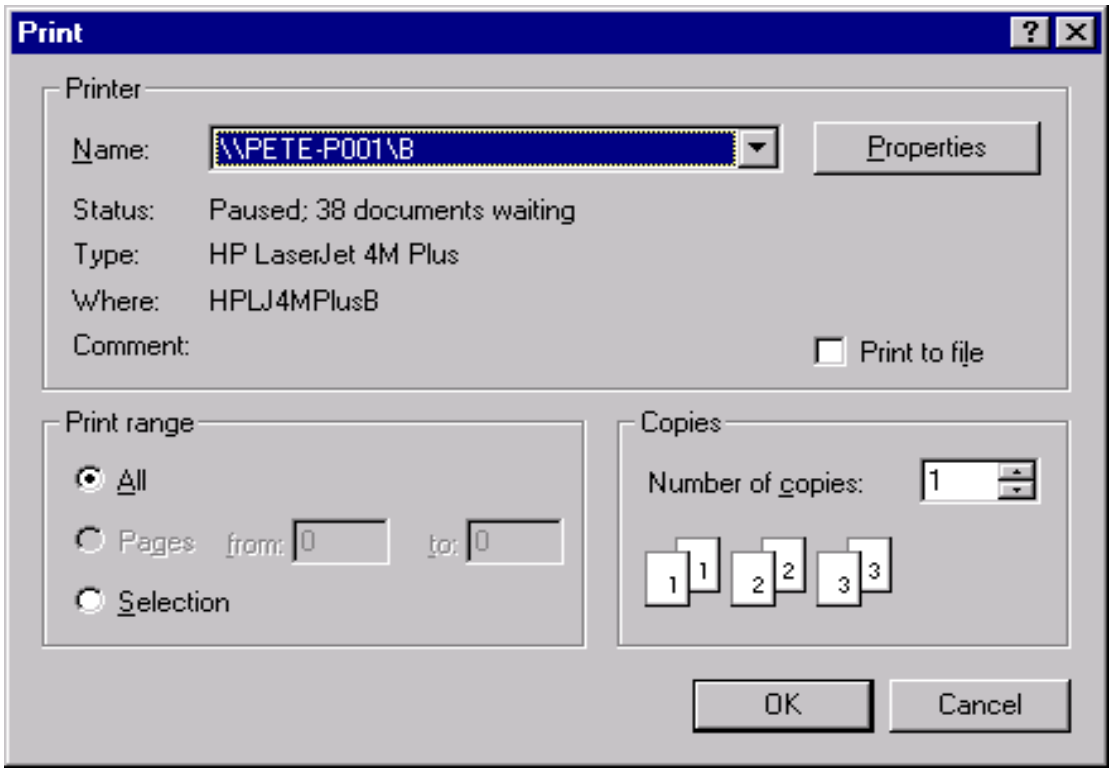

Figure 59. Selecting a printer.

Figure 60 shows the interface screen of the fracture-analysis module. On the screen, the *Fracture Analysis* and *Fracture Shape* buttons are used to perform the analysis and show the results and graphics on the screen.

The *Leak-off Test Analysis* screen in Figure 61 controls the LOT simulator module. Two sets of dialog boxes are displayed, *LOT Contribution Mechanisms* and *View LOT*. The LOT mechanism set allows the user to perform a sensitivity study of the test result for individual (or combined) mechanisms contributing to the LOT response. The *LOT Curve Color* boxes give different colors to the plots drawn from the LOT analyses. The *View LOT* button summarizes the whole analysis by making a conventional pressure-volume plot similar to those prepared by field engineers.

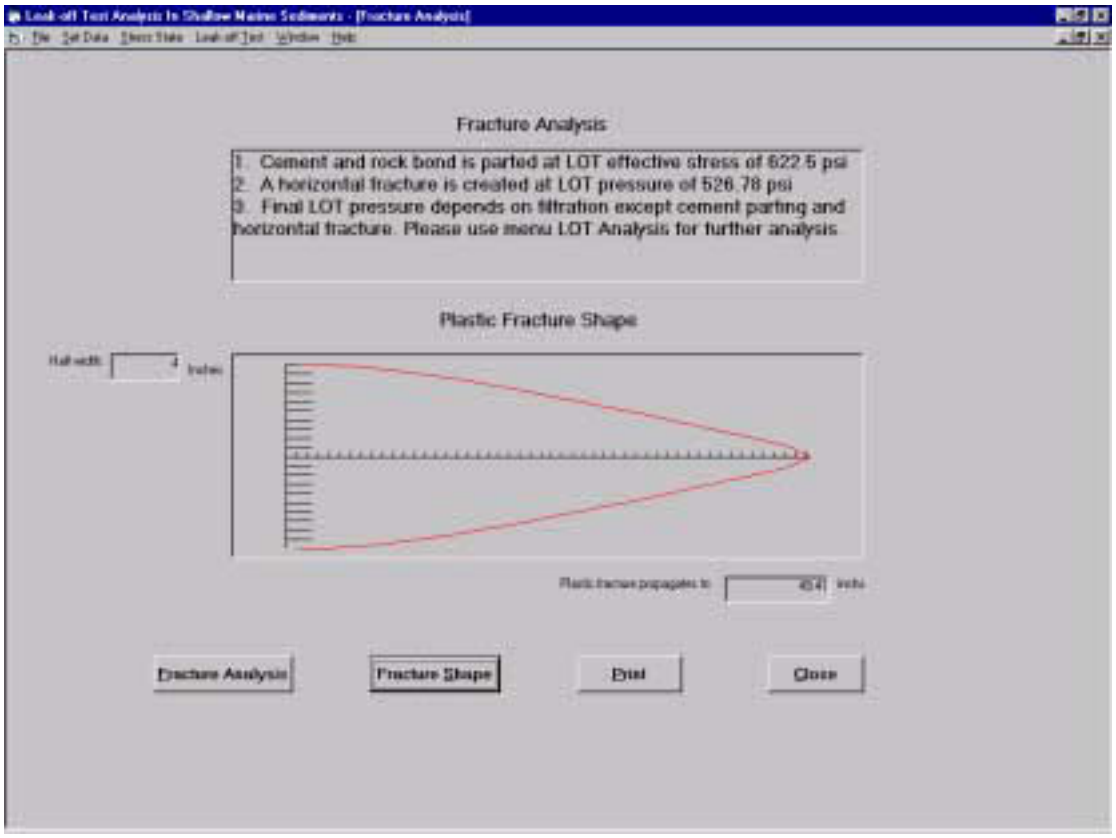

Figure 60. Fracture analysis screen.

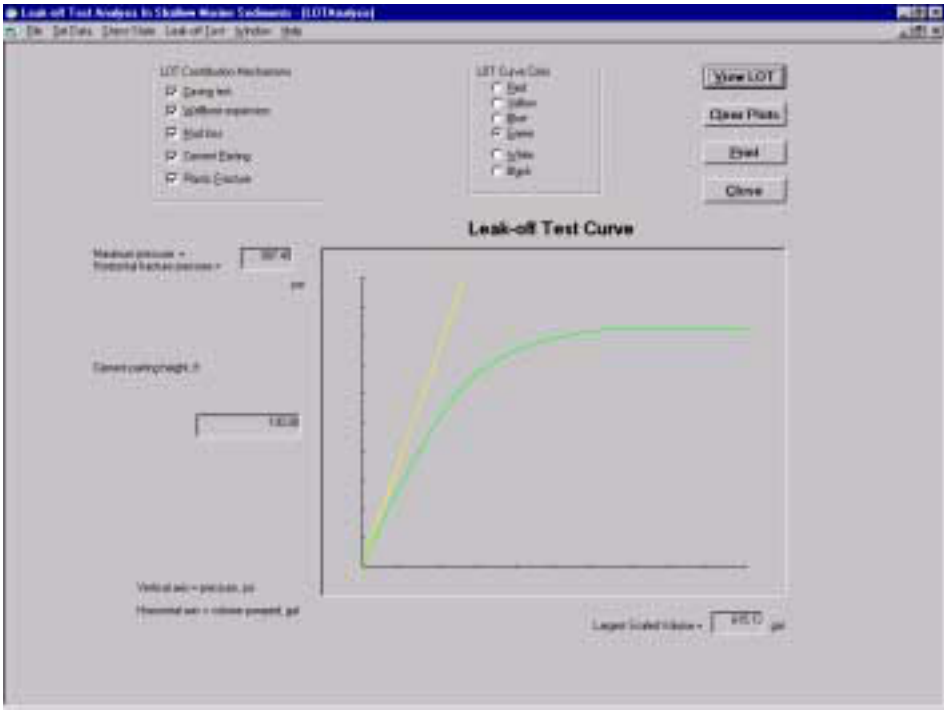

Figure 61. Leak-off test analysis screen.

5.3 Use of LOTUMS Software for Simulation Studies

This section presents examples showing how to use LOTUMS for studying various mechanism affecting LOTs in SMS. It also familiarizes potential users with the software.

To start the software, double click the icon of LOTUMS or LOTUMS.exe in the software directory. An information window appears as shown in Fig. 62, and the software file is opened. Legal users click the "Yes" button to enter the software. The "No" button is provided to exit the system. The underline letter is provided for users operating without the mouse. They should press simultaneously the "Alt" button on the keyboard and the underlined letter. For example, pressing "Alt+Y" is equivalent to clicking the "Yes" button with the mouse.

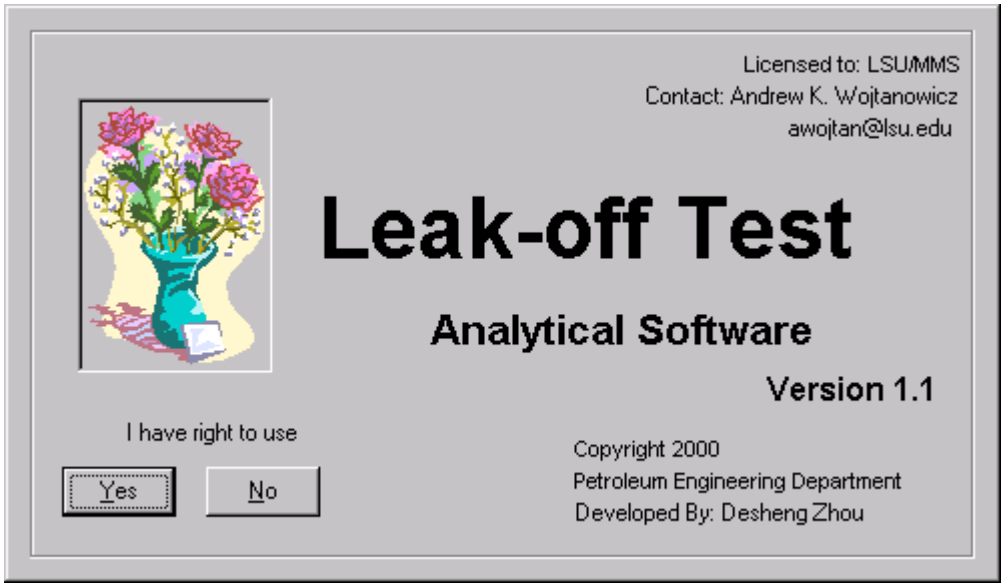

Figure 62. Starting LOTUMS.

The main screen, Fig. 63 gives the date and time and provides menu bar and the software's name. The menu comprises options: File, Set Data, Stress State, Leak-off Test, Windows, and Help. (Again, "Alt" key plus the underline letter key letter could be used instead of mouse'es left button to open menu options).

The "File" menu contains "Set Printer" and "Exit" functions. The "Set Printer" function helps to set up a printer if one wants to print out analytical results. The "Exit" function terminates the software and returns to the main screen. The "Window" menu enables multi-screen operation in various formats; "Cascade", "Tilt Horizontal", and "Tilt Vertical." The

"Help" menu provides simple information on using the software. Users familiar with Windows can use the software without "Help."

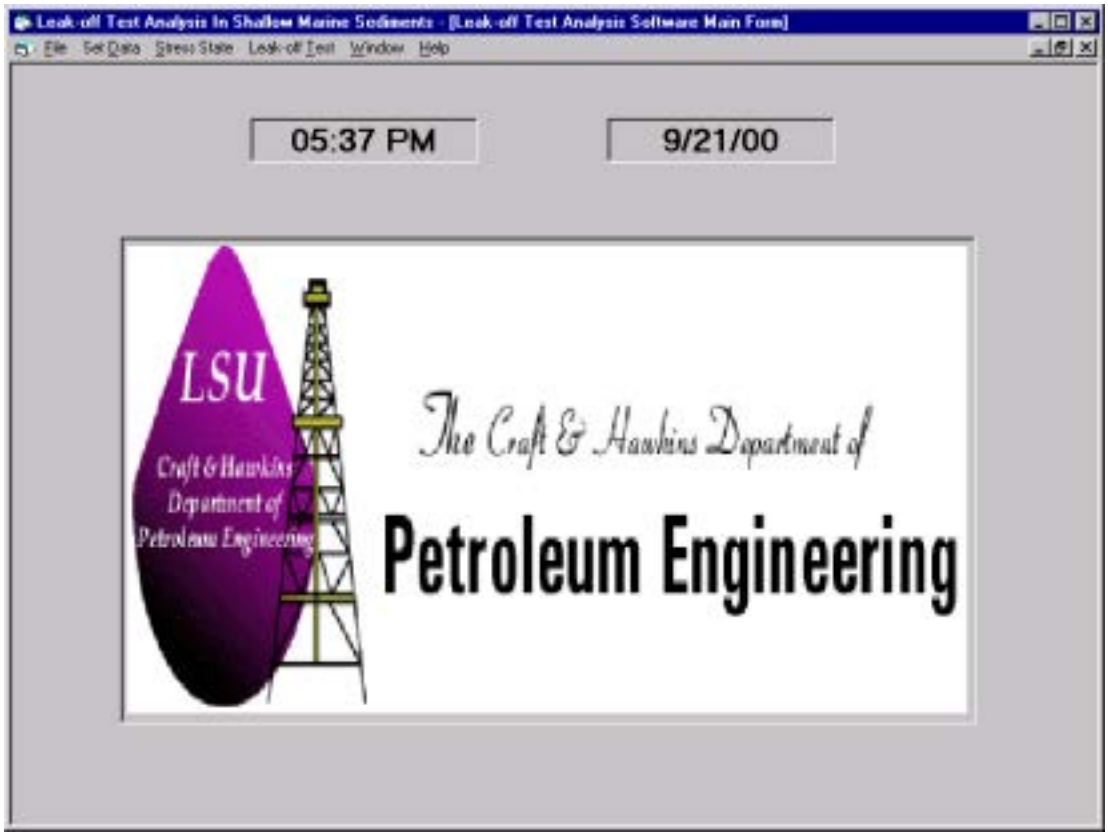

Figure 63. Main screen of LOTUMS.

5.3.1 Data Input

Input data for LOTUMS is organized as geology-specific and well-specific in four screens: Well and Casing String, Mud and Leak-off Test, Cement Slurry, and Rock. The use of these screens is demonstrated using data from a real well. The well was drilled offshore with water depth of 387 ft. Sea water density was 8.6 ppg. Elevation of kelly bushing (KB) above sea level wass 95 ft. The top well section was drilled with 26-in bit and a 20-in. conductor casing string was set at 3,439 ft below kelly bushing.

Well and Casing Data. To input the data, open the Well and Casing String Data screen in the Set Data menu, Fig. 64, input the following data:

In the "Well"section:

Diameter - enter well diameter, 26 in.;
Depth below KBm - enter depth of casing shoe, 3439 ft;
KB above sea - enter 95 ft;
Sea water depth - enter 387 ft;
Sea water density: enter 8.6 ppg.

In the "Casing" section:

Outside diameter - enter 20 in;
Inside diameter: enter casing ID = 18.73 in;
Young's modulus: enter steel modulus 30E6 psi;
Casing string length: enter the calculated value: 3439-95-387=2957 ft.

Once the screen was filled with data press "OK" button to accept the input data. If one wants to correct some data after hitting "OK" button, he needs to fill out the screen again from the "Set Data" menu. One may choose "Set Default" button to use default data and change some values according to his needs. Default data are provided as an example and they are useful for learning and demonstrating the software. Default data for the four input screens could be set by clicking "Set All Default" in the "Set Data" menu, or the "Set Default" command in each input screen. Also, note that the "Clear" button clears all the data in the screen and the "Print" button prints the screen content on the printer selected in the "Set Printer" screen.

Hidden submenus are provided for the four data screens. Using the right button of one's mouse and clicking at any place within the window will show the submenus. The submenus are the same as the command button on a form as "Set Default", "Clear", "Print" and "OK". The submenus provide shortcut to handle data screens.

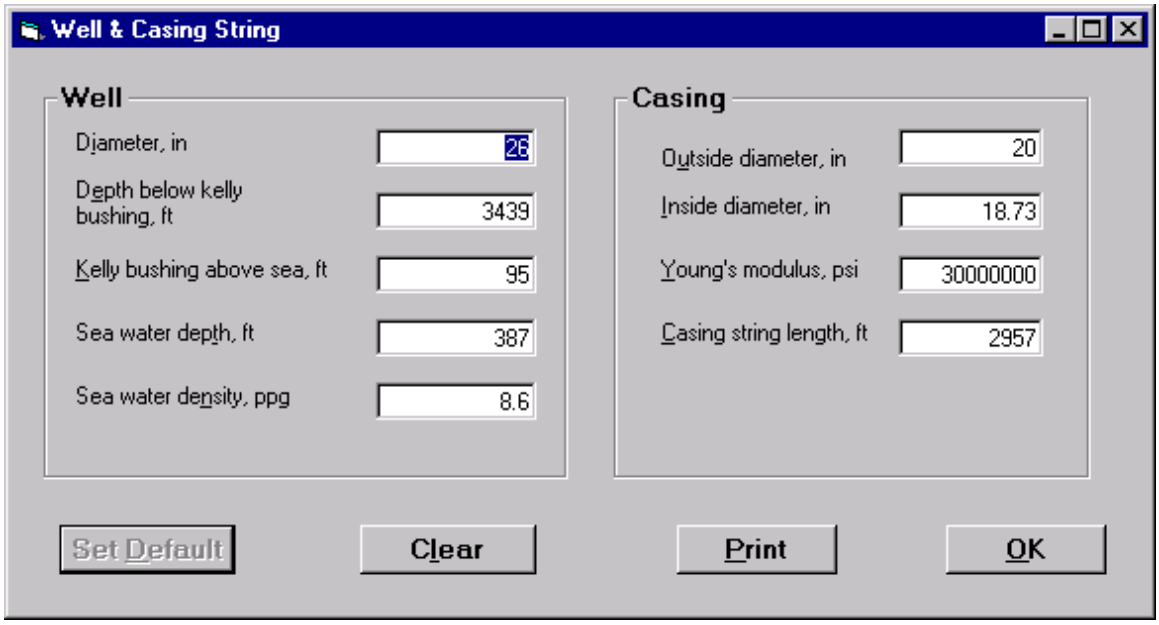

Figure 64. Well and Casing String screen with example input data.

Mud and Leak-off Test Data. In the example well the drilling mud used for the leak-off test has density of 10 ppg, compressibility,1.9E-6 1/psi, plastic viscosity, 15 cp, and yield point, 5 lbf/100 sq ft. The data fills out the Mud section in Fig. 65 leaving the values of mud compressibility and contact stress coefficient to complete this section.

If mud compressibility is unknown, it can be estimated as,

$$C_{mud} = C_w f_w + C_o f_o + C_s f_s$$

where: c_{mud} , c_w, c_o, c_s, stand for mud, water, oil and solids compressibility, respectively; and, *fw, fo, fs* are volume fractions of water, oil, and solids the mud, respectively. Typically, water compressibility is 3.0E-6 1/psi; oil compressibility, 5.0E-6 1/psi; and solids compressibility, 0.2E-6 1/psi.

Contact stress coefficient is a wellbore parameter determined by the mud and rock interaction at the casing shoe. Its value be estimated using LOT data from offset wells. Contact stress coefficient is a major factor controlling the cement-rock parting. Here, it's value is assumed as 1.5.

The LOT section data in Fig. 65 includes pump rate, open-hole length and mud loss coefficient. During the LOT operation in the example well, drilling mud was pumped at a rate of ¼ bbl/min into a newly-drilled 10-ft open-hole section below the cemented wellbore. Mud loss coefficient is a major factor of mud filtration through pre-existed channels and fractures or rock pores. Its value could also be estimated from offset LOT data. In the example, it's value is assumed as 0.0001 gal/min*psi*sq ft.

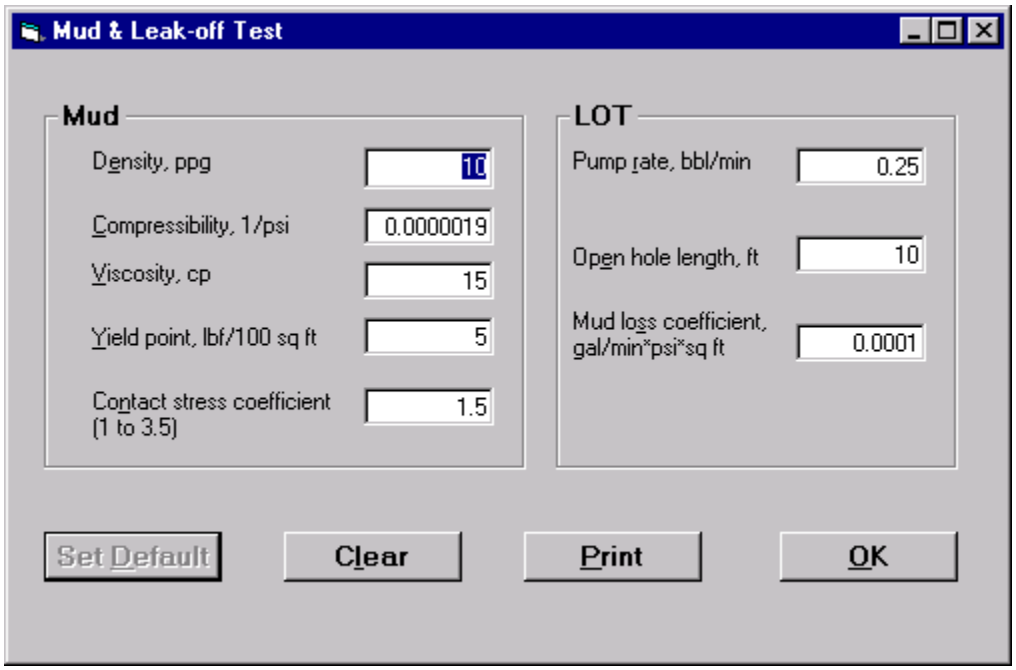

Figure 65. Mud and Leak-off Test screen with example input data.

Cement Slurry Data. In the example well, density of the lead cement slurry was 13.2 ppg and the lead slurry section length in the annulus was 2465 ft. Also, a batch of tail cement slurry with density of 15.8 ppg and height of 492 ft was placed in the annulus after pumping the lead slurry that was displaced to the sea floor. The casing was cemented 29 ft off-bottom. After slurry setting, the top cement level dropped 50 ft. The average slurry compressibility was 2E-6 1/psi. (Similarly to mud, the compressibility of cement slurry can be estimated from the slurry composition.) The Cement Slurry screen in Fig. 66 demonstrates this data input.

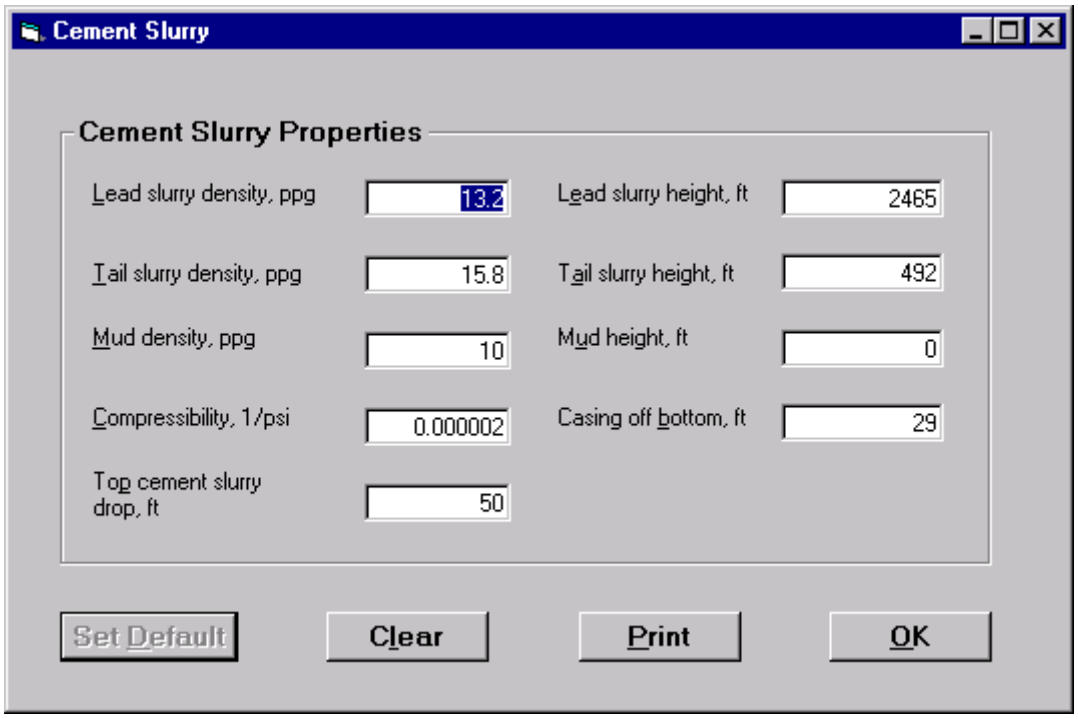

Figure 66. Cement Slurry screen with example input data.

Rock Data. Rock properties for the open-hole section below the casing shoe are input into the Rock screen, shown in Fig. 67, to calculate rock deformation and fracturing. The rock at the casing shoe of the example well has Young's modulus of 2E5 psi, Poisson's ratio, 0.25, cohesive strength, 10 psi, friction angle, 15 degree, and temperature, 100 deg F. The average bulk density of the overburden rock above the casing shoe is 16 ppg, with pore water density of 8.5 ppg.

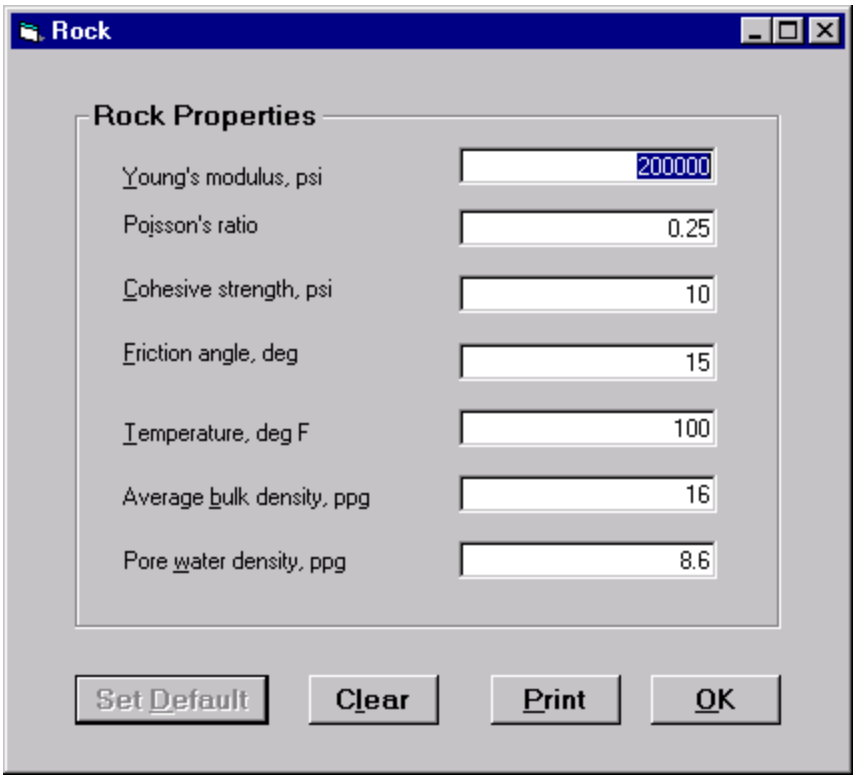

Figure 67. Rock screen with example input data.

5.3.2 Stress Analysis

The LOTUMS software provides analysis of stresses in the Stress State menu item of the main screen. After clicking on the "Stress State," a stress-analysis screen pops up, as shown in Fig. 68. Three command buttons are provided in the Stress Analysis screen, In Situ Stress, Plastic Analysis, and Find Contact Stress. Also provided are the buttons of Clear, Print and Close. Clicking on the In-situ Stress button gives calculated values of vertical stress, horizontal stress, and overburden pressure at the casing shoe. Also calculated are the mud pressure and pore pressure at the casing shoe. These results are shown in Fig. 68.

Clicking on the Plastic Analysis button gives the information whether (or not) the wellbore is in a plastic state of stress, together with the size (radius) of plastic zone around the well and a graph of the wellbore and plastic zone around it. Finally, clicking on the Find Contact Stress button gives the calculated value of contact stress at the casing shoe.

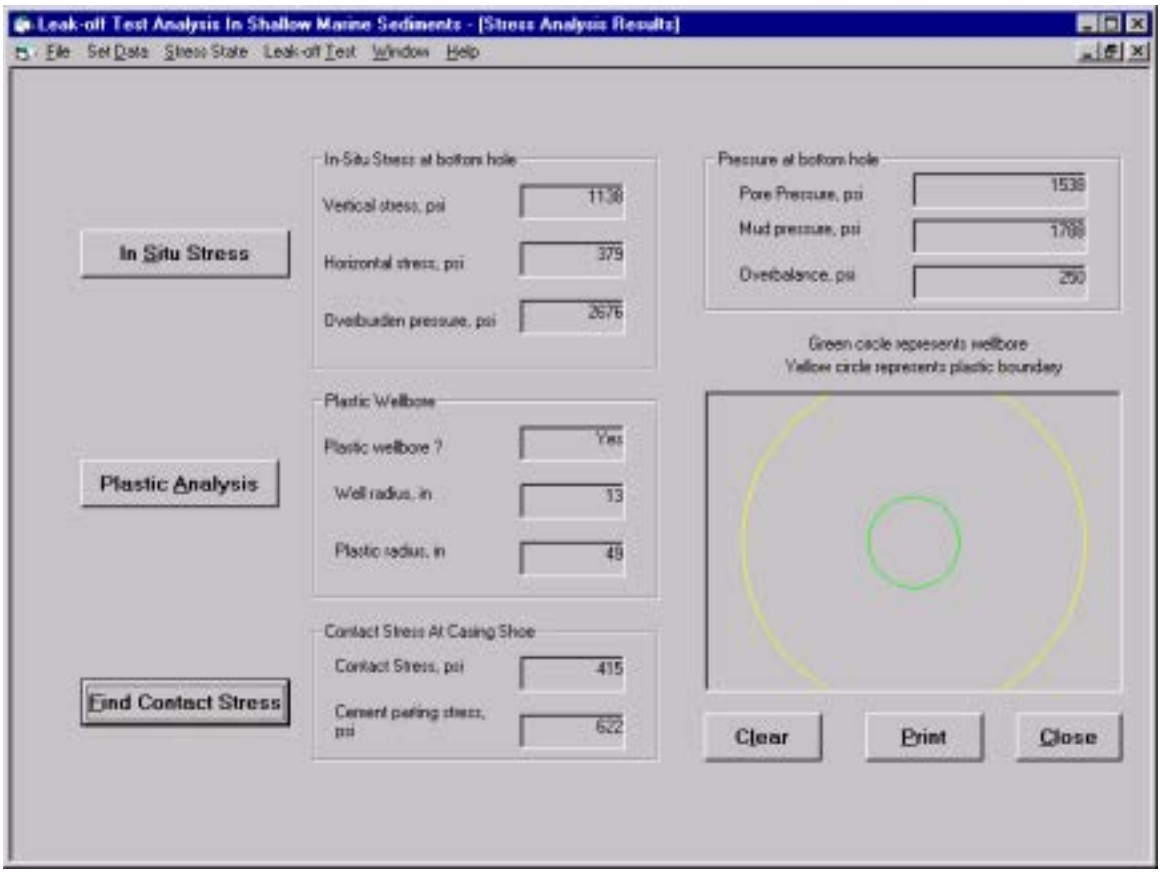

Figure 68. Stress analysis screen with example output data.

5.3.3 Fracture Analysis

The borehole failure analysis is performed from the main menu by choosing the "Leak-off Test"option. There are two types of analysis under this option, "Fracture Analysis" and "LOT Analysis". Selecting "Fracture Analysis" gives the fracture analysis screen shown in Fig.69.

There are five command buttons in this screen, Fracture Analysis, Fracture Shape, Clear, Print and Close. The Clear button clears the screen windows. The Print button sends the screen content to the printer. The Close button terminates the analysis.

Clicking on the "Fracture Analysis" button delivers a description of wellbore failure to the text window on the top of the form. After clicking on the "Fracture Shape" button a plot of the horizontal plastic fracture appears in the central window if the screen. Also, the two small windows display with and length of the horizontal fracture when the fracture propagates to the plastic-elastic boundary.

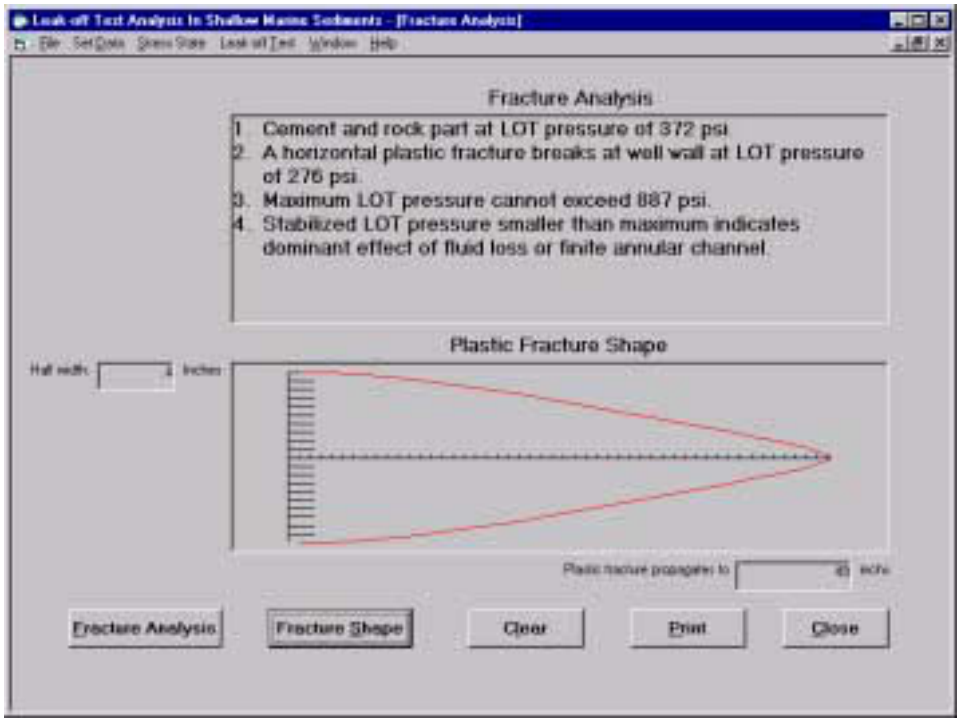

Figure 69. Fracture analysis screen with example output data.

5.3.4 Leak-off Test Analysis

Another option in the "LOT Analysis" menu item is "Leak-off Test" that provides a graphical analysis of a simulated LOT plots of surface pumping pressure vs. cumulative volume pumped into the well. The LOT analysis screen is shown in Fig. 70.

In the analysis, the user may select a combination of mechanisms involved in the well's response to the LOT from the selection box, LOT Contribution Mechanisms, in the upper left corner of the screen. Checking only the Casing Test box would give a plot exclusively resulting from mud compressibility in the well, i.e. all other factors, including open-hole compressibility were ignored in the analysis. The second box, "Wellbore expansion," produces a plot of pressure versus volume when only open-hole expansion is considered. The third box, "Mud loss," provides thye sole effect of mud leaking through pre-existing channels or fractures around the casing shoe. Checking only this box would simulate the mud leak effect during the leak-off test. The fourth and fifth boxes separately consider the two mechanisms of casing shoe failure, "Cement Parting," and "Plastic Fracture," repectively.

The LOT Curve Color menu controls the plot colors. In the result LOT a family of curves with different colors can be generated in one plot. Note, however, that only one color can be selected for a single selection from the LOT Contribution Mechanisms box. After the selection is made and one color checked, the user makes a simulation run by clicking the View Plot button in the upper top section of the screen. The resulting plot represents the well response to the selected combination of mechanisms. Then, another selection can be made resulting in different plot (and color). Thus, several simulation runs can be made to complete a multi-curve analysis based on a single plot.

Figure 70 shows a yellow plot representing the casing pressure test (only casing test box is checked). Ordinate of the plot is scaled in pressure, psi. The horizontal maximum-pressure line

is the horizontal fracture propagation pressure, 887 psi at the casing shoe. Abscissa of the plot is scaled in in volume pumped, gallons.

There are three horizontal lines in the plot. The top red line represents propagation pressure for horizontal fracture, 887 psi. The yellow line, below, corresponds to the initiation pressure for plastic fracture, 372 psi. The green line delineates initiation pressure for cement-rock parting, 276 psi.

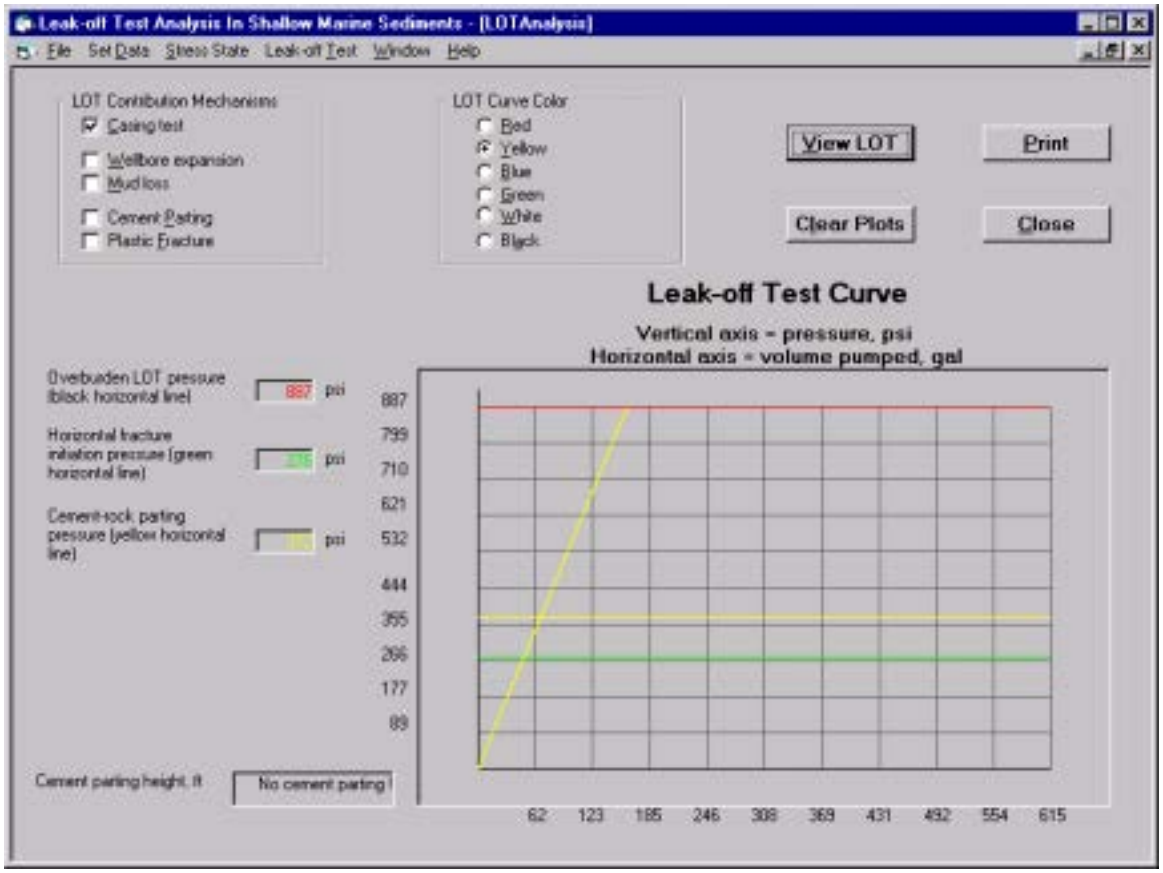

Figure 70. LOT analysis screen with example output data for casing pressure test.

Figure 71 shows the well response when mud compressibility and wellbore expansion are considered. The second curve (in black) is very close to the yellow plot of the casing test leading to the conclusion that borehole expansion is linear and little contributes to the overall volumetric effect. The conclusion is consistent with theoretical data for elastic and plastic wellbores.

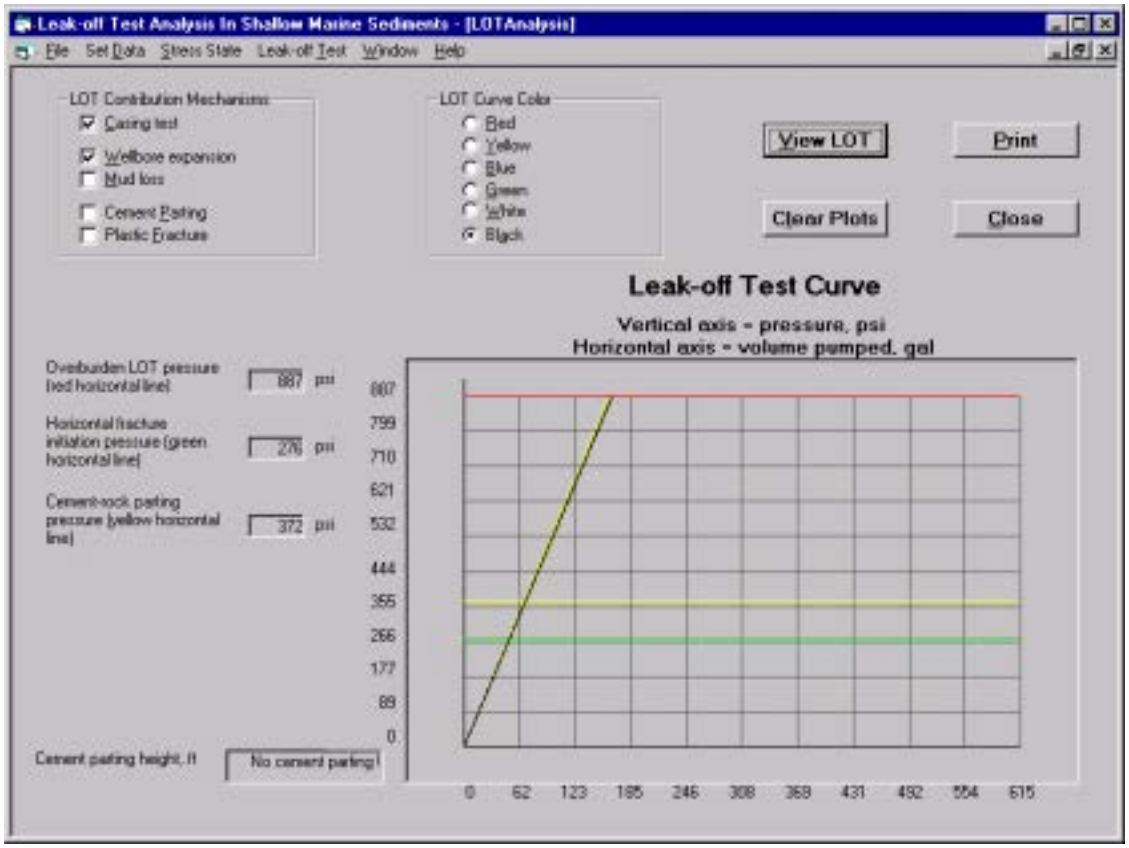

Figure 71. Example output data for combined effects of mud compression and wellbore expansion.

Figure 72 depicts the well response when additional effect of mud loss has been added to the other two mechanisms of mud compression and wellbore expansion. The new plot (in red) is nonlinear and indicates strong volumetric effect.

The two mechanisms of casing shoe failure, cement parting and rock fracturing also produce a non-linear behavior of the LOT curve. Figure 73 shows a LOT result involving combined effects of mud compression (casing test), wellbore expansion, leak (mud loss), and rock fracturing (plastic fracture). The plot (in blue) becomes asymptotic at pressure value lower than that for horizontal fracture propagation pressure (maximum pressure line). Consequently, the plot shows that rock fracture has been initiated early during the test but it did not propagate because, at later stage (and higher pressure) most of the pumped mud was lost into the rock. The result indicates that fluid loss controlled this test. The pumping rate was too low to generate conclusive result (i.e. casing shoe failure).

The plot in Figure 74 demonstrates the effect of adding cement parting to all other mechanisms the green curve. The result shows that initially cement parting occurred and propagated upward to 118 ft from the casing shoe before breaking into another formation above.

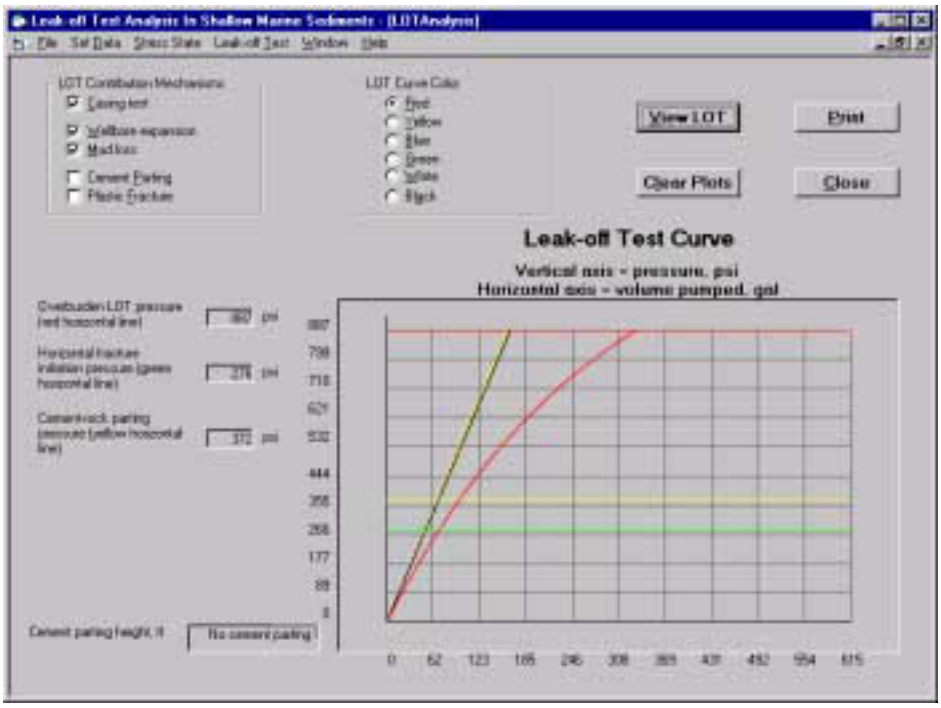

Figure 72. Non-linear response resulting from mud loss in presence of mud compression and wellbore expansion effects.

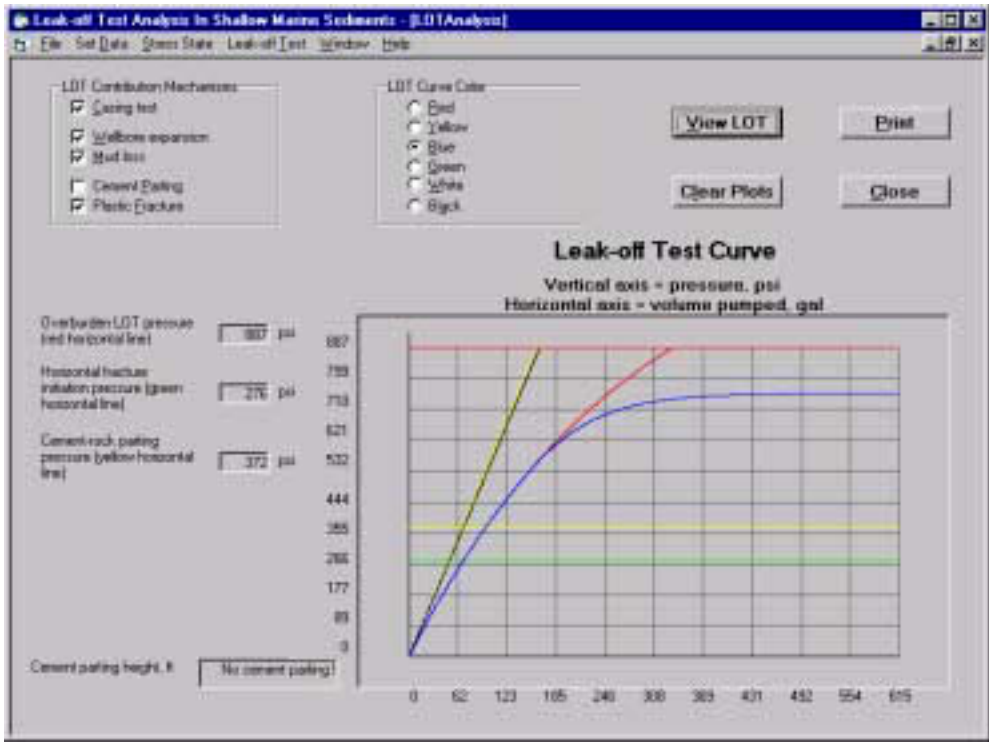

Figure 73. Example output data for combined effects of mud compression, wellbore expansion, mud loss, and rock fracture.

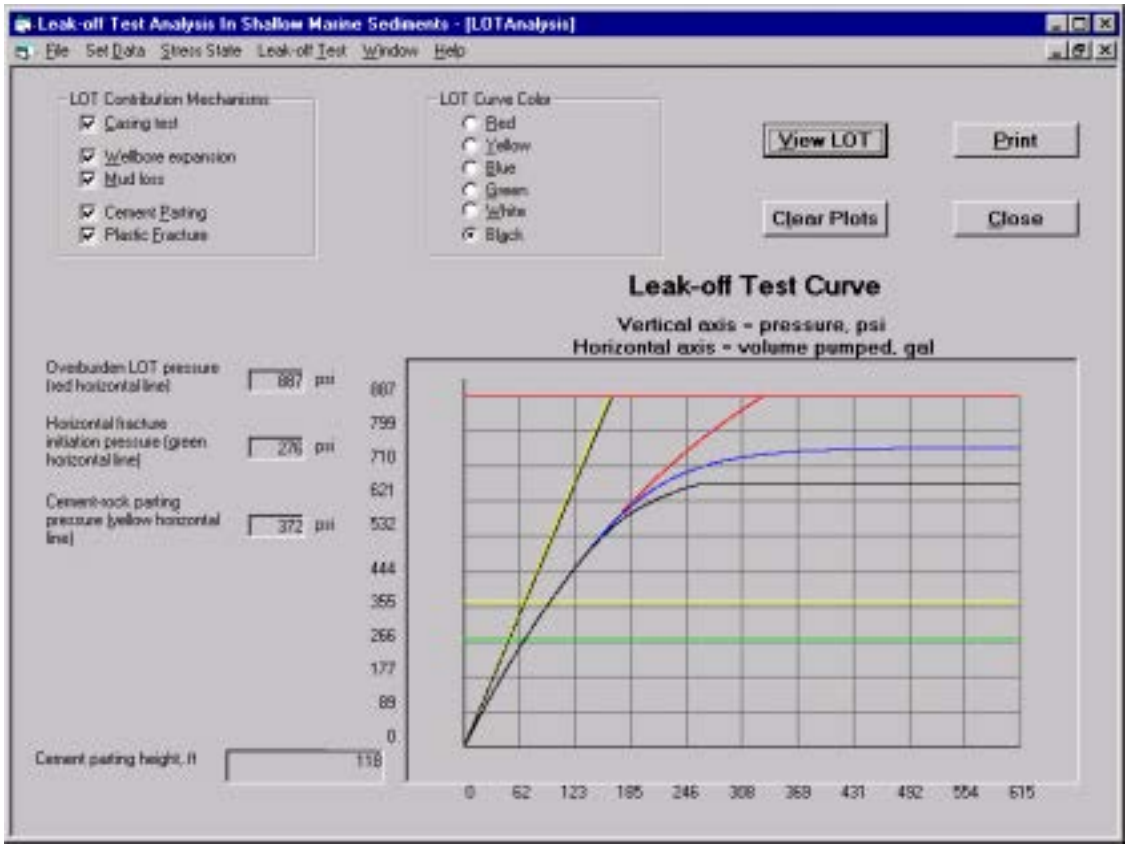

Figure 74. Example output data for combined effects of mud compression, wellbore expansion, mud loss, rock fracture, and cement parting.

5.3.5 Example Simulation Study

The LOTUMS software enables simulation studies of LOT or fluid migration at the casing shoe. In the latter application the user may use the analogy between LOT and fluid migration phenomenon. During LOT the casing shoe is pressurized for the purpose of testing. During fluid migration the casing shoe is pressurized by reservoir fluid moving upwards outside the well. Thus, the response of the casing shoe to LOT becomes indicative of the fate of pressurized fluid migration outside the well. In such studies, the user could change any data and observe theoretical results showing how the casing shoe would fail and where the migrating fluid would go. In the case of direct LOT simulations the results would help to make decisions regarding actual strength of the shoe and the need for remedial cement squeezing.

In this simulation study we use data from the example well above to evaluate the effect of fluid filtration/loss into the rock on the LOT plot pattern. We modify the "Set Data" menu by selecting the submenu of "Mud & Leak-off Test" where we increase the mud loss coefficient by 50%, from 0.0001 to 0.00015 gal/min*psi*sq ft. Then, we call the LOT Analysis screen, check the Casing test, Wellbore expansion, and Mud loss boxes and click on the command button View LOT to get the LOT plot shown in Fig. 75.

As shown in Fig. 75, the LOT plot becomes horizontally asymptotic at the pressure lower than the maximum pressure line. Thus, comparing with the previous result in Fig. 72, we conclude that:

- for mud loss coefficient is 0.0001 gal/min*psi*sq ft - well response is controlled by horizontal fracturing; and,
- for mud loss coefficient 0.00015 gal/min*psi*sq ft - well response is ultimately controlled by fluid loss to the rock matrix.

Even though the box of plastic fracture is not checked the result indicates that the fracture may form but it would no propagate beyond the plastic zone around the well. Obviously, this study disregards a possibility of cement - rock parting (the box is not checked).

Our second example demonstrates the effect of casing setting procedure on the strength of cement seal around the casing shoe and cement-rock parting potential. In this study we again use all the data from the example well except for casing shoe setting distance off-bottom that we reduce. To do so we modify the Cement Slurry screen and change data in the Casing off-bottom box from 29 ft to 10 ft. In the result, contact stress becomes 599 psi as shown in Fig. 76. Comparing with Fig. 68 we observe that the reduction of casing off-bottom setting significantly improved cement seal at the shoe; contact stress increased by 45 percent, from 415 psi to 593 psi.

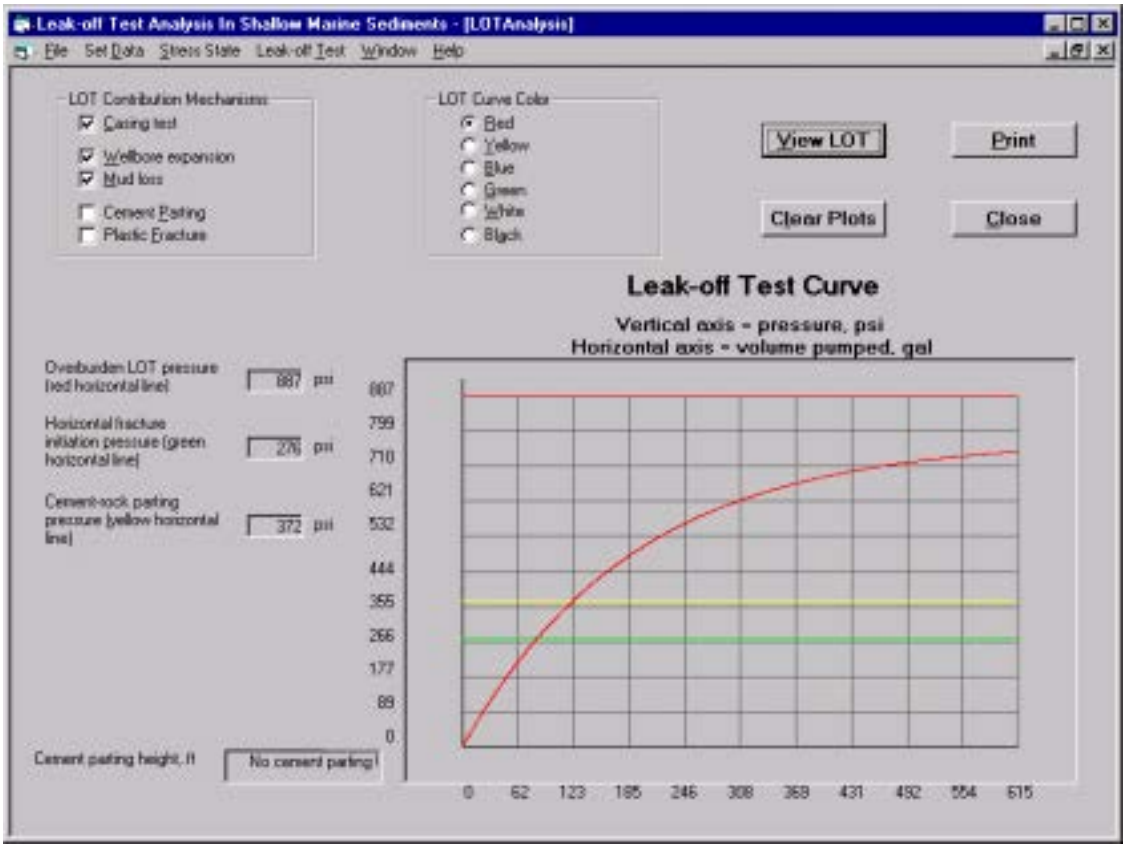

Figure 75. Simulated LOT - mud loss coefficient = 0.00015 gal/min*psi*sq ft.

Cement parting potential is demonstrated in Fig. 77. All mechanisms are considered (all boxes checked) and the plot stabilizes above the cement parting pressure 640 psi (yellow line). However, the parting extends only 4 ft above the casing shoe thus indicating that mud loss to the rock controls the test.

Plastic zone and therefore plastic fracture could be eliminated by increasing mud density resulting in the change of stress at the wellbore. For example, after increasing mud density from 10 ppg to 13 ppg the plastic zone (Fig. 76) would be eliminated as shown in Fig. 78. The change would convert the wellbore state of stress from plastic to elastic and significantly increase the fracture initiation pressure from 276 psi up to 887 psi.

Figures 79 and 80 show the LOT results when there is no mud loss around a wellbore, i.e. the rock is practically impermeable. (Note the unchecked box "Mud loss" in the "LOT Contribution Mechanism" section of the screen.) For such case horizontal fracture or cement parting are the only two mechanisms of LOT pressure stabilization.

Horizontal fracture would propagate and control the LOT when cement-rock parting pressure value is large - close or higher than the overburden pressure. This occurs for large values of the contact stress or contact stress coefficient. Figure 79 presents such case - demonstrated above in Fig. 76 - when the casing was set closer to bottom (10 ft off bottom) and the contact stress increased to 593 psi resulting in cement parting pressure 735 psi. As shown in Figure 79, plastic fracture developed at 276 psi and grew in the plastic zone as pressure increased from 276 psi to 735 psi. Then, cement parted at pressure of 735 psi and propagated upwards only 11 ft above the shoe when the fracture reached and propagated into the elastic zone with no further increase of pumping pressure. Thus, the LOT record in Fig. 79 demonstrates a case when the the casing shoe response to pressurization is controlled by the mechanism of rock fracturing.

Figure 80 demonstrates the case when the mechanism of cement parting prevails. In this example, cement parts at 372 psi and the parting continuous upwards together with growing plastic fracture. However, before the rock fracture (3-foot long at the time) breaks into the elastic zone a 139-ft long vertical annual channel develops and the mud is all lost onto the channel. As shown in Figure 80 the LOT plot turns to horizontal line at the pressure value 680 psi - lower than that required for rock fracture propagation, 887 psi. It should be pointed out that, unlike Fig. 80, the actual LOT plot should turn into horizontal line smoothly. The reason for discontinuity in Fig. 80 was the numerical procedure used for calculating maximum length of the annual channel.

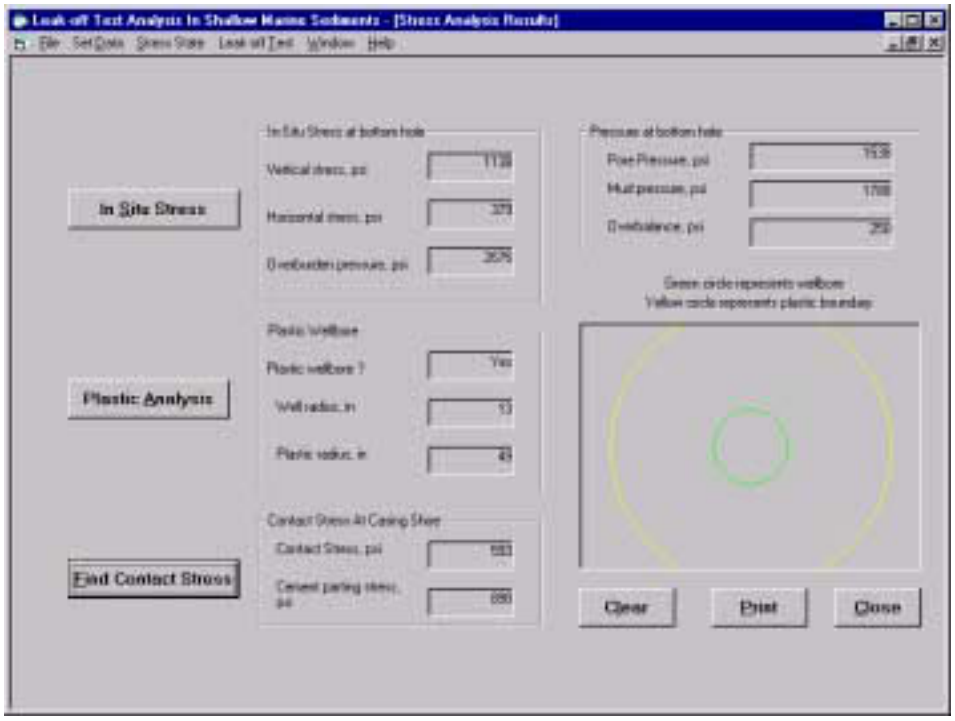

Figure 76. Simulated contact stress 593 psi for casing set 10 ft off bottom.

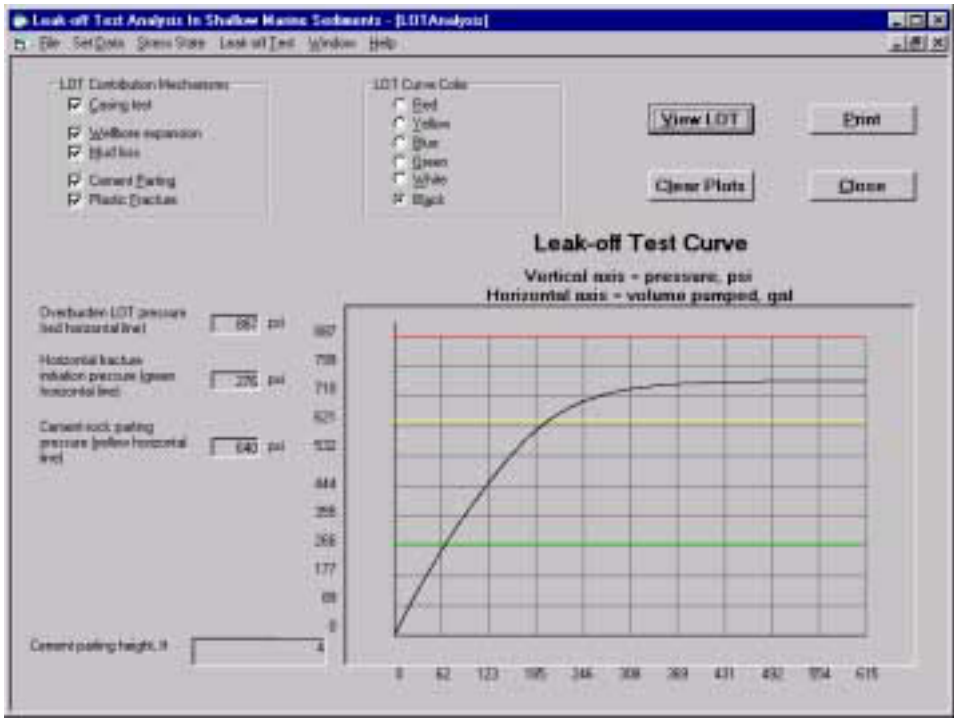

Figure 77. No cement parting propagation after setting casing closer to bottom.

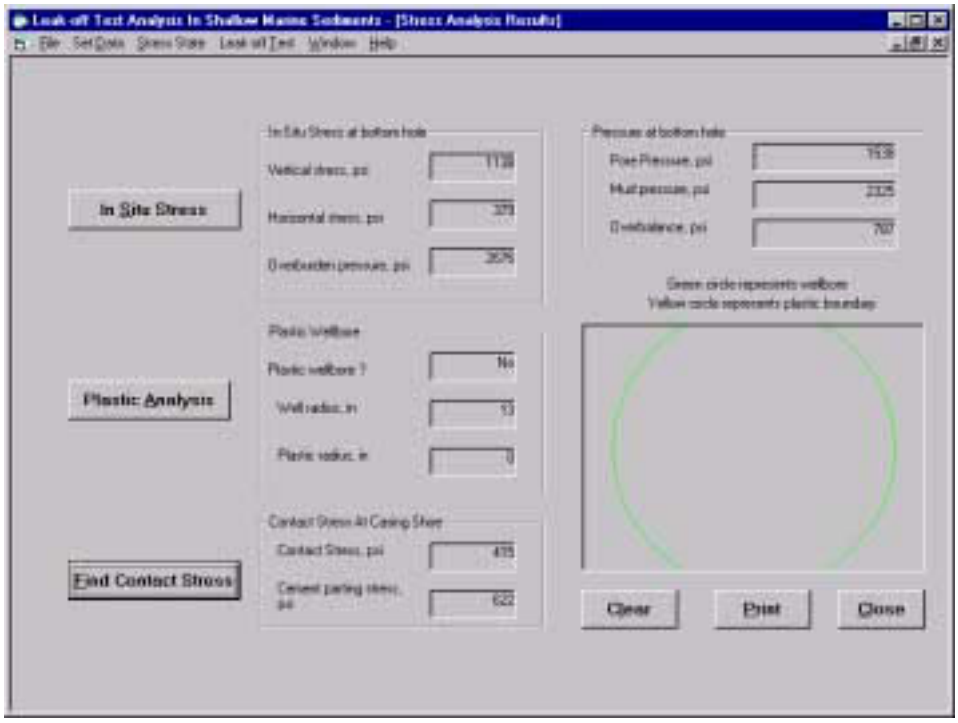

Figure 78. Increase of mud density to 13 ppg eliminates plastic zone around the well.

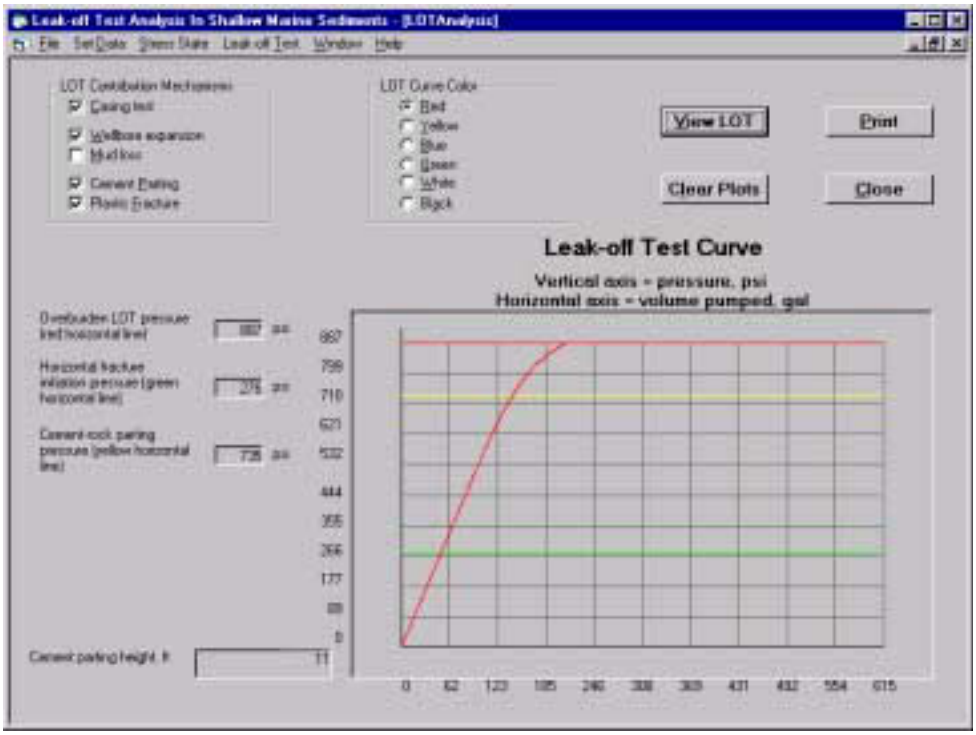

Figure 79. Impermeable rock - LOT response controlled by rock fracturing.

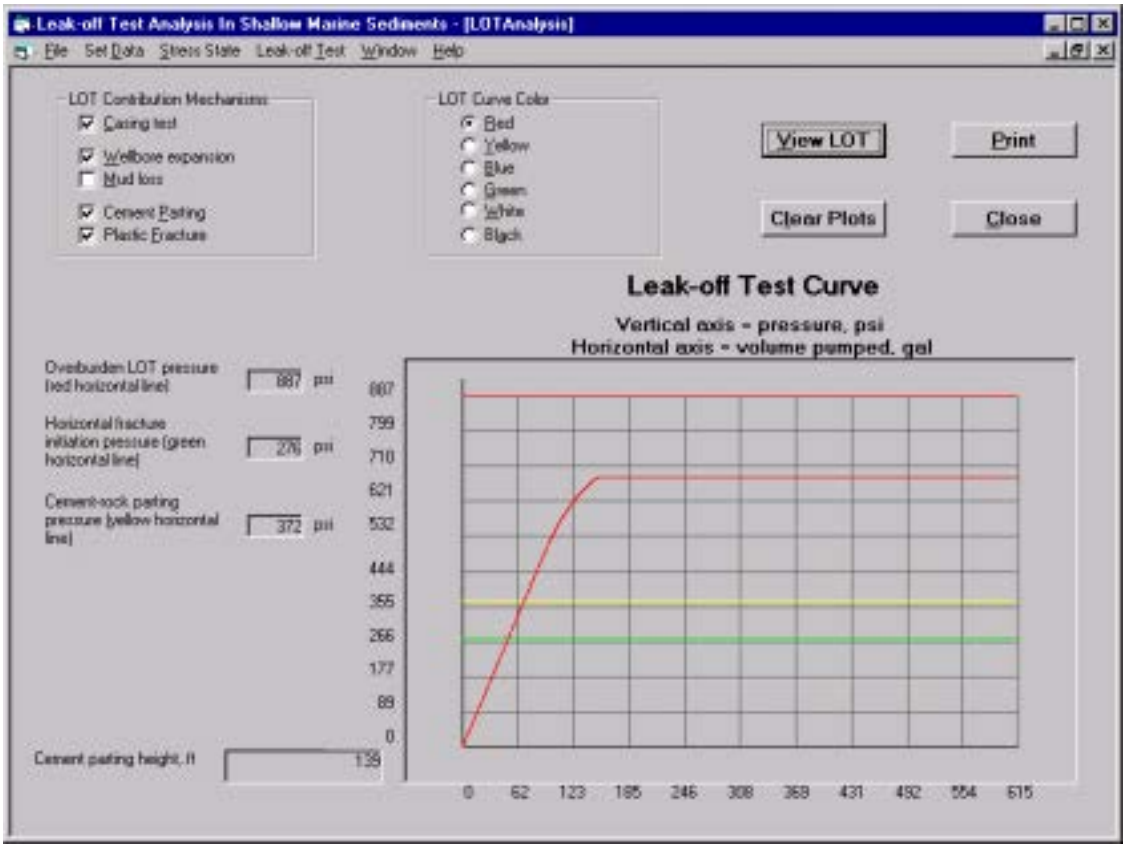

Figure 80. Impermeable rock - LOT response controlled by cement parting.

6. LEAK-OFF TEST ANALYSIS PROCEDURE IN SMS

Conventional analysis of a typical linear leak-off test (LOT) data involves finding the leak-off point at which the plot deviates from the linear trend. However, in the shallow marine sediments LOT plots are inherently nonlinear which brings about some differences in the testing procedure and analysis of results.

Figure 81 shows a complete conceptual LOT plot in SMS to be used for analysis. Unlike conventional testing in deep wells with clear sign of casing shoe failure (two consecutive test points deflect from the linear trend) in SMS the pumping is continued over the entire nonlinear pressure buildup (pressure buildup section OAB) until pressure no longer increases with the pumped volume - pressure stabilization section BC. Thus the decision to stop pumping is verified by the evidence of pressure stabilization. Stabilized pressure value is the maximum pressure for the test. Duration of pressure stabilization should be sufficient to verify the constant pressure value - typically, additional two - four minutes of pumping (up to one bbl of mud).

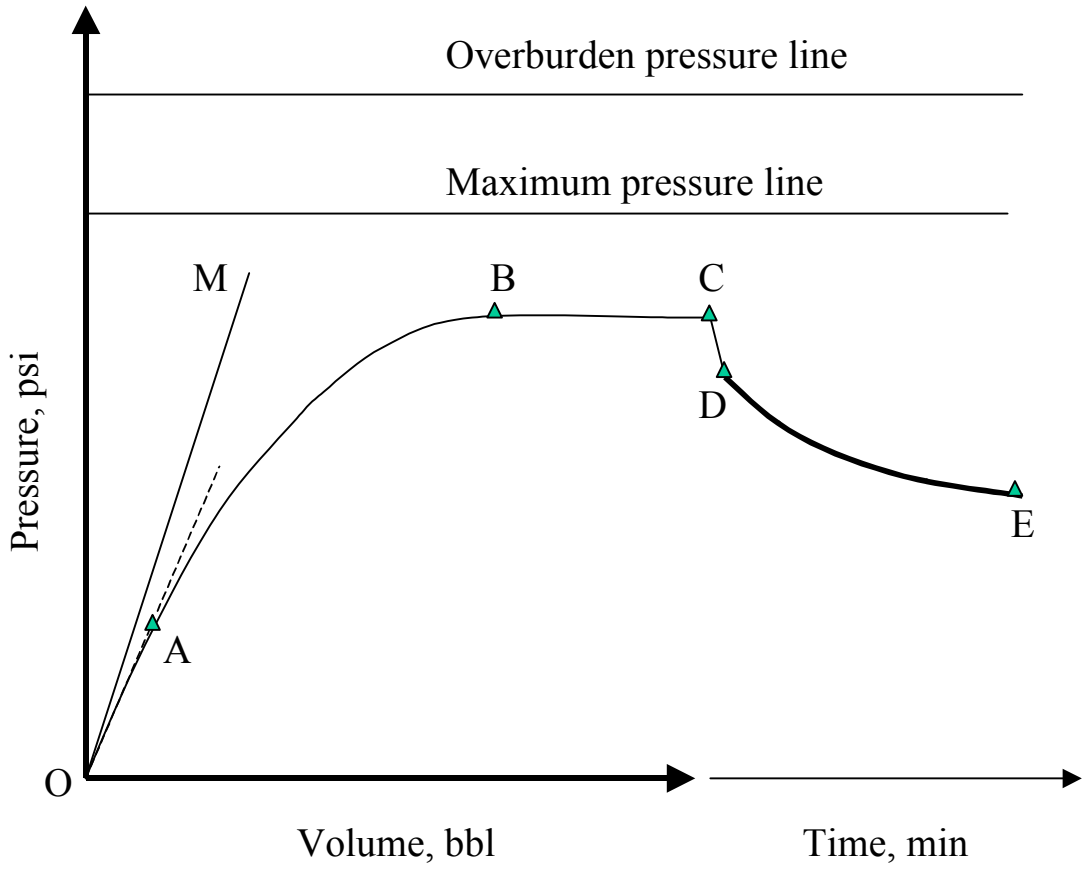

Figure 81. Conceptual leak-off test plot from shallow marine sediment.

Point A in Fig. 81 represents departure from the early straight line. This point is usually difficult to identify and the whole section OAB is called pressure buildup section. Point B is the beginning of maximum stabilized pressure stage of the test.

At point C the pumping is stopped. Section CD represents the sharp pressure drop due to elimination of the frictional pressure loss after the pump is stopped. Then, there is a gradual pressure reduction depicted by section DE in the plot - a pressure fall-off stage of the test. During the fall-off stage, the well losses fluid either to the rock matrix (screen-off), the annular channel behind the cement, or the rock fracture.

Analysis of the pressure buildup section of LOT is inconclusive and difficult to perform. As shown in the simulation studies above, pressure buildup is usually controlled by combined effect of all volumetric mechanisms working simultaneously, compressibility, growth of plastic rock fracture, propagation of cement parting and filtration to the rock matrix. All the mechanisms superimpose similar nonlinear patterns of pressure buildup with no characteristic points. Thus, the analysis of the buildup section alone is not effective and should be performed only in conjunction with the pressure drop-off section as explained in the following chapters.

Pressure stabilization stage of provides useful data for analysis - the maximum pressure. Maximum pressure represents either hydrodynamic balance of pressure losses due drilling fluid

flow (annular channel or rock matrix) or a constant-pressure loss of mud into the horizontal fracture of infinite extend. Comparison of the stabilized pressure from the test with known values of overburden and cementing pressures may help to find the actual mechanism of casing shoe failure.

6.1 Analysis of Maximum Stabilized LOT Pressure

Two horizontal lines are drawn for reference in Fig. 81. The top line corresponds to the overburden pressure at the casing shoe. Its value is the difference of overburden pressure and mud hydrostatic pressure at the casing shoe. The second line is the maximum pressure line at the casing shoe and corresponds to the cementing pressure. Its value is the difference of the maximum hydrostatic pressure during cementing and the hydrostatic mud pressure before LOT. The two lines help to identify mechanisms of pressure stabilization during LOT. Equation 81 gives the values to draw the two lines.

$$\begin{aligned} p_{overLOT} &= p_{over} - p_w \\ p_{\max LOT} &= p_{\max} - p_w \end{aligned} \tag{81}$$

where:

p_{over} = overburden pressure at casing shoe;
p_w = mud pressure the casing shoe;
p_{max}= maximum cementing pressure at casing shoe.

Mud pressure at casing shoe is

$$p_w = 0.052 \rho_m D_{shoe} \tag{82}$$

Horizontal rock fracture can only be propagated when the early plastic fracture grows and breaks into the elastic zone. Moreover, fracture propagation occurs when the maximum stabilized LOT pressure is equal or greater than overburden pressure. Thus, overburden pressure represents maximum possible strength of the rock at the casing shoe in SMS.

If the bulk rock density (ρ_b) is known as a function of depth, the overburden pressure for each depth interval can calculated by integrating the bulk density for each depth interval as

$$p_{over} = \int_{o}^{D_w} g\, \rho_w \, dD + \int_{D_w}^{D} g\, \rho_b \, dD \tag{83}$$

where; D_w, ρ_w, and D are water depth, water density, and vertical depth, respectively.

If rock density is unknown, overburden pressure can be estimated using the porosity trend with depth (Bourgoyne et al.,1991) as

$$p_{over} = g\rho_w D_w + g\rho_g D_s - \frac{(\rho_g - \rho_{fl})g\phi_o}{K}\left(1 - e^{-KD_s}\right) \tag{84}$$

where; ϕ_0 and K are surface porosity and porosity decline constants, respectively.

As shown in Appendix B, the porosity trend model in Eq. 84 does not apply to shallow marine sediments. Instead, a regression model has been developed in this work using data from geotechnical borings. For SMS comprising mostly clay deposits overburden pressure can be calculated as

$$p_{over} = g\rho_w D_w + 1.2D_s - 240(1 - e^{-D_s/400}) \quad (85a)$$

for, $0 < Ds < 100$ ft;

$$p_{over} = g\rho_w D_w + 66.9 + 3929.5e^{-D_s/5500} + 1.4289D_s - 4001.56 \quad (85b)$$

for, $100 < Ds < 650$ ft;

$$p_{over} = g\rho_w D_w + 485.6 + 5888.8e^{-D_s/8000} + 1.4722D_s - 6386.19 \quad (85c)$$

for, $650 < Ds < 3000$ ft.

For SMS comprising mixed layers of sand and clay overburden pressure can be estimated as

$$p_{over} = p_{over-clay} + 0.86D_{sand} \quad (85d)$$

where;

p_{over} = overburden pressure, psi;
D_s = depth (or total thickness) of sediment (clay), feet;
$g\rho_w D_w$ = pressure of sea water, psi;
D_{sand} = depth (or total thickness) of sand, ft;
D = depth, ft
$p_{over\text{-}clay}$ = overburden pressure from Eqs. 8.5a-c for clay deposit thickness:
$D_s = D - D_{sand}$.

If no geotechnical, drilling or logging data is available for an area, a common approximation of the overburden pressure gradient, 1.0 psi/ft, (Harrison et al, 1954; Hubbert and Willis, 1957) could be used as a maximum-limit reference of overburden pressure in SMS.

Maximum cementing pressure occurs at the end of cement placement when hydrostatic column of cement slurry in annulus is still in liquid state and no cement gellation developed. The value represents the maximum pressure actually "liquid-tested" at the casing setting depth before the casing shoe was cemented in place. It also represents maximum value of contact stress between the cement and rock.

Maximum cementing pressure can be estimated from the fluid columns in casing annulus as

$$p_{\max} = p_o + 0.052 \sum_{i=1}^{n} \rho_i (D_i - D_{i-1}) \quad (86)$$

where;

p_o = surface casing pressure (if any), psi

ρ_i and D_i = density and height of the i-th liquid column in the annulus (tail, lead, spacer, preflush, and mud), ppg and ft, respectively.

Better determination of maximum cementing pressure could be made by direct measurement of pressure at the end of displacement process when the pump is stopped. No top plug is used in such operation and bottomhole pressure change can be calculated form the recorded change of the surface pressure.

Once the two pressure reference lines are drawn the analysis of the stabilized- pressure section of the LOT plot would include the following reasoning:

1. If the stabilized LOT pressure value is close to the overburden pressure line, horizontal rock fracturing likely occurred during the test;

2. If the stabilized LOT pressure is smaller than overburden pressure but greater than maximum hydrostatic pressure line, two other volume loss mechanisms (fluid loss or cement parting) are possible but the more likely one is cement-rock parting. The reason is that, theoretically, maximum cementing pressure represents minimum contact stress between cement and rock so cement parting should occur only at pressures higher than contact stress. However fluid loss to rock matrix can still account for some volume loss as the new rock surface is exposed to drilling mud.

3. If the stabilized LOT pressure is below the maximum hydrostatic pressure line the two mechanism of volume loss (fluid loss or cement parting) might be at work again but the more likely one is mud loss to unconsolidated rock matrix. The LOT pressure is constant because the rate of mud loss equals the low pumping rate during the test and pressure stabilizes at the value below cementing pressure. (Note that cement was pumped at rate much higher than that during the LOT.)
   Stabilization of LOT pressure caused by parting of casing shoe cement from the rock at pressures lower than cementing pressure is theoretically possible if the contact stress is lower than the bottomhole pressure at the end of cementing. This could only happen due hydrostatic pressure loss in the annulus after cementing - a phenomenon observed in a few reported field tests.

Analysis of the stabilized LOT pressure, presented above, identifies the maximum strength of the casing shoe controlled by the rock stress (overburden pressure) and the failure by rock fracturing. When the stabilized LOT pressure is smaller than the maximum strength at the shoe the method provides some guidelines regarding most likely mechanism of pressure stabilization. Unfortunately, the analysis is only qualitative and does clearly distinguish between the two mechanisms. However, the method may be sufficient when the LOT stabilized pressure value is high enough to drill the next section of the well so no remedial treatment of casing shoe is required. Otherwise, combined analysis of the pressure buildup and fall-off stages will be needed as explained later in this report.

Examples of Stabilized LOT Pressure Analysis

Figure 82 shows data collected during Leak-off test performed at depth 1029 ft (TVD) in a well drilled offshore in water depth 196 ft. Water level below kelly bushings was 86 ft. The mud weight before LOT was 8.8 ppg and sea water density was about 8.8 ppg.

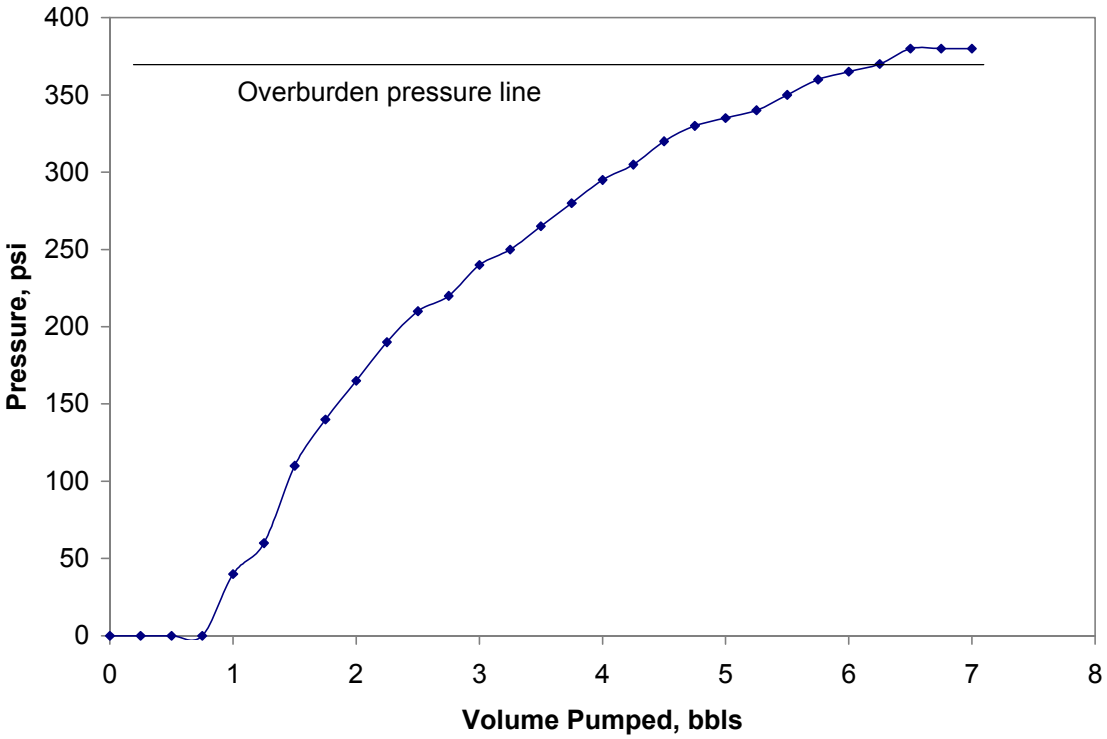

Figure 82. LOT plot indicates horizontal rock fracturing.

No detail rock density information and cementing data is available for this well. We calculate the overburden pressure line based on the maximum average overburden pressure gradient in sediments, 1psi/ft. The sediment depth is 1029-196-86 = 747 ft. The overburden pressure at the casing shoe by the rock is 747 ft × 1 psi/ft = 747 psi. Overburden pressure from sea water is 0.052× 8.8×196 = 90 psi. Total overburden pressure at the casing shoe is 747 + 90 = 837 psi. Mud pressure at the casing shoe is 0.052×8.8×1029 = 471 psi. The overburden pressure line is 837 – 471 = 366 psi. As shown in Fig. 82 the LOT stabilized pressure is 380 psi - slightly above the overburden pressure line indicating horizontal fracturing of the rock during the test.

Shown in Fig. 83 is another example of LOT performed at 821 ft. (KB) in an offshore well drilled in 195 ft of water with kelly bushings 95 ft above sea level. Drilling mud and seawater pressure gradients were 0.442 psi/ft and 0.44 psi/ft., respectively. The rock depth to casing shoe is 821-195-92= 534 ft. With an average overburden pressure is 84 psi/ft, the overburden pressure from rock is 534 psi. Overburden pressure from sea water is 0.44×195 = 86 psi. Total overburden pressure at the casing shoe is 534 + 86 = 620 psi. The mud pressure at the casing shoe is 0.442× 821 = 363 psi. Therefore, the overburden pressure line is 620 – 363 = 257 psi.

The well was cemented to the mud line with 13.8 lb/gal class A slurry having 0.72 psi/ft pressure gradient, which represents the maximum pressure line value: $0.72 \times 534 + 195 \times 0.44 - 821 \times 0.442 = 107$ psi .

As shown in Fig. 83, the maximum tested LOT pressure was 170 psi which is below the overburden pressure line and above the maximum pressure line. Therefore, cement-rock parting or fluid loss leaking might occur at the casing shoe during the test.

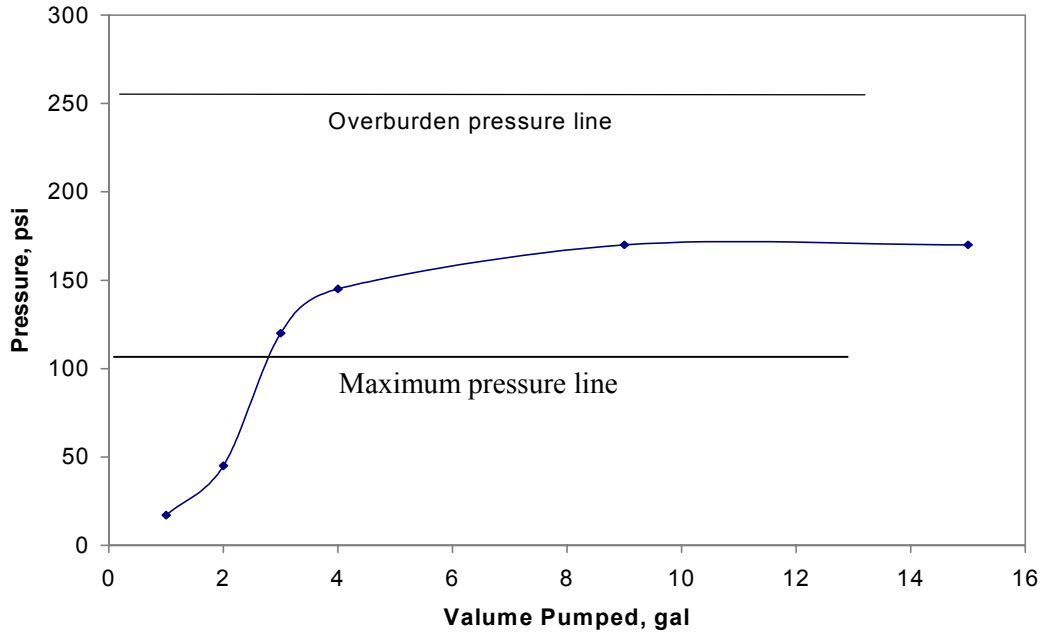

Figure 83. LOT plot indicates cement parting or fluid loss.

6.2 Analysis of LOT Pressure Fall-off

When stabilized LOT pressure is small and insufficient to drill ahead a remedial treatment is needed. The treatment would depend upon the mechanism of drilling mud volume loss at the shoe; whether the mud is lost into the rock matrix, or to the annular channel cause by cement-rock parting. If the mud is lost into the rock matrix remediation would be limited to sealing-of the open hole rock surface with plugging/loss circulation materials or gunk squeezes. However, in case of cement-rock parting the remedial treatment involves squeezing cement between cement and rock in order to increase contact stress and eliminate upward fluid migration behind the well cement. Obviously, costs of the treatments are quite different. Also different is the risk of leaving the casing shoe untreated. Therefore, further analysis of LOT is needed to better distinguish the two mechanisms of pressure stabilization. Combined analysis of pressure buildup and fall-off patterns, described below, may provide such information.

As shown in Fig. 81 a typical record of the pressure fall-off is a plot of pressure vs. time. Shape of such a plot strongly depends upon the time scale selected by the operator; For the same test, a slow pressure fall-off would be recorded with large time scale or, alternatively, a dramatic pressure loss would result from applying a fine time scale. Moreover, the record shows no direct relationship between the pressure buildup and fall-off plots since the former relates to volume and the latter to time.

Fig. 84 presents a plot of data from the same test with three patterns of pressure fall-off (sections DE, DE', and DE") resulting from three different arbitrary time scales. Pattern DE' implies that the casing shoe holds the fluid because of very slow fluid transfer comparing to the pressure buildup stage. In contrast, pattern DE" suggests a fast leaking wellbore with rapid volumetric loss. Thus, with no buildup-falloff conversion, an interpretation of the pressure fall-off is arbitrary and meaningless. The conversion would provide a reference fall-off pattern derived from the pressure buildup plot as explained below. Also, although the technique has been designed for LOTs in shallow marine sediment, it should also work for testing deep wells.

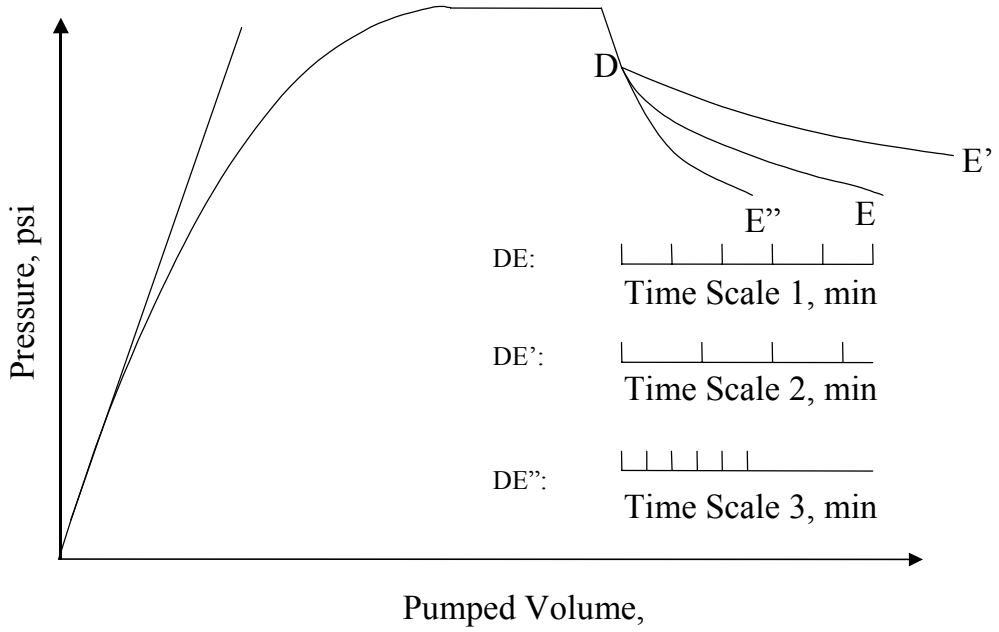

Figure 84. Three patterns of pressure fall-off from the same test.

6.2.1 Normalized Time Scale

In order to relate the pressure buldup and fall-off plots the time scale must be normalized. Typically, the LOT plot ordinate is scaled in 10 or 100 psi pressure increments depending on the recorded maximum pressure. The abscissa is scaled in two units, volume (bbls) and time (min). The problem is that the two scales do not relate to each other.. The size of the units representing one barrel and one minute is made arbitrarily - often based on the grid paper used to make the plot.

In order to make the two plots comparable, a conversion between the time and volume scales is introduced using the pumping rate as a conversion factor. As shown in Fig. 8, the abscissa is scaled using uniform increments of volume and time. However, the volume increments represent barrels pumped in each minute (i.e. numerically equal to pumping rate, q), while the time increments represent minutes.

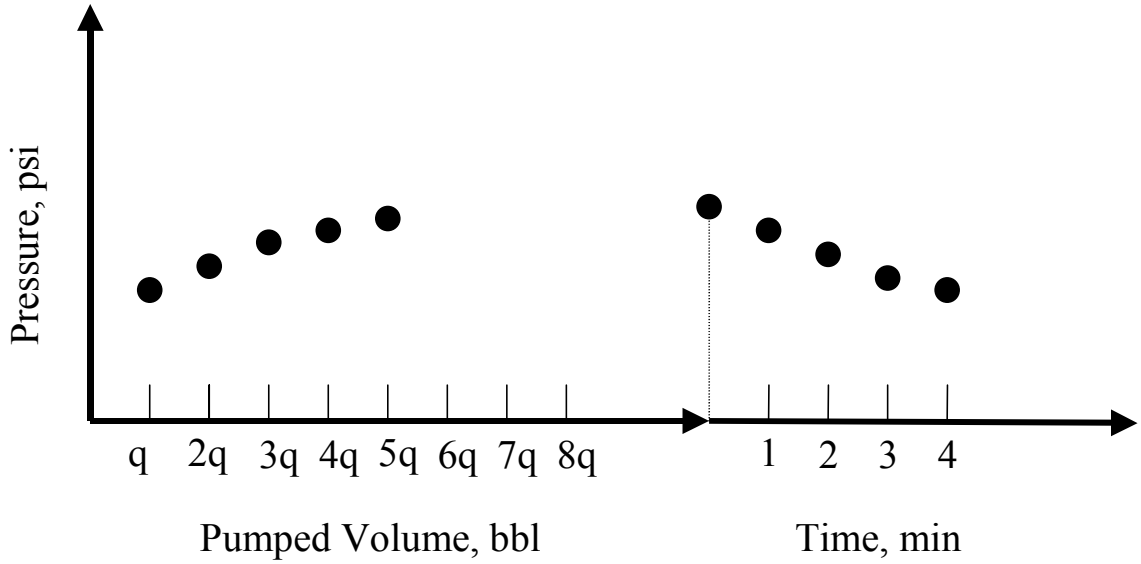

Figure 85. Normalized LOT plot.

6.2.2 Equivalent Plot of LOT Pressure Fall-off

A reference (equivalent) plot of pressure fall-off is added to the actual one using the pressure buildup data as a basis for the reference. The plot describes fall-off pattern for a hypothetical case when the loss of liquid to the rock matrix was the only mechanism of pressure change during LOT. Obviously, a deviation from this pattern would represent contribution of the second mechanism, cement-rock parting. Thus, a comparison of actual pressure fall-off with the equivalent one helps to find out what happened at the casing shoe during LOT. The concept underlines the LOT analysis procedure described below.

Using normalized LOT plot, divide the pressure build-up section into a series of small segments. For each segment, the relationship between incremental increase of pressure (Δp) versus volume (ΔV_p) is

$$\Delta p=\Delta V_p /(C_c V_o) \tag{87}$$

Consequently, the same relationship for the pressure fall-off should be

$$\Delta p=(\Delta V_p-\Delta V_{loss}) /(C_c V_o) \tag{88}$$

where:

ΔV_{loss} = volume loss to rock permeability and newly-opened fractures;
C_c = well system compressibility (approximated with casing test plot);
V_o = total mud in the well.

Shown in 86(a) is a small segment AE of the pressure build-up plot. Fig. 86(b) magnifies the segment AE for graphical analysis. As shown in Fig. 8.6(b), for a given pumped volume AC, the pressure increase should be CF according to Eq. 8.6 if all the mud were used to increase

wellbore pressure. However, the actual pressure increase is CE is smaller than CF because some mud is lost to the rock. Pressure increase represented by CE involves volumetric increase, AB, according to Eq. 8.7. Thus, the volume lost from the pumped volume AC is equal to BC.

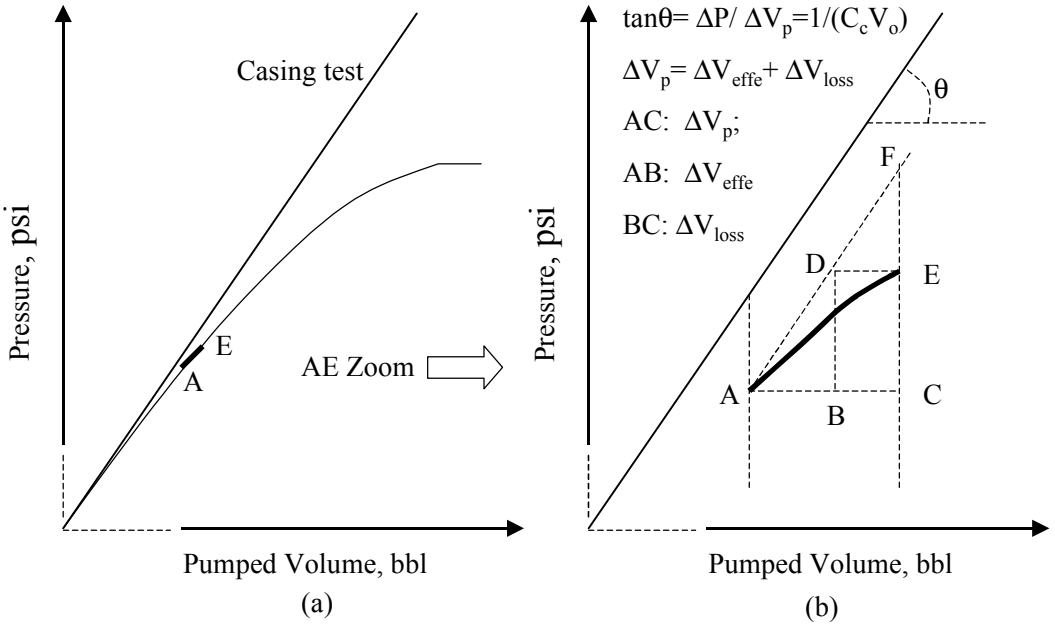

Figure 86. Graphical interpretation of LOT pressure build-up.

Figure 87 demonstrates how to make a plot of equivalent pressure fall-off using graphical data from the pressure build-up section. Theoretical basis for the procedure is the compressibility formula describing incremental pressure fall-off equal the to incremental pressure build-up for the same rate of fluid volume loss

$$\Delta p=(-\Delta V_{loss}) /(C_c V_o) \tag{89}$$

The procedure for making the fall-off plot, shown in Fig. 87 is described as follows:

1. Make normalized plot of the LOT buildup and fall-off data;
2. Identify the well compressibility trendline
3. Determine vertical shift in the pressure values for the buildup and drawdown plots equal to frictional pressure loss during mud pumping;
4. Consider the top increment of the pressure buildup plot AE and find the beginning of pressure fall-off - point A';
5. Draw the well compressibility line A'F' having negative slope angle Θ defined by the casing test;
6. Draw time increment: A'C' = AC;
7. Find equivalent volume loss during the pressure fall-off: A'B'= BC;
8. Find point D' on the compressibility line A'F' as an intercept of the vertical line through B';
9. Find point of E' as an intercept of a horizontal line through point D' and a vertical line through point C';

10. Segment A'E' is a segment of the equivalent pressure fall-off corresponding to the pressure build-up segment AE;
11. Rename point E' as A'; and add the next segment to the pressure fall-off plot by repeating steps 4 through 10. Continue the procedure until the equivalent fall-off pressure plot is completed.

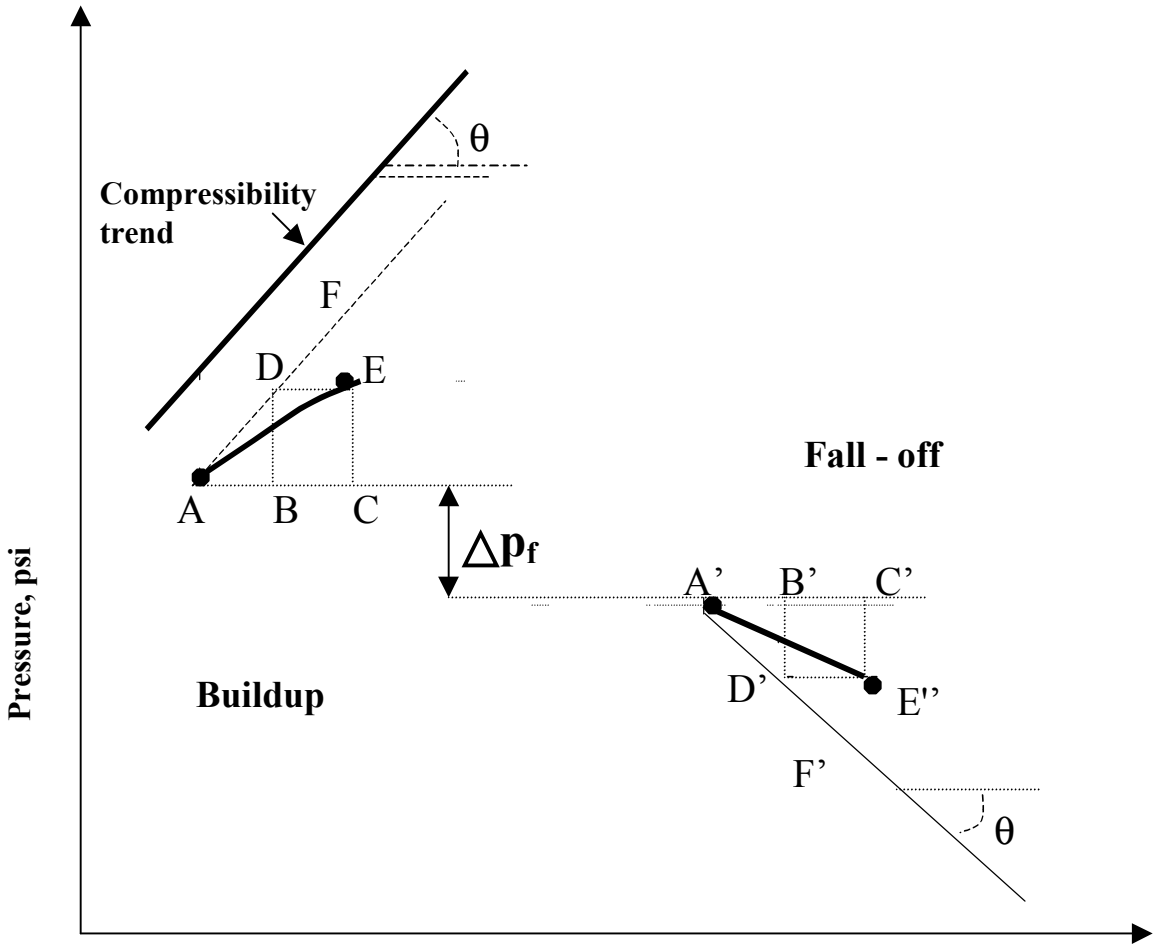

Figure 87. Graphical construction of equivalent pressure fall-off plot.

For most of actual LOTs, stopping the pump produces a sharp pressure drop due to elimination of frictional pressure loss. In the result, the pressure build-up plot is shifted upwards comparing to the fall-off plot. The shift should be considered in the analysis by adjusting point A' upwards by the value of frictional pressure drop.

6.2.3 Graphical Analysis of LOT Pressure Fall-off

In this method, the assumption is that during the pressure build-up and fall-off stages of LOT volumetric rates of fluid loss are the same for the same values of bottomhole pressure. The assumption is true when there is no cement parting so the well fluid loss into the rock depends only on pressure overbalance and the rock area open to flow (Darcy Law).

Comparing the plots of actual and equivalent pressure fall-off provides a pattern-recognition method to identify the presence of cement-rock parting or fluid loss to the rock. After the cement parts from the rock an annular channel is initiated between the cement and the rock surface covered by mud filter cake. As pumping continues drilling fluid fills up and propagates the annular channel upwards outside the well. Size of the channel (height and width) is controlled be the pressure equilibrium conditions involving bottomhole pressure, contact stress and frictional pressure loss in the channel.

When pumping stops new pressure equilibrium develops due to the lack of frictional losses. Then, the value of pressure at the entry to the annual channel remains constant resulting in no pressure fall-off. Thus, theoretically, in the absence of fluid loss mechanism there should be no pressure fall-off at all. Obviously, such idealized case never occurs and some pressure fall-off takes place. However, for the cement parting the recorded pressure fall-off should be markedly smaller than the equivalent fall-off. In the other words, if the recorded fall-off plot stays above the equivalent fall-off plot cement-rock parting occurred during LOT. Two examples below demonstrate this technique

.

Example 1 - Cement parting.

Shown in Fig. 8.8 is a LOT data recorded in a well drilled offshore in 102-foot of water. The MN line is the casing test plot. Estimated value of the overburden pressure line for this well was 190 psi. Since the stabilized pressure falls markedly below the overburden pressure line either cement parting or fluid loss may have occurred during the test.

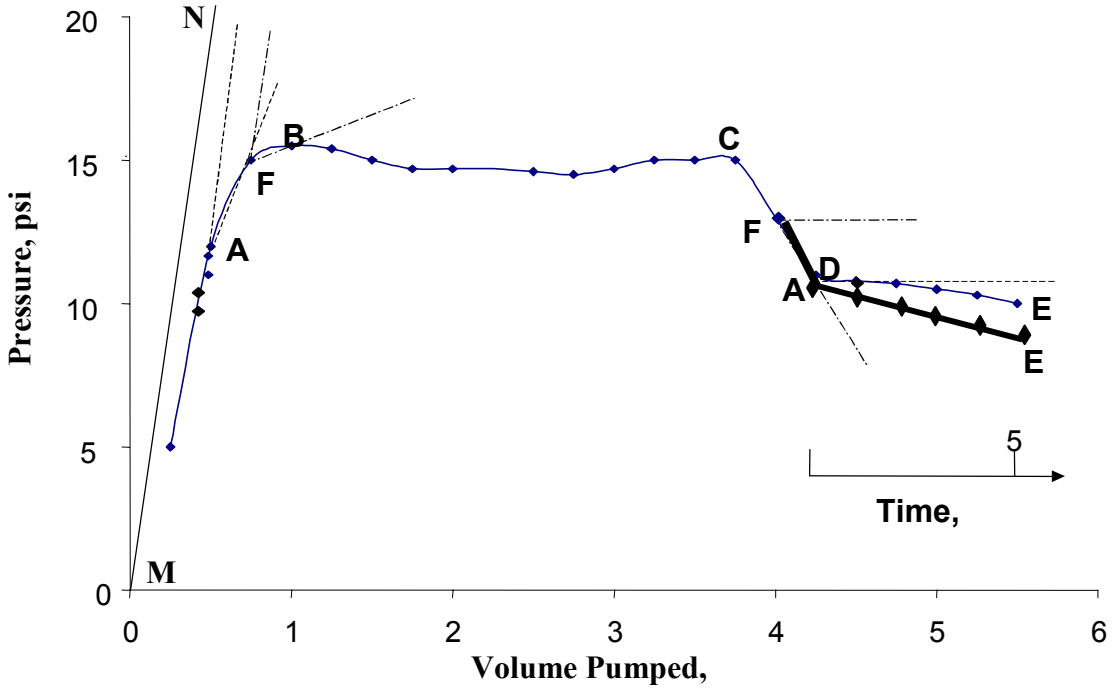

Figure 88. Fall-off pressure analysis - Example 1.

The pressure buildup plot is similar to LOT data from deep wells with clearly indicated deviation form linear trend at the leak-off point A. Below point A, the linear section of the plot shows that the open hole holds pressure and does not leak mud. Point A may indicate either

initiation of cement parting or the beginning of fluid loss caused by opening a non-propagating fracture in plastic zone around the well. Thus, analysis of the fall-off section is needed to identify one of the two mechanisms.

The well was shut-in at point C. Section CF' represents pressure drop after shut-in. Point F' has been found by subtracting pressure difference between points A and A'. (Note that point A' in the fall-off plot corresponds to point A in the buildup plot because the well holds pressure below these points.) Thus, the analysis starts at point F' that represents the beginning of pressure fall-off. The construction procedure for the equivalent fall-off plot is as follows:

- Normalize time scale;
- Select the last one-minute time increment FB in the pressure build-up plot and find *the mud volume loss* from the well during the last minute of buildup;
- At point F', use *the mud volume loss* and the negative trend-line of compressibility (negative slope of line MN) and draw the pressure fall-off line section F'A';
- Consider the one-minute time increment AF in the pressure build-up plot and find the mud volume lost from the well during the previous minute of pressure buildup;
- Starting at point A', draw five consecutive sections of the pressure fall-off line A'E using five points on the buildup line below A.

Comparison of the actual pressure fall-off F'DE with the equivalent fall-off F'A'E' shows that the upper part of actual fall-off F'A' is very steep and almost identical to the equivalent one F'D which implies that the fall-off begins with fluid loss to the rock. However, at lower pressure (points A" and D) the fall-off plots split and level-off with the actual plot markedly above the equivalent one.

The analysis shows that cement parting occurred during LOT pressure buildup (point A). Than the upward propagating annular channel entered a fluid-loss zone so the pressure stabilized at point B. When the pumping stopped (point F') the fluid loss continued causing rapid pressure loss (F'D) until the pressure dropped to its cement-parting value (point A') and the annular channel closed (point D). Then, the wellbore stopped leaking and the pressure stabilized (section DE).

Example 2 - Fluid Loss

Figure 89 shows a LOT data from a well at TVD= 802 ft drilled offshore in 102-foot deep water. The well was drilled with 8.9 ppg mud and the sea water pressure gradient was 0.442 psi/ft. Also, as shown in Fig. 89 the maximum stabilized LOT pressure was 220 psi. The approximated value of overburden pressure using 1psi/ft pressure gradient gives the overburden pressure line at 256 psi. The line indicates that cement parting might have occurred during the LOT. However, estimation of the overburden pressure with new correlations for SMS in Equ. (85) (for sandy sediment) gives much lower value of the overburden pressure line, 170 psi. The smaller value of overburden pressure eliminates possibility of cement parting but the pressure fall-off analysis is still needed to explain the mud transfer mechanism during this test.

The leak-off happens around point C when plastic (non-propagating) fracture is initiated. The fracture grows and new rock surface is progressively exposed to the mud inflow. At point O the plastic fracture breaks into the elastic zone and horizontal fracture propagates at almost constant pressure. Thus the test shows that overburden pressure in this well corresponds to the stabilized pressure value of about 220 psi.

After the shut-in, the fracture in elastic zone is closed and the pressure fall-off begins at point A'. As shown in Fig. 89, the actual pressure fall-off is identical to the equivalent fall-off.

Thus, during the fall-off the mud is lost into slowly- reversing plastic fracture until the fracture closes up at point E'.

The analysis shows that no remedial treatment is needed in this well. The casing shoe has integrity and the maximum pressure equals overburden pressure at this depth.

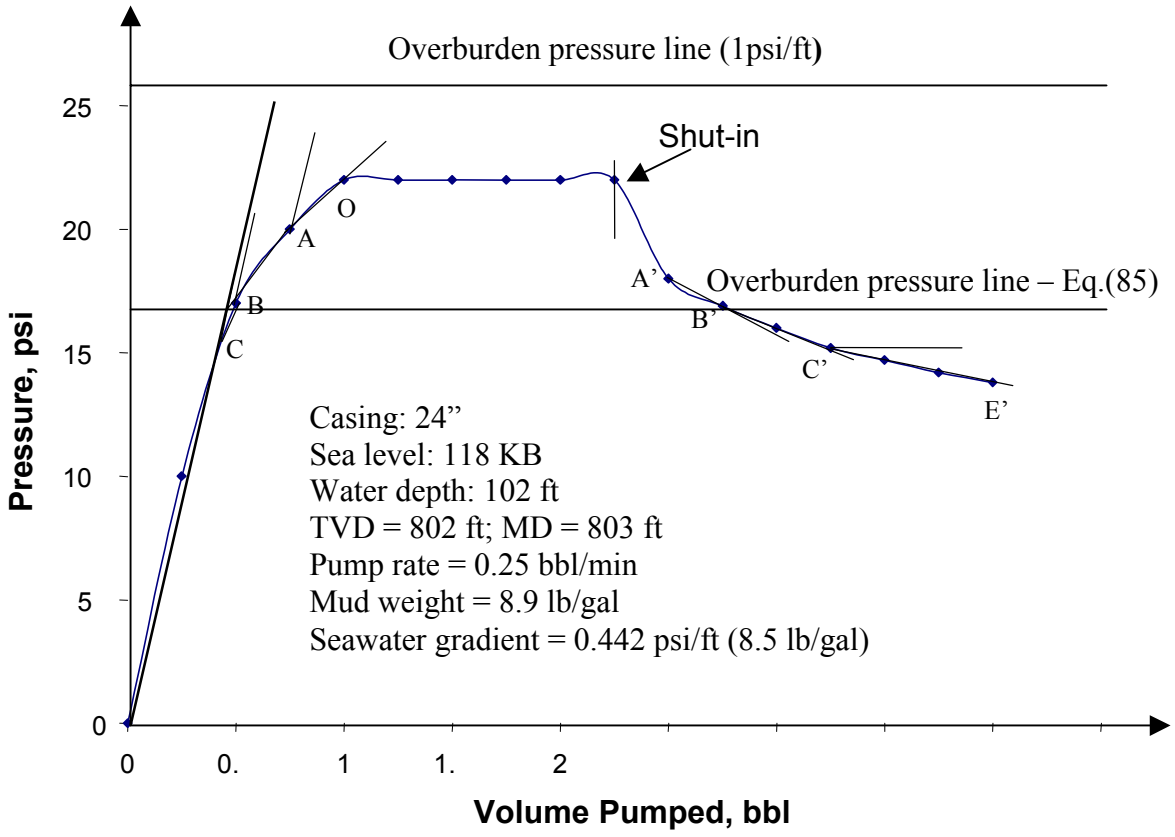

Figure 89. Fall-off pressure analysis - Example 2.

CONCLUSIONS

The study examined geomechanical properties, stresses, strains and failure conditions for wells drilled and cemented in upper marine sediments at shallow depths subsea. Some theoretical observations have been made that are summarized below.

- Very soft sediments may be in plastic state. Their in-situ stresses should be calculated from the presented formula based on elasto-plastic theory;
- Analysis based on elasto-plastic properties of SMS shows that vertical fractures cannot be induced by LOTs in these type of sediments. Therefore, LOT analysis in SMS cannot be extrapolated from the theory developed for conventional LOTs in deep wells;
- Plastic zone develops generally around wells in SMS. However, plastic deformation of the open hole does not result in non-linear pressure-volume behavior. Wellbore expansion during LOT can be calculated from elastic relationship no matter whether the well is in the elastic or plastic state;

- Non-linear behavior of the LOT pressure build-up section results from fluid loss, cement-rock parting, and plastic (non-propagating) fracture in the plastic zone around a wellbore;
- Linear behavior of the LOT pressure build-up section results from mud compression and wellbore expansion. The combination of the two linear and three non-linear factors give possible pressure build-up patterns of LOT in SMS.
- Theoretically, the three mechanisms could be recognized from the analysis of the LOT plot patterns if rock properties were known;

This project makes several theoretical contributions to the knowledge of well integrity in SMS; It provides: new theoretical analysis of stress distribution in SMS and well before and during LOT; new models for non-propagating fracture and cement-rock parting; a software for LOT simulation; and a new concept of contact stress resulting from well cementing.

The project also provides data and statistical analysis of LOTs at shallow depths onshore and off-shore. The analysis leads to the conclusion that - unlike deep wells - no generalized fracture gradient correlation could be made for SMS from statistical analysis of LOTs in the area. The reason is that geology-related (overburden, rock consolidation) and drilling-related (cementing, contact stress) mechanisms may control the test and contribute to large data scatter.

Finally, several specific conclusions can be made from this work:

1. In contrast to LOT data from deep wells showing the maximum breakdown pressure "hump", the plots from shallow LOTs indicate the well failure as pressure stabilization in response to continuous pumping;

2. The plots of LOT data from SMS are inherently non-linear with no indication of the onset of the casing shoe failure.

3. Analysis of field LOT data based upon mathematical model (and software) of casing shoe failure mechanism is difficult because most of the system properties are unknown so there is no reliable data input for the application software. Such software could only be used either for simulation studies or demonstration and training .

4. Analysis of the LOT pressure buildup section alone would be inconclusive and difficult to perform. LOT pressure buildup is usually controlled by combined effect of all volumetric mechanisms working simultaneously: compressibility, growth of plastic rock fracture, propagation of cement parting and filtration to the rock matrix.

5. Porosity trend model in Eq. 4 does not apply to shallow marine sediments. Instead, a regression model has been developed using data from geotechnical borings.

6. Analysis of the stabilized LOT pressure, presented above, identifies the maximum strength of the casing shoe controlled by the rock stress (overburden pressure) and the failure by rock fracturing. When the stabilized LOT pressure is smaller than the maximum strength at the shoe the method provides guidelines regarding most likely mechanism of pressure stabilization.

7. The presented graphical procedure for comparing the plots of actual and equivalent pressure fall-off provides a pattern-recognition method to distinguish the mechanism of cement-rock parting from the fluid loss mechanism.

REFERENCES

Aadnoy, B. S., Soteland, T., Ellingsen, B., 1989, "Casing Point Selection at Shallow Depth", SPE 18718, SPE/IADC Drilling Conference, New Orleans, Louisiana, Feb. 28-Mar. 3, 1989, pp825-836.

Adams, N., and Thompson, J., "How a Geothermal Blowout was Controlled," World Oil, June 1989, 36-40

Arifun and Sumpeno, W. H.: 1994 "A New Approach to Casing Setting Depth Selection in Unocal East Kalimantan Operations", IADC Well Contral Conference of the Americas, Houston Texas, November 16-17.

Bender, C. V., Bourgoyne, A. T., Suheyda, J. N., 1995, "Use of Soil Borings Data for Estimating Break-Down Pressure of Upper Marine Sediments", LSU/MMS Well Control Workshop, May 23-24, 1995.

Bourgoyne, Adam T., Chenevert, Martin E., Millheim, Keith K., Young, F.S., 1991, "*Applied Drilling Engineering*", SPE Textbook Series, Vol. 2., Richardson, Texas.

Cassagrande, A., " Research of Atterberg Limits of Soils," Public Roads, Vol. 13, No. 8, 121-136,1932.

Chen, W. F. and Han, D. J.: *Plasticity for Structural Engineering*, Springer-Verlag New York Inc., 1988.

Chenevert, M. E., and McClure, L. J. 1978, "How to run casing and open-hole pressure tests", *Oil and Gas Journal*, Mar. 06, 1978, pp.66-76.

Danenberger, EP. (1993), "Outer Continental Shelf Drilling Blowouts, 1971-1991" OTC 7248, 2~th Annual OTC in Houston, Texas, May 1993, USA.

Eaton, Ben A., Eaton, Travis L., 1997 "Fracture gradient prediction for the new generation", Wold Oil, October 1997, pp. 93-100.

Harrison, E., Kieschnick, Jr., W. F., McGuire, W. J., 1954, "The Mechanics of Fracture Induction and Extension", AIME Petroleum Transactions, Vol. 201, 1954, pp. 252-263.

Hazov, V. A., Hurshudov, V. A., 1993, "Leak-off tests help determine well bore compressibility", *Oil and Gas Journal*, Nov. 29, 1993, pp. 71-73.

Hubbert, M. K., Willis, D. G., 1957, "Mechanics of Hydraulic Fracturing", Petroleum Transactions (AIME), Vol. 210, pp153-166.

Hughes, Virgina M., P., "Reducing Blowout Incidents Through a Computer Assisted Analysis of Trends of Gulf Blowouts," MS Thesis, The University of Texas at Austin, 1986.

Iskima and Rogiers…….

Jaeger, J. C., and Cook, N. G. W., 1976, "*Fundamentals of Rock Mechanics*", Second Edition, John Wiley & Sons, Inc., New York, USA.

Moria, N. and Black, A. D.: "Theory of Lost Circulation Pressure", 65th Annual Conference and Exhibition, Sept. 1990, SPE 20409.

Morita, N., Fuh, G-F., Boyd, P. A., 1991, "Safety of Casing Shoe Test and Casing Shoe Integrity After Testing", SPE 22557, Proceedings of the 66th Annual Technical Conference and Exhibition of the Society of Petroleum Engineers, Dallas, Texas, Oct. 6-9, 1991.

Nelson, E. B., 1990, *Well Cementing*, Schlumberger Educational Services.

Obert, L., and Duvall, W. I., 1967, *Rock Mechanics and the Design of Structures in Rock,* John Wiley & Sons.

Postler, D. P., 1997, "Pressure Integrity Test Interpretation", Paper SPE 37589, presented at the 1997 SPE/IADC Drilling Conference, Amsterdam, The Netherlands, 4-6 March 1997.

Risnes, R., Bratli, R. K., and Horsrud, P., 1982, “Sand Stresses Around a Well”, SPEJ, Dec. 1982, pp. 883-898.
Rocha, L. A. S., 1993, “Mechanisms of Crater Formation While Drilling a Well”, Dissertation, Louisiana State University, Baton Rouge, LA.
Rocha, L. A. S., Bourgoyne, A. T., 1996, “ A New Simple Method To Estimate Fracture Pressure Gradient”, SPE Drilling and Completion, Sept. 1996, pp153-159.
Sneddon, I. N. and Lowengrub, M., 1969, “*Crack Problems in the Classical Theory of Elasticity*”, John Wiley & Sons, Inc.
Steiger, R. P., Leung, P. K., 1992, “Quantitative Determination of the Mechanical Properties of Shales”, SPE Drilling Engineering Journal, Sept. 1992, pp. 181-185.
Warpinski, N. R. and Smith, M. B.: "Rock Mechanics and Fracture Geometry, in Recent Advances in Hydraulic Fracturing", SPE Monograph, Vol. 12, 57-80.
Wojtanowicz, A. K, and Zhou, D.: 1998, “Borehole Failure Resulting From Formation Integrity (Leak-Off) Testing in Upper Marine Sediments Offshore”, Journal of Energy Resources Technology, Vol. 120, 111-117.
Wojtanowicz, A. K., and Zhou, D., 1996, “Finite Element Analysis of Soft Sediment Behavior During Leak-Off Test,” LSU/MMS Well Control Workshop, Baton Rouge, LA.
Zhou, Desheng, "Well Integrity Mechanism, Failure, and Testing in Shallow Marine Sediments," PhD Dissertation, Louisiana State University, Baton Rouge, Louisiana, August, 2000

APPENDIX A:

FINITE ELEMENT ANALYSIS

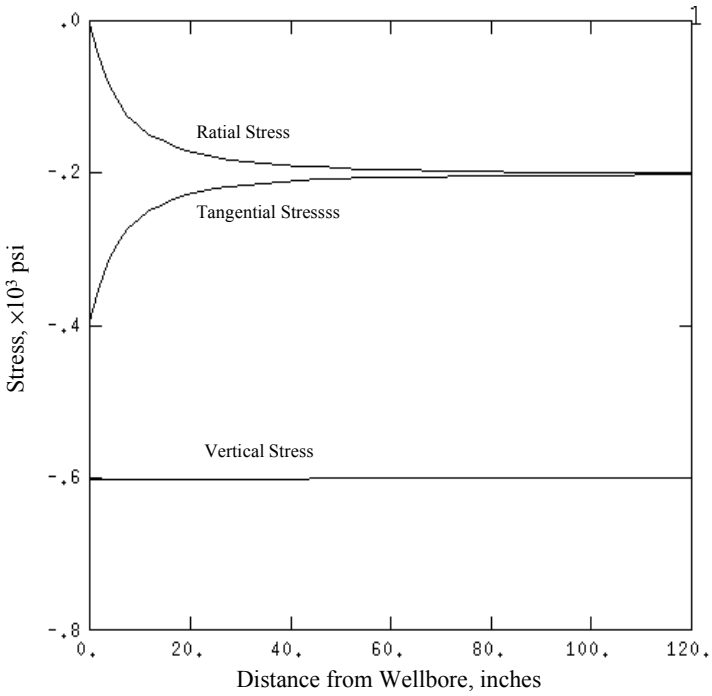

Figure A.1 Stress distribution along line 3 in Figure 15 before LOT - elastic well bore (Case 1).

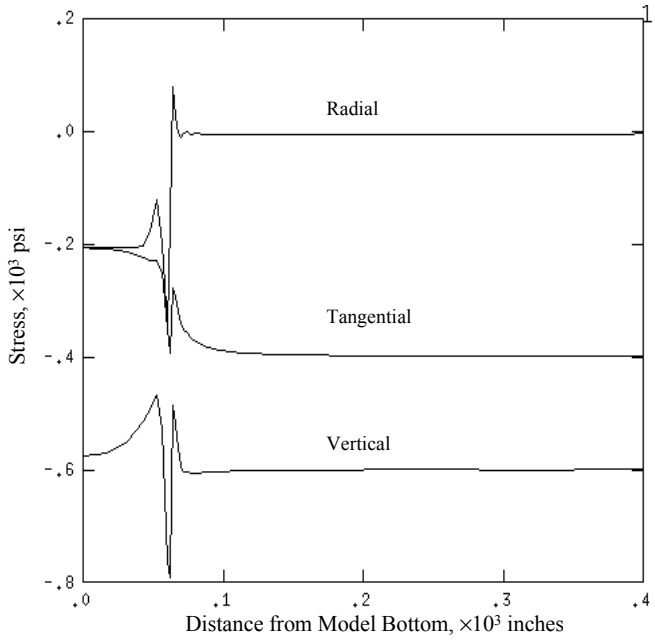

Figure A.2 Stress along Line 5 in Figure 15 for Case 1.

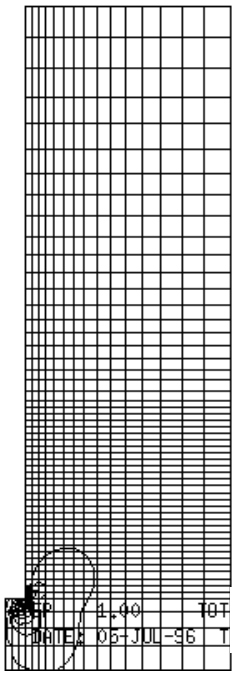

Figure A.3 Shear stress contour around the hole bottom for Case 1 before LOT.

Shear stress concentrates around casing shoe and bottom hole and makes them the most possible places of fracturing.

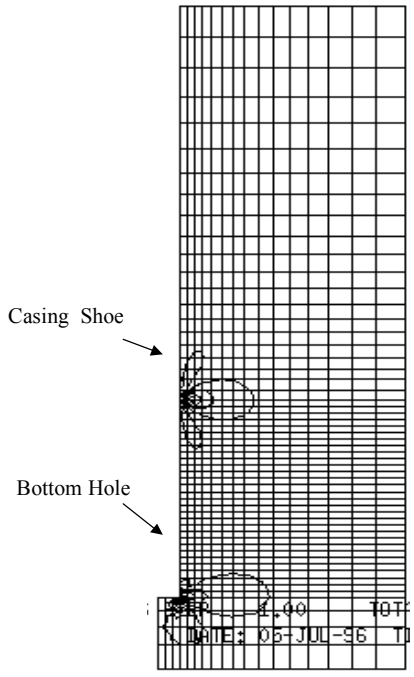

Figure A.4 Shear stress contour for Case 1 during LOT.

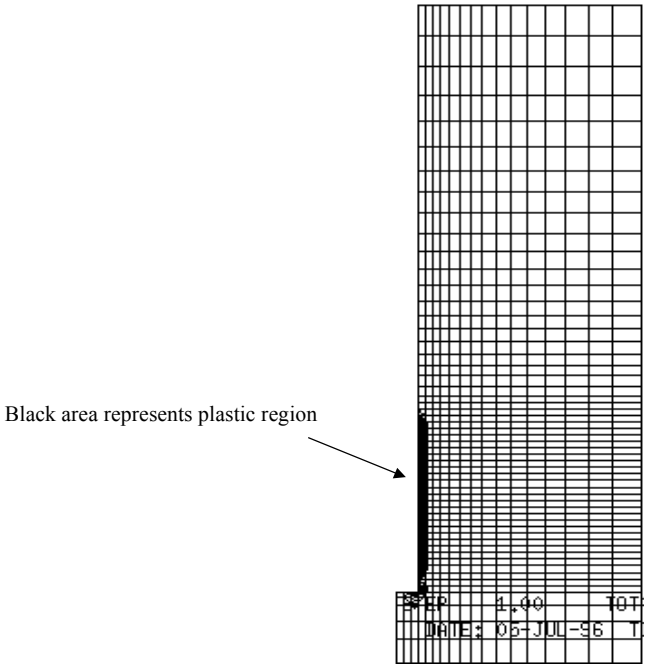

Figure A.5 LOT generates plastic zone around initially elastic wellbore (Case 1 in Figure 15).

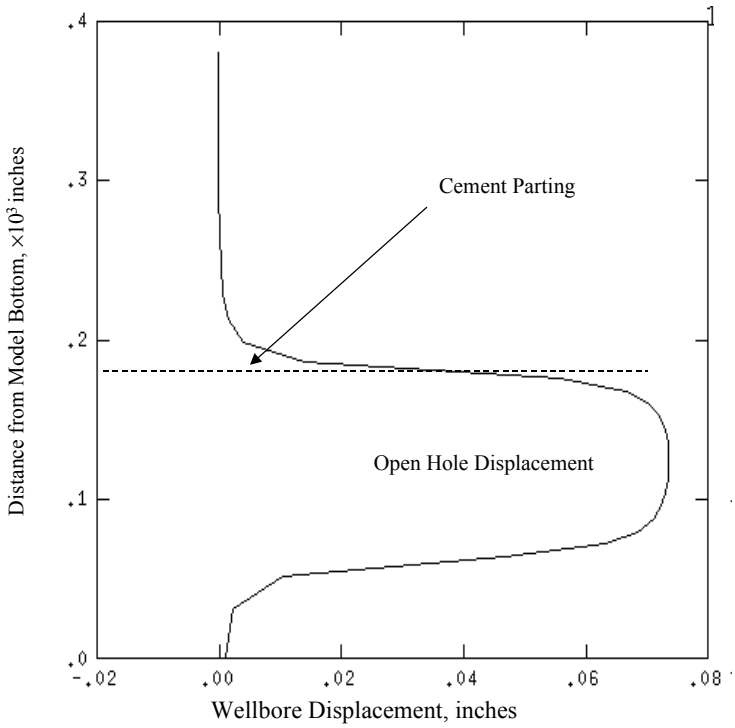

Figure A.6 Cement parting caused by LOT (Case 1).

There was a pre-existing plastic zone around wellbore. Note a rapid drop of tangential and vertical stress at the wellbore

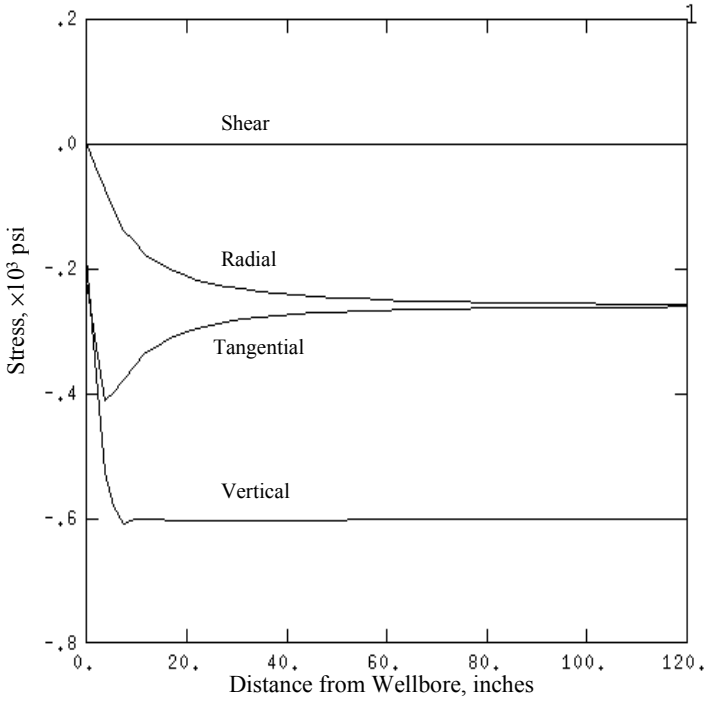

Figure A.7 Effect of pre-existing plastic annulus (Case 2).

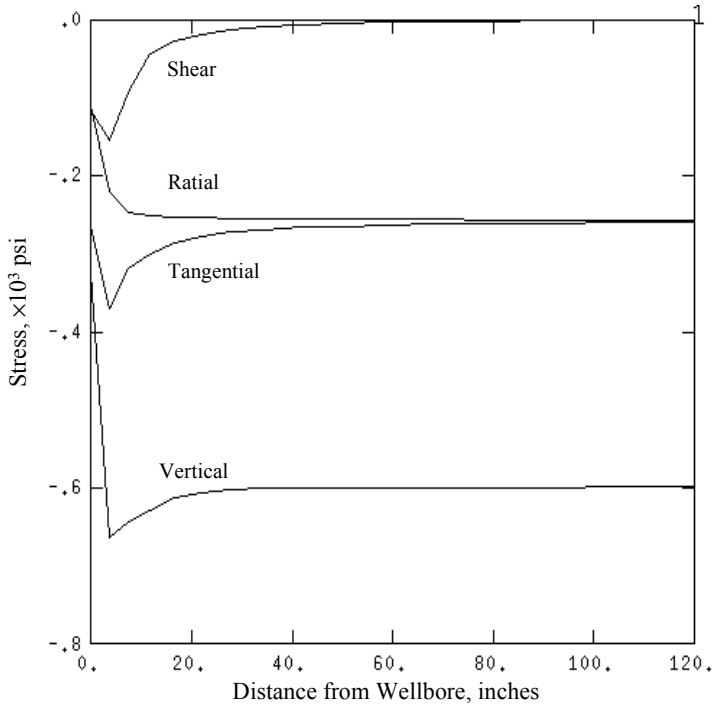

Figure A.8 Stress distribution along Line 4 in Fig. 15 (Case 2, before LOT).

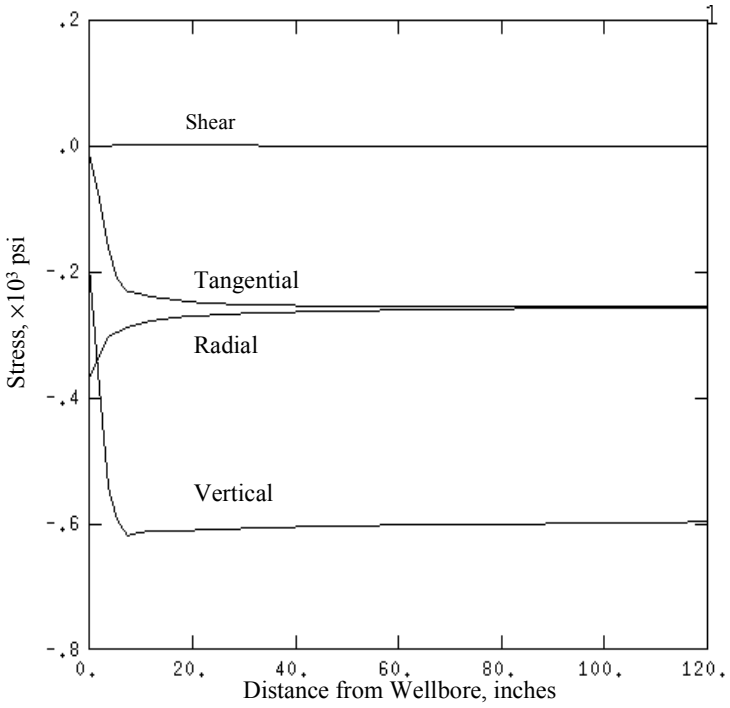

Figure A.9 Tangential stress decreases and radial stress increases during LOT (Case 2).

Tangential compression stress recovers instead of going to tension

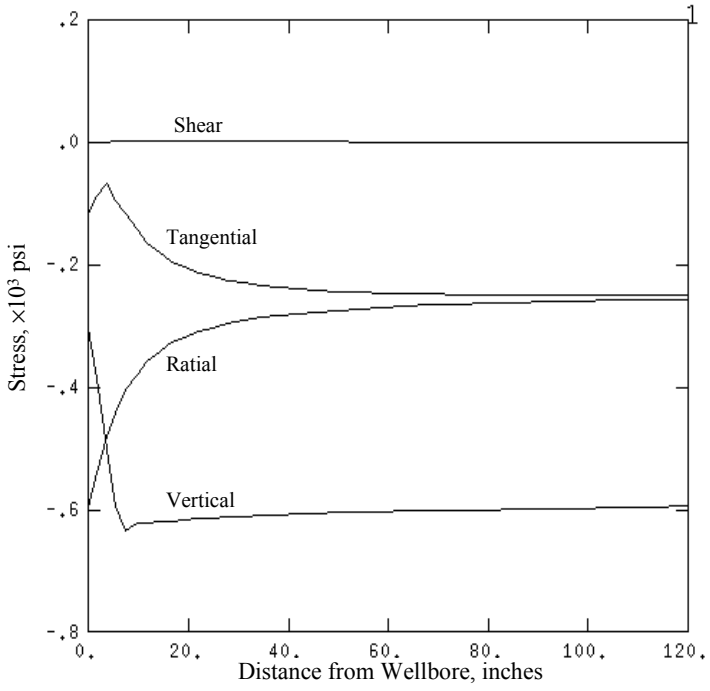

Figure A.10 No vertical fracture possible - even at high wellbore pressure (Case 2).

Plastic yield occurs instead of fracture at bottom of open hole

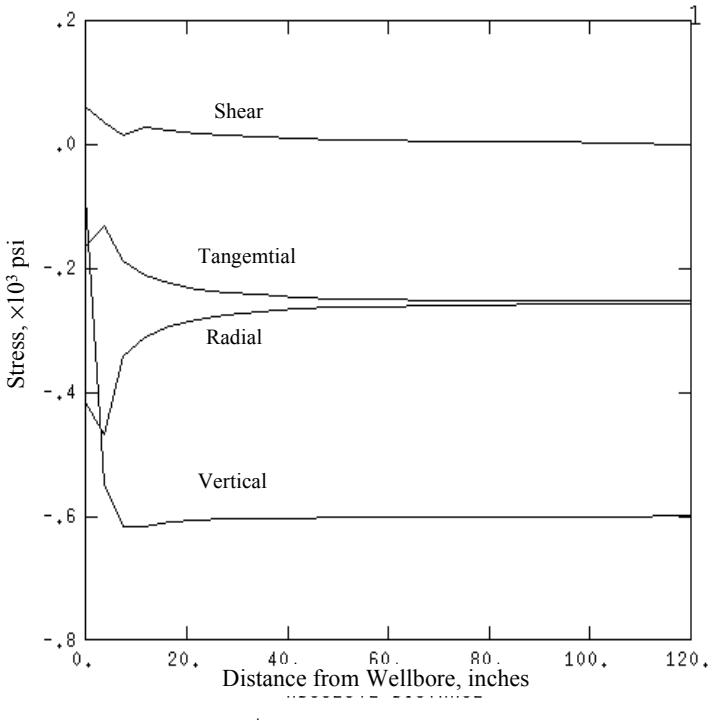

Figure A.11 Stress distribution along line 4 in Figure 15 during LOT (Case 2).

No vertical fracture below casing shoe

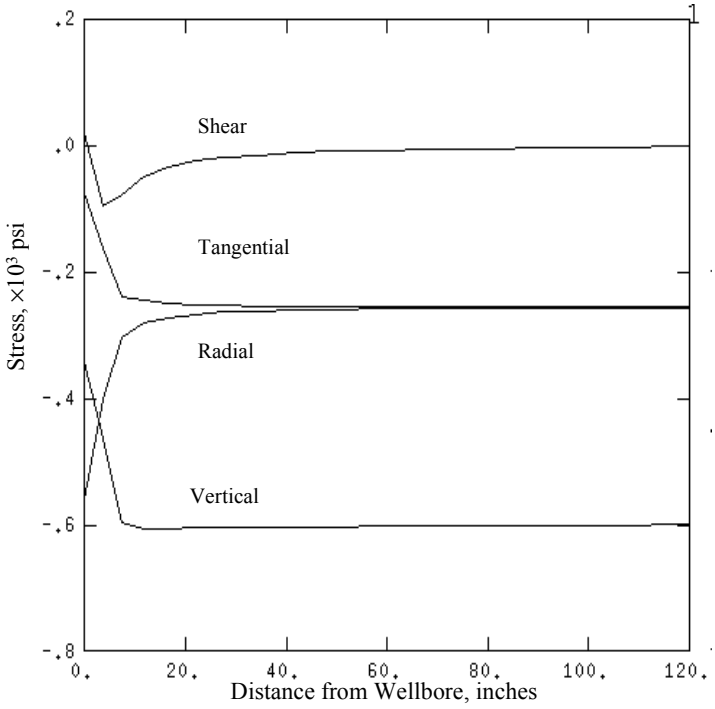

Figure A.12 Stress distribution along Line 2 in Figure 15 for Case 2 during LOT.

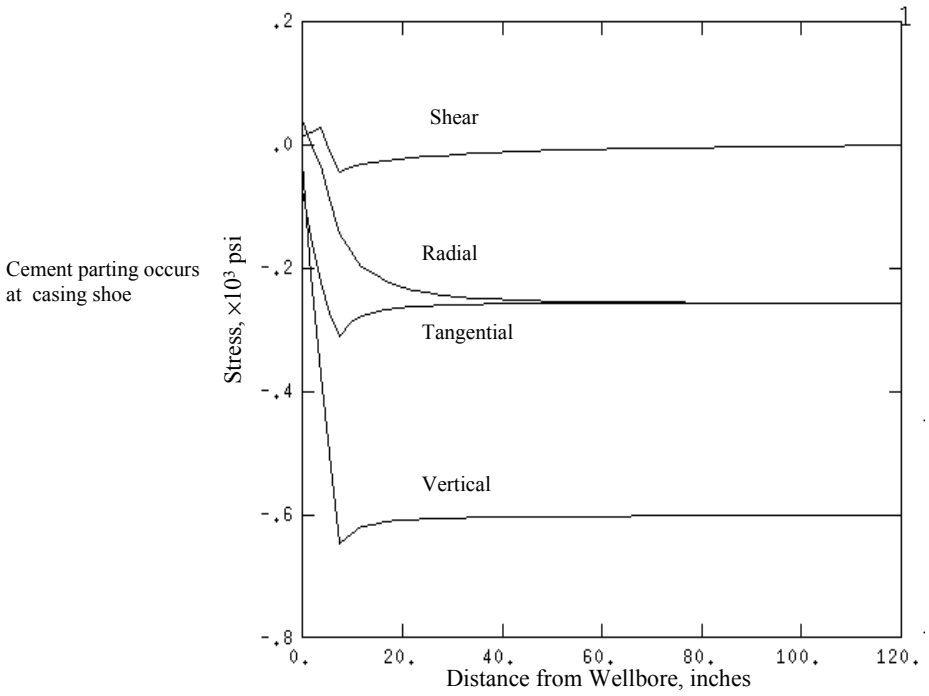

Figure A.13 Stresses along Line 1 of Figure 15 for Case 2 during LOT.

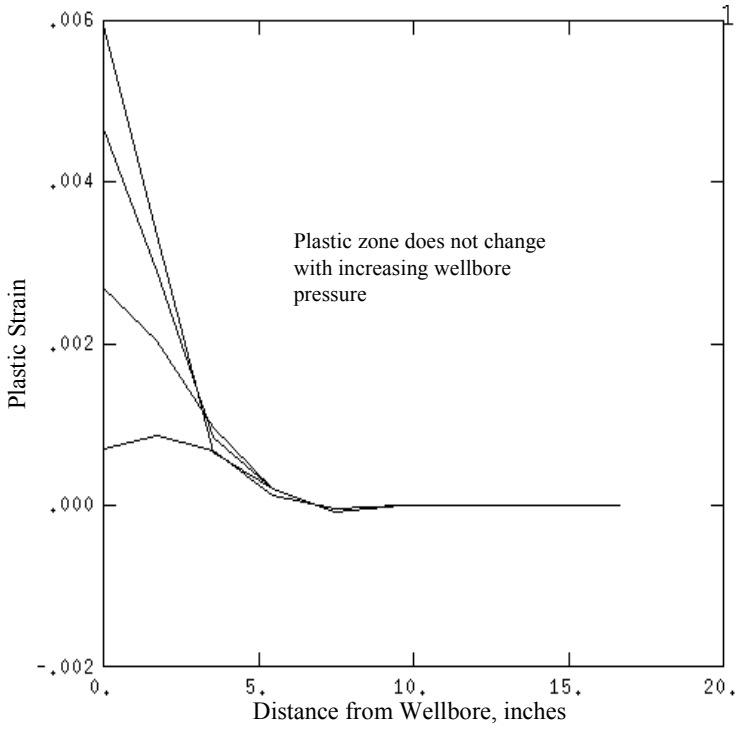

Figure A.14 Plastic strains during LOT for Case 2.

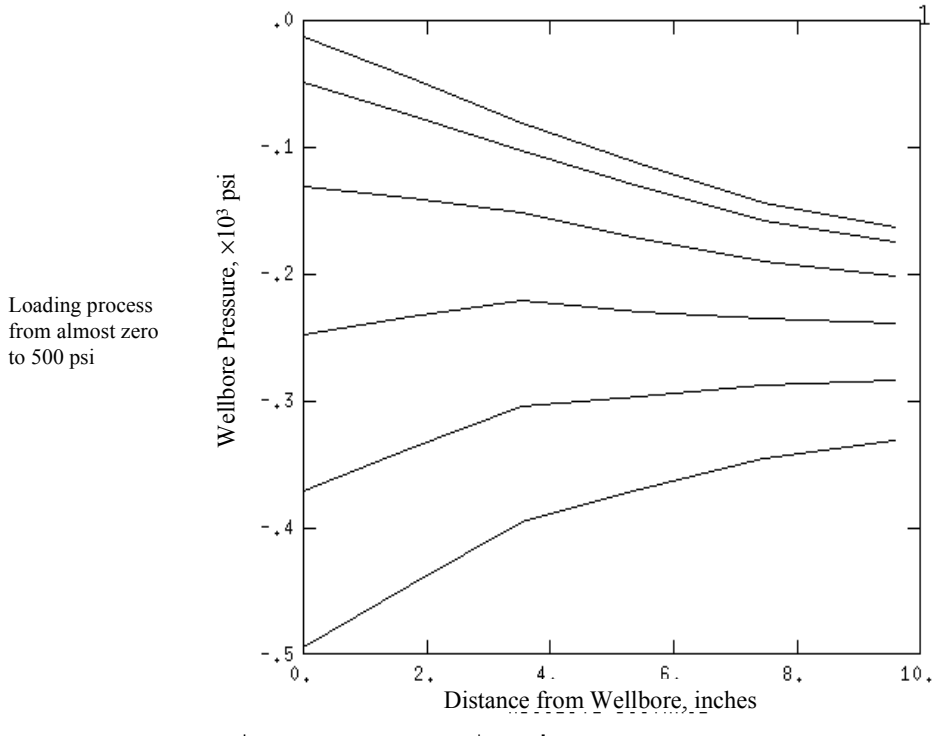

Figure A.15 Selected LOT for further analysis.

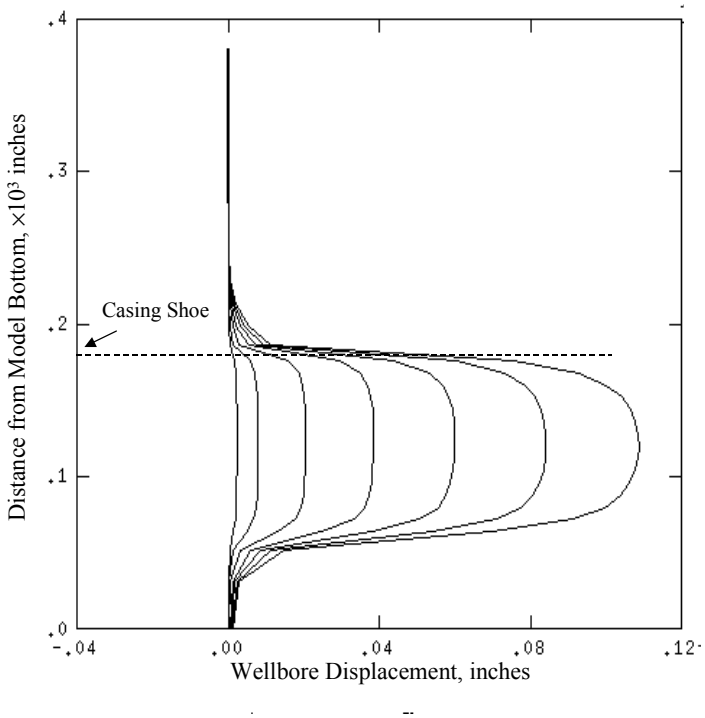

Figure A.16 Radial displacements along Line 5 of Figure 15 for Case 2 at different LOT pressure. Cement parting is obvious.

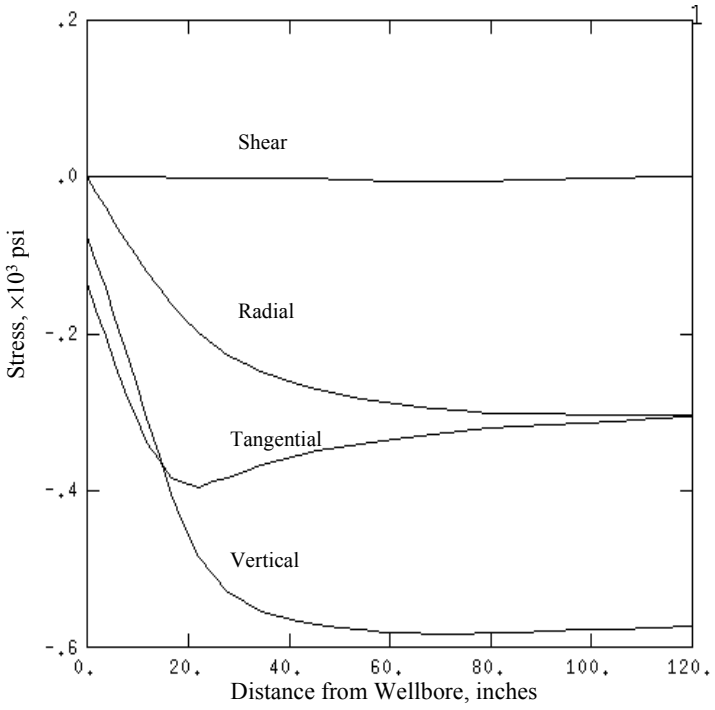

Figure A.17 Stress distribution along Line 3 of Fig. 15 before LOT for Case 3.

No vertical fracture possible

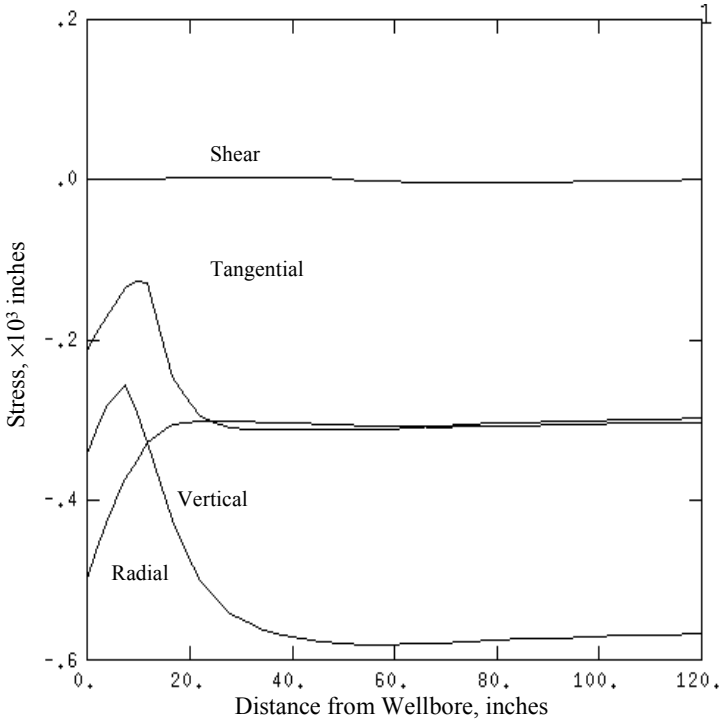

Figure A.18 Stresses during LOT for Case 3.

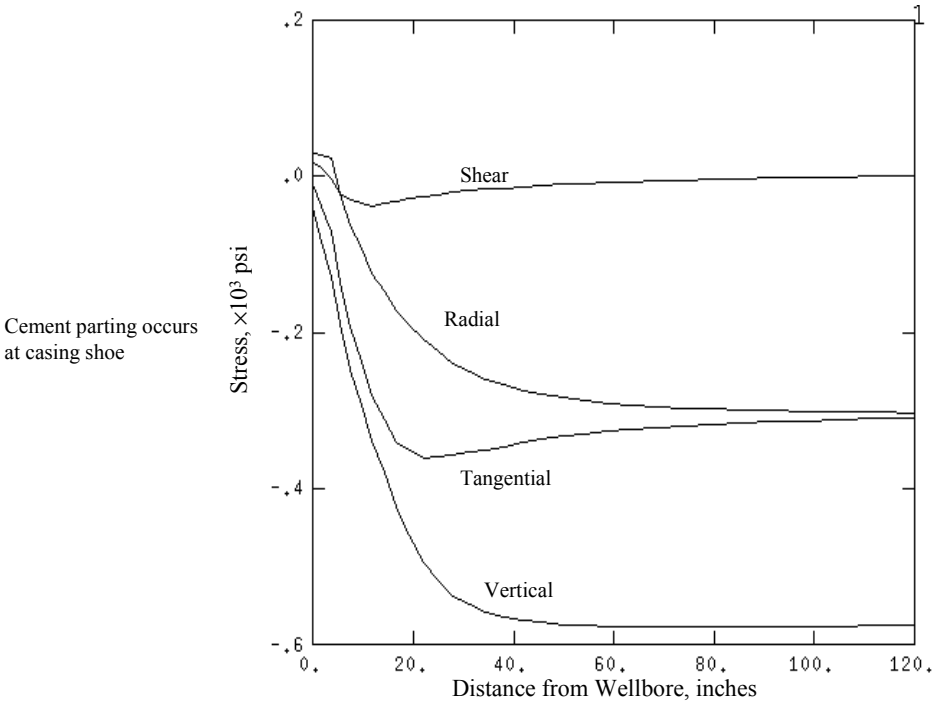

Figure A.19 Stress distribution along Line 1 in Fig. 15 for Case 3 during LOT.

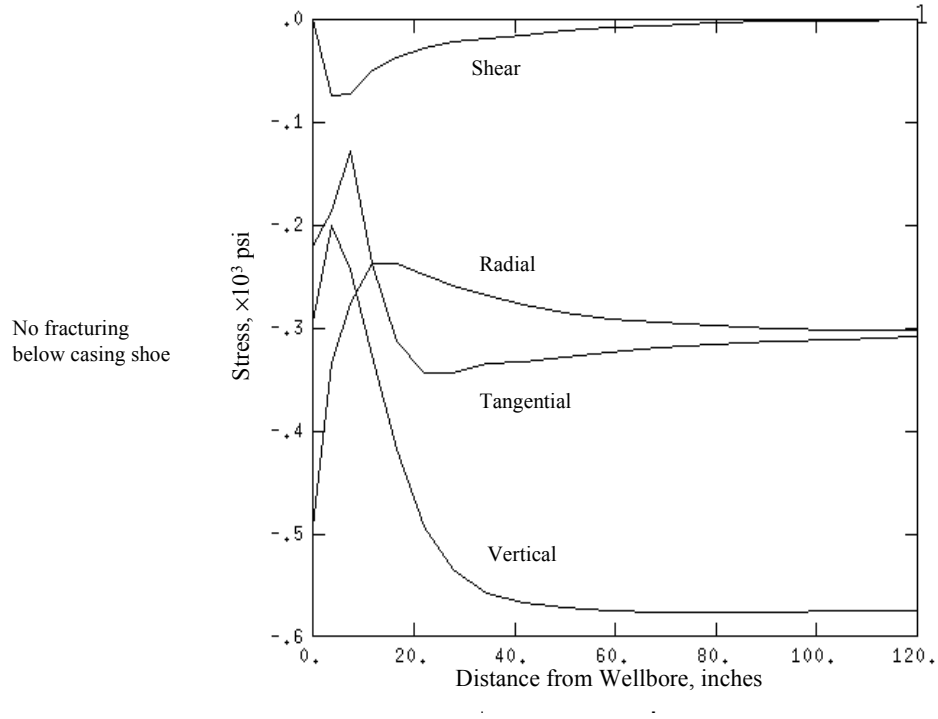

Figure A.20 Stress distribution along Line 2 in Fig. 15 for Case 3 during LOT.

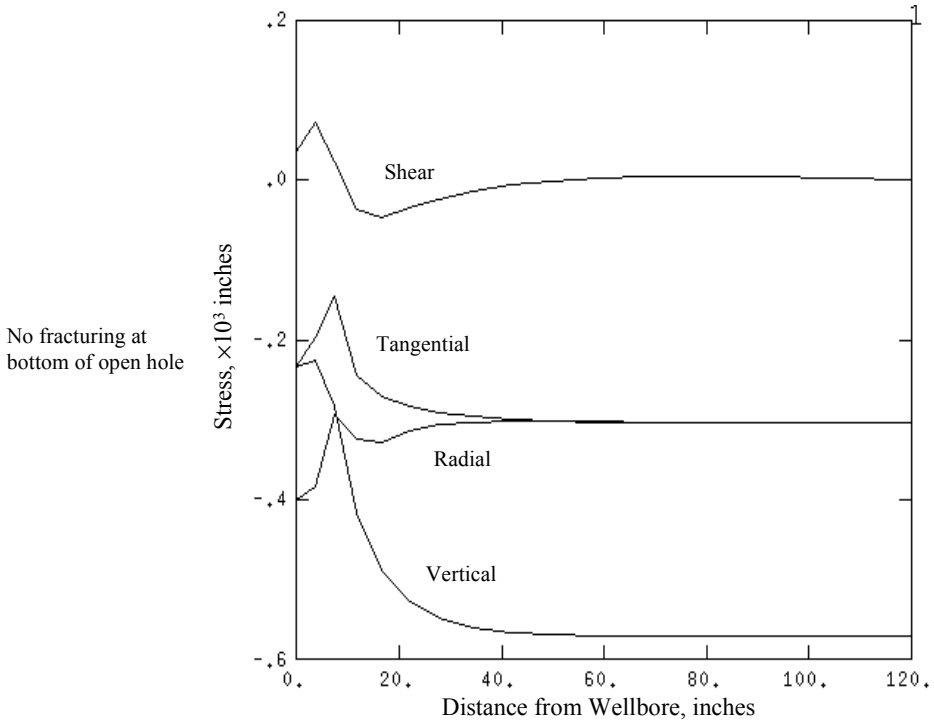

Figure A.21 Stresses along Line 4 in Figure 15 for Case 3 during LOT.

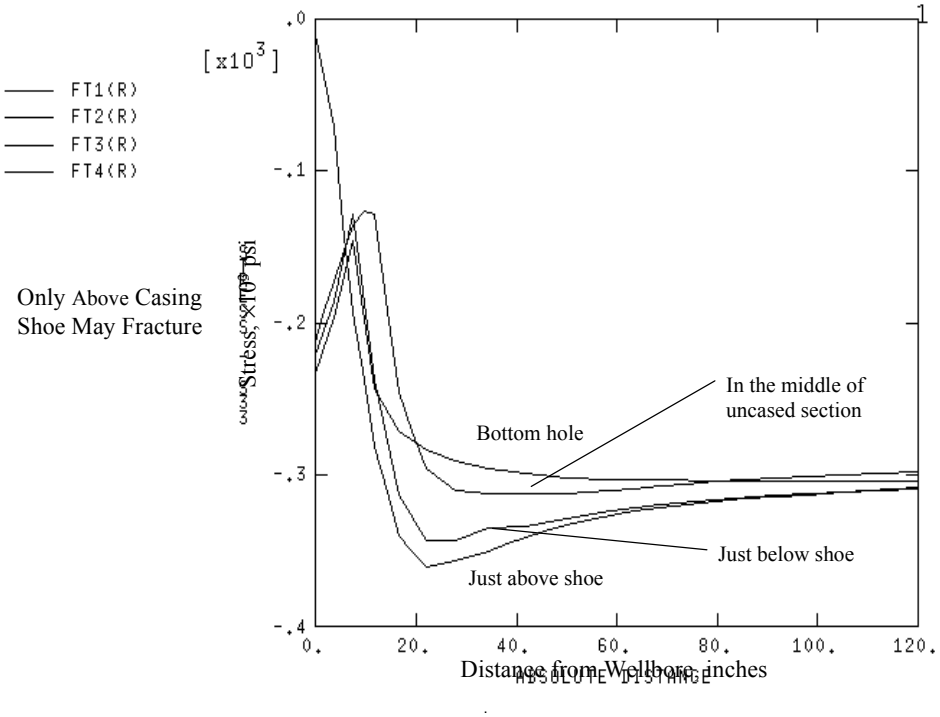

Figure A.22 Tangential stresses along different horizontal lines in Fig. 15.

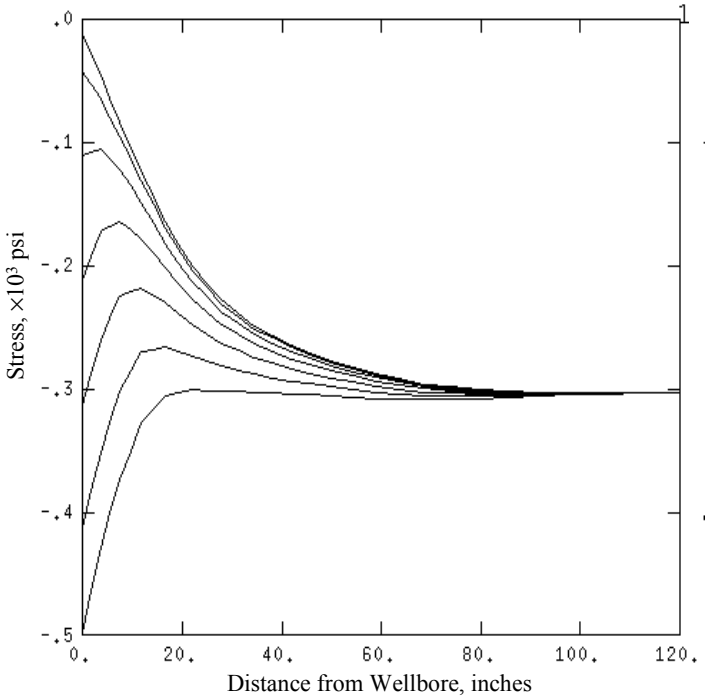

Figure A.23 Radial stresses along Line 3 in Fig. 15 for Case 3 at different LOT pressures.

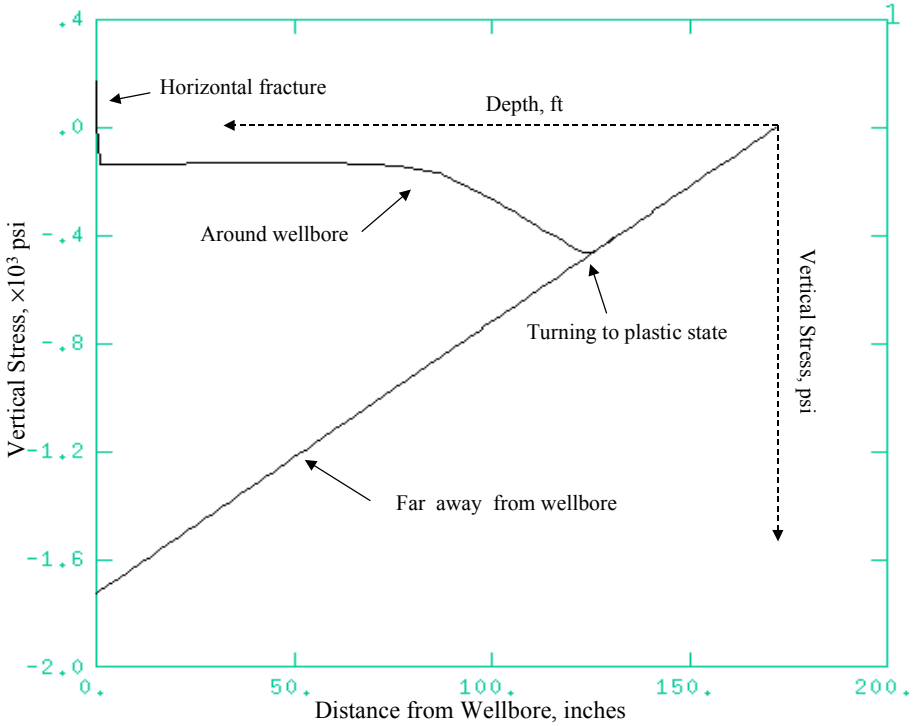

Figure A.24 Vertical stress distribution around and away from the wellbore.

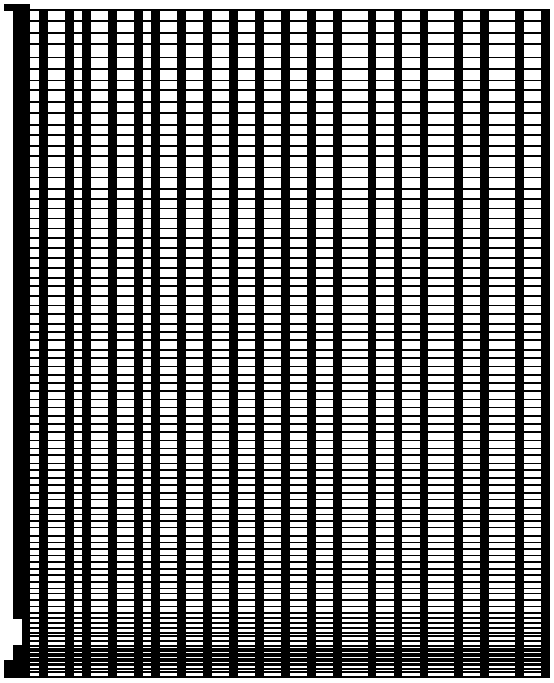

Figure A.25 Finite elements and nodes for the analysis of horizontal fracture.

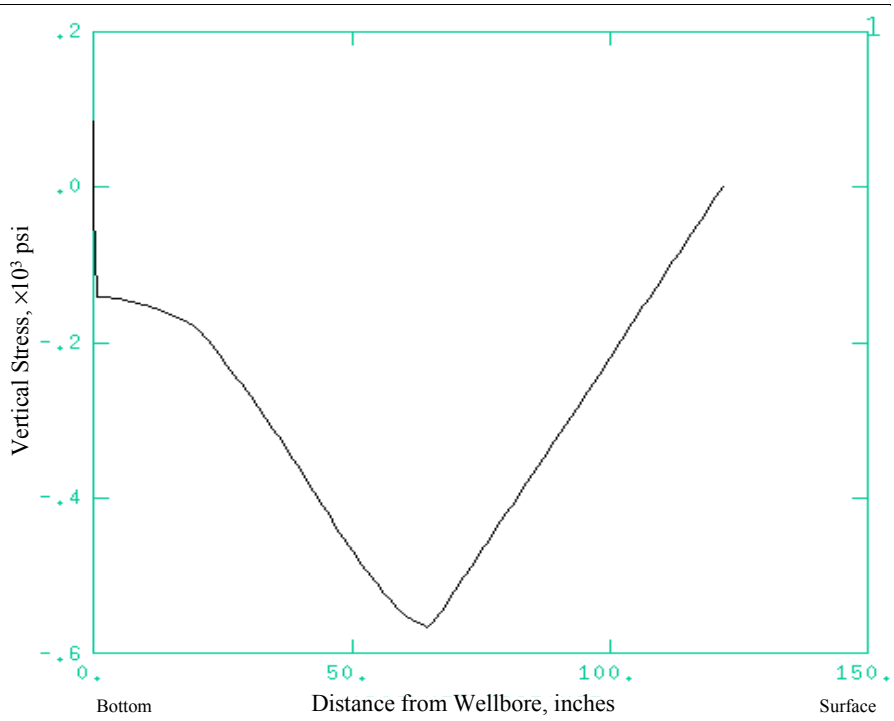

Figure A.26 Effect of casing diameter (Table 3).

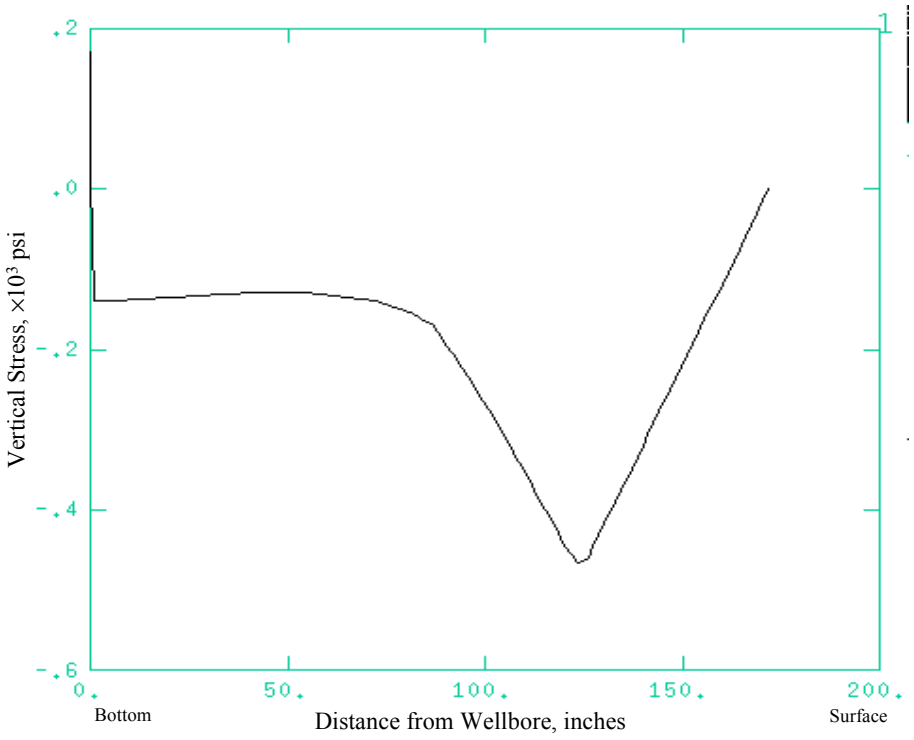

Figure A.27 Effect of formation depth (Table3).

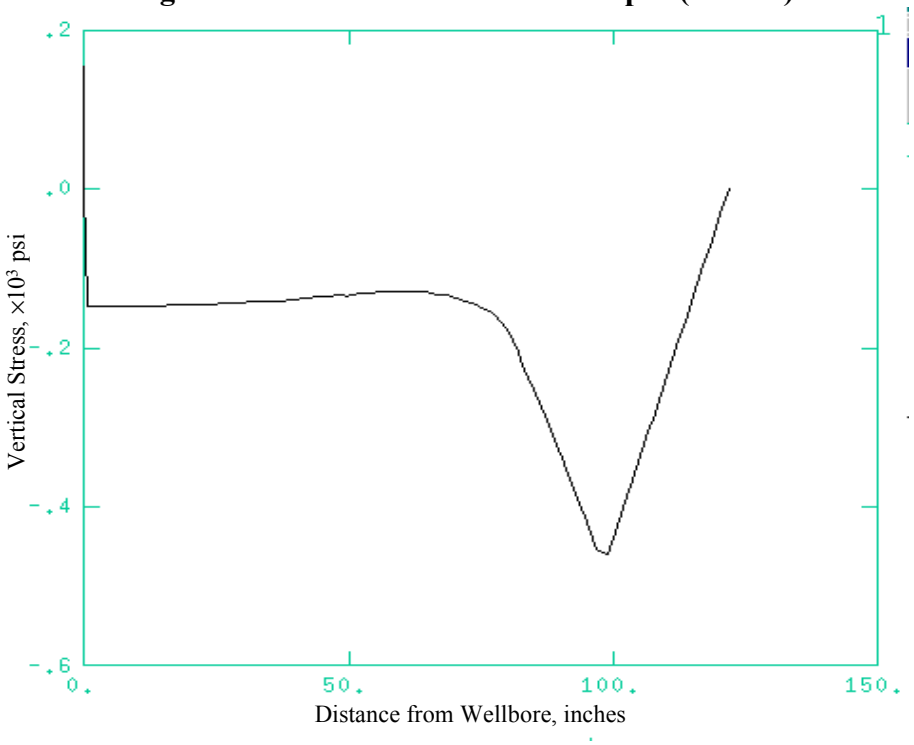

Figure A.28 Effect of formation density (Table 3).

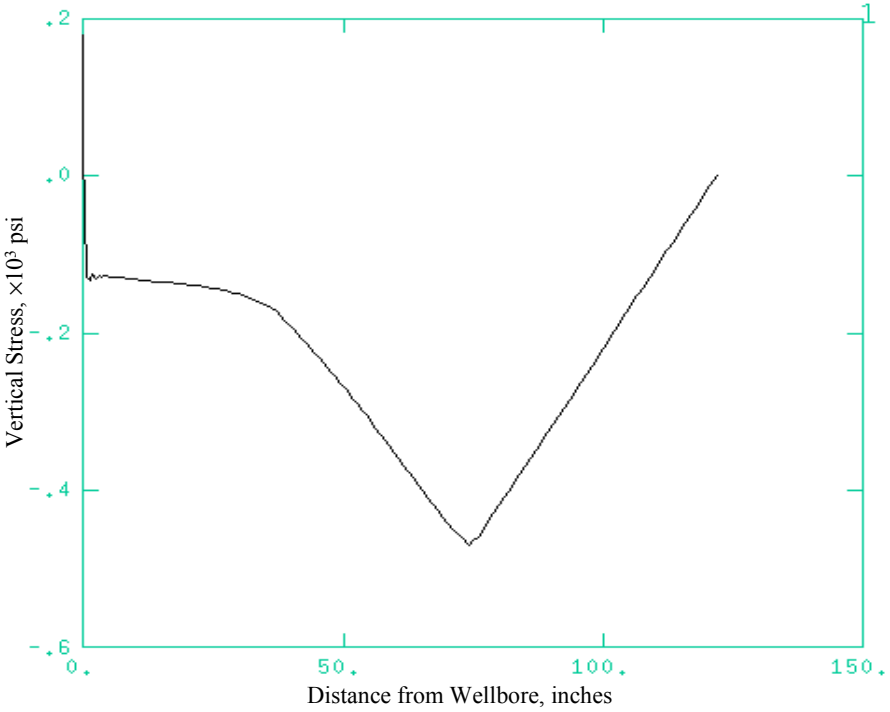

Figure A.29 Effect of formation Young's modulus (Table 3).

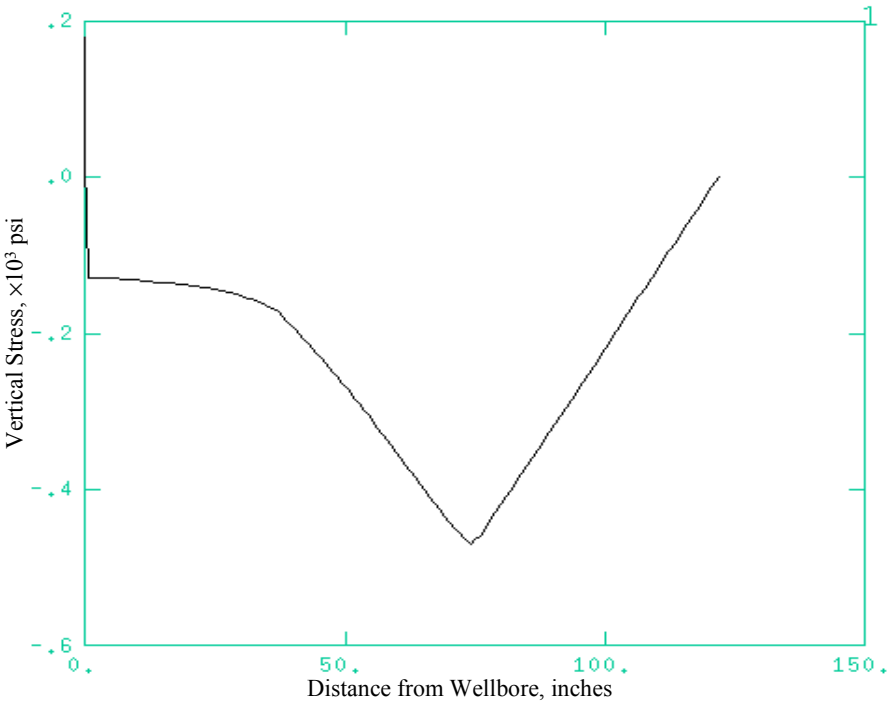

Figure A.30 Effect of casing Young's modulus (Table 3).

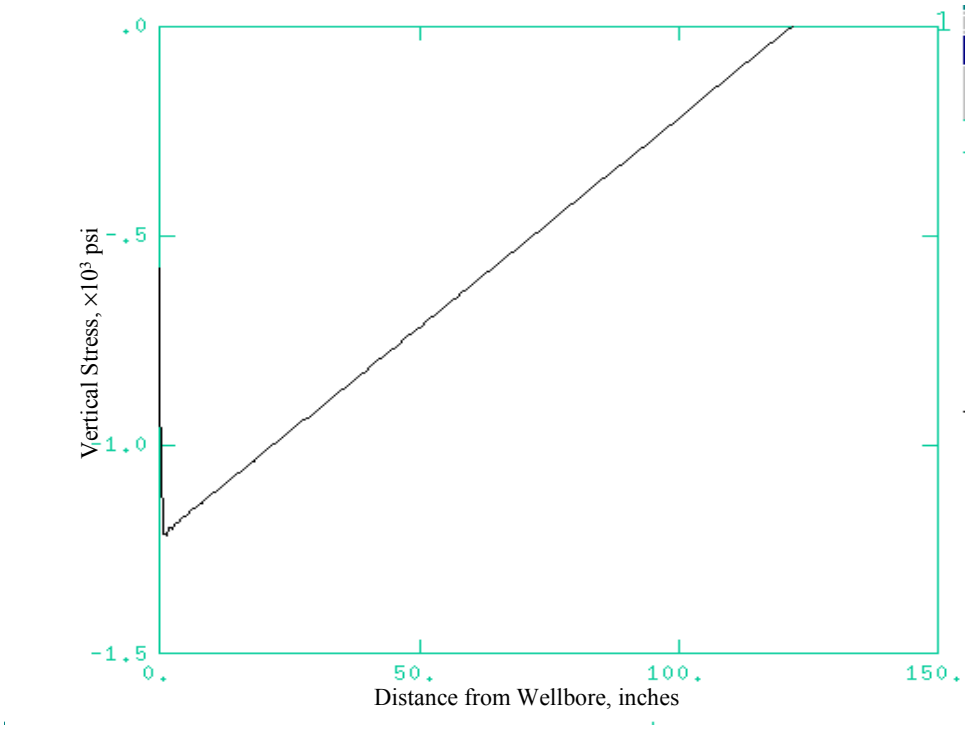

Figure A.31 Elastic wellbore case: no vertical stress reduction around wellbore and no horizontal fracture.

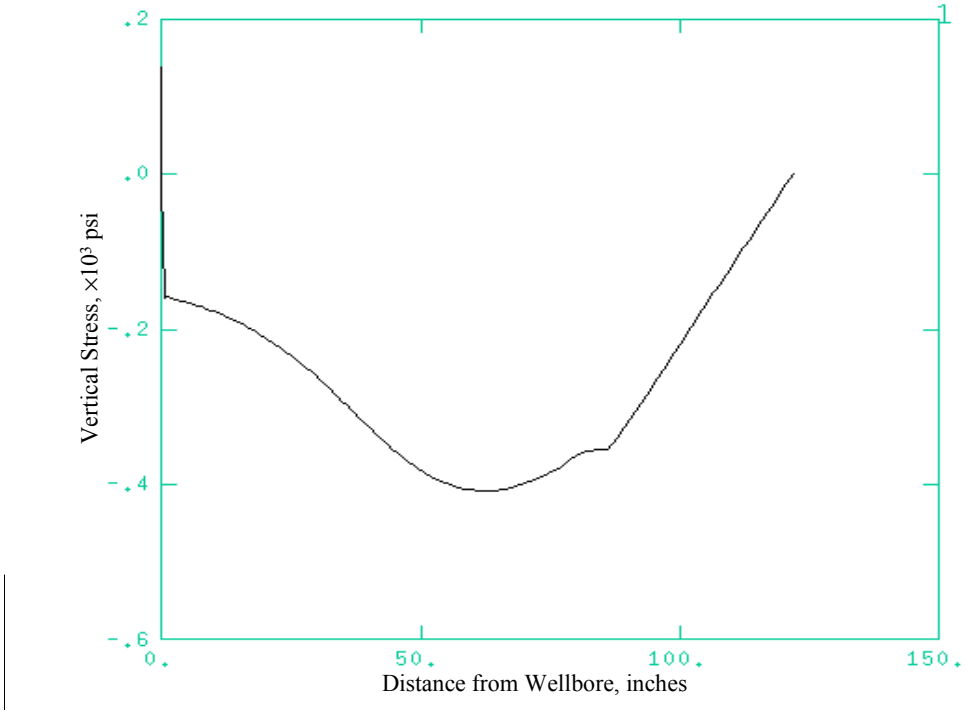

Figure A.32 Effect of Poisson's ratio (Table 3).

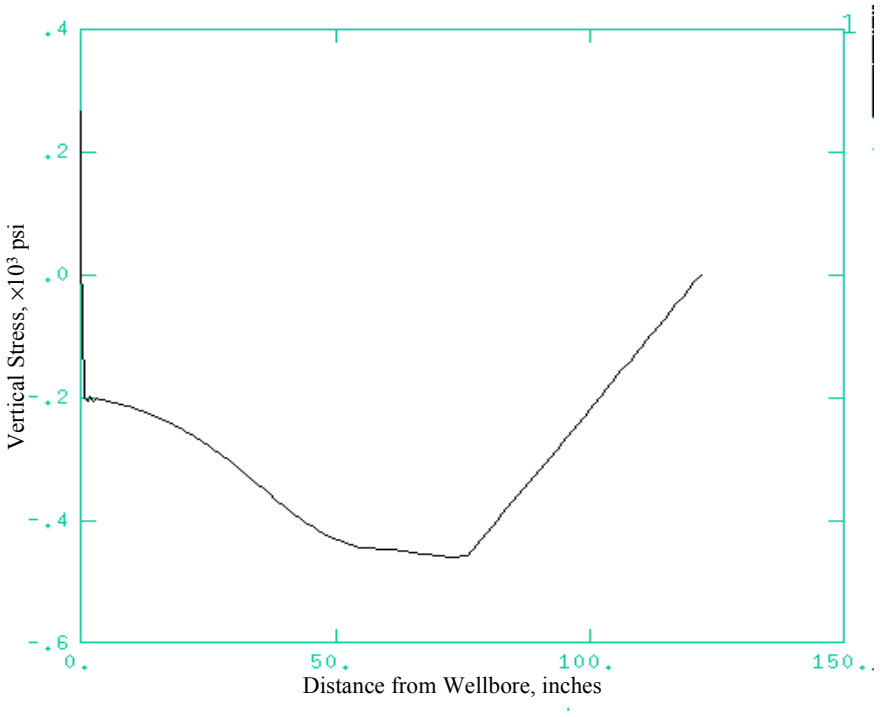

Figure A.33 Effect of friction angle (Table 3).

APPENDIX B:

DETERMINATION OF OVERBURDEN PRESSURE IN SMS

Overburden pressure can be calculated from bulk rock density data available from well logs, cores, or geotechnical tests. If the bulk density (ρ_b) is known as a function of depth, overburden pressure is calculated by integrating the bulk density,

$$p_{over} = \int_{o}^{D_w} g\,\rho_w\,dD + \int_{D_w}^{D} g\,\rho_b\,dD \qquad \text{(B.1)}$$

where; D_w and ρ_w are water depth and density, D and ρ_b are the vertical depth and bulk density - a function of depth below the sea floor.

Bourgoyne et al (1991) presented a porosity method to estimate bulk density at any depth as,

$$\rho_b = (1-\phi_0 e^{-KD_s})\rho_{grain} + \phi_0 e^{-KD_s}\rho_{fluid} \qquad \text{(B.2)}$$

Where:

ϕ_0, and K = surface porosity and porosity decline exponent, respectively;
ρ_{grain}, and ρ_{fluid} = densities of sediment matrix and pore fluid, respectively;
D_s = sediment's depth.

Formula (B.2) applies to the deep sediments in the Gulf of Mexico. However, as shown in Fig.B-1, it does not match the density data from SMS in the Green Canyon area in the Gulf of Mexico (Rocha, 1993; and Bender et al.,1995). (Parameter values used in Eq. B.2 are: grain density $\rho_{grain}= 2.65$, surface porosity $\phi_0=0.77$ and porosity decline constant $K=323E\text{-}6$.) Figure B-1 indicates that the porosity-based model underestimates sediment density and, therefore, it would underestimate overburden pressure in SMS.

Correlations for shaly SMS

Empirical correlations have been developed by considering sediment lithology and curve fitting bulk density data from soil borings in the Green Canyon area. For the sediment comprising mostly shale and clay deposits the empirical model provides three different formulas based on the depth range as follows:

$$\begin{aligned} \rho_1 &= 1.37(2-e^{-D/400}) && 0 \le D < 100 \\ \rho_2 &= 1.65(2-e^{-D/5500}) && 100 \le D < 650 \\ \rho_3 &= 1.7(2-e^{-D/8000}) && 650 \le D < 3000 \end{aligned} \qquad \text{(B.3)}$$

Where:

ρ = density, gm/cc; and,
D = depth, ft.

Figure B.2 compares density data in the Green Canyon area and the calculated value from Eq. B-3. In the figure, the plots named Model 1, 2, and 3 have been based on the formulas for ρ_1, ρ_2, ρ_3 in Eq. B-3, respectively.

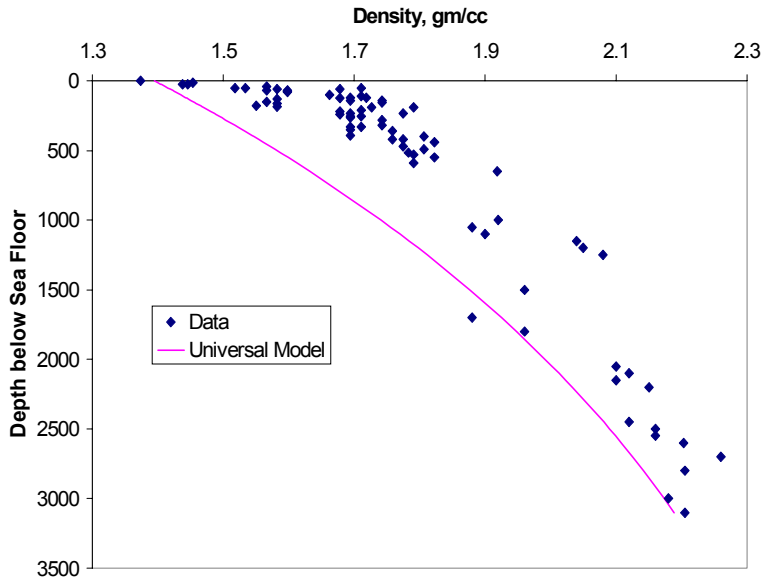

Figure B.1 Comparison of SMS bulk density from Green Canyon area with prediction from the porosity-based model.

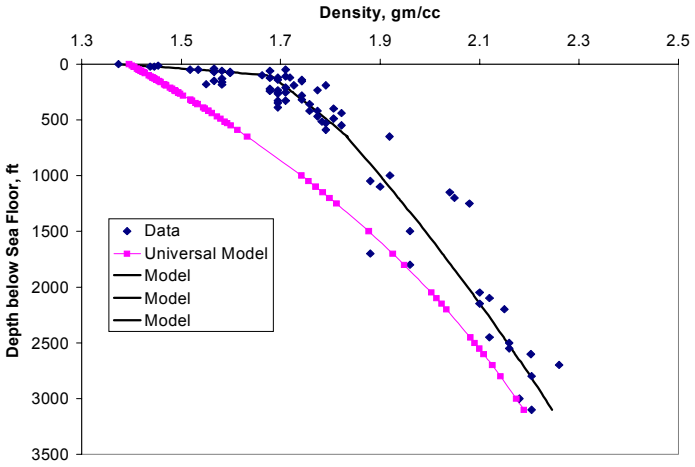

Figure B.2 Difference between the porosity-based model and the correlation proposed in this report.

To derive overburden pressure correlations we substitute Eqs. B.3 into Eq. B.1 and after integration obtain the following formulas:

$$\begin{aligned} p_{over} &= g\rho_w D_w + 1.2D_s - 240(1 - e^{-D/400}): && 0 \le D_s < 100 \\ p_{over} &= g\rho_w D_w + 66.9 + 3929.5e^{-D_s/5500} + 1.4289D_s - 4001.56: && 100 \le D_s < 650 \\ p_{over} &= g\rho_w D_w + 485.6 + 5888.8e^{-D_s/8000} + 1.4722D_s - 6386.19: && 650 \le D_s < 3000 \end{aligned} \quad \text{(B.4)}$$

Where:

p_{over} = overburden pressure, psi;
D_s = sediment depth, feet.

Correlations for SMS comprising sand and shale

Sediments in the Green Canyon area from 0 to 650 ft below sea floor are mostly clays. Thus, the correlation in Eq. B.3 applies only to shales. However, for sediments with sand layers in shallow marine sediments, the correlation of density versus depth is different.

As shown in Fig. B-3, sediment density is approximately 1.98 gm/cc (0.86 psi/ft) for sand, and 1.90 gm/cc (0.82 psi/ft) for shaly sand. Data from other areas in the Gulf of Mexico (such as Ship Shoal, Vermilion , West Delta, Grand Isle) support the approximation as shown in Fig. B.4.

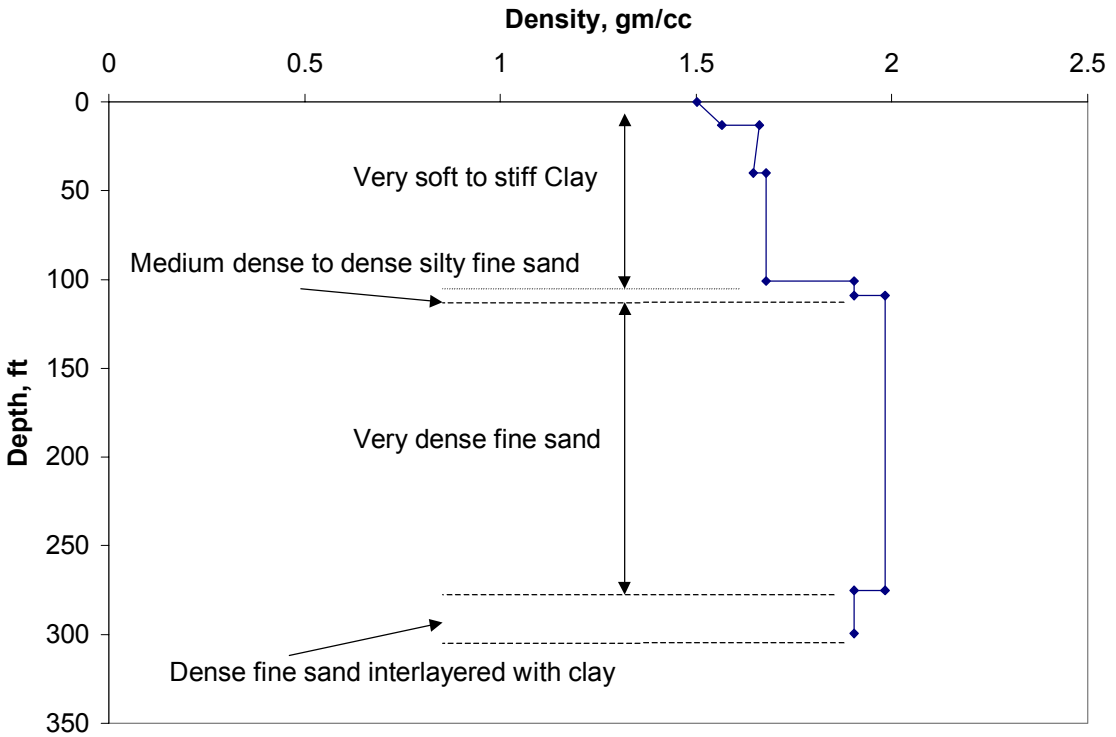

Figure B.3 Densities of SMS comprising sand and shale (Grand Isle area).

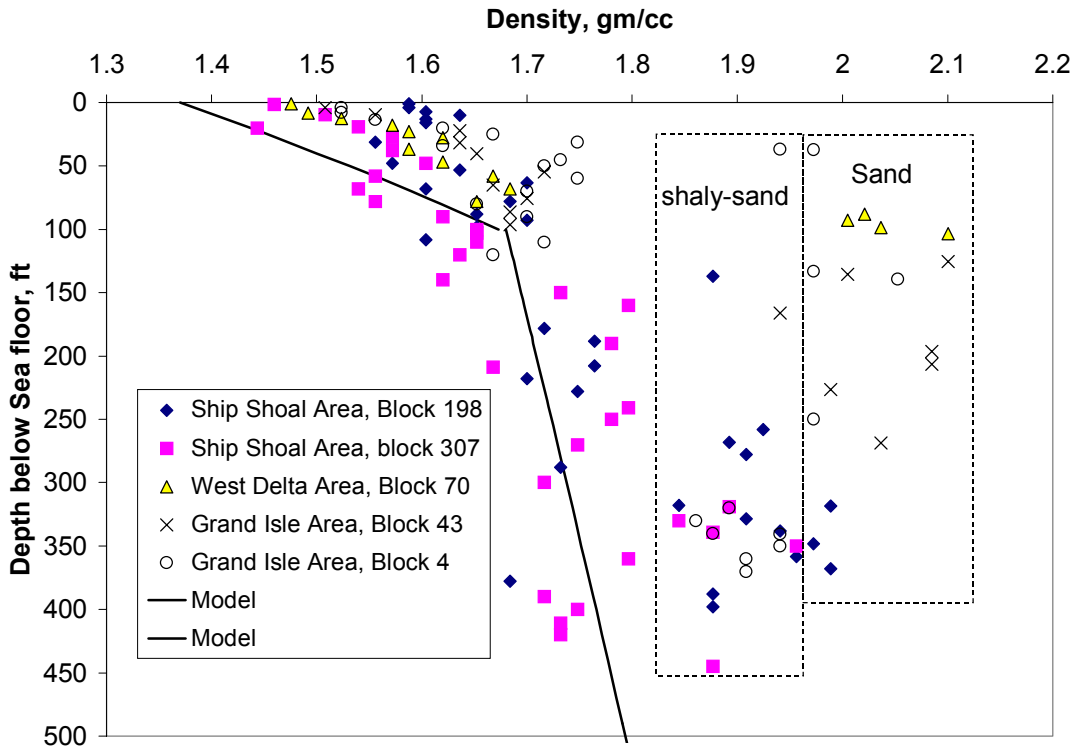

Figure B.4 Densities of SMS containing sand and shale in the Gulf of Mexico.

The proposed model in Eq. B-3 represents overburden pressure of pure shale sediments and gives the minimum values for SMS. If the sediment contains sand or sand-clay mixture, its density will be greater. Figure B.5 shows a comparison of the model results with soil borings data from the Vermilion and Ship Shoal areas.

As shown in Fig. B-4 sandy sediment density value of 1.98 gm/cc is constant and independent from depth. Thus, unlike the shale model in Eq. B-3 representing compaction of shale the sand density model is just a constant.

For SMS comprising mixed layers of sand and clay overburden pressure can be estimated as

$$p_{over} = p_{over-clay} + 0.86 D_{sand} \qquad \text{(B.5)}$$

where;

p_{over}	=	overburden pressure, psi;
D_s	=	depth (or total thickness) of sediment (clay), feet;
$g\rho_w D_w$	=	pressure of sea water, psi;
D_{sand}	=	depth (or total thickness) of sand, ft;
D	=	depth, ft
$p_{over\text{-}clay}$	=	overburden pressure from Eqs. (B-4) for clay deposit thickness: $D_s = D - D_{sand}$.

For example, if the depth of interest is 1000 ft below the sea floor (1,750 ft of water having gradient 0.442 psi/ft) and the total sand thickness within this depth range is 400 ft then, overburden pressure from the sand is (0.86*400=) 344 psi; overburden pressure from the clay is (66.9+3929.475e$^{-600/5500}$+1.4289*600-4001.56=) 446 psi; and overburden pressure from the sea water is (0.442*1750=) 773.5 psi. Therefore, the total overburden pressure at 1000 ft is (344+446+773.5=) 1563.5 psi.

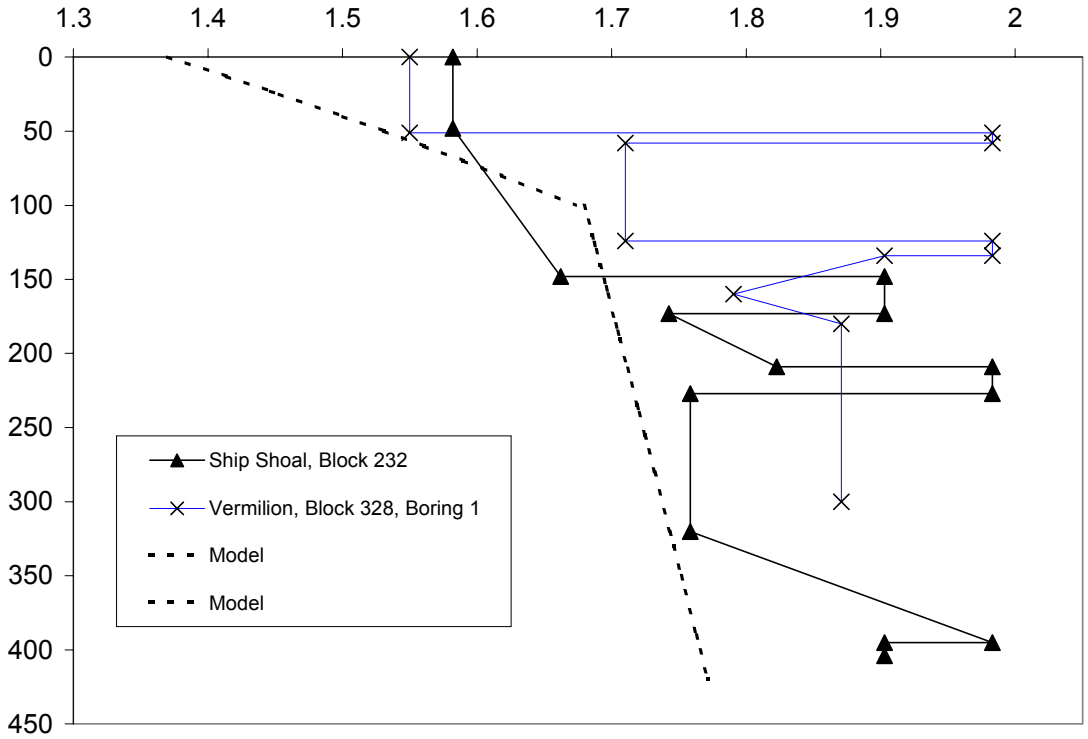

Figure B.5 Comparison of shale model (Eq. B-3) with data from shaly-sand SMS.

APPENDIX C:

LOTUMS SOFTWARE INSTALLATION AND USE

LOTUMS, leak-off test in upper marine sediments, is developed for simulating leak-off test. The basic principle of the software was discussed in Chapter 7.

LOTUMS Installation

The file is stored in a CD with a name of LOTUMS.exe. It can be run on the CD directly. If copied on hard drive a computer with MS Windows, LOTUMS runs better from hard drive. Skilled computer user can skip this section.

To install the software just copy the file (LOTUMS.exe) from CD to the directory of one's hard drive. The detail procedure is:

(1). Insert the disk in CD driver.
(2). Create a directory in one's computer (using File Manager, Windows Explorer or DOS) as C:\LOTUMS.
(3). Copy the file from CD drive to C:\LOTUMS.
(4). Check the file LOTUMS.exe in one's C:\LOTUMS otherwise copy again.

For some computer without dynamic link library, the direct copy method may fail. The disk provides an install package to install the software on any PC. To install from the package (in the CD or coped file in one's hard drive), go to package directory and double click "setup.exe" file, the installation begins. Follow the guides of the installation to complete the installation.

Use LOTUMS

The usage of the software is very simple. Double click the file LOTUMS.exe using one's mouse from Windows Explorer to execute the program. Note that the windows of the software may not fit one's computer screen very well but it will not affect his executing.

After the software is running on one's computer, windows appear. Users can follow the guides of the software and do leak-off test analysis following the menu of the software. Users may follow the procedure as follows:

(1). Double click the file LOTUMS.exe on you CD or hard drive.
(2). A flash window appears. If one is a legal user, click *Yes Button* on the window using the left button of his mouse or press and hold *Alt* key and press letter *Y* (represented as *Alt + Y*) on his keyboard if he doesn't want to use mouse. Otherwise, click *No Button* or hit *Alt + N* to end this execution. If one wants to choose any bottom or menu without mouse, he can use *Alt + ?* way. The ? here represents the underlined character on the bottom or menu, such as using *Alt + Y* to execute the bottom Yes.
(3). The main window called "Leak-off Test Analysis Software" appear on one's screen after entering the software system. On the top of the window are menus named "*File, Set Data, Stress State, Leak-off Test, Window and Help*".
(4). Click the *File* menu or *Alt+F* to enter the submenu. *Set Printer* and *Exit* submenus are provided under the *File* menu. Click *Exit (or Alt + X)* to end the execution of the software. You can terminate the program any time by click the *Exit* menu. Any form of

the software could be printed out on one's printer. Choose and connect the right printer using the *Set Printer* submenu.

(5). *Set Date* menu provides the entrance of all the data needed for the analysis. Under the menu are five submenus named as *Set All Default, Well and Casing String, Mud and leak-off test, Cement Slurry and Rock*.

Well and Casing String submenu asks for data of well planning and casing string size. A new form will pop-up if one choose to execute the submenu. One can input data one by one or use *Set Default* button to set all provided data for the form. The default data are used for practicing. One can change the data on the form whenever he wants to. Choose *Ok* button to accept the data and terminate the form. Note that the data entered by *Set Default* don't represent they are the best values. They are just a sample of data set.

Same as *Well and Casing String* submenu, *Mud and leak-off test, Cement Slurry and Rock* submenus ask for data of mud and leak-off test properties, the properties of cement slurry and the properties of rock respectively.

If one don't want to set data one by one form, he can choose *Set All Default* to set all the needed data for mud, cement, rock, well and so on. He can change any data by clicking the appreciate form. Again, the data set by *Set All Default* do not mean they are the best data.

(6). After setting all the necessary data, one could do analysis through *In-situ Stress Analysis, Fracture Analysis* and/or *Leak-off Test analysis* submenus. One could find out whether the wellbore is in plastic state and how large the plastic region is as well as the in-situ stresses by choose *Calculate* button on the *In-situ Stress Analysis* menu. Click *Close* to end the form.

(7). *Leak-off Test* menu is the major part of the analysis. It contains *Fracture Analysis* and *LOT Analysis* submenus. On the *Fracture Analysis* form, choose button of *Fracture Analysis* to see the result of fracture way. *Fracture Shape* button shows the horizontal plastic fracture shape and size. Choose *Close* button to end the form.

LOT Analysis submenu provide leak-off test analysis. On the form of *LOT Analysis,* there are three command buttons named *View LOT, Print, Clear,* and *Close. View LOT* button executes calculation and draw its LOT curve on the form. *Clear, Print* and *Close* buttons clear the plots, print the form on one's printer and end the form respectively. Two frames *of LOT component* and *LOT Curve Color* are provided. LOT components include *Compressing Mud, Wellbore Expansion, Filtration, Cement Parting* and *Plastic Fracture.* One can watch any combination effect by check the appropriate boxes and then click *View LOT*. One could draw LOT curves in different color by choosing the color he likes by choosing the color option in color frame.

Compressing Mud set the function of analysis of only mud compression. It gives casing test result. *Wellbore Expansion* sets the function of the analysis of the expansion of the open hole section during leak-off test. *Filtration* considers the effect of leak through any pre-existed channel or pre-existed formation fracture as well as filtration into rock pores. Changing the properties of mud on *Mud and Leak-off Test,* one'll see the effect of the filtration. Check *Cement Parting* box allow one to analyze the effect of cement parting of the leak-off test. *Plastic Fracture* adds the effect of horizontal plastic fracture on the LOT. The result of plastic fracture and filtration through the newly created surfaces will be added on the LOT curve once these boxes are checked.

(8). Menus of *Window* contains the current opened windows during the execution of the software. Users can shift form from one to another directly by using the submenus under the *Window*. Functions of multi-form operation are also provided under the *Window* menu. One may arrange forms in layer, horizontal and vertical. Menu *Help* contains simple guides of using the software, and a *About* form which gives the information about the software is also provided under *Help* menu.